U.S.NRC
United States Nuclear Regulatory Commission
Protecting People and the Environment

NUREG/CR-7306
ORNL/TM-2023/2938

Fuel Assembly and Irradiation Parametric Study for Extended-Enrichment and High-Burnup Light-Water Reactor Spent Nuclear Fuel in Dry Storage Casks and Transportation Packages

Office of Nuclear Regulatory Research

AVAILABILITY OF REFERENCE MATERIALS IN NRC PUBLICATIONS

NRC Reference Material

As of November 1999, you may electronically access NUREG-series publications and other NRC records at NRC's Library at www.nrc.gov/reading-rm.html. Publicly released records include, to name a few, NUREG-series publications; *Federal Register* notices; applicant, licensee, and vendor documents and correspondence; NRC correspondence and internal memoranda; bulletins and information notices; inspection and investigative reports; licensee event reports; and Commission papers and their attachments.

NRC publications in the NUREG series, NRC regulations, and Title 10, "Energy," in the *Code of Federal Regulations* may also be purchased from one of these two sources.

1. **The Superintendent of Documents**
   U.S. Government Publishing Office
   Washington, DC 20402-0001
   Internet: https://bookstore.gpo.gov/
   Telephone: (202) 512-1800
   Fax: (202) 512-2104

2. **The National Technical Information Service**
   5301 Shawnee Road
   Alexandria, VA 22312-0002
   Internet: https://www.ntis.gov/
   1-800-553-6847 or, locally, (703) 605-6000

A single copy of each NRC draft report for comment is available free, to the extent of supply, upon written request as follows:

Address: **U.S. Nuclear Regulatory Commission**
Office of Administration
Digital Communications and Administrative Services Branch
Washington, DC 20555-0001
E-mail: Reproduction.Resource@nrc.gov
Facsimile: (301) 415-2289

Some publications in the NUREG series that are posted at NRC's Web site address www.nrc.gov/reading-rm/doc-collections/nuregs are updated periodically and may differ from the last printed version. Although references to material found on a Web site bear the date the material was accessed, the material available on the date cited may subsequently be removed from the site.

Non-NRC Reference Material

Documents available from public and special technical libraries include all open literature items, such as books, journal articles, transactions, *Federal Register* notices, Federal and State legislation, and congressional reports. Such documents as theses, dissertations, foreign reports and translations, and non-NRC conference proceedings may be purchased from their sponsoring organization.

Copies of industry codes and standards used in a substantive manner in the NRC regulatory process are maintained at—

The NRC Technical Library
Two White Flint North
11545 Rockville Pike
Rockville, MD 20852-2738

These standards are available in the library for reference use by the public. Codes and standards are usually copyrighted and may be purchased from the originating organization or, if they are American National Standards, from—

American National Standards Institute
11 West 42nd Street
New York, NY 10036-8002
Internet: www.ansi.org
(212) 642-4900

Legally binding regulatory requirements are stated only in laws; NRC regulations; licenses, including technical specifications; or orders, not in NUREG-series publications. The views expressed in contractor prepared publications in this series are not necessarily those of the NRC.

The NUREG series comprises (1) technical and adminis-trative reports and books prepared by the staff (NUREG–XXXX) or agency contractors (NUREG/CR–XXXX), (2) proceedings of conferences (NUREG/CP–XXXX), (3) reports resulting from international agreements (NUREG/IA–XXXX),(4) brochures (NUREG/BR–XXXX), and (5) compilations of legal decisions and orders of the Commission and Atomic and Safety Licensing Boards and of Directors' decisions under Section 2.206 of NRC's regulations (NUREG–0750),and (6) Knowledge Management prepared by NRC staff or agency contractors.

U.S.NRC
United States Nuclear Regulatory Commission
Protecting People and the Environment

NUREG/CR-7306
ORNL/TM-2023/2938

Fuel Assembly and Irradiation Parametric Study for Extended-Enrichment and High-Burnup Light-Water Reactor Spent Nuclear Fuel in Dry Storage Casks and Transportation Packages

Manuscript Completed: June 2023
Date Published: April 2024

Prepared by:
A. Alpan
N. Kucinski
A. Shaw
B. Hiscox
G. Radulescu

Oak Ridge National Laboratory
Oak Ridge, TN 37831-6170

Lucas Kyriazidis, NRC Project Manager

Office of Nuclear Regulatory Research

ABSTRACT

There is an increased interest in operating commercial light-water reactors (LWRs) in the United States with improved economics that would result from longer fuel cycle lengths, fewer and shorter refueling outages, and fewer fuel assemblies requiring storage at the back end of the fuel cycle. To support this, fuel discharge burnups, as well as initial ^{235}U enrichments, must be higher than those used in current commercial LWRs. The typical upper limit considered for assembly average burnup in this report is 75 gigawatt-days (GWd) per metric ton of uranium (MTU), as opposed to the current typical upper bound of approximately 62 GWd/MTU. The upper limit considered for initial ^{235}U enrichment is 8 weight percent (8 wt %), as opposed to the current regulatory limit of 5 wt %. The enrichment range from 5 to 8 wt % is referred to in this report as *extended enrichment*. To investigate the effect of high burnup and extended enrichment conditions on dose rates and burnup credit for dry storage casks and transportation packages, a fuel assembly and irradiation parametric study was performed. The conclusions from this study will assist U.S. Nuclear Regulatory Commission staff in reviewing applications for dry storage casks and transportation packages that contain high-burnup and extended enrichment fuel.

TABLE OF CONTENTS

LIST OF FIGURES

LIST OF TABLES

EXECUTIVE SUMMARY

To assess the effect of extended enrichment (i.e., uranium enriched between 5 and 8 weight percent (wt %) uranium-235 (^{235}U) and high-burnup fuel—assembly average burnup up to 75 gigawatt-days per metric ton uranium (GWd/MTU)—on radiation shielding and criticality safety analyses for transportation packages and dry storage casks, a parametric study on fuel assembly, irradiation conditions, and decay was performed to evaluate trends and were compared with current experience with low-enriched uranium (^{235}U enrichment up to 5 wt %) light-water reactor operation. A few subject areas were excluded in the study, including accident-tolerant fuel, assemblies used in pressure vessel fluence reduction programs, and boiling-water reactor (BWR) burnup credit (BUC).

Various fuel assembly, irradiation, and decay parameters were evaluated for pressurized-water reactors (PWRs) and BWRs separately. These parameters included assembly average burnup; initial ^{235}U enrichment; fuel specific power; soluble boron concentration (modeled as an average concentration and using a boron letdown curve); moderator density; fuel temperature; fuel density; burnable absorbers (integral fuel burnable absorbers, gadolinium oxide [Gd_2O_3] fuel rods, and wet annular burnable absorbers); rod control cluster assemblies; and cooling time for PWRs. For BWRs, assembly average burnup, maximum initial ^{235}U enrichment, fuel specific power, coolant void, fuel temperature, fuel density, burnable absorbers (Gd_2O_3 fuel rods), control rod blades, and cooling time were included. The ranges for these parameters were determined from low-enriched uranium plus (LEU+) assembly designs, as well as low-enriched uranium (LEU) assembly designs. LEU+ refers to uranium enriched between 5 and 10 wt % ^{235}U.

The SCALE code system, version 6.3.0, was used in all of the analyses. Polaris was used for fuel depletion, Oak Ridge Isotope GENeration (ORIGEN) for decay, OPUS for ORIGEN postprocessing, ORIGEN Assembly Isotopics (ORIGAMI) for interpolations on ORIGEN cross section libraries, Monaco with Automated Variance Reduction using Importance Calculations (MAVRIC) for shielding, and criticality safety analysis sequence with KENO V.a transport module (CSAS5) for criticality safety calculations. ENDF/B-VII.1 cross section libraries were used throughout the study: the continuous-energy library was used for shielding calculations, and the multigroup library (252 neutron group) was used for criticality safety calculations. ENDF/B-VII.1 has been validated using SCALE for nuclear criticality safety, reactor physics, and radiation shielding and was therefore found appropriate to use in this analysis. The multigroup bias of criticality safety calculations was assessed by comparing multigroup and continuous-energy library results for verification purposes.

Shielding calculations with MAVRIC included two simplifications: a simplified geometry was used for transportation packages and dry shielding casks, and an on-the-fly dose rate calculation was used, involving the generation of response functions that were combined with source intensities. The simplifications enabled efficient dose rate calculations with relative errors that were generally no more than a maximum of a few percent within an energy group. The simplified geometrical models were compared with detailed transportation package and dry storage cask models and were verified to be appropriate for the current analyses. Criticality safety calculations with CSAS5 used the Generic Burnup Credit (GBC)-32 cask model in 3D geometry.

Nuclide importance to decay heat, source terms, and BUC was determined for extended enrichment and high-burnup fuel. Results were compared with those from previous publications using LEU and LEU+ fuel, if available. The parametric study for shielding included analyses for PWRs and BWRs. Results are presented in plots for each parameter analyzed. The output of interest was the trend in dose rate, presented for neutrons and gammas separately. Additionally, a cobalt impurity concentration of 20 ppm was included in the fuel cladding, and ^{60}Co dose rates were calculated. This cobalt impurity represents the upper bound of the range of cobalt impurity in Zircaloy-4 cladding. Dose rates were given as absolute values, relative values with respect to a baseline assembly model, or normalized to a maximum value within a dataset when analyzing trends. Similar dose rate trends were generally observed for burnup, initial enrichment, cooling time, specific power, moderator density/temperature, coolant void fraction, and fuel density compared to LEU publications. The parametric study for criticality safety included analyses for PWRs only. The output of interest was the trend in k_{eff} and the resulting Δk_{eff} with respect to the parameter of interest. Trends were compared with those from previous publications using LEU and LEU+ fuel, if available. Criticality safety behavior for high-burnup and extended enrichment assemblies followed expectations established by decades of BUC analysis in most instances.

ACKNOWLEDGMENTS

This report was written under U.S. Nuclear Regulatory Commission (NRC) Interagency Agreement 31310022N0002. The authors thank Lucas Kyriazidis and Andrew Barto of the NRC, for their invaluable support and guidance that facilitated the successful completion of this report. The authors are grateful for the thorough review of and comments on this report by Andrew Barto, Andrew Bielen, Nathanael Hudson, Lucas Kyriazidis, and Michael Rose of the NRC. The authors also thank Cihangir Celik and B.J. Marshall of Oak Ridge National Laboratory, for their technical review of the report.

ABBREVIATIONS AND ACRONYMS

ADAMS	Agencywide Documents Access and Management
AIC	Ag-In-Cd
AF	absorption fraction
AFP	actinide and fission product
ATF	accident-tolerant fuel
BOC	beginning-of-cycle
BUC	burnup credit
BWR	boiling-water reactor
CE	continuous-energy
cm	centimeter
CSAS5	criticality safety analysis sequence with KENO V.a transport module
DOE	U.S. Department of Energy
EALF	energy of average neutron lethargy causing fission
eV	electron-volt
ENDF	Evalauted Nuclear Data File
g	gram
GBC-32	generic burnup credit-32
GEH	GE Hitachi Nuclear Energy
GWd	gigawatt-days
HI-STAR	Holtec International Storage, Transport and Repository
HI-STORM	Holtec International Storage Module
ICSBEP	International Criticality Safety Benchmark Evaluation Project
IFBA	integral fuel burnable absorber
K	kelvin
k_{eff}	effective multiplication factor
k_{inf}	infinite multiplication factor
LEU	low-enriched uranium
LEU+	low-enriched uranium plus
LWR	light-water reactor
MAVRIC	Monaco with Automated Variance Reduction using Importance Calculations
mrem/h	millirem per hour
MeV	mega electron-volt
MPC	multipurpose canister
MTU	metric ton of uranium
MW	megawatt
n	neutrons
NRC	U.S. Nuclear Regularory Commission
OFA	optimized fuel assembly

ORIGAMI	ORIGEN Assembly Isotopics
ORIGEN	Oak Ridge Isotope GENeration
ORNL	Oak Ridge National Laboratory
p	photons
pcm	per cent mille
ppm	parts per million
PWR	pressurized-water reactor
RCCA	rod cluster control assembly
RFA	robust fuel assembly
s	second
SFA	shielding fuel assembly
SNF	spent nuclear fuel
$T_{1/2}$	half-life
VALID	verified, archived library of inputs and data
W	watts
WABA	wet annular burnable absorber
WEC	Westinghouse Electric Company LLC
wt %	weight percent
yr	year(s)

1 INTRODUCTION

The U.S. nuclear industry has an increased interest in improving the economic operation of nuclear power plants. Proposed improvements include operating with longer fuel cycles, reducing refueling outage frequency and duration, and generating fewer fuel assemblies to transport and store. Such operational changes require higher burnups and initial ^{235}U enrichments compared to those currently used in light-water reactors (LWRs). This report evaluates the effect of high-burnup (up to assembly average burnup of 75 gigawatt days per metric ton of uranium (GWd/MTU) and extended-enrichment (between 5 weight percent (wt %) to 8 wt % uranium-235 (^{235}U) enrichment) fuel on shielding and criticality safety analyses for transportation packages and dry storage casks.

The present study excluded a few subjects, including accident-tolerant fuel, assembly designs for reactor pressure vessel fluence reduction programs that were treated as special cases, and boiling-water reactor (BWR) burnup credit (BUC)—only pressurized-water reactor (PWR) BUC was considered. Note that the shielding analyses included PWR and BWR fuel.

The SCALE computer code system version 6.3.0 was used for all analyses recorded in this report. SCALE has been validated for criticality safety, reactor physics, and radiation shielding analyses using the Evaluated Nuclear Data File (ENDF)/B-VII.1 library [1]. The ENDF/B-VII.1 continuous-energy (CE) library was used in shielding (dose rate) calculations, and the ENDF/B-VII.1-based 252 neutron group library was used in criticality safety (burnup credit) calculations. A verification of the 252-neutron-group library was demonstrated by comparing results against the CE library.

The shielding analyses used simplified geometrical models representing transportation packages and dry storage casks, as well as on-the-fly dose rate calculations, as discussed in Appendix A. A verification of the use of simplified shielding models was demonstrated by comparing results against detailed geometrical models. A verification of the simplifications to the geometrical model and calculation method enabled efficient calculation of dose rates. BUC calculations for criticality safety used the generic burnup credit-32 (GBC-32) cask computational benchmark [2] with a 3D model.

A set of fuel assembly, irradiation, and decay parameters was selected for a parametric study. For PWR fuel, Westinghouse Electric Company LLC (WEC) 17 × 17 optimized fuel assembly (OFA) and robust fuel assembly (RFA) rod designs were used. For BWR fuel, GE Hitachi Nuclear Energy (GEH) 10 × 10 GE14 fuel assembly was used. Studied parameters for PWR fuel included assembly average burnup, initial ^{235}U enrichment, specific power, soluble boron, moderator density, fuel temperature, fuel density, burnable absorbers, rod control cluster assemblies, and cooling times. Studied parameters for BWR fuel included assembly average burnup, initial ^{235}U enrichment, specific power, moderator density (coolant void), fuel temperature, fuel density, burnable absorbers, control blades, and cooling times.

The analysis methodology in the SCALE modules and geometrical models, as well as the parametric study methodology, is discussed in this report. Nuclide importance to decay heat, source terms, and BUC was evaluated for high burnup and extended enrichments and compared with previously published data. Parametric studies for shielding and criticality safety were analyzed separately in dedicated sections.

2 SCOPE LIMITATIONS

Several topics were excluded from the scope of this work and listed below.

- Accident tolerant fuel (ATF) designs have not been included in this report. Extended-enrichment ATF isotopic and lattice parameter trends were analyzed in ORNL/TM-2021/1961 [3], and the effects of extended-enrichment and ATF on fresh fuel storage criticality safety were analyzed in ORNL/TM-2021/2330 [4].
- Assembly designs used in reactor pressure vessel fluence reduction programs, such as peripheral power suppression assemblies involving the use of half- or full-length hafnium rods [5] and shielding fuel assemblies (SFAs) involving rows of stainless-steel rods and axial-zoned SFA fuel rods [6], are not analyzed. These are considered special cases and should be taken into account on a case-by-case basis.
- BWR BUC is excluded because the technical basis for BWR BUC in spent nuclear fuel (SNF) storage containers has not been fully developed [7-9].
- Variation of burnup within a fuel pellet was not modeled in this study. This study applies a constant assembly average burnup in fuel depletion calculations.
- Actinide and fission product (AFP) sets of isotopes were used for BUC analysis because it is currently the preferred approach used in industry.

3 FUEL ASSEMBLY, IRRADIATION, AND DECAY PARAMETERS AND RANGES

The PWR fuel assembly models analyzed herein are the WEC 17 × 17 assembly containing RFA [10-12] and OFA) [11, 12] fuel rod designs. Fuel designs based on WEC RFA and OFA are used in the majority of WEC nuclear power plants [13]. These WEC designs have been used in various analyses for high-burnup and extended-enrichment fuel [14-20]. The BWR fuel assembly model analyzed herein is the GEH10 × 10-8 [12, 21] GE14 assembly. The "-8" following the 10 × 10 lattice array represents two large water holes that effectively replace 8 fuel rods. The GE14 design has been used in the neutronics analysis of high-burnup and extended-enrichment fuel [22, 23].

High-burnup and extended-enrichment uranium oxide (UO_2) fuel is characterized by higher beginning-of-cycle (BOC) reactivity compared to current LWR fuel that operates at initial ^{235}U enrichments up to 5 wt %. Available means to suppress PWR BOC reactivity include the use of burnable absorbers and soluble boron. Burnable absorbers are divided into two groups: integral burnable absorbers and burnable poison rods [24-26]. Integral burnable absorbers consist of neutron-absorbing material that are an integral part of the fuel assembly. Examples are fuel pellets coated by a thin layer of zirconium diboride (ZrB_2), referred to as integral fuel burnable absorber (IFBA) [24, 26, 27], and burnable absorbers such as gadolinium oxide (Gd_2O_3) or erbium oxide (Er_2O_3) mixed with UO_2 fuel [24, 26]. Burnable poison rods consist of rods with neutron-absorbing material inserted into PWR assembly guide tubes. Two examples of burnable poison rods are (i) wet annular burnable absorber (WABA) rods that contain annular alumina-boron carbide (Al_2O_3/B_4C) pellets within two concentric Zircaloy-4 tubes [24, 25, 28] and (ii) a pyrex borosilicate (B_2O_3/SiO_2) glass tube enclosed within a stainless steel clad [24, 25]. Soluble boron in PWRs is not considered as a burnable absorber because its reactivity is controlled by changing the boron concentration with burnup within a fuel cycle [29]. For BWRs, burnable absorber in the form of Gd_2O_3 is widely used for reactivity hold-down at BOC [26, 29].

3.1 Pressurized-Water Reactors

In this report, the PWR *baseline assembly* refers to a PWR fuel assembly with physical characteristics given in Table 3-1 and selected fuel assembly and irradiation parameters. The values that are underlined in Table 3-2 are associated with the baseline assembly parameters. In the parametric study, when a parameter was varied, other parameters were kept constant and corresponded to the baseline values.

The 17 × 17 array PWR baseline assembly included 80 IFBA fuel rods, 0 Gd_2O_3 fuel rods, and 0 burnable poison rods; no RCCA insertion occurred. IFBA fuel rod, Gd_2O_3 fuel rod, WABA rod, and rod cluster control assembly (RCCA) specifications are given in Table 3-3, Table 3-4, Table 3-5, and Table 3-6, respectively. 2D geometric models of a PWR assembly without burnable poison rods are illustrated in Figure 3-1 (a) and with 24 WABA rods inserted into assembly guide tubes in Figure 3-1 (b).

A cobalt impurity concentration of 20 parts per million (ppm) [30] was included in the Zircaloy-4 composition in the fuel assembly model. The cobalt impurity was depleted by flux to determine ^{60}Co activity trends with depletion parameters. The 20 ppm cobalt concentration represents an upper bound of cobalt impurity in Zircaloy-4. The cobalt impurity concentration in assembly structural materials (e.g., stainless steel or inconel in spacer grids or assembly upper and lower

nozzles) is typically higher than 300 ppm [12]. However, assembly structural materials were not included in the assembly model in depletion calculations because their presence can modify the neutron flux and spectrum and lead to incorrect conclusions about the inventories of nuclides in an irradiated fuel assembly.

Table 3-1 Physical Characteristics of PWR Fuel Assemblies Used in Fuel Depletion Calculations

Parameter	Data[a]	
	WEC RFA	WEC OFA
Fuel pellet material	UO_2	UO_2
Assembly array size	17 × 17	17 × 17
Number of fuel rods	264	264
Fuel rod pitch (cm)	1.26	1.26
Pellet radius (cm)	0.410	0.392
UO_2 effective density (g/cm^3)	10.26	10.26
Clad material	Zircaloy-4[b]	Zircaloy-4[b]
Clad outer radius (cm)	0.475	0.457
Clad inner radius (cm)	0.418	0.400
Number of guide tubes	24	24
Guide tube material	Zircaloy-4[b]	Zircaloy-4[b]
Guide tube outer radius (cm)	0.602	0.602
Guide tube inner radius (cm)	0.561	0.561
Number of instrument tubes	1	1
Instrument tube material	Zircaloy-4[b]	Zircaloy-4[b]
Instrument tube outer radius (cm)	0.605	0.605
Instrument tube inner radius (cm)	0.559	0.559

[a] Data is from the U.S. Department of Energy (DOE) report DOE/RW—0184-Vol.3 [11], except guide and instrument tube dimensions and UO_2 density, which are from [31]. WEC Standard fuel rod dimensions in [11] specified as "WEC Std" are the same as WEC RFA fuel rod dimensions [10].
[b] ZIRLO® and Optimized ZIRLO™ have replaced Zircaloy-4 for enhanced corrosion resistance and dimensional stability [13, 32-34]. [1] In this report, Zircaloy-4 was used for the fuel cladding, guide tubes, and instrument tubes. Using Zircaloy-4 instead of ZIRLO or optimized ZIRLO has no significant effect on the dose rate and BUC analysis in this study since most of the composition remains zirconium in all three alloys. Furthermore, since trends are being analyzed in this report, the use of either of these three alloys would not affect the conclusions driven from the trends.

[1] Optimized ZIRLO and ZIRLO are trademarks or registered trademarks of Westinghouse Electric Company LLC, its affiliates and/or its subsidiaries in the United States and may be registered in other countries throughout the world. All rights reserved. Unauthorized use is strictly prohibited.

Table 3-2 PWR Fuel Assembly, Irradiation, and Decay Parameters

Parameter	Data
Assembly average burnup (GWd/MTU)[a]	15, 20, 25, 30, 35, 40, 45, 50, 55, 60, 65, 70, 75
Initial ^{235}U enrichment (wt %)[b]	5.0, 5.5, 6.0, 6.5, 7.0, 7.5, 8.0
Fuel specific power (MW/MTU)	15, 20, 30, 40, 50
Average soluble boron concentration in the coolant (ppm)	600, 1,000, 1,800
Moderator density (g/cm^3)/corresponding moderator temperature (K)	0.76971/550, 0.70045/585, 0.63/610, 0.60811/615
Fuel temperature (K)	560, 800, 900, 1600
Fuel density (g/cm^3)	10, 10.26, 10.75
Integral burnable absorber types	IFBA, gadolinia[c]
Number of IFBA fuel rods	0, 80, 104, 128, 156, 200
Number of Gd_2O_3 fuel rods[d]	12
Burnable poison rod types	None, WABA
Number of WABA rods	8, 20, 24
Number of RCCA rods	None, 24
Cooling Time (years)	1, 2, 5, 10, 20, 30, 40, 50, 60, 70, 80, 90, 100

[a] 20, 30, 40, 50, 60, 70, 75 GWd/MTU were used in shielding, 15, 25, 35, 45, 55, 65, 75 GWd/MTU were used in criticality safety calculations.

[b] Enrichments of 5 and 8 wt % were used in shielding calculations. Enrichments of 5, 6.5, and 8 wt % were used in criticality safety calculations. The 7 wt % enrichment was used in the Gd_2O_3 study only.

[c] Gadolinia refers to Gd_2O_3.

[d] Gd_2O_3 was used in the hybrid IFBA/Gd_2O_3 assembly design, in which the baseline initial ^{235}U enrichment was 7 wt % for UO_2 rods and 5 wt % for Gd_2O_3 fuel rods, consistent with the assembly design in [15].

Table 3-3 PWR IFBA Fuel Rod Specification

Parameter	Data	
	WEC RFA[a]	WEC OFA[b]
Poison material	ZrB_2	ZrB_2
^{10}B enrichment (wt %)	50	50
^{10}B loading (mg/in)	2.355	2.355
Coating thickness (micron)	10	10.441
Coating density (g/cm^3)	3.85	3.85

[a] Data is from [35].

[b] The WEC OFA IFBA coating thickness was calculated using the WEC OFA fuel pellet radius and WEC RFA IFBA ^{10}B enrichment, ^{10}B loading, and coating density.

Table 3-4 PWR Gadolinia Fuel Rod Specification

Parameter	Data[a]
Poison material	Gd_2O_3
Gd_2O_3 concentration (wt %)	8

[a] Poison material is from [27]; Gd_2O_3 concentration is from [36]. The same Gd_2O_3 concentration was used in [20].

Table 3-5 PWR WABA Rod Specification

Parameter	Data[a]
Poison material	B_4C-Al_2O_3
Poison inner radius (cm)	0.353
Poison outer radius (cm)	0.404
Poison density (g/cm^3)	3.65
B_4C-Al_2O_3 composition (atoms/[barn · cm])	$^{10}B = 2.98553 \times 10^{-3}$ $^{11}B = 1.21192 \times 10^{-2}$ $C = 3.77001 \times 10^{-3}$ $^{16}O = 5.85563 \times 10^{-2}$ $Al = 3.90223 \times 10^{-2}$
Cladding material	Zircaloy-4
Inner clad inner radius (cm)	0.286
Inner clad outer radius (cm)	0.339
Outer clad inner radius (cm)	0.418
Outer clad outer radius (cm)	0.484

[a] Data is from [35] except the B_4C-Al_2O_3 composition, which was calculated.

Table 3-6 PWR RCCA Specification

Parameter	Data[a]
Poison material	80/15/5% Ag-In-Cd (AIC) (lower) and 100% B_4C (upper)
AIC density (g/cm^3)	10.2
AIC radius (cm)	0.382
B_4C density (g/cm^3)	1.76
B_4C radius (cm)	0.373
Cladding material	Stainless steel 304
Cladding inner radius (cm)	0.386
Cladding outer radius (cm)	0.484

[a] Data is from [31, 35, 37].

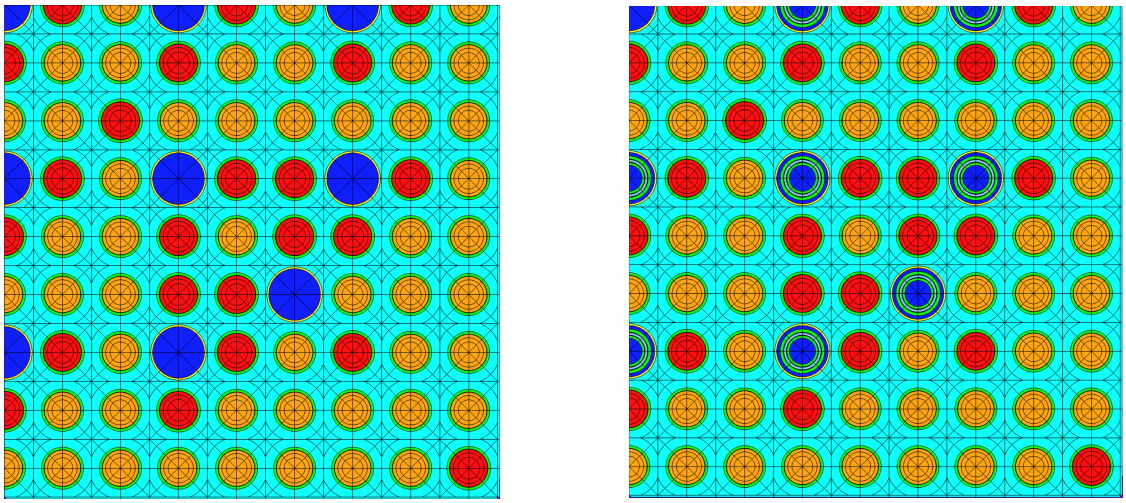

(a) (b)

Figure 3-1 2D View of the PWR Assembly Models (Quadrant Symmetry) (a) with UO_2 and IFBA Fuel Rods and (b) with UO_2, IFBA Fuel, and WABA Rods
(IFBA fuel rods are shown in red and UO_2 rods are shown in orange; Zircaloy-4 fuel cladding and WABA tubes is shown in green; alumina-boron carbide in the WABA is shown in blue gray; Zircaloy-4 WABA tube is shown in yellow; the moderator outside the fuel rods, guide tubes, and instrument tube is shown in light blue; the moderator inside guide tubes, instrument tube, and WABA is shown in deep blue; each UO_2 region has three fuel depletion rings (three rings inside the fuel), and other regions have one ring)

Details about the parameters listed in Table 3-2 are given in the following paragraphs.

Assembly average burnup: Assembly average burnups of 0.1, 1, 2, 4, 6, 8, 10, 12, 14, 16, 18, 20, 25, 30, 35, 40, 45, 50, 55, 60, 65, 70, 75, 80, and 85 GWd/MTU were used in the Polaris fuel depletion calculations; among these values, results from 20, 30, 40, 50, 60, 70, and 75 GWd/MTU were presented for the parametric studies for shielding calculations. With the use of the Oak Ridge Isotope GENeration Assembly Isotopics (ORIGAMI) module, results from 15, 25, 35, 45, 55, 65, and 75 GWd/MTU were presented for the parametric studies for criticality safety calculations.

Initial fuel enrichment: Extended-enrichment fuel ranges up to 8.0 wt % initial ^{235}U were used. Results from 5.0, 5.5, 6.0, 6.5, 7.0, 7.5, and 8.0 wt % ^{235}U initial enrichments were presented in the parametric studies.

Fuel specific power: Specific power of fresh batch, once-burned batch, twice-burned batch, and core-average low-enriched uranium plus (LEU+) cores are 48.8, 39.2, 14.8, and 40.4 megawatt (MW) per MTU, respectively, in [17]; thus, the range of specific powers were chosen between 15 and 50 MW/MTU.

Average soluble boron concentration in the coolant: The maximum critical soluble boron concentration is 1,582 ppm for the LEU+ core in [17]. Five LEU+ core design options in [20] have peak critical boron concentration at full power ranging from 1,332 to 1,795 ppm. Critical boron peaks range from 1,396 to 1,516 ppm in [14] for LEU+ core designs. The average soluble boron concentrations included in this study are 600, 1,000, and 1,800 ppm. In addition to the average soluble boron concentration, a boron letdown curve was modeled.

Moderator density/corresponding moderator temperature: A moderator temperature of 600 kelvin (K) was used for the pin cell benchmark and 2D analysis of the LEU+ core in [15] and [16], respectively. A hot full-power moderator temperature of 585 K is given in [17] for LEU+ cores. Four moderator temperatures were included in this study: 550 K, 585 K, 610 K and 615 K. A burnup-averaged hot-assembly outlet temperature for PWRs is approximately 610 K [38]; this value has previously been used as a conservative moderator temperature for BUC criticality safety analysis in [39]. The 610 K moderator temperature is within the single-phase liquid region that is near the saturation liquid temperature (i.e., 623.15 K [40]). Moderator densities for each temperature were determined using a typical PWR coolant system pressure of 2,250 pounds per square inch [35].

Fuel temperature: A fuel temperature of 900 K was used for the pin cell benchmark and 2D analysis of the LEU+ core in [15] and [16], respectively. A hot full-power fuel temperature of approximately 860 K is given in [17] for LEU+ cores. Four fuel temperatures were included in this study: 560, 800, 900, and 1,600 K.

Fuel density: The fuel density that was calculated as 10.26 gram (g) per cubic centimeter (cm^3) in [35] was used in this study. Two other fuel densities, accounting for approximately −2 and +5 percent change in 10.26 g/cm^3, were added in the parametric study [41]. The lower value of the fuel density corresponds to the density of UO_2 for fuel that is radially homogenized within the cladding inner radius while maintaining a constant fuel mass.

Integral burnable absorbers: IFBA-only burnable absorbers were used in LEU+ cores in [17]. In this study, the number of IFBA fuel rods (80, 104, 128, 156, and 200 in an assembly) and their

locations were taken from [17]; additionally, a zero-IFBA fuel rod assembly was modeled. IFBA/Gd_2O_3 hybrid designs were used in LEU+ lattices in [15] and [20]. In this study, the hybrid IFBA/Gd_2O_3 design was taken from [15], and Gd_2O_3 loading was taken from [36]. The IFBA/Gd_2O_3 assembly that was modeled was one representative assembly design for LEU+ cores.

Burnable poison rods: WABA rods were used in LEU+ cores in [17]. In this study, the number of WABA rods (8, 20, and 24 in an assembly) and their locations were taken from [17]. Each WABA rod assembly design also contained 200 IFBA fuel rods. Additionally, 24 WABA rods and 80 IFBA rods were modeled in a fuel assembly where the IFBA and WABA locations were taken from [17].

RCCA rods: Models included the following scenarios, which are similar to those analyzed in [42].

(i) RCCA with In-Cd-Ag alloy fully inserted up to 45, 55, 65, and 75 GWd/MTU
(ii) RCCA with In-Cd-Ag alloy fully inserted for 5 GWd/MTU from 70 to 75 GWd/MTU
(iii) RCCA with B_4C fully inserted up to 75 GWd/MTU

Cooling time: The analyzed cooling time spans from 1 to 100 yr. Spent fuel has a minimum cooling time of 1 yr [43]. Spent fuel might be in dry storage for a long period of time (e.g., 100 yr or more) depending on the availability of a permanent spent fuel repository in the United States.

3.2 Boiling-Water Reactors

In this report, the BWR *baseline assembly* refers to a BWR fuel assembly with physical characteristics given in Table 3-8 and selected fuel assembly and irradiation parameters. The values that are underlined in Table 3-8 are associated with the baseline assembly parameters. In shielding calculations, relative dose rates were plotted that were ratios of dose rates generated using an assembly with varying parameters to the dose rates generated using the baseline assembly for transportation packages and dry storage casks.

BWR assemblies are typically divided into axial zones based on axial variations in initial ^{235}U enrichment, burnable absorber loading, and number of fuel rods. For example, in the GE14 fuel design, an assembly has 14 part-length fuel rods [21]. In this study, only the *dominant* axial zone that contains fuel rods occupying every position in the fuel pin array was modeled.

The 10 × 10-8 array BWR baseline assembly included 67 UO_2 rods with eight different initial ^{235}U enrichments, 20 UO_2-Gd_2O_3 rods with three different Gd_2O_3 loadings, and 2 water rods that effectively replaced 8 fuel rods. The BWR baseline assembly did not include control blades. Gadolinia fuel rod and control blade specifications are given in Table 3-9 and Table 3-10, respectively. BWR assembly geometric models without and with a control rod blade are shown in Figure 3-2. The maps of initial ^{235}U enrichments and Gd_2O_3 loading associated with Figure 3-2 are shown in Figure 3-3; an assembly design with a maximum initial ^{235}U enrichment of 7 wt % is presented in Figure 3-3 [23]. For the enrichment parametric study, all initial ^{235}U enrichments in Figure 3-3 were scaled using the maximum initial ^{235}U enrichment of 7 wt % and the varied maximum initial ^{235}U enrichment. For example, to create a new assembly having a maximum initial ^{235}U enrichment of 8 wt %, all ^{235}U enrichments in Figure 3-3 were multiplied by 8/7 (i.e., 1.143). The Gd_2O_3 loading was unchanged in creating new assemblies with different maximum initial ^{235}U enrichments.

A cobalt impurity concentration of 20 ppm [30] was included in the Zircaloy-2 composition. The cobalt impurity was depleted by flux to determine ^{60}Co activity trends with fuel depletion parameters.

Table 3-7 Physical Characteristics of the BWR Fuel Assembly Used in Fuel Depletion Calculations

Parameter	GE14 Data	Reference
Fuel pellet material	UO_2	[21]
Assembly array size	10 × 10	[21]
Number of fuel rods	92	[21, 44]
Number of UO_2-Gd_2O_3 rods	25	[23]
Fuel rod pitch (cm)	1.295	[21]
Pellet radius (cm)	0.438	[21, 44]
UO_2 effective density (g/cm^3)	10.64	[22]
Clad material	Zircaloy-2	[44]
Clad outer radius (cm)	0.513	[21]
Clad inner radius (cm)	0.447	[21]
Water tube clad material	Zircaloy-2	[21]
Water tube outer radius (cm)	1.24[a]	[21]
Water tube inner radius (cm)	1.2	[21]
Channel width (inside) (cm)	13.406	[21]
Channel box thickness (cm)	0.203	[22]
Corner-fuel-rod-center to channel-box-inner-corner (cm)	0.965	[22]

[a] 1.28 has been used in the fuel depletion analysis. The 0.04 cm difference in Zircaloy-2 between the value used and the reference value has no effect on the conclusions due to the material and small difference. Furthermore, this small difference would not have any effect in analyzing dose rate trends.

Table 3-8 BWR Fuel Assembly, Irradiation, and Decay Parameters

Parameter	Data
Average assembly burnup (GWd/MTU)	20, 30, 40, 50, 60, 70, 75
Maximum initial ^{235}U enrichment (wt %)	5.0, 5.5, 6.0, 6.5, 7.0, 7.5, 8.0
Fuel specific power (MW/MTU)	15, 20, 25, 30, 40, 50
Coolant void (%)	20, 40, 45.5, 60, 80
Fuel temperature (K)	500, 700, 800, 900, 1,100, 1,300
Fuel density (g/cm^3)	10.26, 10.64, 10.96
Gd_2O_3 concentration (wt %)	4, 6, 8 (see Figure 3-3) Four additional cases, each having uniform Gd_2O_3 loadings of 1.5, 4, 6, and 8 wt % in the baseline assembly Gd_2O_3 rods
Burnable poison rod types	None
Control rod blades	None, with control rod blade
Cooling Time (years)	1, 2, 5, 10, 20, 30, 40, 50, 60, 70, 80, 90, 100

Table 3-9 BWR Gadolinia Fuel Rod Specification

Parameter	Data[a]
Poison material	Gd_2O_3
Gd_2O_3 loading (wt %)	4, 6, 8

[a] Poison material is from [21]; Gd_2O_3 loading is from the BWR assembly design having a maximum initial ^{235}U enrichment of 7 wt % in [23], as shown in Figure 3-3.

Table 3-10 BWR Control Rod Blade Specification

Parameter	Data[a]
Poison material	B_4C
Cladding and sheath material	Stainless steel 304
Tube inner radius (cm)	0.175
Tube outer radius (cm)	0.239
Control rod blade tip radius (cm)	0.396
Sheath thickness (cm)	0.142
Central structure wing length (cm)	1.985

[a] Data is from [45].

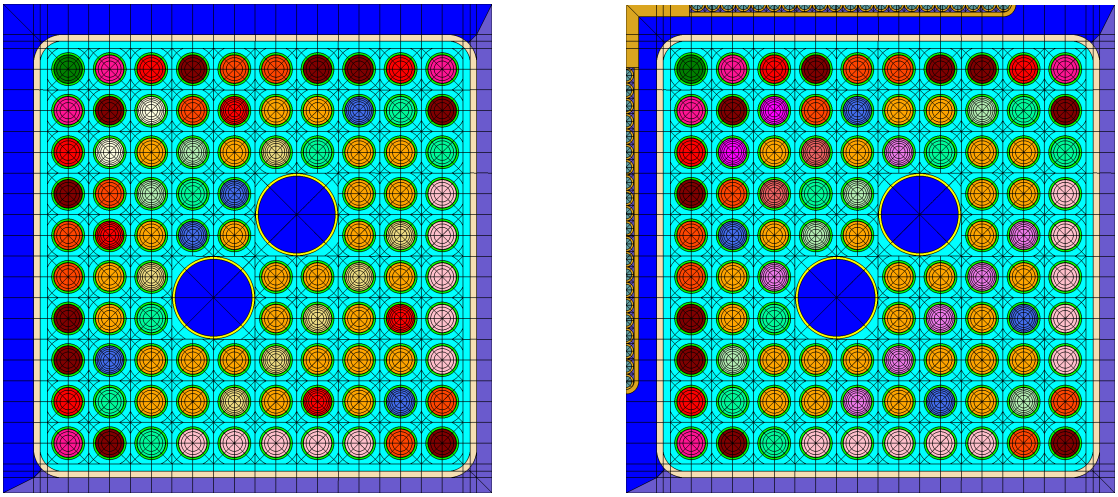

(a) (b)

Figure 3-2 2D View of the BWR Assembly Model (a) Without a Control Blade and (b) with a Control Rod Blade (Each fuel pin color represents a combination of the ^{235}U enrichment and gadolinia loading; the moderator outside the fuel rods, water holes is shown in light blue; the moderator inside the water holes is shown in deep blue)

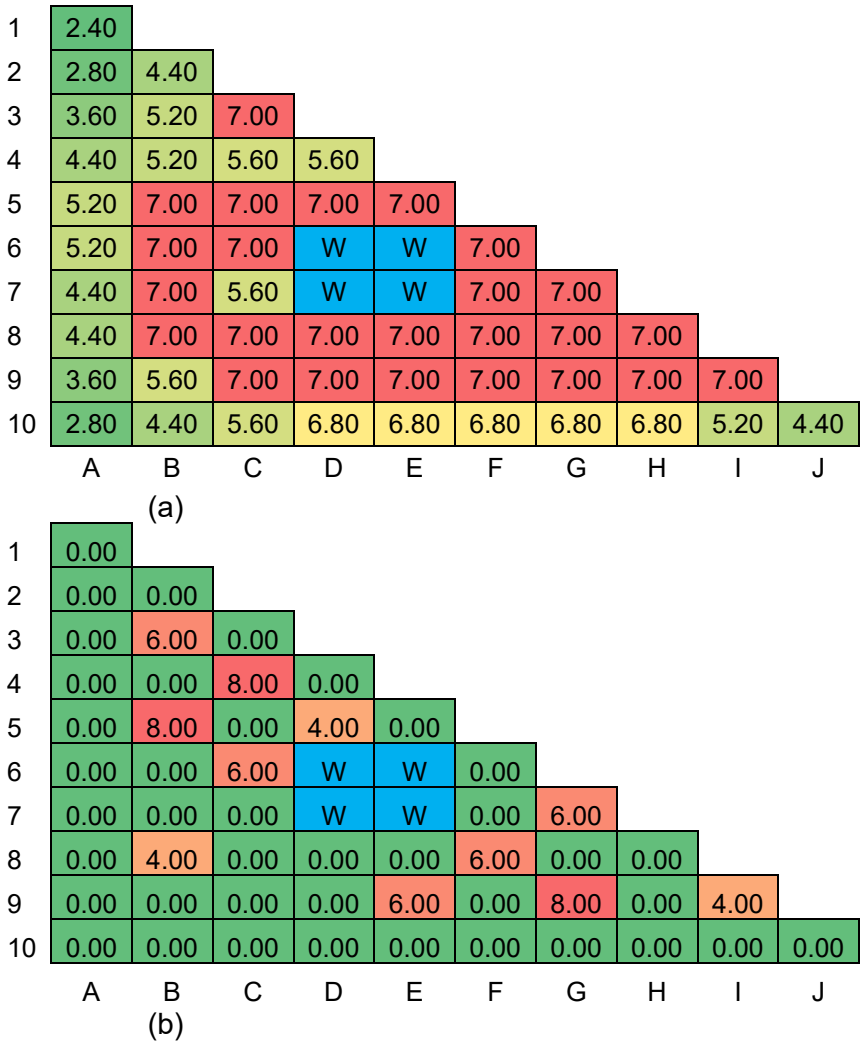

Figure 3-3 **2D BWR Assembly Maps of (a) Initial Uranium Enrichment (wt %) and (b) Gd_2O_3 loading (wt %) Associated with Figure 3-2 for a Maximum Initial ^{235}U Enrichment of 7 wt %** (Bottom region from the diagonal line of symmetry is shown; "W" in the blue-colored cell shows one water rod that effectively replaces four fuel rods; wt % color scale is red–yellow–green, where red shows the highest and green shows the lowest values)

Details about the parameters listed in Table 3-8 are given in the following paragraphs.

Assembly average burnup: Assembly average burnups of 0.1, 1, 2, 4, 6, 8, 10, 12, 14, 16, 18, 20, 25, 30, 35, 40, 45, 50, 55, 60, 65, 70, 75, 80, and 85 GWd/MTU were used in the fuel depletion calculations; among these values, results from 20, 30, 40, 50, 60, 70, and 75 GWd/MTU were presented for the parametric studies.

Initial fuel enrichment: Extended-enrichment fuel ranges up to 8 wt % initial ^{235}U. Results from 5.0, 5.5, 6.0, 6.5, 7.0, 7.5, and 8.0 wt % ^{235}U initial enrichments were presented in the parametric studies.

Fuel specific power: Typical BWR fuel specific power is approximately 25 GWd/MTU [21]. The range of BWR specific powers was chosen to be between 15 and 50 MW/MTU. The broadness of this range might not be physical, but this range of values was chosen such that the values expected for increased enrichment and higher burnup BWR fuel are sufficiently included in this range.

Coolant void: The range for core-average void fractions is given as 0.415 to 0.429 in [21]. All possible coolant voids were included, from 0% to 100%.

Fuel temperature: A fuel temperature of 1,100 K and branch cases of 900 K and 1,300 K were used in [22]. Approximately 800 K was used in [23]. These fuel temperatures were included in this study, as well as select lower temperatures.

Fuel density: Nominal fuel density is approximately 97 percent of UO_2 theoretical density. The analyzed fuel density ranges from the UO_2 theoretical density to the density of UO_2 fuel radially homogenized within the clad inner radius. The values used is this study are from [41].

Gd_2O_3 loading: Gadolinia loadings of 4, 6, and 8 wt % were used in the baseline assembly, as shown in Figure 3-3. Variations in Gd_2O_3 loadings were not performed.

Control rod blade: The control blade is illustrated in Figure 3-2 (b), and its design parameters are provided in Table 3-10 [45]. Models included the following scenarios.

(i) Control rod blade fully inserted up to 45, 55, 65, and 75 GWd/MTU
(ii) Control rod blade fully inserted for 5 GWd/MTU from 70 to 75 GWd/MTU

Cooling time: The analyzed cooling time spans from 1 to 100 yr. Spent fuel has a minimum cooling time of 1 yr [43]. Spent fuel might be in dry storage for a long period of time (e.g., 100 yr or more) depending on the availability of a permanent spent fuel repository in the United States.

4 ANALYSIS METHODOLOGY AND MODELS

Fuel depletion, decay, shielding, and criticality safety computer codes available in the SCALE computer code system [46] were used to perform the calculations documented herein. SCALE is a comprehensive modeling and simulation suite for nuclear safety analysis and design developed and maintained by Oak Ridge National Laboratory (ORNL) to perform reactor physics, criticality safety, radiation shielding, and spent fuel characterization for nuclear facilities and transportation/storage package designs. The SCALE calculational sequences and computer codes used in these calculations include Polaris for fuel depletion, Oak Ridge Isotope GENeration (ORIGEN) for decay, decay heat, and source terms, ORIGAMI for burnup-dependent fuel composition, Monaco with Automated Variance Reduction using Importance Calculations (MAVRIC) for shielding, and the criticality safety analysis sequence with KENO V.a transport module (CSAS5) for criticality safety. Appendix A provides details on the transportation package and dry storage cask shielding models and the method employed herein to assess the effects of depletion parameters on external dose rates.

SCALE version 6.3.0 was used in this study. The calculations documented in this report used nuclear cross-section libraries based on ENDF/B-VII.1. The 252-neutron-group ENDF/B-VII.1 library was used in Polaris and CSAS5, a one-group ENDF/B-VII.1 library was used in ORIGEN, and the CE ENDF/B-VII.1 library was used in MAVRIC. A limited set of comparisons between CSAS5 CE and multigroup library results are provided in Appendix B to verify the use of multigroup cross sections instead of CE.

4.1 SCALE Computer Codes

This section provides a methodology description of the SCALE 6.3.0 modules used in these analyses.

4.1.1 Polaris Fuel Depletion Calculations

Polaris is a module dedicated to 2D LWR lattice physics analyses. This module uses the embedded self-shielding method for multigroup cross-section processing and a particle transport solver based on the method of characteristics. The point depletion calculations within Polaris are performed with the ORIGEN code.

Polaris provides an intuitive input format that allows users to set up lattice models with minimal input and effort. The Polaris output containing stacked ORIGEN binary concentration files (.f71) for each material depleted or irradiated in the problem at the end of each burnup state point and ORIGEN binary cross-section libraries (.f33) were utilized in subsequent ORIGEN and ORIGAMI calculations, respectively, for source term and fuel composition characterization.

Polaris in SCALE 6.3.0 was used herein instead of TRITON because Polaris has a series of advantages; it was developed specifically for LWR fuel depletion problems, has a shorter input providing simplicity in verification, and has faster computing times.

4.1.2 ORIGEN Decay Calculations

The ORIGEN code [46, 47] is used within SCALE to solve the system of differential equations that describes nuclide generation, depletion, and decay. It can be used as a standalone code

and as a functional module within SCALE's depletion modules and sequences (i.e., Polaris, TRITON, and ORIGAMI). Besides its use in Polaris, ORIGEN was used as a standalone code to perform decay calculations and to generate neutron and gamma emission spectra during decay. SNF neutron source terms calculated with ORIGEN include neutrons from spontaneous fission and from (α,n) reactions with light elements in the fuel oxide material. SNF photon source terms calculated with ORIGEN include photons from radionuclide decay, spontaneous fission, and (α,n) reactions, as well as bremsstrahlung in UO_2.

4.1.3 OPUS for ORIGEN Postprocessing

OPUS [46] is a utility program that reads and processes an ORIGEN binary concentration file (.f71) into a format suitable for plotting. It was used to print various radiation source terms following ORIGEN decay calculations.

4.1.4 ORIGAMI for Interpolations on ORIGEN Cross-Section Libraries

ORIGAMI [48] is a SCALE sequence that performs point-depletion calculations from pregenerated, problem-dependent ORIGEN cross-section libraries (.f33 files) for irradiated light water reactor fuel assemblies. ORIGAMI was used to perform point-depletion calculations using pregenerated, problem-dependent ORIGEN cross-section libraries generated by Polaris for criticality safety analyses. ORIGAMI performs interpolations on cross-section library states, such as burnup, moderator density, and enrichment, based on the methodology originally developed for ORIGEN-ARP [49]. In this study, interpolations were performed on burnup. Moderator densities and enrichments were consistent with the baseline data except for the parametric studies in which variations on these parameters were performed.

In ORIGAMI, axial zone-wise relative burnups were provided as user input, which were used in interpolation calculations using ORIGEN cross-section libraries. For criticality safety analyses, GBC-32 cask models having 18-axial-zone burnup profiles were used in this study. Burnups greater than 75 GWd/MTU were required to allow interpolations between high burnups for central axial nodes because a maximum assembly average burnup of 75 GWd/MTU would result in a nodal burnup of approximately 83 GWd/MTU. Therefore, Polaris included burnup steps up to 85 GWd/MTU (e.g., 0.1, 1, 2, 4, 6, 8, 10, 12, 14, 16, 18, 20, 25, 30, 35, 40, 45, 50, 55, 60, 65, 70, 75, 80, and 85 GWd/MTU). ORIGAMI can produce different types of output files in addition to the standard ORIGEN output for each depletion zone [46]. In this study, nuclide concentrations by axial zone, written as a SCALE *standard composition block*, were created as input for the KENO Monte Carlo transport code in CSAS5.

4.1.5 MAVRIC Shielding Calculations

MAVRIC is a SCALE sequence that performs Monte Carlo shielding calculations using automated variance reduction methods [50-52]. MAVRIC was used to perform shielding calculations, as described in Appendix A. Figure 4-1 shows the workflow using Polaris and ORIGEN to generate neutron and gamma emission spectra that is combined with response functions described in Appendix A to calculate dose rates on simplified dry storage cask and transportation package models.

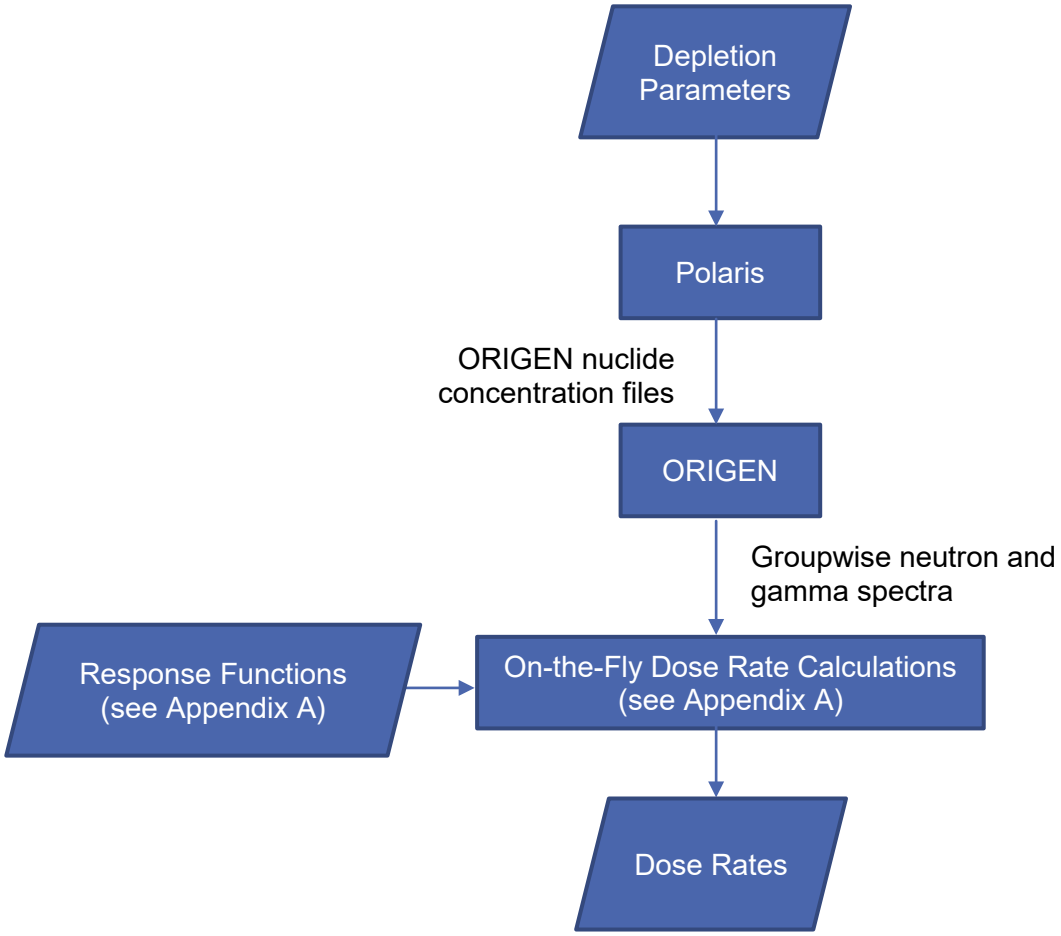

Figure 4-1 SCALE Workflow for Shielding Analysis

MAVRIC has the capability to automatically generate variance reduction parameters based on input geometry and source specifications. MAVRIC performs forward and adjoint discrete ordinates calculations with the Denovo computer code [53] to determine energy- and space-dependent particle importance functions. The Denovo computer code input data are specified in the MAVRIC input, including the SCALE 27n19g library, problem geometry discretization on a cartesian grid, and a response function definition. The forward-weighted, consistent adjoint–driven importance sampling variance reduction method implemented in MAVRIC was used, which estimates dose rates with low statistical relative errors outside the dry storage cask and transportation package models (see Appendix A).

4.1.6 CSAS5 Criticality Safety Calculations

The SCALE 6.3.0 package offers several sequences for criticality safety analysis: CSAS5, Criticality Safety Analysis Sequence with KENO-VI transport module (CSAS6), Criticality Safety Analysis Sequence with Shift transport module and KENO V.a geometry (CSAS5-Shift), and Criticality Safety Analysis Sequence with Shift transport module and KENO-VI geometry (CSAS6-Shift). Criticality safety calculations in this report used the CSAS5 sequence. The primarily purpose is to generate eigenvalues, whether in an infinite system (infinite multiplication factor (k_{inf}) or fully contained as an independent system (effective multiplication factor (k_{eff})).

The GBC-32 PWR cask [2] was selected as a generic cask model to perform criticality safety related sensitivity calculations for the storage and transportation of SNF. The GBC-32 model is shown in Figure 4-2. The CSAS5 model of GBC-32 contained WEC 17 × 17 OFAs or WEC 17 × 17 RFAs. The GBC-32 model, as defined in [2], contained 18 axial fuel zones, boral panels between storage cells, and 32 fuel assemblies. Fuel compositions in each axial zone were determined using ORIGAMI interpolations of Polaris-generated ORIGEN cross-section libraries. Burnable absorbers built into the fuel depletion models (i.e., Polaris) were not modeled in CSAS5, which results in a conservative k_{eff} in the GBC-32 (e.g., by eliminating residual poison in the GBC-32 model). Figure 4-3 shows the workflow using Polaris and ORIGAMI to generate depleted fuel compositions for the CSAS5 for calculations in the GBC-32 [2] cask containing 32 PWR fuel assemblies.

ORIGAMI fuel compositions included the AFP set of isotopes for BUC analysis. The AFP nuclide set was selected as it is currently the preferred BUC approach in industry. Nuclides included for AFP BUC are listed in Table 4-1. The interpolated burnups at which compositions were generated applied the axial profiles given in Section 8.1.12 to the assembly average burnups; central fuel nodes were more heavily depleted than the top and bottom nodes [54]. All assemblies placed within the cask are identical.

Monte Carlo calculations were executed to obtain a statistical uncertainty in the calculated k_{eff} of at most 0.0001, or 10 per cent mille (pcm), with 10,000 particles per generation and 200 skipped generations. In all cases, the transport calculation was terminated by achieving the requested uncertainty.

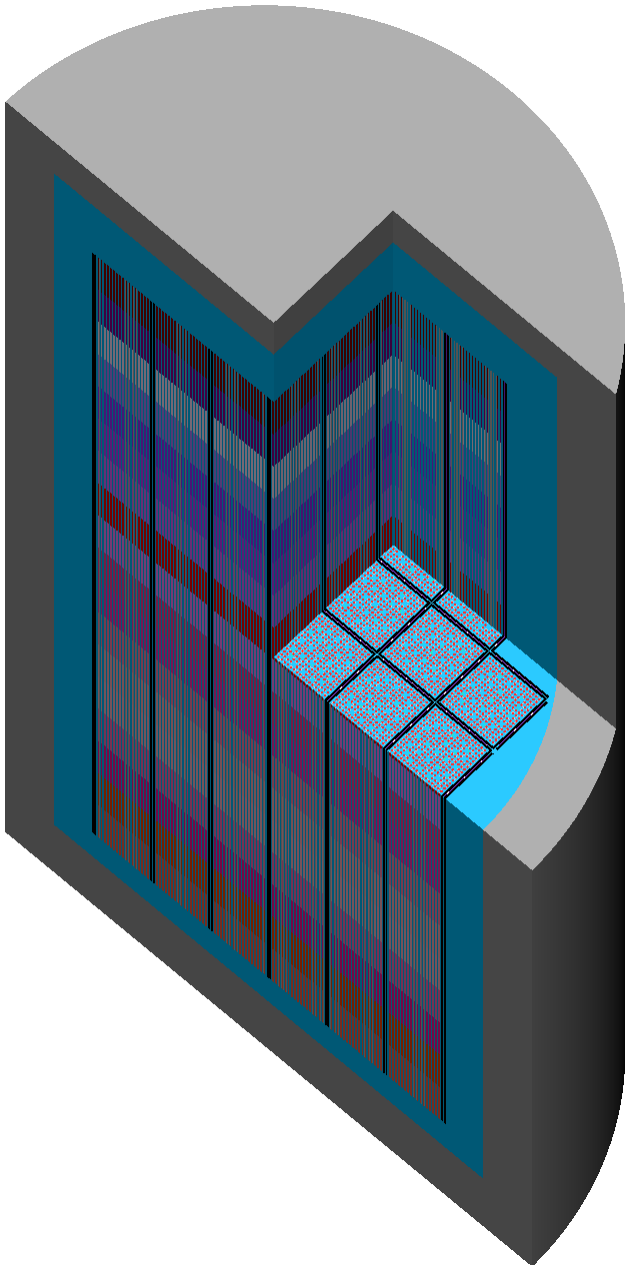

Figure 4-2 GBC-32 Cask Model Used for Criticality Safety Calculations

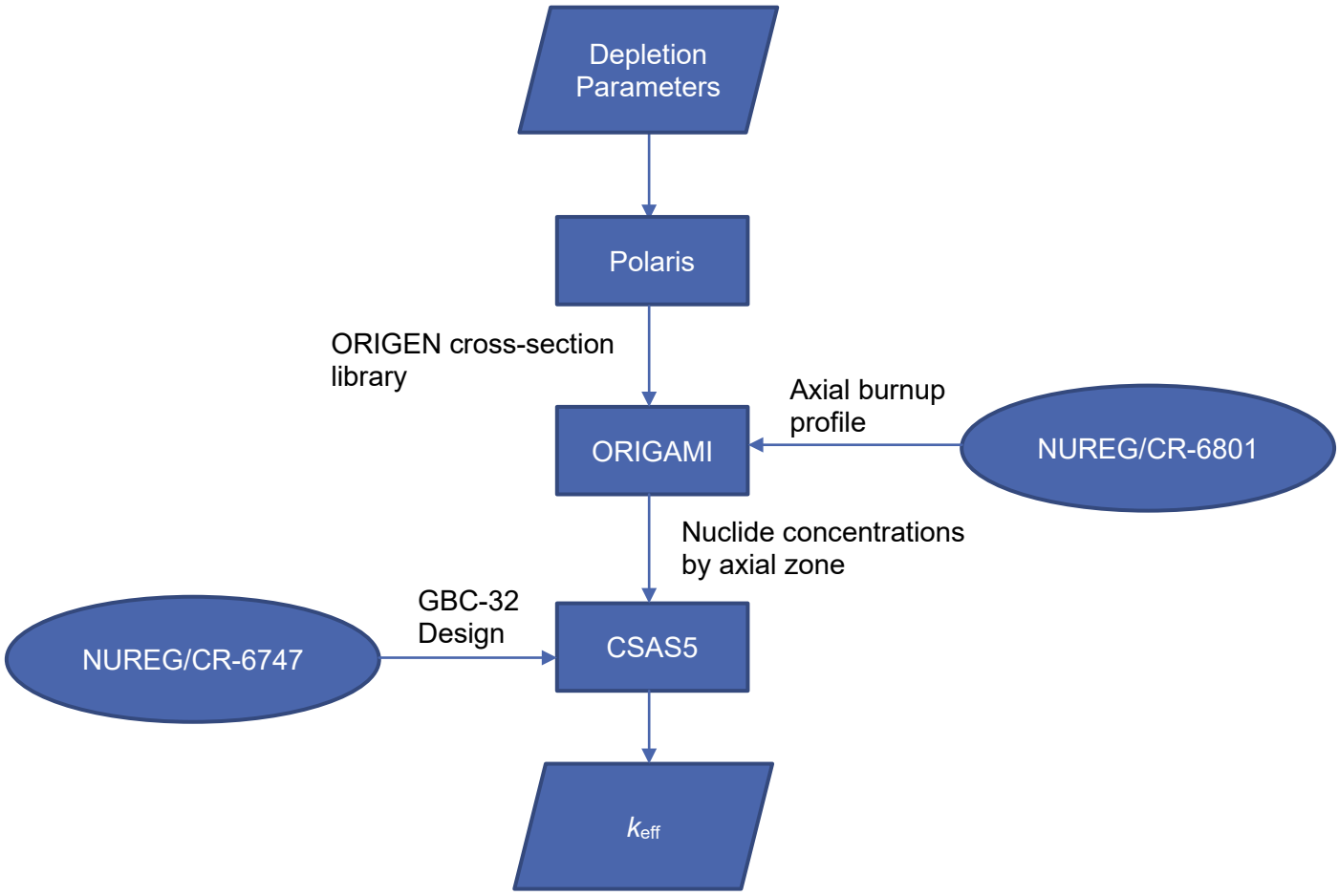

Figure 4-3 SCALE Workflow for Criticality Safety Analysis Using the GBC-32 Cask Design (NUREG/CR-6801 and NUREG/CR-6747 are in [55] and [2], Respectively)

Table 4-1 AFP Nuclide Set

Type of Burnup Credit	Recommended Set of Nuclides [7, 8]
Actinide-only BUC	^{234}U, ^{235}U, ^{238}U, ^{238}Pu, ^{239}Pu, ^{240}Pu, ^{241}Pu, ^{242}Pu, ^{241}Am
Additional nuclides for AFP BUC	^{95}Mo, ^{99}Tc, ^{101}Ru, ^{103}Rh, ^{109}Ag, ^{133}Cs, ^{143}Nd, ^{145}Nd, ^{147}Sm, ^{149}Sm, ^{150}Sm, ^{151}Sm, ^{152}Sm, ^{151}Eu, ^{153}Eu, ^{155}Gd, ^{236}U, ^{237}Np, ^{243}Am

4.2 Parametric Studies

The concentrations of nuclides in irradiated fuel vary as a function of burnup and depend on irradiation and fuel assembly parameters. Nuclide production and depletion rates are sensitive to changes in the neutron flux magnitude and spectrum that are induced by the varying parameters. The purpose of the parametric study is to determine the variations of dry storage and transportation cask external dose rates and k_{eff} with changes in fuel assembly parameters (e.g., initial ^{235}U enrichment, number of burnable absorbers) and irradiation parameters (e.g., burnup, specific power, moderator density, fuel temperature). In this parametric study, a single modeling parameter was varied within a range of values and other parameters were maintained at their reference values (see Section 3). Major effects expected on nuclide concentrations due to varying depletion parameters are briefly discussed in this section. Dose rate and k_{eff} variations determined by the parametric study are presented in Sections 7 and 8, respectively.

4.2.1 Assembly Average Burnup

By increasing fuel burnup, more fissile nuclides are depleted and more fission products, transuranic nuclides, and activation products are produced.

4.2.2 Initial Fuel Enrichment

Nuclide concentrations at fixed burnup exhibit significant sensitivity to initial fuel enrichment. Fuel with higher initial enrichment will need a lower neutron flux to achieve the same power density compared with fuel with lower initial enrichment. An increase of the initial fuel enrichment causes an increase in the ^{235}U absorption rate, a decrease in the absorption rates of other nuclides, a reduction in the thermal neutron flux, and neutron spectrum hardening [18]. To achieve the same power density, the ^{239}Pu depletion rate in fuel with higher initial enrichment will be lower than that in low-enriched fuel.

Figure 4-4 shows the variations of ^{235}U, ^{238}U, and ^{239}Pu concentrations determined in irradiated WEC 17 × 17 OFA fuel as a function of burnup for initial fuel enrichments of 8 wt % and 5 wt % and identical depletion conditions (see reference parameters in Section 3). The values presented in this figure were taken from the f71 file generated by Polaris (i.e., 2D depletion calculations). The ^{235}U concentration and its rate of change are higher in fuel with 8 wt % initial fuel enrichment throughout the irradiation history compared to those in fuel with 5 wt % initial enrichment for a fixed burnup. The ^{238}U concentration and its rate of change are higher in fuel with 5 wt % initial enrichment throughout the irradiation history compared to those in fuel with 8 wt % initial fuel enrichment for a fixed burnup. Up to approximately 20 GWd/MTU, ^{239}Pu concentration is higher for a 5 wt % initial fuel enrichment, compared to the 8 wt % initial enrichment. Beyond 20 GWd/MTU, ^{239}Pu concentration is higher for an 8 wt % initial fuel enrichment, compared to that of the 5 wt % initial fuel enrichment. The ^{239}Pu concentrations achieve their maximum values at approximately 65 GWd/MTU and 50 GWd/MTU with initial fuel enrichments of 8 wt % and 5 wt %, respectively.

To achieve the same power density, fuel with lower initial enrichment needs a higher neutron flux compared with fuel with higher initial enrichment. Higher neutron flux will deplete ^{235}U faster, which hardens the neutron spectrum and initially builds ^{239}Pu faster in low enriched fuel compared to high enriched fuel. To maintain constant power, ^{239}Pu would have to be burned at

a higher rate in the lower enriched fuel. Therefore, ^{239}Pu concentration reaches a maximum value earlier in the cycle in low enriched fuel compared with higher enriched fuel.

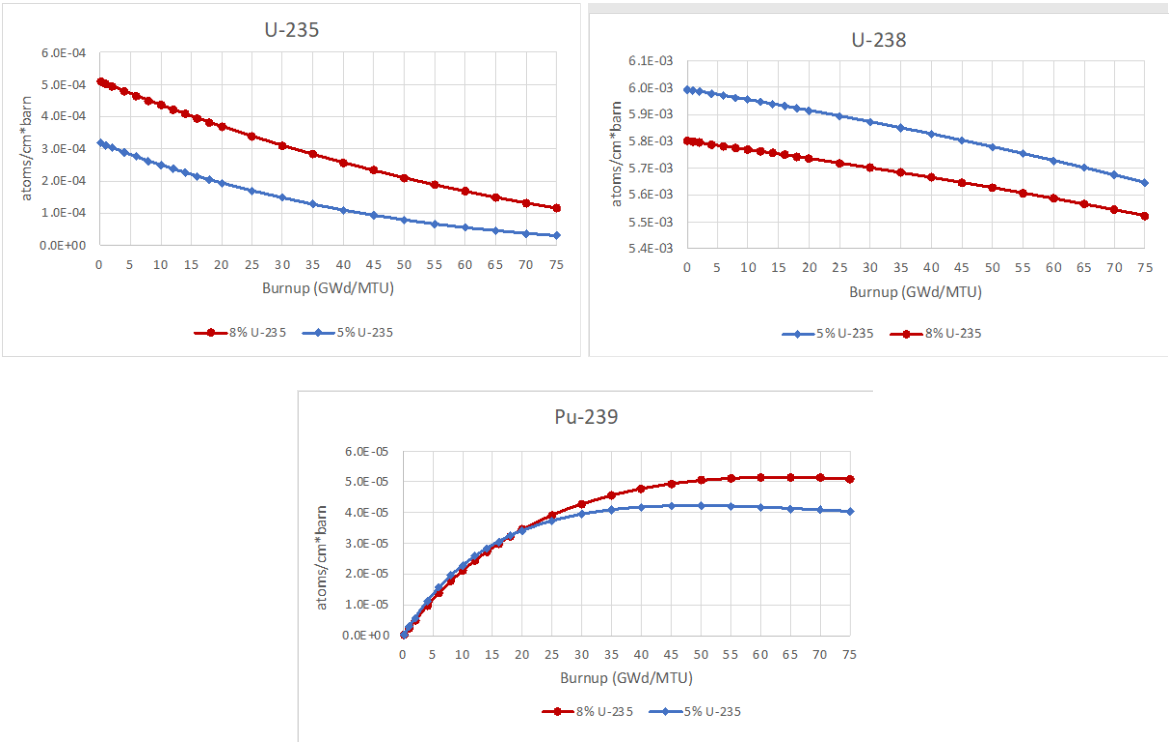

Figure 4-4 Variations of ^{235}U, ^{238}U, and ^{239}Pu Concentrations in Irradiated PWR Fuel as a Function of Burnup for Initial ^{235}U Enrichments of 8 wt % and 5 wt %

Nuclides important to radiation source terms/dose rates found in greater concentrations at high burnup in the 5 wt % enriched fuel as compared to 8 wt % enriched fuel are the main neutron emitters ^{242}Cm (half-life ($T_{1/2}$) = 0.45 yr) and ^{244}Cm ($T_{1/2}$ = 18.1 yr), fission products ^{106}Ru ($T_{1/2}$ = 1.02 yr) and ^{134}Cs ($T_{1/2}$ = 2.0652 yr), and ^{60}Co ($T_{1/2}$ = 5.271 yr). Additionally, ^{154}Eu ($T_{1/2}$ = 8.593 yr) has higher concentrations in the 5 wt % enriched fuel as compared to 8 wt % enriched fuel only up to a burnup of approximately 60 GWd/MTU. The fission product ^{106}Ru is primarily produced by fission, and this nuclide has a much higher cumulative fission yield from ^{239}Pu as compared to ^{235}U. The primary production paths for ^{134}Cs and ^{154}Eu are by thermal capture in ^{133}Cs and ^{153}Eu, respectively.

Nuclides important to radiation source terms/dose rate found in greater concentrations at high burnup in 8 wt % enriched fuel as compared to 5 wt % enriched fuel include fission products ^{144}Ce ($T_{1/2}$ = 284.89 days) and ^{90}Sr ($T_{1/2}$ = 28.78 yr), the ^{235}U cumulative fission yields of which are higher as compared to those of ^{239}Pu. Also, ^{137}Cs ($T_{1/2}$ = 30.1 yr) concentration slightly increases with increasing initial fuel enrichment.

4.2.3 Specific Power

During fuel irradiation, the total neutron flux varies proportionally with specific power at fixed burnup. The equilibrium level of unstable nuclides, where the decay rate approaches the production rate, is directly proportional to the specific power [41]. Fission product and minor actinide inventories are directly correlated with the specific power. Therefore, radiation source terms and dose rates increase with increasing specific power. The k_{eff} is expected to decrease with increasing specific power at very high burnups because of increased neutron absorption by the fission products specified in BUC AFP compositions. Increased enrichment is expected to slightly lower k_{eff} sensitivity to the specific power because of its increasing sensitivity to main actinides.

4.2.4 Fuel Temperature

Fuel temperature increase has a broadening effect on the resonance capture cross section of fertile nuclides (e.g., ^{238}U and ^{240}Pu), which increases the probability of neutrons with energies near the resonance being captured in fuel and increases the production of transuranic nuclides. [41]. Less ^{238}U resonance capture reactions exist in the fuel with extended enrichment compared to the regular fuel because the fuel with extended enrichment contains less ^{238}U than the regular fuel. The effect decreases with increasing fuel initial enrichment.

4.2.5 Fuel Density

Neutron absorption probability is higher near the outer surface of the fuel pellet than the inner region of the pellet (i.e., spatial self-shielding), especially at high burnup values. A higher fuel density will increase neutron absorptions near the outer pellet surface and decrease neutron absorptions in the inner pellet region.

4.2.6 Moderator Density

By increasing moderator density, the thermal flux is increased, the thermal absorption reactions are increased, and the resonance absorption reactions are decreased. The result is lower ^{239}Pu and transplutonium nuclide production rates [41].

4.2.7 Soluble Boron Concentration in Pressurized-Water Reactor Coolant

Neutron absorption by the boron diluted in coolant results in hardening of the neutron energy spectrum, increased resonance captures in fertile nuclides (e.g., ^{238}U and ^{240}Pu), and increased production of transuranic nuclides.

4.2.8 Discrete Absorbers

In discrete absorbers, such as WABA rods, RCCAs, and control rod blades, neutron absorption and moderator displacement result in hardening of the neutron energy spectrum, which increases resonance captures in fertile nuclides (e.g., ^{238}U and ^{240}Pu) and production of transuranic nuclides.

5 SCALE VALIDATION

SCALE 6.2.4 nuclear criticality safety, reactor physics, and radiation shielding analysis capabilities and nuclear data libraries based on ENDF/B-VII.0 or ENDF/B-VII.1 data were validated and are documented in a series of ORNL reports [56-58]. The calculations documented in this report used SCALE 6.3.0 and nuclear data libraries based on ENDF/B-VII.1 data. The conclusions of the SCALE 6.2.4 validation studies are considered to be applicable for this report because the ENDF library (ENDF/B-VII.1) used in this report was also used in the SCALE 6.2.4 validation study.

The performance of the KENO V.a Monte Carlo code within the SCALE 6.2.4 system for nuclear criticality safety was assessed using models from the Verified, Archived Library of Inputs and Data (VALID) [59] and both multigroup and CE cross sections based on ENDF/B-VII.1. VALID contains SCALE input files for more than 600 cases documented in the International Handbook of Evaluated Criticality Safety Benchmark Experiments, which have been vetted by the International Criticality Safety Benchmark Evaluation Project (ICSBEP). The VALID files have been prepared, reviewed, and continuously maintained at ORNL. The bias of the calculated k_{eff} was less than 150 pcm for pin array experiments containing low-enriched uranium (LEU) or mixtures of uranium and plutonium oxide.

SCALE fuel depletion code validations were based on comparisons with radiochemical assay data. The comparison between calculation and experiment results showed good agreement on average for many of the 40 measured nuclides of importance to BUC, decay heat, and radiation shielding applications. The two major actinides ^{235}U and ^{239}Pu were well-predicted, on average. The bias values for ^{235}U in PWR and BWR fuel were approximately 1 (σ = 4 percent) and 3 percent (σ = 11 percent), respectively; the bias values for ^{239}Pu in PWR and BWR fuel were approximately 2 (σ = 3 percent) and 3 percent (σ = 8 percent), respectively [57].

MAVRIC validation was based on eight representative benchmark experiments from the Shielding Integral Benchmark Archive and Database (SINBAD), the ICSBEP Handbook, and other publicly available shielding validation studies. Either CE cross-section libraries generated from ENDF/B-VII.1 nuclear data or ENDF/B-VII.0 multigroup (200-neutron and 47-gamma-ray groups) were used in the validation study. The set of selected experiments included four types: (1) shielding experiments testing radiation attenuation in individual shielding materials (e.g., iron, steel, polyethylene, lead, and tungsten), as well as combinations of various thicknesses of steel and polyethylene; (2) an experiment involving neutron streaming through ducts; (3) a skyshine experiment using ^{60}Co sources; and (4) a criticality alarm experiment providing foil activation measurements. The reported measurements of uncertainties varied greatly among these experiments, from very small values (e.g., 1 percent) to 100 percent. Generally, MAVRIC calculations and the experimental values agreed within measurement uncertainty. Rare outliers were explained by either a lack of information or large uncertainties in the experiment conditions, material, or dimensions [58].

6 NUCLIDE IMPORTANCE TO DECAY HEAT, SOURCE TERMS, AND CRITICALITY SAFETY

6.1 Decay Heat

Before determining nuclides important to high-burnup and extended-enrichment fuel, decay heat as a function of burnup was calculated using an initial ^{235}U enrichment of 5 wt % and compared with results in NUREG/CR-6700 [60] for a verification of the calculational method. The plots shown in Figure 6-1 were generated by executing the ORIGEN) and OPUS modules on the ORIGEN binary concentrations file (.f71) that resulted from the Polaris execution. Figure 6-1 shows the decay heat release rate from actinides and fission products, as well as the total decay heat release rate at 5-year and 100-year cooling times for the WEC 17 × 17 OFA; plots are similar to Figures 7 and 8 in NUREG/CR-6700 [60].

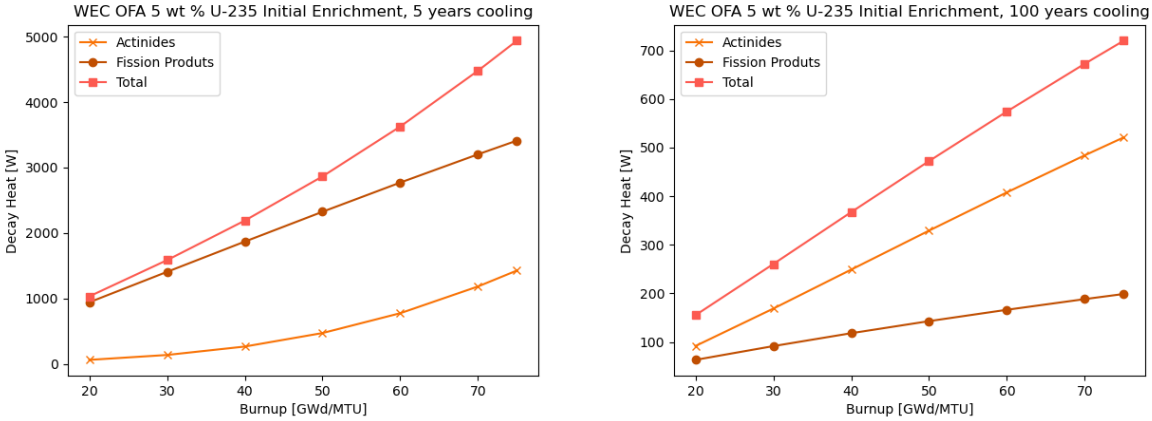

Figure 6-1 Decay Heat for WEC OFA with Initial ^{235}U Enrichment of 5 wt % for 5-year and 100-year Cooling Times

Decay heat calculations were repeated for 8 wt % initial ^{235}U enrichment and plotted in Figure 6-2. To compare decay heat as a function of burnup for highly contributing nuclides, the fraction of decay heat to the total decay heat for the highest contributing 16 nuclides were plotted in Figure 6-3 for an initial ^{235}U enrichment of 5 wt % at 5-year and 100-year cooling times for the WEC 17 × 17 OFA. Plots in Figure 6-3 are similar to Figures 9 and 10 in NUREG/CR-6700 [60]. This calculation was repeated for 8 wt % initial ^{235}U enrichment; results are shown in Figure 6-4.

The fractional contribution of nuclides to decay heat generation were calculated for various combinations of burnup, enrichment, and cooling time. Although these calculations were performed for WEC 17 × 17 OFA and GEH 10 × 10 GE14 assemblies, the relative nuclide rankings were determined to be essentially identical, and only the results for the WEC 17 × 17 OFA are presented in Table 6-1, Table 6-2, and Table 6-3.

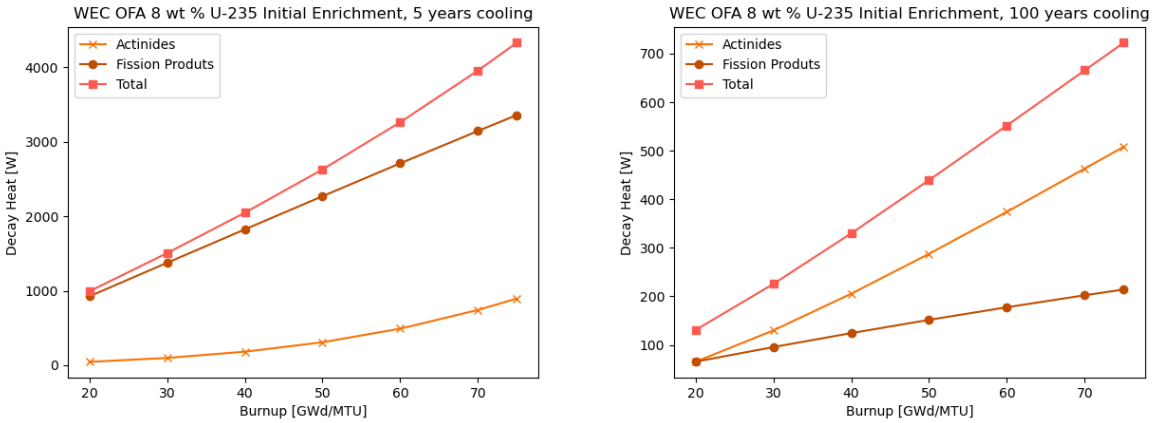

Figure 6-2 Decay Heat for WEC OFA with Initial ^{235}U Enrichment of 8 wt % for 5-year and 100-year Cooling Times

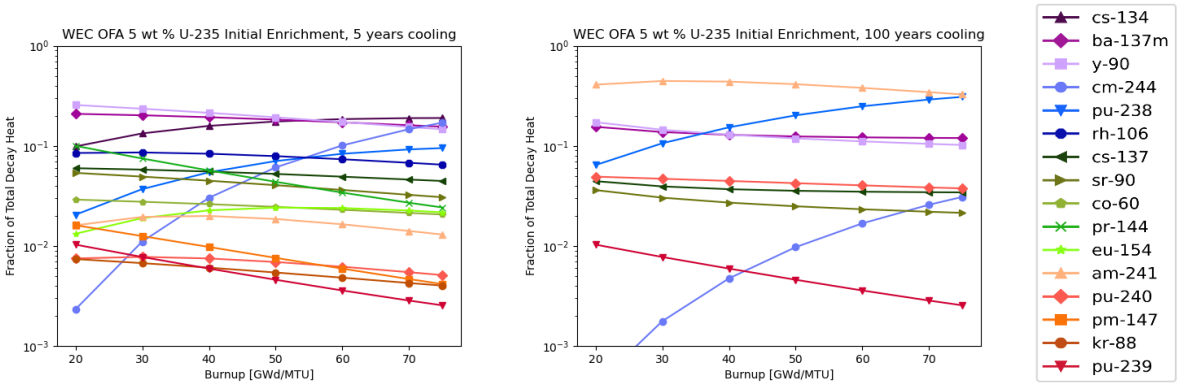

Figure 6-3 Fraction of Decay Heat Generation for WEC OFA with Initial ^{235}U Enrichment of 5 wt % for 5-year and 100-year Cooling Times

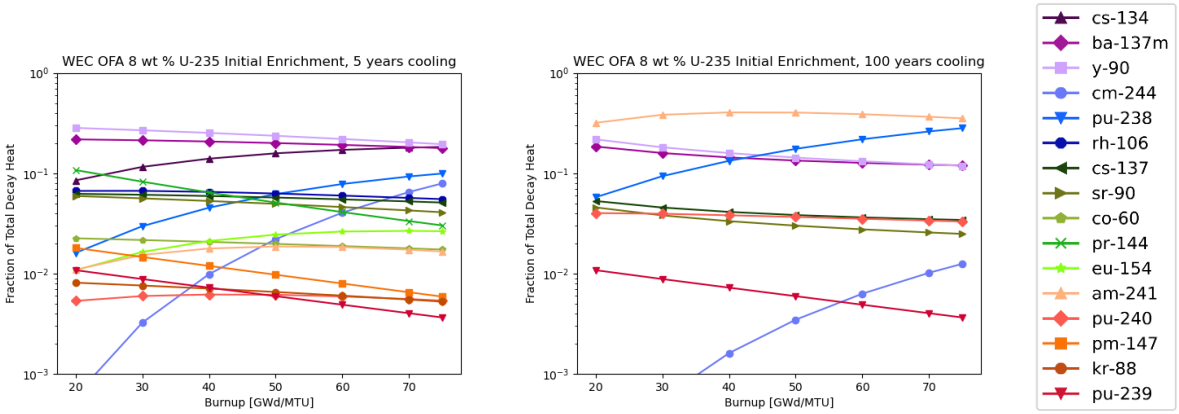

Figure 6-4 Fraction of Decay Heat Generation for WEC OFA with Initial ^{235}U Enrichment of 8 wt % for 5-year and 100-year Cooling Times

Decay heat nuclide rankings are provided for 5 wt % initial ^{235}U enrichment at 75 GWd/MTU, 8 wt % initial ^{235}U enrichment at 40 GWd/MTU, and 8 wt % initial ^{235}U enrichment at 75 GWd/MTU, each at up to 100 yr of cooling time. In comparing the decay heat rankings of 5 wt % initial ^{235}U enrichment at 70 GWd/MTU in NUREG/CR-6700 [60] and 5 wt % initial ^{235}U enrichment at 75 GWd/MTU from the current study at a 5-year cooling time, it is observed that the top five highest contributors are the same, but the order of second-, third-, and fourth-ranked nuclides are different. The highest-ranked nuclide is ^{134}Cs. For the 100-year cooling time, the top five highest contributors are the same and are ranked in the same order. The highest-ranked nuclide is ^{241}Am.

In keeping the assembly average burnup, the same (75 GWd/MTU) and increasing the initial ^{235}U enrichment from 5 to 8 wt %, the top five contributors are the same, but their rankings are changed at 5-year cooling time. The top contributors are ^{90}Y and ^{134}Cs for 8 wt % and 5 wt % enrichments, respectively, at 5-year cooling time. ^{244}Cm ranked at number two for 5 wt % enrichment with 17.0 percent of total decay heat contribution and is ranked at number five for 8 wt % enrichment with 7.9 percent of total decay heat contribution. For the 100-year cooling time, the top four nuclide contributors remain the same and are ranked in the same order; the fifth and sixth nuclide rankings change order. Results indicate that changing the enrichment at high assembly average burnups does not cause a change in the top contributors, but the rankings of the top contributors show more variability at the 5-year cooling time compared to the 100-year cooling time.

Finally, the assembly average burnup is decreased to 40 GWd/MTU while keeping the initial ^{235}U enrichment at 8 wt %. The highest contributor remains the same (i.e., ^{90}Y), the second and third rankings switch order (^{134}Cs and ^{137m}Ba), and the fourth and fifth contributors are different at the 5-year cooling time. The fourth contributor, ^{239}Pu at 9.9% of total decay heat, moves to the eighth contributor, at 4.5% of total decay heat. The fifth contributor, ^{244}Cm at 7.9% of total decay heat, moves to the 13th contributor, at 1.0% of total decay heat. At the 100-year cooling time, the top contributor remains the same (i.e., ^{241}Am), the second and forth contributors switch their ranking (i.e., ^{90}Y and ^{238}Pu), the third-ranked nuclide remains the same (^{137m}Ba), and the

fifth-ranked nuclide becomes the sixth ranked nuclide. Results indicate that changing burnup at 8 wt % initial ^{235}U enrichment can cause more variability in ranking at the 5-year cooling time compared to the 100-year cooling time.

Table 6-1 Nuclide Ranking for Decay Heat; WEC 17 × 17 OFA, 5 wt % at 75 GWd/MTU Assembly Average Burnup

Rank	1-year cooling time			5-year cooling time			50-year cooling time			100-year cooling time		
	Isotope	Decay heat (W)	Percent of total decay heat (%)	Isotope	Decay heat (W)	Percent of total decay heat (%)	Isotope	Decay heat (W)	Percent of total decay heat (%)	Isotope	Decay heat (W)	Percent of total decay heat (%)
1	^{106}Rh	4.87×10^{3}	25.8	^{134}Cs	9.34×10^{2}	18.9	^{238}Pu	3.28×10^{2}	23.4	^{241}Am	2.34×10^{2}	32.5
2	^{144}Pr	4.17×10^{3}	22.1	^{244}Cm	8.40×10^{2}	17.0	^{137m}Ba	2.71×10^{2}	19.3	^{238}Pu	2.21×10^{2}	30.7
3	^{134}Cs	3.58×10^{3}	19.0	^{137m}Ba	7.66×10^{2}	15.5	^{90}Y	2.44×10^{2}	17.4	^{137m}Ba	8.58×10^{1}	11.9
4	^{242}Cm	1.14×10^{3}	6.0	^{90}Y	7.20×10^{2}	14.6	^{241}Am	2.32×10^{2}	16.5	^{90}Y	7.31×10^{1}	10.2
5	^{244}Cm	9.80×10^{2}	5.2	^{238}Pu	4.68×10^{2}	9.5	^{244}Cm	1.50×10^{2}	10.7	^{240}Pu	2.69×10^{1}	3.7
6	^{137m}Ba	8.40×10^{2}	4.5	^{106}Rh	3.19×10^{2}	6.5	^{137}Cs	7.78×10^{1}	5.5	^{137}Cs	2.46×10^{1}	3.4
7	^{90}Y	7.92×10^{2}	4.2	^{137}Cs	2.19×10^{2}	4.4	^{90}Sr	5.11×10^{1}	3.6	^{244}Cm	2.22×10^{1}	3.1
8	^{238}Pu	4.78×10^{2}	2.5	^{90}Sr	1.51×10^{2}	3.1	^{240}Pu	2.68×10^{1}	1.9	^{90}Sr	1.53×10^{1}	2.1
9	^{144}Ce	3.72×10^{2}	2.0	^{144}Pr	1.19×10^{2}	2.4	^{239}Pu	1.26×10^{1}	0.9	^{239}Pu	1.25×10^{1}	1.7
10	^{95}Nb	3.22×10^{2}	1.7	^{154}Eu	1.07×10^{2}	2.2	^{154}Eu	2.84×10^{0}	0.2	^{242}Cm	2.60×10^{-1}	0.0
11	^{137}Cs	2.41×10^{2}	1.3	^{60}Co	1.02×10^{2}	2.1	^{85}Kr	1.09×10^{0}	0.1	^{154}Eu	5.05×10^{-2}	0.0
12	^{60}Co	1.72×10^{2}	0.9	^{241}Am	6.40×10^{1}	1.3	^{242}Cm	3.32×10^{-1}	0.0	^{85}Kr	4.34×10^{-2}	0.0
13	^{90}Sr	1.66×10^{2}	0.9	^{240}Pu	2.52×10^{1}	0.5	^{60}Co	2.73×10^{-1}	0.0	^{60}Co	3.81×10^{-4}	0.0
14	^{95}Zr	1.57×10^{2}	0.8	^{147}Pm	2.05×10^{1}	0.4	^{134}Cs	2.58×10^{-4}	0.0	^{125}Sb	7.56×10^{-10}	0.0
15	^{154}Eu	1.47×10^{2}	0.8	^{85}Kr	1.98×10^{1}	0.4	^{125}Sb	2.16×10^{-4}	0.0	^{147}Pm	2.57×10^{-10}	0.0
16	^{147}Pm	5.89×10^{1}	0.3	^{125}Sb	1.76×10^{1}	0.4	^{147}Pm	1.40×10^{-4}	0.0	^{134}Cs	1.33×10^{-11}	0.0
17	^{125}Sb	4.81×10^{1}	0.3	^{239}Pu	1.26×10^{1}	0.3	^{106}Rh	1.57×10^{-11}	0.0	^{106}Rh	2.56×10^{-26}	0.0
18	^{85}Kr	2.56×10^{1}	0.1	^{144}Ce	1.07×10^{1}	0.2	^{144}Pr	5.13×10^{-16}	0.0	^{144}Pr	2.59×10^{-35}	0.0
19	^{240}Pu	2.48×10^{1}	0.1	^{242}Cm	2.69×10^{0}	0.1	^{144}Ce	4.58×10^{-17}	0.0	^{144}Ce	2.32×10^{-36}	0.0
20	^{241}Am	2.07×10^{1}	0.1	^{95}Nb	4.60×10^{-5}	0.0	^{95}Nb	2.38×10^{-82}	0.0	^{95}Zr	0.00×10^{0}	0.0
21	^{239}Pu	1.26×10^{1}	0.1	^{95}Zr	2.12×10^{-5}	0.0	^{95}Zr	1.14×10^{-82}	0.0	^{95}Nb	0.00×10^{0}	0.0
total=		**1.88×10^{4}**	**98.8**		**4.94×10^{3}**	**99.6**		**1.40×10^{3}**	**99.6**		**7.20×10^{2}**	**99.4**

Table 6-2 Nuclide Ranking for Decay Heat; WEC 17 × 17 OFA, 8 wt % at 40 GWd/MTU Assembly Average Burnup

Rank	1-year cooling time			5-year cooling time			50-year cooling time			100-year cooling time		
	Isotope	Decay heat (W)	Percent of total decay heat (%)	Isotope	Decay heat (W)	Percent of total decay heat (%)	Isotope	Decay heat (W)	Percent of total decay heat (%)	Isotope	Decay heat (W)	Percent of total decay heat (%)
1	^{144}Pr	4.60×10^{3}	42.7	^{90}Y	5.16×10^{2}	25.2	^{90}Y	1.74×10^{2}	27.5	^{241}Am	1.33×10^{2}	40.4
2	^{106}Rh	2.03×10^{3}	18.8	^{137m}Ba	4.23×10^{2}	20.7	^{137m}Ba	1.50×10^{2}	23.6	^{90}Y	5.23×10^{1}	15.9
3	^{134}Cs	1.09×10^{3}	10.1	^{134}Cs	2.85×10^{2}	13.9	^{241}Am	1.32×10^{2}	20.8	^{137m}Ba	4.74×10^{1}	14.4
4	^{90}Y	5.68×10^{2}	5.3	^{106}Rh	1.33×10^{2}	6.5	^{238}Pu	6.50×10^{1}	10.2	^{238}Pu	4.38×10^{1}	13.3
5	^{137m}Ba	4.64×10^{2}	4.3	^{144}Pr	1.31×10^{2}	6.4	^{137}Cs	4.30×10^{1}	6.8	^{239}Pu	1.48×10^{1}	4.5
6	^{144}Ce	4.11×10^{2}	3.8	^{137}Cs	1.21×10^{2}	5.9	^{90}Sr	3.66×10^{1}	5.8	^{137}Cs	1.36×10^{1}	4.1
7	^{95}Nb	3.90×10^{2}	3.6	^{90}Sr	1.08×10^{2}	5.3	^{239}Pu	1.48×10^{1}	2.3	^{240}Pu	1.26×10^{1}	3.8
8	^{242}Cm	2.26×10^{2}	2.1	^{238}Pu	9.27×10^{1}	4.5	^{240}Pu	1.26×10^{1}	2.0	^{90}Sr	1.10×10^{1}	3.3
9	^{95}Zr	1.90×10^{2}	1.8	^{154}Eu	4.32×10^{1}	2.1	^{244}Cm	3.60×10^{0}	0.6	^{244}Cm	5.31×10^{-1}	0.2
10	^{137}Cs	1.33×10^{2}	1.2	^{60}Co	4.23×10^{1}	2.1	^{154}Eu	1.15×10^{0}	0.2	^{242}Cm	1.47×10^{-1}	0.0
11	^{90}Sr	1.19×10^{2}	1.1	^{241}Am	3.63×10^{1}	1.8	^{85}Kr	7.97×10^{-1}	0.1	^{85}Kr	3.18×10^{-2}	0.0
12	^{238}Pu	9.46×10^{1}	0.9	^{147}Pm	2.44×10^{1}	1.2	^{242}Cm	1.87×10^{-1}	0.0	^{154}Eu	2.04×10^{-2}	0.0
13	^{60}Co	7.16×10^{1}	0.7	^{244}Cm	2.02×10^{1}	1.0	^{60}Co	1.14×10^{-1}	0.0	^{60}Co	1.59×10^{-4}	0.0
14	^{147}Pm	7.01×10^{1}	0.7	^{239}Pu	1.48×10^{1}	0.7	^{147}Pm	1.67×10^{-4}	0.0	^{125}Sb	4.00×10^{-10}	0.0
15	^{154}Eu	5.96×10^{1}	0.6	^{85}Kr	1.45×10^{1}	0.7	^{125}Sb	1.14×10^{-4}	0.0	^{147}Pm	3.06×10^{-10}	0.0
16	^{125}Sb	2.54×10^{1}	0.2	^{240}Pu	1.27×10^{1}	0.6	^{134}Cs	7.87×10^{-5}	0.0	^{134}Cs	4.05×10^{-12}	0.0
17	^{244}Cm	2.35×10^{1}	0.2	^{144}Ce	1.17×10^{1}	0.6	^{106}Rh	6.55×10^{-12}	0.0	^{106}Rh	1.07×10^{-26}	0.0
18	^{85}Kr	1.87×10^{1}	0.2	^{125}Sb	9.31×10^{0}	0.5	^{144}Pr	5.65×10^{-16}	0.0	^{144}Pr	2.86×10^{-35}	0.0
19	^{239}Pu	1.48×10^{1}	0.1	^{242}Cm	6.86×10^{-1}	0.0	^{144}Ce	5.05×10^{-17}	0.0	^{144}Ce	2.56×10^{-36}	0.0
20	^{240}Pu	1.27×10^{1}	0.1	^{95}Nb	5.57×10^{-5}	0.0	^{95}Nb	2.89×10^{-82}	0.0	^{95}Zr	0.00×10^{0}	0.0
21	^{241}Am	1.16×10^{1}	0.1	^{95}Zr	2.57×10^{-5}	0.0	^{95}Zr	1.38×10^{-82}	0.0	^{95}Nb	0.00×10^{0}	0.0
total=		**1.08×10^{4}**	**98.6**		**2.05×10^{3}**	**99.6**		**6.35** $\times 10^{2}$	**99.8**		**3.30** $\times 10^{2}$	**99.8**

Table 6-3 Nuclide Ranking for Decay Heat; WEC 17×17 OFA, 8 wt % at 75 GWd/MTU Assembly Average Burnup

Rank	1-year cooling time			5-year cooling time			50-year cooling time			100-year cooling time		
	Isotope	Decay heat (W)	Percent of total decay heat (%)	Isotope	Decay heat (W)	Percent of total decay heat (%)	Isotope	Decay heat (W)	Percent of total decay heat (%)	Isotope	Decay heat (W)	Percent of total decay heat (%)
1	^{144}Pr	4.56×10^{3}	27.0	^{90}Y	8.41×10^{2}	19.4	^{238}Pu	3.01×10^{2}	22.2	^{241}Am	2.54×10^{2}	35.1
2	^{106}Rh	3.63×10^{3}	21.5	^{134}Cs	7.90×10^{2}	18.2	^{90}Y	2.85×10^{2}	20.9	^{238}Pu	2.03×10^{2}	28.1
3	^{134}Cs	3.03×10^{3}	17.9	^{137m}Ba	7.69×10^{2}	17.7	^{137m}Ba	2.73×10^{2}	20.1	^{137m}Ba	8.62×10^{1}	11.9
4	^{242}Cm	9.99×10^{2}	5.9	^{238}Pu	4.29×10^{2}	9.9	^{241}Am	2.52×10^{2}	18.5	^{90}Y	8.54×10^{1}	11.8
5	^{90}Y	9.26×10^{2}	5.5	^{244}Cm	3.43×10^{2}	7.9	^{137}Cs	7.81×10^{1}	5.8	^{137}Cs	2.47×10^{1}	3.4
6	^{137m}Ba	8.43×10^{2}	5.0	^{106}Rh	2.38×10^{2}	5.5	^{244}Cm	6.12×10^{1}	4.5	^{240}Pu	2.38×10^{1}	3.3
7	^{238}Pu	4.39×10^{2}	2.6	^{137}Cs	2.20×10^{2}	5.1	^{90}Sr	5.97×10^{1}	4.4	^{90}Sr	1.79×10^{1}	2.5
8	^{144}Ce	4.07×10^{2}	2.4	^{90}Sr	1.76×10^{2}	4.1	^{240}Pu	2.38×10^{1}	1.8	^{239}Pu	1.57×10^{1}	2.2
9	^{244}Cm	3.99×10^{2}	2.4	^{144}Pr	1.30×10^{2}	3.0	^{239}Pu	1.58×10^{1}	1.2	^{244}Cm	9.03×10^{0}	1.2
10	^{95}Nb	3.55×10^{2}	2.1	^{154}Eu	1.14×10^{2}	2.6	^{154}Eu	3.04×10^{0}	0.2	^{242}Cm	4.13×10^{-1}	0.1
11	^{137}Cs	2.42×10^{2}	1.4	^{60}Co	7.50×10^{1}	1.7	^{85}Kr	1.25×10^{0}	0.1	^{154}Eu	5.40×10^{-2}	0.0
12	^{90}Sr	1.94×10^{2}	1.2	^{241}Am	7.16×10^{1}	1.7	^{242}Cm	5.28×10^{-1}	0.0	^{85}Kr	4.98×10^{-2}	0.0
13	^{95}Zr	1.73×10^{2}	1.0	^{147}Pm	2.55×10^{1}	0.6	^{60}Co	2.02×10^{-1}	0.0	^{60}Co	$2.81E \times 10^{-4}$	0.0
14	^{154}Eu	1.58×10^{2}	0.9	^{240}Pu	2.32×10^{1}	0.5	^{134}Cs	2.18×10^{-4}	0.0	^{125}Sb	6.62×10^{-10}	0.0
15	^{60}Co	1.27×10^{2}	0.8	^{85}Kr	2.27×10^{1}	0.5	^{125}Sb	1.89×10^{-4}	0.0	^{147}Pm	3.19×10^{-10}	0.0
16	^{147}Pm	7.32×10^{1}	0.4	^{239}Pu	1.58×10^{1}	0.4	^{147}Pm	1.75×10^{-4}	0.0	^{134}Cs	1.12×10^{-11}	0.0
17	^{125}Sb	4.21×10^{1}	0.2	^{125}Sb	1.54×10^{1}	0.4	^{106}Rh	1.17×10^{-11}	0.0	^{106}Rh	1.91×10^{-26}	0.0
18	^{85}Kr	2.94×10^{1}	0.2	^{144}Ce	1.17×10^{1}	0.3	^{144}Pr	5.61×10^{-16}	0.0	^{144}Pr	2.84×10^{-35}	0.0
19	^{241}Am	2.50×10^{1}	0.1	^{242}Cm	2.66×10^{0}	0.1	^{144}Ce	5.01×10^{-17}	0.0	^{144}Ce	2.54×10^{-36}	0.0
20	^{240}Pu	2.31×10^{1}	0.1	^{95}Nb	5.07×10^{-5}	0.0	^{95}Nb	2.62×10^{-82}	0.0	^{95}Zr	0.00×10^{0}	0.0
21	^{239}Pu	1.58×10^{1}	0.1	^{95}Zr	2.34×10^{-5}	0.0	^{95}Zr	1.25×10^{-82}	0.0	^{95}Nb	0.00×10^{0}	0.0
total=		**1.69×10^{4}**	**98.8**		**4.33×10^{3}**	**99.6**		**1.36×10^{3}**	**99.7**		**7.23×10^{2}**	**99.6**

6.2 Source Terms

This section presents major nuclides that contribute to neutron and photon source terms of high-burnup and extended-enrichment UO_2 fuel. For the neutron source, the identified nuclides contribute more than 1% of the total neutron source strength. For the gamma source, these nuclides are provided for nine energy groups in the 0.4–4 mega electron-volt (MeV) energy range based on the SCALE 27 neutron and 19 gamma group library energy group structure. Gamma sources with energy outside this energy range have been demonstrated to have negligible contributions to the external dose rates of transportation packages and dry storage casks because of either their low energy or their low source strength (see NUREG-2216 [8], NUREG-2215 [7], and Appendix A of this report). The nuclides contributing more than 1% of the total gamma strength for each energy group are presented.

Table 6-4 through Table 6-17 give the important nuclides, the total source strength, and nuclide percentage contribution to the total source strength. The specific values in the tables characterize neutron and photon sources of WEC 17 × 17 OFA and GEH 10 × 10 GE14 assemblies with a 6 wt % enrichment and a 75 GWd/MTU burnup value at various cooling times. The neutron source strength is provided in neutrons per second (s) per MTU, and the photon source strength is provided in photons per s per MTU.

The 6 wt% fuel enrichment was selected for the fuel with extended enrichment (i.e., 5 to 8 wt %) because at fixed burnup, a lower fuel enrichment is typically more conservative than a higher fuel enrichment with respect to dose rate [7, 8]. The nuclides identified in this section are the same nuclides previously identified as important for shielding analyses of UO_2 fuel with initial ^{235}U enrichment less than 5 wt % [60-62] and equal to 8 wt % [41].

Table 6-4 WEC OFA (6% Initial ^{235}U and 75 GWd/MTU)—Neutron Sources

Cooling Time (years)	1	2	5	10	20	50	100
Spontaneous fission							
Strength (n/s)	3.09×10^9	2.83×10^9	2.47×10^9	2.03×10^9	1.40×10^9	4.72×10^8	1.05×10^8
Nuclide	**Percent of total source strength (%)**						
^{240}Pu	—	—	—	—	—	—	3.6
^{242}Pu	—	—	—	—	—	—	2.3
^{242}Cm	5.8	1.4	—	—	—	—	—
^{244}Cm	90.6	95.3	97.3	97.5	96.9	91.0	60.2
^{246}Cm	1.1	1.2	1.4	1.7	2.5	7.3	32.5
^{252}Cf	2.1	1.8	—	—	—	—	—
(α,n) reactions							
Strength (n/s)	2.60×10^7	1.55×10^7	1.22×10^7	1.13×10^7	9.77×10^6	7.02×10^6	5.00×10^6
Nuclide	**Percent of total source strength (%)**						
^{238}Pu	17.6	29.6	36.9	38.3	40.8	44.8	42.4
^{239}Pu	—	—	—	1.0	1.2	1.6	2.3
^{240}Pu	—	1.3	1.7	1.9	2.2	3.1	4.4
^{241}Am	—	2.1	5.3	9.6	17.1	33.0	46.8
^{242}Cm	50.3	17.9	—	—	—	—	—
^{244}Cm	29.7	48.0	54.4	48.6	38.2	16.9	3.5

Table 6-5 GE14 (6% Initial ^{235}U and 75 GWd/MTU)—Neutron Sources

Cooling Time (years)	1	2	5	10	20	50	100
Spontaneous fission							
Strength (n/s)	4.11×10^9	3.78×10^9	3.24×10^9	2.62×10^9	1.79×10^9	6.18×10^8	1.54×10^8
Nuclide	**Percent of total source strength (%)**						
^{240}Pu	—	—	—	—	—	—	2.59
^{242}Pu	—	—	—	—	—	—	1.75
^{242}Cm	3.79	—	—	—	—	—	—
^{244}Cm	86.16	90.24	93.97	95.86	95.62	87.88	52.03
^{246}Cm	1.61	1.75	2.04	2.52	3.68	10.62	42.33
^{252}Cf	8.16	6.83	3.64	1.21	—	—	—
(α,n) reactions							
Strength (n/s)	6.49×10^6	4.10×10^6	3.26×10^6	2.93×10^6	2.42×10^6	1.54×10^6	1.01×10^6
Nuclide	**Percent of total source strength (%)**						
^{238}Pu	15.2	24.1	29.6	31.7	35.5	43.8	45.2
^{239}Pu	—	—	—	—	—	1.3	1.9
^{240}Pu	—	1.1	1.5	1.6	2.0	3.2	5.0
^{241}Am	—	1.6	3.7	6.7	12.5	26.9	41.5
^{242}Cm	45.4	15.2	—	—	—	—	—
^{244}Cm	37.5	57.2	64.0	58.8	48.7	24.1	5.5

Table 6-6 WEC OFA (6% Initial ^{235}U and 75 GWd/MTU)—Gamma Sources for 1-year Cooling Time

Average group energy (MeV)									
	0.5	0.7	0.9	1.165	1.495	1.83	2.25	2.75	3.5
Strength (p/s)	8.54×10^{15}	3.69×10^{16}	1.86×10^{15}	1.69×10^{15}	1.02×10^{15}	5.68×10^{13}	1.83×10^{14}	9.04×10^{12}	1.06×10^{12}
Nuclide	**Percent of total source strength (%)**								
^{60}Co	—	—	—	21.8	36.2	—	—	—	—
^{95}Zr	—	3.2	—	—	—	—	—	—	—
^{95}Nb	—	7.0	—	—	—	—	—	—	—
^{90}Y	1.4	—	1.2	—	—	—	—	—	—
^{103}Ru	1.2	—	—	—	—	—	—	—	—
^{106}Rh	49.3	6.0	14.4	29.8	9.1	74.4	15.2	84.1	95.3
^{110m}Ag	—	—	8.9	—	6.3	—	—	—	—
^{125}Sb-125	2.5	—	—	—	—	—	—	—	—
^{134}Cs	36.2	61.0	57.5	20.2	36.4	—	—	—	—
^{137m}Ba	—	19.3	—	—	—	—	—	—	—
^{144}Pr	8.5	1.8	9.3	7.0	10.1	23.6	84.6	15.9	4.9
^{154}Eu	—	—	8.6	20.3	1.6	—	—	—	—

Table 6-7 WEC OFA (6% Initial ^{235}U and 75 GWd/MTU)—Gamma Sources for 5-year Cooling Time

Average group energy (MeV)									
	0.5	0.7	0.9	1.165	1.495	1.83	2.25	2.75	3.5
Strength (p/s)	1.33×10^{15}	1.28×10^{16}	4.41×10^{14}	6.03×10^{14}	3.39×10^{14}	3.65×10^{12}	6.31×10^{12}	5.42×10^{11}	6.79×10^{10}
Nuclide	**Percentage of total source strength (%)**								
^{60}Co	—	—	—	36.0	64.3	—	—	—	—
^{90}Y	8.2	—	4.7	2.0	—	12.9	—	—	—
^{106}Rh	20.7	1.1	4.0	5.5	1.8	75.9	28.9	91.9	97.3
^{125}Sb	6.0	—	—	—	—	—	—	—	—
^{134}Cs	60.7	45.9	63.3	14.8	28.5	—	—	—	—
^{137m}Ba	—	50.9	—	—	—	—	—	—	—
^{144}Pr	1.6	—	1.1	—	—	10.5	70.4	7.6	2.2
^{154}Eu	2.5	0.9	26.3	41.1	3.5	—	—	—	—

Table 6-8 WEC OFA (6% Initial ^{235}U and 75 GWd/MTU)—Gamma Sources for 10-year Cooling Time

Average group energy (MeV)									
	0.5	0.7	0.9	1.165	1.495	1.83	2.25	2.75	3.5
Strength (p/s)	3.05×10^{14}	7.05×10^{15}	1.49×10^{14}	3.07×10^{14}	1.42×10^{14}	5.27×10^{11}	1.49×10^{11}	1.98×10^{10}	2.51×10^{9}
Nuclide	**Percentage of total source strength (%)**								
^{60}Co	—	—	—	36.8	79.8	—	—	—	—
^{90}Y	31.5	—	12.5	3.5	1.8	79.2	23.1	—	—
^{106}Rh	3.0	—	—	—	—	17.5	40.6	83.7	87.7
^{125}Sb	7.4	—	—	—	—	—	—	—	—
^{134}Cs	49.4	15.6	35.0	5.4	12.8	—	—	—	—
^{137m}Ba	—	82.3	—	—	—	—	—	—	—
^{144}Pr	—	—	—	—	—	—	35.0	2.4	—
^{154}Eu	7.4	1.2	52.0	54.1	5.6	2.3	—	—	—
^{208}Tl	—	—	—	—	—	—	—	12.2	—
^{244}Cm	—	—	—	—	—	—	—	1.6	11.5

Table 6-9 WEC OFA (6% Initial ^{235}U and 75 GWd/MTU)—Gamma Sources for 20-year Cooling Time

Average group energy (MeV)									
	0.5	0.7	0.9	1.165	1.495	1.83	2.25	2.75	3.5
Strength (p/s)	9.52×10^{13}	4.72×10^{15}	5.09×10^{13}	1.13×10^{14}	3.64×10^{13}	3.34×10^{11}	2.79×10^{10}	2.84×10^{9}	2.05×10^{8}
Nuclide	**Percentage of total source strength (%)**								
^{60}Co	—	—	—	26.7	83.1	—	1.3	—	—
^{90}Y	79.5	—	28.5	7.4	5.5	98.2	97.1	1.3	—
^{125}Sb	1.9	—	—	—	—	—	—	—	—
^{134}Cs	5.5	—	3.6	—	1.7	—	—	—	—
^{137}Cs	1.1	—	—	—	—	—	—	—	—
^{137m}Ba	—	97.7	—	—	—	—	—	—	—
^{154}Eu	10.6	—	67.7	65.4	9.7	1.6	—	—	—
^{208}Tl	—	—	—	—	—	—	—	90.2	—
^{244}Cm	—	—	—	—	—	—	1.3	7.5	95.5
^{246}Cm	—	—	—	—	—	—	—	—	2.1

Table 6-10 WEC OFA (6% Initial ^{235}U and 75 GWd/MTU)—Gamma Sources for 50-year Cooling Time

Average group energy (MeV)									
	0.5	0.7	0.9	1.165	1.495	1.83	2.25	2.75	3.5
Strength (p/s)	3.85×10^{13}	2.33×10^{15}	1.02×10^{13}	1.13×10^{13}	1.87×10^{12}	1.60×10^{11}	1.33×10^{10}	2.02×10^{9}	6.84×10^{7}
Nuclide	**Percentage of total source strength (%)**								
^{60}Co	—	—	—	5.2	31.3	—	—	—	—
^{90}Y	95.6	—	69.5	36.0	51.8	99.5	99.3	—	—
^{137}Cs	1.4	—	—	—	—	—	—	—	—
^{137m}Ba	—	99.3	—	—	—	—	—	—	—
^{154}Eu	2.3	—	30.3	58.8	16.8	—	—	—	—
^{208}Tl	—	—	—	—	—	—	—	95.4	—
^{244}Cm	—	—	—	—	—	—	2.8	3.4	91.1
^{246}Cm	—	—	—	—	—	—	—	—	6.3

Table 6-11 WEC OFA (6% Initial ^{235}U and 75 GWd/MTU)—Gamma Sources for 100-year Cooling Time

Average group energy (MeV)									
	0.5	0.7	0.9	1.165	1.495	1.83	2.25	2.75	3.5
Strength (p/s)	1.13×10^{13}	7.34×10^{14}	2.18×10^{12}	1.34×10^{12}	2.98×10^{11}	4.78×10^{10}	3.98×10^{9}	1.19×10^{9}	1.51×10^{7}
Nuclide	**Percentage of total source strength (%)**								
^{90}Y	97.5	—	97.3	91.3	97.8	99.9	99.3	—	—
^{137}Cs	1.5	—	—	—	—	—	—	—	—
^{137m}Ba	—	99.3	—	—	—	—	—	—	—
^{154}Eu	—	—	2.5	8.8	1.9	—	—	—	—
^{208}Tl	—	—	—	—	—	—	—	98.4	—
^{238}Pu	—	—	—	—	—	—	—	—	1.7
^{240}Pu	—	—	—	—	—	—	—	—	4.7
^{242}Pu	—	—	—	—	—	—	—	—	2.9
^{244}Cm	—	—	—	—	—	—	—	—	61.0
^{246}Cm	—	—	—	—	—	—	—	—	28.2

Table 6-12 GE14 (6% Initial ^{235}U and 75 GWd/MTU)—Gamma Sources for 1-year Cooling Time

Average group energy (MeV)									
	0.5	0.7	0.9	1.165	1.495	1.83	2.25	2.75	3.5
Strength (p/s)	6.44×10^{15}	2.98×10^{16}	1.51×10^{15}	1.44×10^{15}	8.86×10^{14}	4.02×10^{13}	1.14×10^{14}	6.48×10^{12}	7.76×10^{11}
Nuclide	**Percentage of total source strength (%)**								
^{60}Co	—	—	—	27.1	44.0	—	—	—	—
^{95}Zr	—	2.4	—	—	—	—	—	—	—
^{95}Nb	—	5.2	—	—	—	—	—	—	—
^{90}Y	1.7	—	1.4	—	—	1.2	—	—	—
^{103}Ru	1.0	—	—	—	—	—	—	—	—
^{106}Rh	48.3	5.5	13.1	25.8	7.7	77.5	17.9	86.5	95.9
^{110m}Ag	—	—	9.0	—	5.9	—	—	—	—
^{134}Cs	—	—	—	—	—	—	—	—	—
^{137m}Ba	2.7	60.5	56.7	19.1	33.5	—	—	—	—
^{144}Pr	38.5	23.1	—	—	—	—	—	—	—
^{154}Eu	6.8	1.3	6.9	5.0	7.0	20.2	82.0	13.4	4.0
^{160}Tb	—	—	8.9	20.0	1.5	—	—	—	—

Table 6-13 GE14 (6% Initial ^{235}U and 75 GWd/MTU)—Gamma Sources for 5-year Cooling Time

Average group energy (MeV)									
	0.5	0.7	0.9	1.165	1.495	1.83	2.25	2.75	3.5
Strength (p/s)	1.06×10^{15}	1.13×10^{16}	3.59×10^{14}	5.48×10^{14}	3.28×10^{14}	2.73×10^{12}	4.07×10^{12}	3.95×10^{11}	5.02×10^{10}
Nuclide	**Percentage of total source strength (%)**								
^{60}Co	—	—	—	41.9	70.2	—	—	—	—
^{90}Y	9.3	—	5.3	2.0	—	15.7	—	—	—
^{106}Rh	19.2	—	3.6	4.4	1.4	75.2	33.2	93.1	97.2
^{125}Sb	6.0	—	—	—	—	—	—	—	—
^{134}Cs	61.2	41.7	62.5	13.1	23.7	—	—	—	—
^{137m}Ba	—	55.4	—	—	—	—	—	—	—
^{144}Pr	1.2	—	—	—	—	8.5	65.9	6.3	1.8
^{154}Eu	2.7	—	27.0	37.9	3.0	—	—	—	—

Table 6-14 GE14 (6% Initial ^{235}U and 75 GWd/MTU)—Gamma Sources for 10-year Cooling Time

Average group energy (MeV)									
	0.5	**0.7**	**0.9**	**1.165**	**1.495**	**1.83**	**2.25**	**2.75**	**3.5**
Strength (p/s)	2.56×10^{14}	6.59×10^{15}	1.24×10^{14}	2.83×10^{14}	1.43×10^{14}	4.62×10^{11}	1.10×10^{11}	1.52×10^{10}	2.01×10^{9}
Nuclide	**Percentage of total source strength (%)**								
^{60}Co	—	—	—	42.0	83.2	—	1.3	—	—
^{90}Y	34.2	—	13.5	3.4	1.6	82.3	28.6	—	—
^{106}Rh	2.6	—	—	—	—	14.8	40.8	80.4	80.6
^{125}Sb	7.1	—	—	—	—	—	—	—	—
^{134}Cs	47.2	13.4	33.6	4.7	10.1	—	—	—	—
^{137m}Ba	—	84.7	—	—	—	—	—	—	—
^{144}Pr	—	—	—	—	—	—	28.7	1.9	—
^{154}Eu	7.4	1.1	52.0	49.1	4.6	2.2	—	—	—
^{208}Tl	—	—	—	—	—	—	—	14.4	—
^{244}Cm	—	—	—	—	—	—	—	2.6	18.2

Table 6-15 GE14 (6% Initial ^{235}U and 75 GWd/MTU)—Gamma Sources for 20-year Cooling Time

Average group energy (MeV)									
	0.5	0.7	0.9	1.165	1.495	1.83	2.25	2.75	3.5
Strength (p/s)	8.52×10^{13}	4.53×10^{15}	4.39×10^{13}	1.03×10^{14}	3.73×10^{13}	3.04×10^{11}	2.56×10^{10}	2.58×10^{9}	2.61×10^{8}
Nuclide	**Percentage of total source strength (%)**								
^{60}Co	—	—	—	31.2	85.7	—	1.5	—	—
^{90}Y	80.8	—	30.1	7.4	4.9	98.1	96.5	1.3	—
^{125}Sb	1.7	—	—	—	—	—	—	—	—
^{134}Cs	5.0	—	3.3	—	1.4	—	—	—	—
^{137}Cs	1.2	—	—	—	—	—	—	—	—
^{137m}Ba	—	97.8	—	—	—	—	—	—	—
^{154}Eu	9.9	—	65.9	60.4	7.9	1.5	—	—	—
^{208}Tl	—	—	—	—	—	—	—	87.2	—
^{244}Cm	—	—	—	—	—	—	1.8	10.5	95.4
^{246}Cm	—	—	—	—	—	—	—	—	3.1

Table 6-16 GE14 (6% Initial ^{235}U and 75 GWd/MTU)—Gamma Sources for 50-year Cooling Time

Average group energy (MeV)									
	0.5	0.7	0.9	1.165	1.495	1.83	2.25	2.75	3.5
Strength (p/s)	3.50×10^{13}	2.24×10^{15}	9.04×10^{12}	9.89×10^{12}	1.77×10^{12}	1.46×10^{11}	1.22×10^{10}	1.80×10^{9}	8.89×10^{7}
Nuclide	**Percentage of total source strength (%)**								
^{60}Co	—	—	—	6.3	35.0	—	—	—	—
^{90}Y	95.8	—	71.0	37.3	49.8	99.6	98.7	—	—
^{137}Cs	1.4	—	—	—	—	—	—	—	—
^{137m}Ba	—	99.2	—	—	—	—	—	—	—
^{154}Eu	2.2	—	28.4	55.9	14.9	—	—	—	—
^{208}Tl	—	—	—	—	—	—	—	93.8	—
^{244}Cm	—	—	—	—	—	—	1.2	4.8	88.7
^{246}Cm	—	—	—	—	—	—	—	—	9.2

Table 6-17 GE14 (6% Initial ^{235}U and 75 GWd/MTU)—Gamma Sources for 100-year Cooling Time

Average group energy (MeV)									
Nuclide	0.5	0.7	0.9	1.165	1.495	1.83	2.25	2.75	3.5
Strength (p/s)	1.03×10^{13}	7.06×10^{14}	1.98×10^{12}	1.21×10^{12}	2.71×10^{11}	4.35×10^{10}	3.63×10^{9}	1.05×10^{9}	2.15×10^{7}
Nuclide	**Percentage of total source strength (%)**								
^{90}Y	97.3	—	97.5	91.8	97.9	99.9	98.8	—	—
^{137}Cs	1.5	—	—	—	—	—	—	—	—
^{137m}Ba	—	99.4	—	—	—	—	—	—	—
^{154}Eu	—	—	2.3	8.1	1.7	—	—	—	—
^{208}Tl	—	—	—	—	—	—	—	97.3	—
^{238}Pu	—	—	—	—	—	—	—	—	1.1
^{240}Pu	—	—	—	—	—	—	—	—	3.4
^{242}Pu	—	—	—	—	—	—	—	—	2.3
^{244}Cm	—	—	—	—	—	—	—	1.2	54.0
^{246}Cm	—	—	—	—	—	—	—	—	37.7

6.3 Criticality Safety

Previous studies [60] have evaluated AFP nuclide importance to criticality safety based on the fractional contribution of each nuclide to the total neutron absorption rate. A set of 28 nuclides, which is listed in Table 4-1, is currently recommended for BUC criticality safety analyses [7, 8, 54]. This set of nuclides was analyzed in this work using the same method used in NUREG/CR-6700 [60] to determine their rankings within the set of all AFP nuclides in irradiated fuel. The WEC 17 × 17 OFA with an average assembly burnup of 75 GWd/MTU was used in this analysis. The absorption fractions (AFs) and nuclide ranks are presented in Table 6-18 for initial ^{235}U enrichments of 6 wt % and 8 wt % and cooling times of 5 and 100 yr. The nuclide ranking in Table 6-18 is based on AFP nuclides in irradiated fuel, the neutron AF of which exceeds 1×10^{-6}. This analysis shows that the combined AFs of this set of nuclides is approximately 0.94 to 0.95 within the cooling time interval 5 to 100 yr. The importance of ^{234}U and ^{151}Eu increases significantly as the fuel cooling time increases. Therefore, this analysis shows that this set of 28 nuclides is also adequate for BUC criticality safety analyses of fuel with extended enrichment and increased burnup.

Table 6-18 Absorption Fractions and Nuclide Ranks for the Set of Burnup Credit Nuclides in WEC 17 × 17 OFA with an Average Assembly Burnup of 75 GWd/MTU

Type of BUC	Nuclide	6 wt % ^{235}U				8 wt % ^{235}U			
		5 year-cooling time		100-year cooling time		5-year cooling time		100-year cooling time	
		AF	Rank	AF	Rank	AF	Rank	AF	Rank
Actinide-only	^{234}U	1.178×10^{-3}	38	3.17×10^{-3}	30	1.612×10^{-3}	34	3.30×10^{-3}	29
	^{235}U	7.454×10^{-2}	4	7.46×10^{-2}	4	1.356×10^{-1}	4	1.36×10^{-1}	4
	^{238}U	2.199×10^{-1}	2	2.20×10^{-1}	2	2.108×10^{-1}	2	2.11×10^{-1}	2
	^{238}Pu	3.578×10^{-3}	25	1.69×10^{-3}	29	2.786×10^{-3}	29	1.32×10^{-3}	30
	^{239}Pu	2.382×10^{-1}	1	2.37×10^{-1}	1	2.297×10^{-1}	1	2.29×10^{-1}	1
	^{240}Pu	1.929×10^{-1}	3	2.02×10^{-1}	4	1.672×10^{-1}	3	1.72×10^{-1}	3
	^{241}Pu	5.231×10^{-2}	5	5.22×10^{-4}	9	4.468×10^{-2}	5	4.47×10^{-4}	9
	^{242}Pu	1.034×10^{-2}	12	1.03×10^{-2}	13	7.134×10^{-3}	16	7.14×10^{-3}	16
	^{241}Am	1.626×10^{-2}	11	5.87×10^{-2}	5	1.496×10^{-2}	11	5.31×10^{-2}	5
Additional nuclides for AFP	^{95}Mo	3.990×10^{-3}	21	3.99×10^{-3}	22	3.987×10^{-3}	20	3.99×10^{-3}	22
	^{99}Tc	9.550×10^{-3}	14	9.54×10^{-3}	16	9.489×10^{-3}	14	9.50×10^{-3}	14
	^{101}Ru	3.654×10^{-3}	23	3.65×10^{-3}	24	3.566×10^{-3}	22	3.57×10^{-3}	23
	^{103}Rh	1.662×10^{-2}	7	1.66×10^{-2}	7	1.545×10^{-2}	8	1.55×10^{-2}	8
	^{109}Ag	3.626×10^{-3}	24	3.62×10^{-3}	25	2.847×10^{-3}	28	2.85×10^{-3}	26
	^{133}Cs	1.145×10^{-2}	9	1.14×10^{-2}	10	1.133×10^{-2}	9	1.14×10^{-2}	10
	^{143}Nd	1.135×10^{-2}	10	1.13×10^{-2}	11	1.096×10^{-2}	10	1.10×10^{-2}	11
	^{145}Nd	4.574×10^{-3}	20	4.57×10^{-3}	21	4.534×10^{-3}	18	4.54×10^{-3}	19
	^{147}Sm	3.311×10^{-3}	32	3.96×10^{-3}	23	3.670×10^{-3}	25	4.38×10^{-3}	21
	^{149}Sm	7.636×10^{-3}	16	7.63×10^{-3}	17	7.393×10^{-3}	15	7.40×10^{-3}	15
	^{150}Sm	2.841×10^{-3}	30	2.84×10^{-3}	27	2.531×10^{-3}	32	2.53×10^{-3}	28
	^{151}Sm	3.902×10^{-3}	22	1.88×10^{-3}	28	3.832×10^{-3}	21	1.85×10^{-3}	27
	^{152}Sm	5.673×10^{-3}	17	5.67×10^{-3}	18	5.393×10^{-3}	17	5.40×10^{-3}	18
	^{151}Eu	1.818×10^{-4}	75	2.51×10^{-3}	33	1.892×10^{-4}	71	2.60×10^{-3}	32
	^{153}Eu	4.945×10^{-3}	19	4.94×10^{-3}	20	4.436×10^{-3}	19	4.44×10^{-3}	20
	^{155}Gd	5.342×10^{-3}	27	1.02×10^{-2}	15	3.895×10^{-3}	31	7.43×10^{-3}	17
	^{236}U	1.919×10^{-2}	6	1.93×10^{-2}	6	2.385×10^{-2}	6	2.40×10^{-2}	6
	^{237}Np	9.511×10^{-3}	15	1.18×10^{-2}	12	9.567×10^{-3}	13	1.17×10^{-2}	12
	^{243}Am	5.451×10^{-3}	18	5.40×10^{-3}	19	3.459×10^{-3}	23	3.43×10^{-3}	24
	Subtotal	9.419×10^{-1}		9.49×10^{-1}		9.449×10^{-1}		9.51×10^{-1}	

7 PARAMETRIC STUDY FOR SHIELDING

The total dose rate for a cask containing SNF depends on many fuel and dry storage cask and transportation package design parameters. The total dose rate contains neutron and gamma components, which vary considerably depending on factors such as enrichment, burnup, and cooling time. All parametric studies were therefore performed for two designs: a dry storage cask containing concrete shielding and a transportation package containing steel and hydrogen-rich polymer impregnated with uniformly dispersed boron carbide shielding material.

In this section, absolute, relative, and normalized dose rates on dry storage casks and transportation packages using simplified geometrical models, as described in Appendix A, are presented. *Relative* indicates that the dose rates of interest are relative to those from the baseline assembly of the appropriate fuel type (WEC OFA, WEC RFA, GEH GE14) and enrichment described in Section 3. *Normalized* dose rates are data normalized to the maximum value in a data set, where a *data set* refers to any data represented by a connected line on a plot. Dose rates that have not been normalized are presented in millirem per hour (mrem/h), with one MTU used as the basis for each assembly in the cask.

Unless otherwise stated, certain plots and discussion are omitted for brevity when no significant difference occurred in results for similar cases, such as when a parameter produced similar trends for dry storage casks and transportation packages or when a parameter produced similar trends at different enrichments. The 6.5 wt % initial ^{235}U enrichment trends were between the 5 and 8 wt % trends and were not presented.

7.1 Dry Storage Cask and Transportation Package Shielding Evaluation for Pressurized-Water Reactors

The parameters considered in this study include burnup, initial ^{235}U enrichment, cooling time, specific power, soluble boron concentration and boron letdown curve, moderator density (and corresponding temperature), fuel temperature, fuel density, burnable absorbers, RCCAs, fuel assembly type, and axial burnup profile. The parametric studies presented in Sections 7.1.1 through 7.1.10 used WEC 17 × 17 OFA. All parametric studies were performed with a dry storage cask and a transportation package; each contained 32 identical PWR fuel assemblies. The dose location for all analysis was the mid-height external surface of the cask/package.

7.1.1 Burnup

The effect of assembly burnup on dry storage cask and transportation package dose rates was analyzed for 5.0, 5.5, 6.0, 6.5, 7.0, 7.5, and 8.0 wt % ^{235}U PWR fuel. The fuel was burned up to a maximum assembly average burnup of 75 GWd/MTU.

7.1.1.1 Neutron Dose Rate Trends

The graphs in Figure 7-1 illustrate the effects on the neutron dose rate of varying burnup for PWR fuel with several different initial ^{235}U enrichments at 5 yr of cooling time. Neutron dose rates for a dry storage cask containing concrete and a transportation package are provided. As described in NUREG/CR-6716 [63], the neutron dose rate has previously been observed to increase with burnup approximately to the power of four. The same effect is observed in this analysis, with the highest burnup producing the highest neutron dose rates. This effect was

most pronounced at lower enrichments. The absolute neutron dose rate was higher for the transportation package than for the dry storage cask because the concrete in the storage cask provides a higher degree of neutron attenuation.

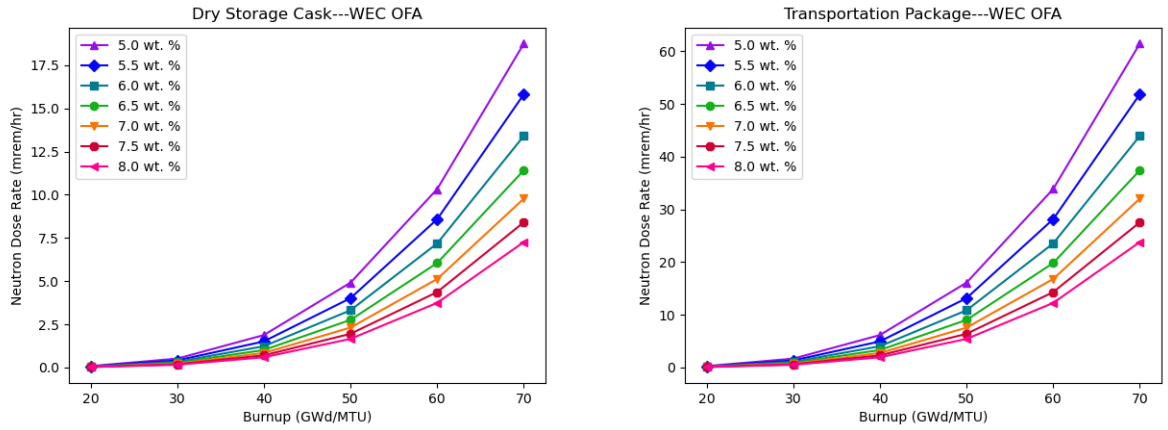

Figure 7-1 Neutron Dose Rate Trends of Variation with PWR Fuel Burnup (GWd/MTU) and Initial Enrichment (^{235}U wt %)

7.1.1.2 Gamma Dose Rate Trends

The graphs in Figure 7-2 illustrate the effects on the primary gamma dose rate of varying burnup for PWR fuel with several different initial enrichments at 5 yr of cooling time. Primary gamma dose rates for a dry storage cask and transportation package are provided. As discussed in Section 3.4.1.1 of NUREG/CR-6716 [63], the gamma dose rate has previously been observed to increase linearly with burnup. This linear relationship was also observed in this analysis, with the highest burnup producing the highest gamma dose rates. The effect of increasing burnup on primary gamma dose rates was most pronounced at lower enrichments.

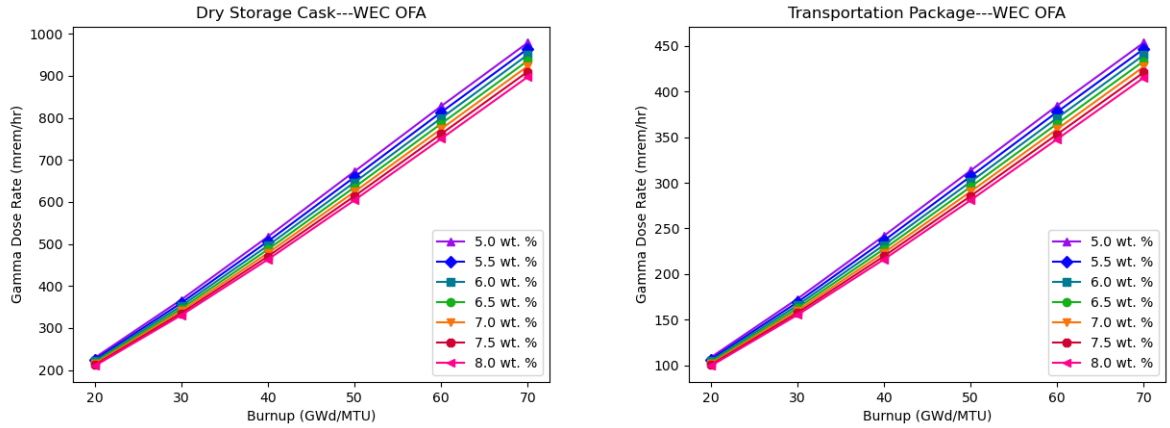

Figure 7-2 Primary Gamma Dose Rate Trends of Variation with PWR Fuel Burnup (GWd/MTU) and Initial Enrichment (^{235}U wt %)

7.1.1.3 Cobalt-60 Dose Rate Trends

The graphs in Figure 7-3 illustrate the effects on the ^{60}Co dose rate of varying burnup for PWR fuel with several different initial enrichments at 5 yr of cooling time. Cobalt-60 dose rates for a dry storage cask and a transportation package are provided. As discussed in Section 3.4.1.1 of NUREG/CR-6716 [63], the primary gamma dose rate has previously been observed to increase linearly with burnup. This linear relationship was also observed with the ^{60}Co dose rates, with the highest burnup producing the highest ^{60}Co dose rates. The effect of increasing burnup on ^{60}Co dose rates was most pronounced at lower enrichments.

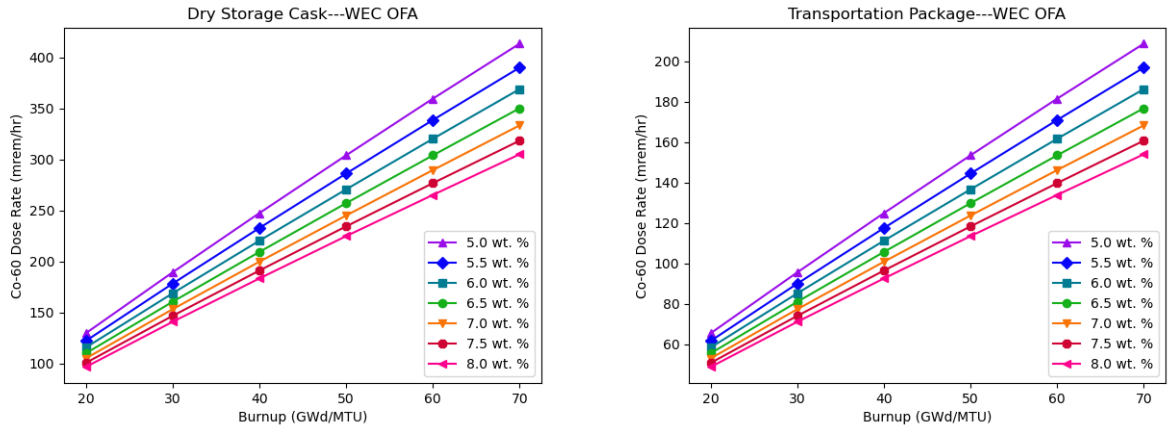

Figure 7-3 Cobalt-60 Dose Rate Trends of Variation with PWR Fuel Burnup (GWd/MTU) and Initial Enrichment (^{235}U wt %)

7.1.2 Initial Fuel Enrichment

The effect of initial ^{235}U enrichment on dry storage cask and transportation package dose rates was analyzed for 5.0, 5.5, 6.0, 6.5, 7.0, 7.5, and 8.0 wt % ^{235}U PWR fuel. The fuel was burned up to 75 GWd/MTU.

7.1.2.1 Neutron Dose Rate Trends

The graphs in Figure 7-4 illustrate the effects on the neutron dose rate of varying enrichment (in ^{235}U wt %) for PWR fuel at constant burnup (75 GWd/MTU) at several different cooling times. Neutron dose rates for a dry storage cask and a transportation package are provided. These graphs show that the neutron dose rate increases with decreasing enrichment. At a constant burnup of 75 GWd/MTU, the neutron dose rate decreased by a factor of two with an increase from 5 to 7 wt % enrichment. Similar effects were observed at lower enrichments (up to 5 wt. % ^{235}U) and burnups (up to 60 GWd/MTU) in Section 3.4.1.2 of NUREG/CR-6716 [63], where neutron dose rate decreased by a factor of two with an increase from 2.5 to 5 wt. %.

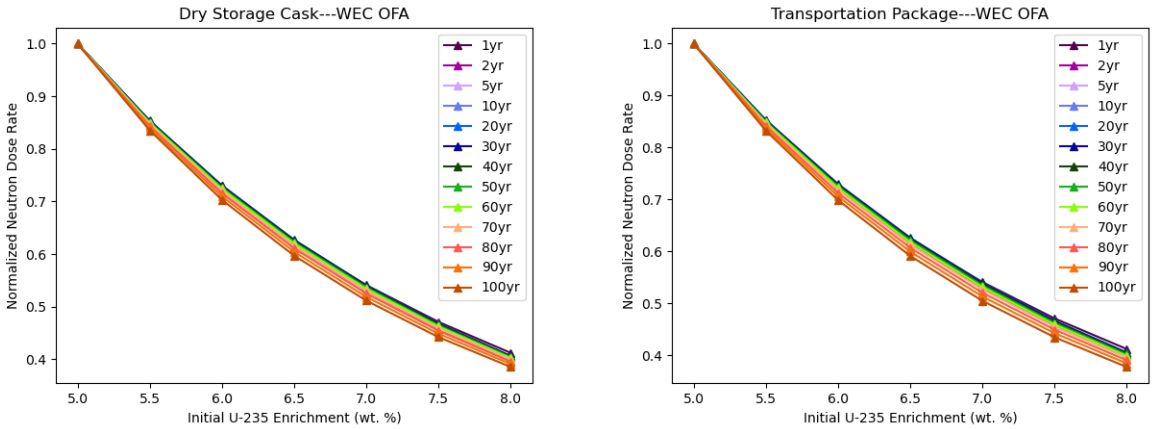

Figure 7-4 Neutron Dose Rate Trends of Variation with PWR Initial Fuel Enrichment (^{235}U wt %) and Cooling Time (years)

7.1.2.2 Gamma Dose Rate Trends

Primary gamma dose rate trends of variation with initial uranium enrichment (in ^{235}U wt %) at constant burnup (75 GWd/MTU) for PWR fuel are illustrated in Figure 7-5. Primary gamma dose rates for a dry storage cask and a transportation package are provided. These graphs show that for cooling times less than or equal to 5 yr, the primary gamma dose rate decreases with increasing fuel enrichment at a constant burnup of 75 GWd/MTU. These same trends were observed at lower enrichments (up to 5 wt % ^{235}U) and burnups (up to 60 GWd/MTU) in Section 3.4.1.2 of NUREG/CR-6716 [63]. Figure 7-5 shows that the primary gamma dose rate changes its trend of variation with initial fuel enrichment at the 10-year cooling time. The primary gamma dose rate increases with increasing initial fuel enrichment for longer cooling times (i.e., greater than 10 yr). These different trends are caused by the effects of fuel enrichment variations on the production of dominating fission products at each of the cooling times analyzed. Primary gamma dose rate is more sensitive to initial fuel enrichment at cooling times less than approximately 10 yr. Initial enrichment had a maximum effect on primary gamma dose rate at the 2-year cooling time, indicating that ^{106}Ru and ^{134}Cs concentrations are more sensitive to the initial fuel enrichment than the other primary gamma dose rate contributors. Beyond an approximately 10-year cooling time, the primary gamma dose rate has a weaker dependence on initial fuel enrichment compared to lower cooling times, indicating that the concentrations of longer-lived fission products ^{154}Eu, ^{137}Cs, and ^{90}Sr are relatively insensitive to the initial fuel enrichment at constant burnup. These same effects were observed at lower enrichments in Section 4.1.2.1 of ORNL/SPR-2373 [41].

Note that NUREG/CR-6716 [63] plots gamma dose rates that include both the primary and secondary gammas produced, as a function of enrichment, whereas this study plots the normalized primary gamma dose rates only since trends in the secondary gamma dose rates are the same as those for the neutron dose rates [41]. A comparison of the total gamma dose rate trends in NUREG/CR-6716 [63] and normalized primary gamma dose rate trends in this study suggest that secondary gammas can be dominating in trends depending on cooling time and burnup.

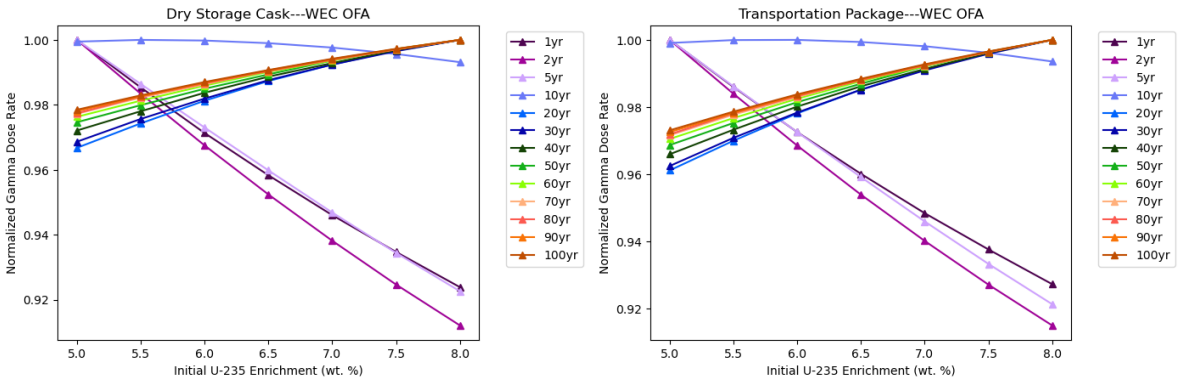

Figure 7-5 Primary Gamma Dose Rate Trends of Variation with PWR Initial Fuel Enrichment (^{235}U wt %) and Cooling Time (years)

7.1.2.3 Cobalt-60 Dose Rate Trends

The graphs in Figure 7-6 illustrate the effects on the ^{60}Co dose rate of varying enrichment for PWR fuel at constant burnup (75 GWd/MTU) at several different cooling times. Cobalt-60 dose rates for a dry storage cask and a transportation package are provided. These graphs show that, for all cooling times analyzed, the ^{60}Co dose rate decreased with increasing fuel enrichment at a rate independent of cooling time. At a constant burnup of 75 GWd/MTU, the ^{60}Co dose rate was observed to be more sensitive to fuel enrichment than the primary gamma dose rate but was not as sensitive to fuel enrichment as the neutron dose rate.

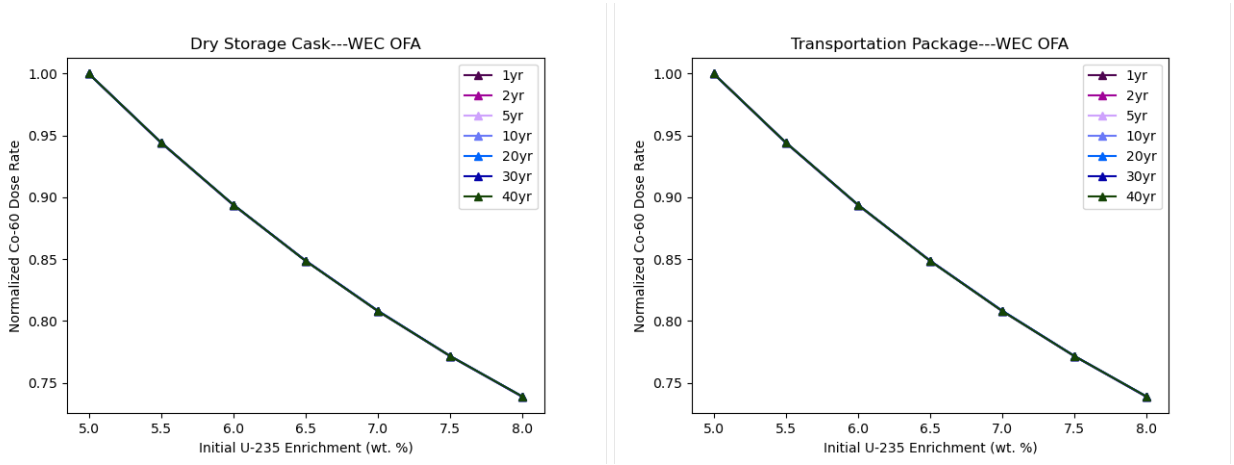

Figure 7-6 Cobalt-60 Dose Rate Trends of Variation with PWR Initial Fuel Enrichment (^{235}U wt %) and Cooling Time (years)

7.1.3 Cooling Time

The effect of post-irradiation cooling time on cask dose rates was analyzed for PWR fuel 5.0, 5.5, 6.0, 6.5, 7.0, 7.5, and 8.0 wt % ^{235}U. The fuel was burned up to 75 GWd/MTU.

7.1.3.1 Neutron Dose Rate Trends

The graphs in Figure 7-7 illustrate the effects on the neutron dose rate of varying cooling times for PWR fuel with several different initial enrichments. Neutron dose rates for a dry storage cask and a transportation package are provided. As discussed in Section 3.4.1.1 of NUREG/CR-6716 [63], the neutron dose rate decreased constantly and approximately exponentially with increasing cooling time over the range of cooling times analyzed.

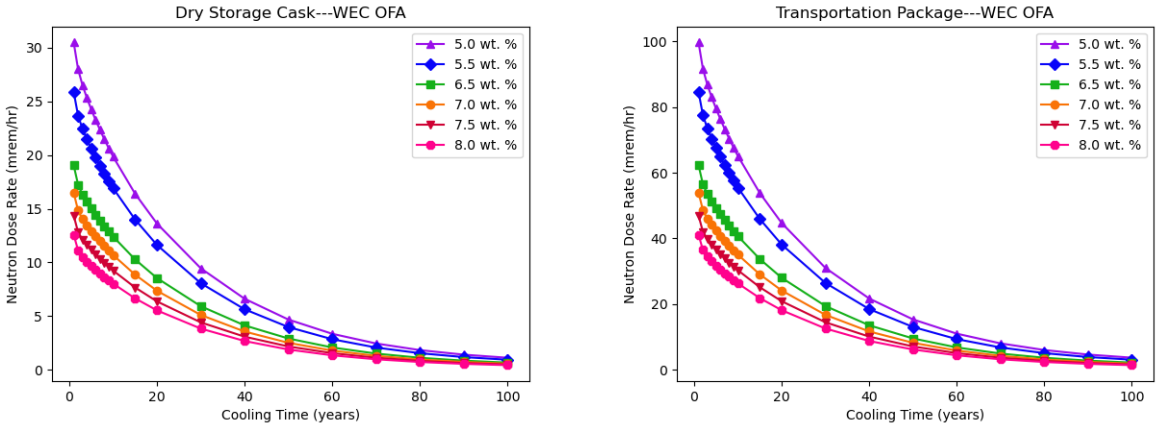

Figure 7-7 Neutron Dose Rate Trends of Variation with PWR Fuel Cooling Time (years)

7.1.3.2 Gamma Dose Rate Trends

The graphs in Figure 7-8 illustrate the effects on the primary gamma dose rate of varying enrichment for PWR fuel at constant burnup (75 GWd/MTU) at several different cooling times. Primary gamma dose rates for a dry storage cask and a transportation package are provided. These graphs show that the gamma dose rate decreases very quickly between 5 and 20 yr of cooling time as the short-lived fission products decay. After 20 yr of cooling time, the dose rate decreases exponentially. This same effect was observed at lower enrichments and burnups in Section 3.4.1.2 of NUREG/CR-6716 [63].

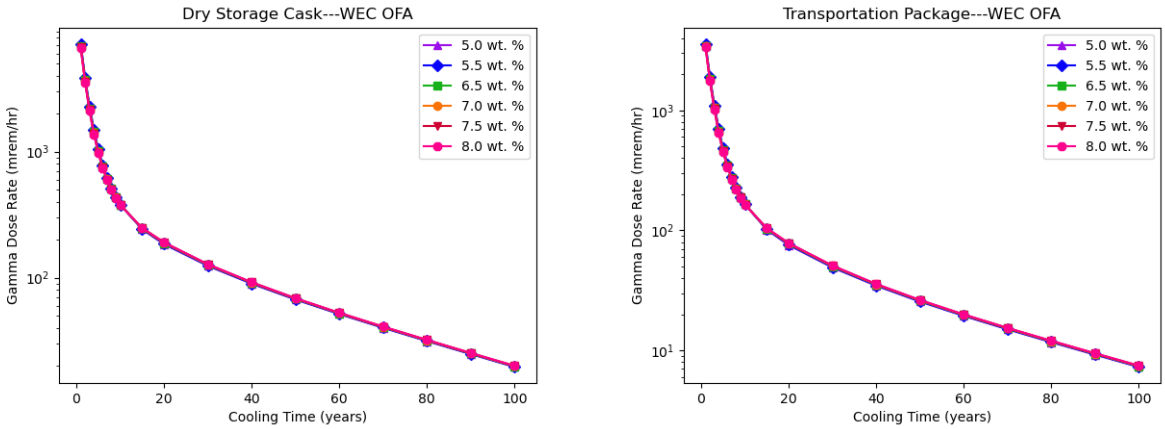

Figure 7-8 Primary Gamma Dose Rate Trends of Variation with PWR Fuel Cooling Time (years)

7.1.3.3 Cobalt-60 Dose Rate Trends

The graphs in Figure 7-9 illustrate the effects on the ^{60}Co dose rate of varying enrichment for PWR fuel at constant burnup (75 GWd/MTU) at several different cooling times. Cobalt-60 dose rates for a dry storage cask and a transportation package are provided. These graphs show that for all cooling times analyzed, the ^{60}Co dose rate decreased with increasing fuel enrichment. At a constant burnup of 75 GWd/MTU, the ^{60}Co dose rate was observed to be more sensitive to fuel enrichment than the primary gamma dose rate but was not as sensitive to fuel enrichment as the neutron dose rate.

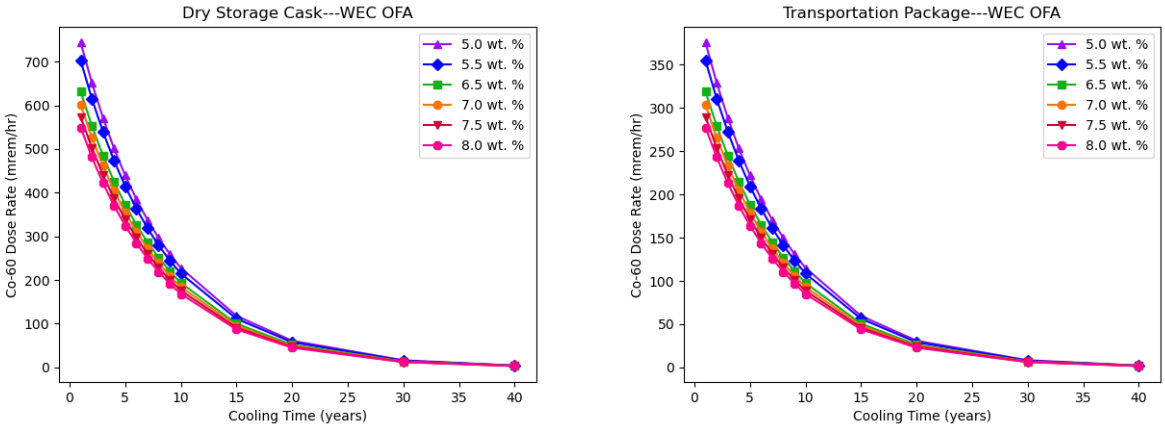

Figure 7-9 Cobalt-60 Dose Rate Trends of Variation with PWR Fuel Cooling Time (years)

7.1.4 Specific Power

The effect of assembly specific power on cask dose rates was analyzed for 5.0, 6.5, and 8.0 wt % ^{235}U PWR fuel. The fuel was burned up to 75 GWd/MTU using specific powers of 15, 20, 30, 40, and 50 MW/MTU.

7.1.4.1 Neutron Dose Rate Trends

Figure 7-10 illustrates the effects on the neutron dose rate of varying specific power for PWR fuel with 8 wt % enrichment at fixed assembly average burnup (75 GWd/MTU) over a range of cooling times. The graphs in Figure 7-11 illustrate these effects at different initial enrichments and cooling time at fixed assembly average burnup (75 GWd/MTU). The slight burnup at low cooling times shows the importance of the contribution of ^{242}Cm (half-life = 162.8 days) to the neutron source term. These graphs show that neutron dose rate increases with increasing specific power, and the effects are slightly greater for a higher initial fuel enrichment (e.g., 8 wt %) compared to a lower initial fuel enrichment (e.g., 5 wt %). These effects decrease with increasing specific power beyond approximately 2 and 4 yr of cooling for the fuel with an initial enrichment of 5 wt % and 8 wt %, respectively, and increase with increasing specific power at shorter cooling times. The relatively small effect of specific power on the neutron dose rate was also observed for 3.5 wt % fuel burned to 40 GWd/MTU over a range of specific powers in Section 3.4.2.4 of NUREG/CR-6716 [63]. As shown in Figure 7-12, for a given cooling time (5 yr), the effect of specific power on neutron dose rate slightly increases with increasing burnup.

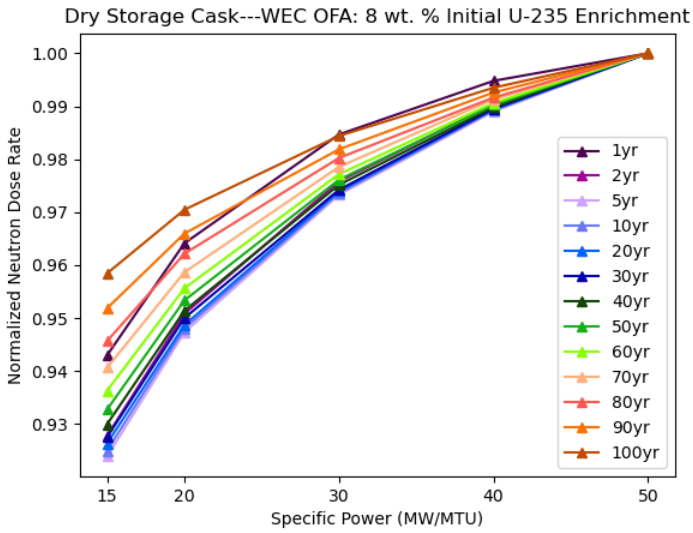

Figure 7-10 PWR Neutron Dose Rate Trends of Variation with Specific Power (MW/MTU) and Cooling Time (years) (Normalization to Highest Dose Rate Value at Each Cooling Time)

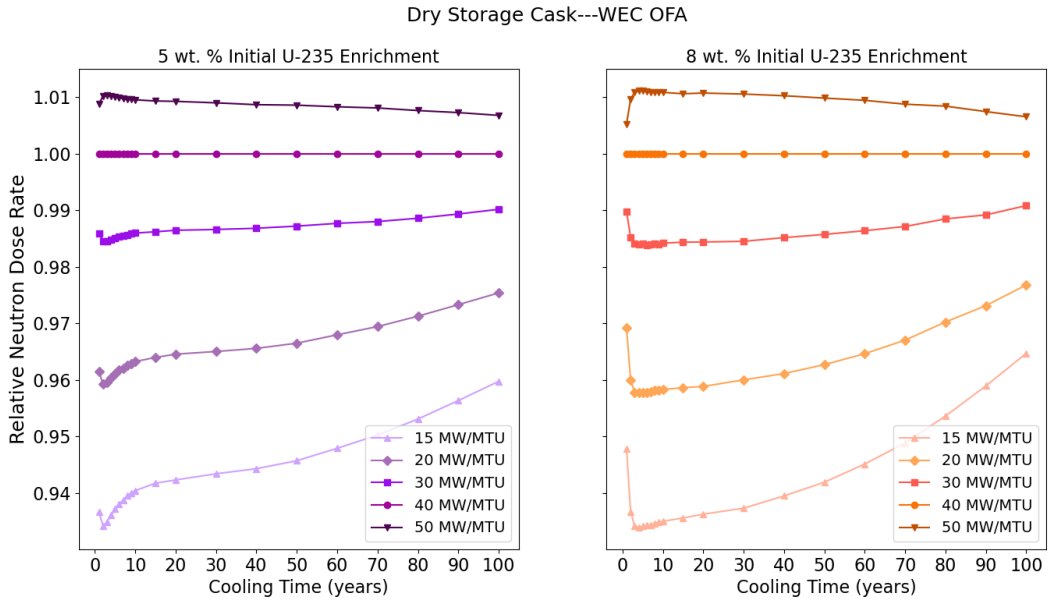

Figure 7-11 Comparative Effects of Varying Specific Power on Neutron Dose Rate from PWR Fuel with Different Enrichments (Normalization to Dose Rate Values for a 40 MW/MTU Specific Power)

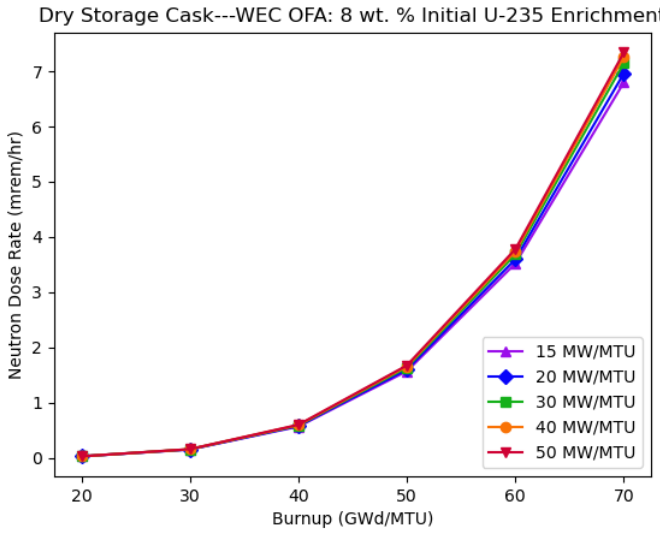

Figure 7-12 Neutron Dose Rate Trends of Variation with PWR Specific Power (MW/MTU) and Burnup (GWd/MTU)

7.1.4.2 Gamma Dose Rate Trends

Figure 7-13 illustrates the effects on the primary gamma dose rate of varying specific power for PWR fuel with 8 wt % enrichment at fixed assembly average burnup (75 GWd/MTU) over a range of cooling times. The graphs in Figure 7-14 illustrate these effects at different initial enrichments and cooling time at fixed assembly average burnup (75 GWd/MTU). These graphs show that primary gamma dose rate increases with increasing specific power within the time interval 1–100 yr. Specific power variations have approximately the same relative effects on primary gamma dose rate produced by fuel with different enrichments. Maximum specific power effects were achieved for the 1-year cooling time, indicating that the concentrations of the shorter-lived fission products ^{144}Ce, ^{106}Ru, and ^{134}Cs are more sensitive to the specific power than the concentrations of the longer-lived fission products ^{154}Eu, ^{137}Cs, and ^{90}Sr. Beyond an approximately 20-year cooling time, the primary gamma dose rate decreases with cooling time at a rate that is independent of specific power. These same effects were observed for 3.5 wt % fuel burned to 40 GWd/MTU over a range of specific powers in Section 3.4.2.4 of NUREG/CR-6716 [63]. As shown in Figure 7-15, for a given cooling time (5 yr), the effect of specific power on primary gamma dose rate increases with increasing burnup.

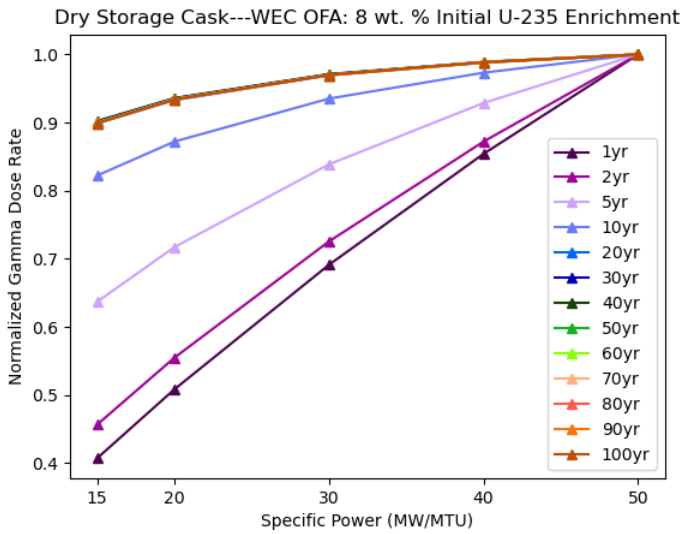

Figure 7-13 PWR Primary Gamma Dose Rate Trends of Variation with Specific Power (MW/MTU) and Cooling Time (years) (Normalization to Highest Dose Rate Value at Each Cooling Time)

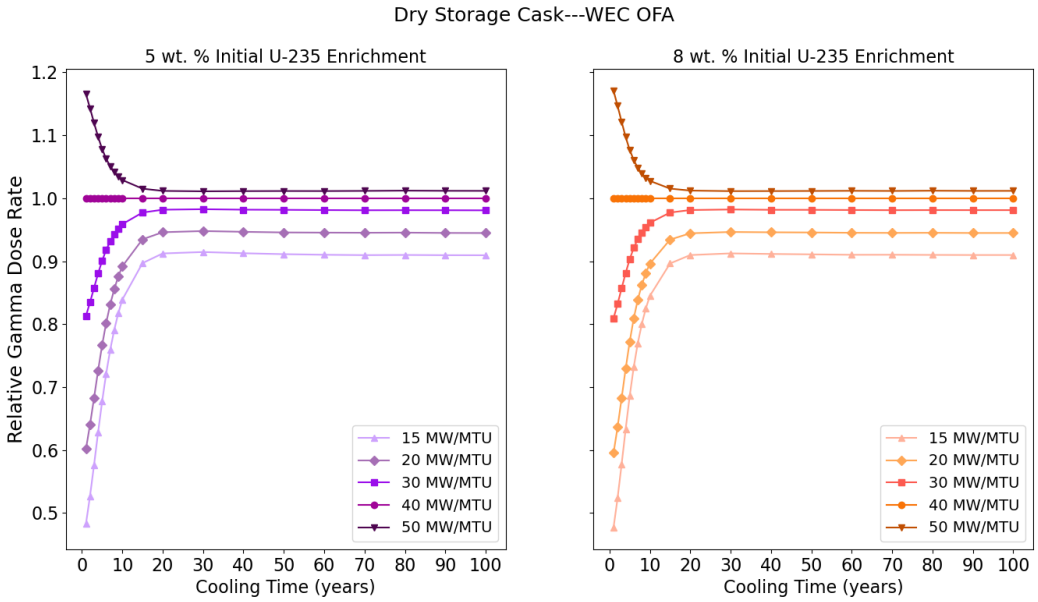

Figure 7-14 Comparative Effects of Varying Specific Power on Primary Gamma Dose Rate from PWR Fuel with Different Enrichments (Normalization to Dose Rate Values for a 40 MW/MTU Specific Power)

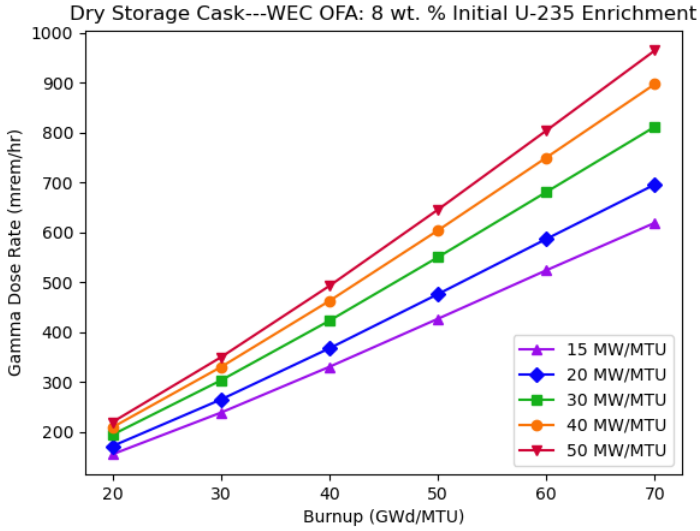

Figure 7-15 Primary Gamma Dose Rate Trends of Variation with PWR Specific Power (MW/MTU) and Burnup (GWd/MTU)

7.1.4.3 Cobalt-60 Dose Rate Trends

Figure 7-16 illustrates the effects on the ^{60}Co dose rate of varying specific power for PWR fuel with 8 wt % enrichment at fixed assembly average burnup (75 GWd/MTU) over a range of cooling times. The graphs in Figure 7-17 illustrate these effects at different initial enrichments and cooling time at fixed assembly average burnup (75 GWd/MTU). These graphs show that ^{60}Co dose rate increases with increasing specific power over the range of cooling times analyzed and the effects are independent of initial fuel enrichment. For a given cooling time (5 yr), the effect of specific power on ^{60}Co dose rate increases with increasing burnup.

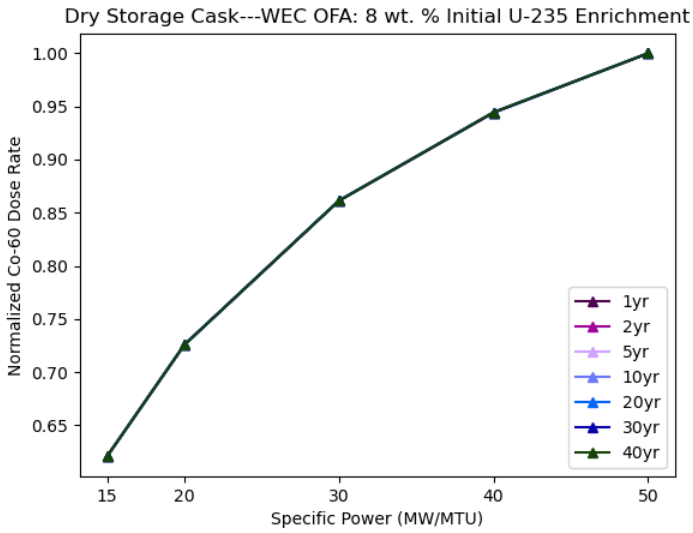

Figure 7-16 PWR ^{60}Co Dose Rate Trends of Variation with Specific Power (MW/MTU) and Cooling Time (years) (Normalization to Highest Dose Rate Value at Each Cooling Time)

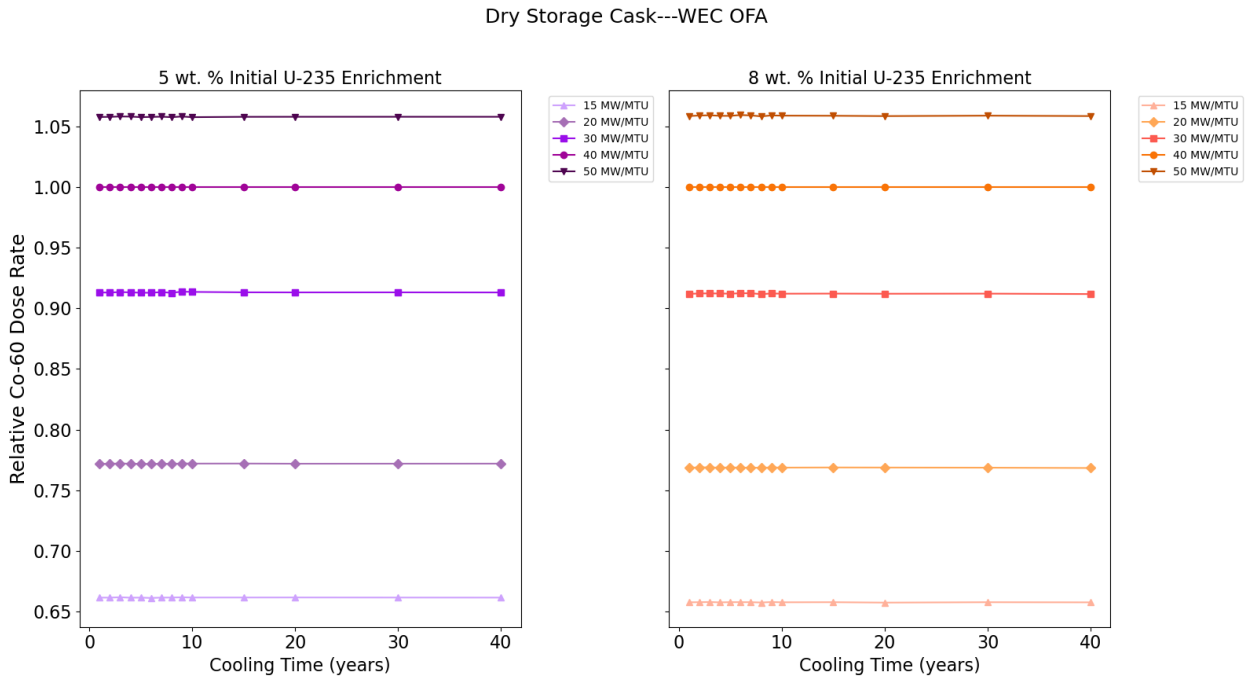

Figure 7-17 Comparative Effects of Varying Specific Power on ^{60}Co Dose Rate from PWR Fuel with Different Enrichments (Normalization to Dose Rate Values for a 40 MW/MTU Specific Power)

7.1.5 Soluble Boron

The effect of soluble boron concentration in the coolant on cask dose rates was presented for 5 and 8 wt % ^{235}U PWR fuel. The fuel was burned up to 75 GWd/MTU using soluble boron concentrations of 600, 1,000, and 1,800 ppm. In each case, the soluble boron level was held at a constant value during the entire irradiation period.

7.1.5.1 Neutron Dose Rate Trends

Figure 7-18 illustrates the effects on the neutron dose rate of varying average boron concentration (in ppm) in the coolant for PWR fuel with 8 wt % enrichment at fixed assembly average burnup (75 GWd/MTU) over a range of cooling times. The graphs in Figure 7-19 illustrate these effects at different initial enrichments and cooling times at fixed assembly average burnup (75 GWd/MTU). These graphs show that neutron dose rate increases with increasing average soluble boron concentration, and the effects are greater for a higher initial fuel enrichment (e.g., 8 wt %) compared with a lower initial fuel enrichment (e.g., 5 wt %). These effects significantly increase with increasing fuel cooling time beyond 10 yr of cooling. As shown in Figure 7-20, for a given cooling time (5 yr), the effect of soluble boron concentration on neutron dose rate increases with increasing burnup.

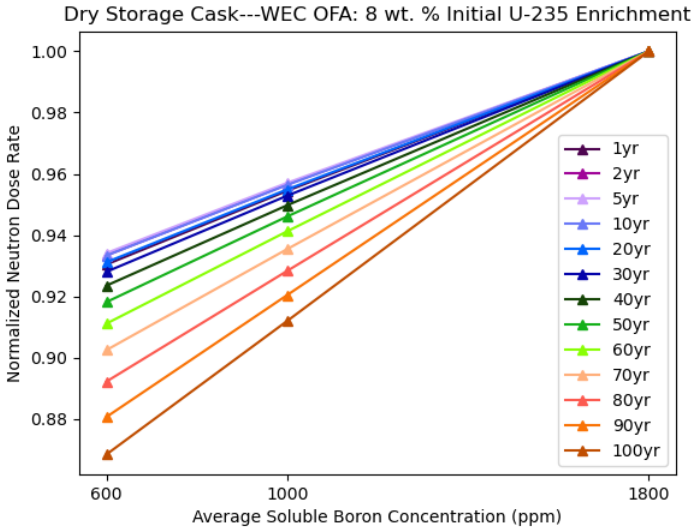

Figure 7-18 PWR Neutron Dose Rate Trends of Variation with Soluble Boron Concentration (ppm) and Cooling Time (year) (Normalization to Highest Dose Rate Value at Each Cooling Time)

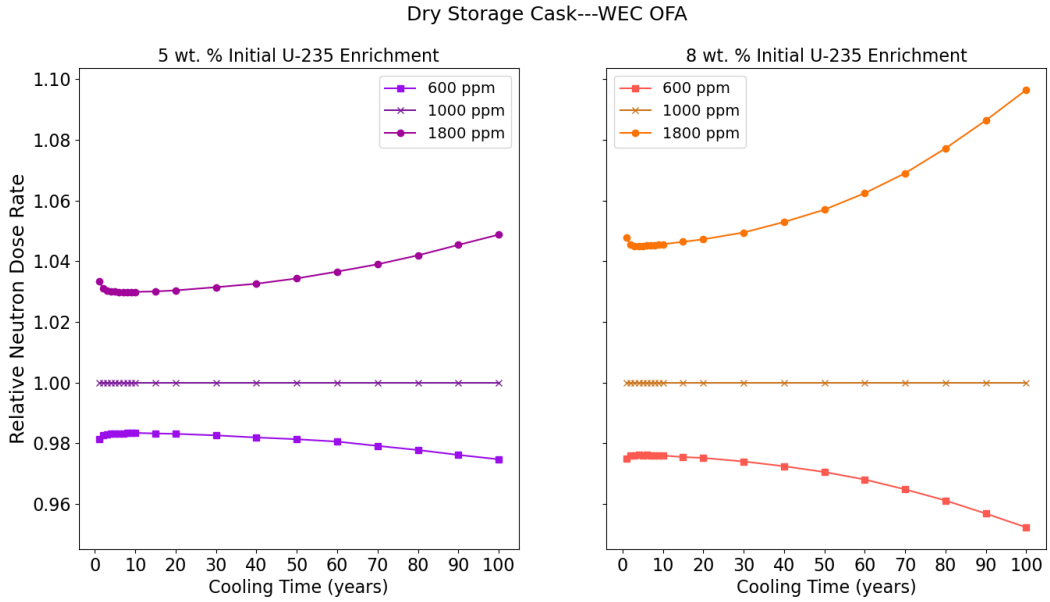

Figure 7-19 Comparative Effects of Varying Average Boron Concentration on Neutron Dose Rate from PWR Fuel with Different Enrichments (Normalization to Dose Rate Values for a 1,000 ppm Boron Concentration)

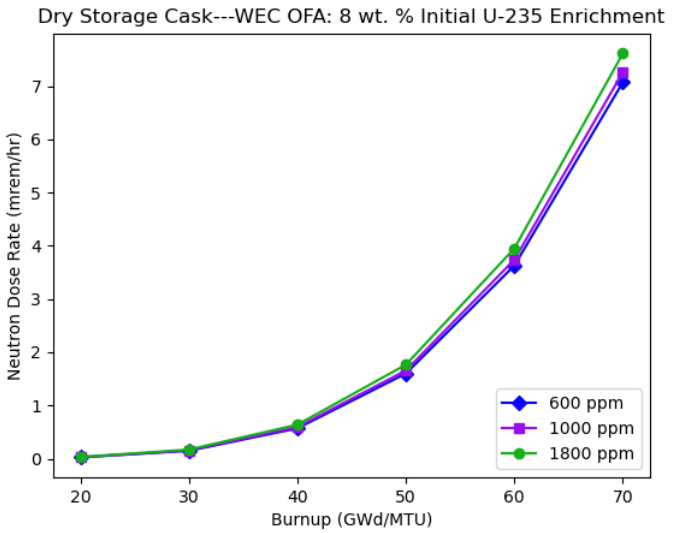

Figure 7-20 Neutron Dose Rate Trends of Variation with PWR Average Boron Concentration and Burnup (GWd/MTU)

7.1.5.2 Gamma Dose Rate Trends

Figure 7-21 illustrates the effects on the primary gamma dose rate of varying average boron concentration (in ppm) in the coolant for PWR fuel with 8 wt % enrichment at fixed assembly average burnup (75 GWd/MTU) over a range of cooling times. The graphs in Figure 7-22 illustrate these effects at different initial enrichments and cooling time at fixed assembly average burnup (75 GWd/MTU). The effects are greater for the 5 wt % enrichment compared to the 8 wt % enrichment up to 50 yr of cooling. For both enrichments, maximum effects are observed for the 10-year cooling time. The effect of soluble boron concentration was smaller for gamma dose rates than for neutron dose rates. As shown in Figure 7-23, for a given cooling time (5 yr), the effect of the soluble boron concentration on the primary gamma dose rate increases with increasing burnup.

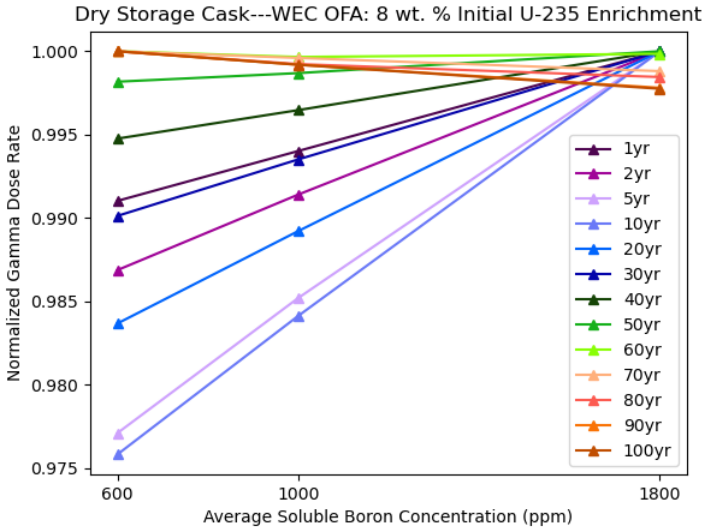

Figure 7-21 PWR Primary Gamma Dose Rate Trends of Variation with Soluble Boron Concentration (ppm) and Cooling Time (year) (Normalization to Highest Dose Rate Value at Each Cooling Time)

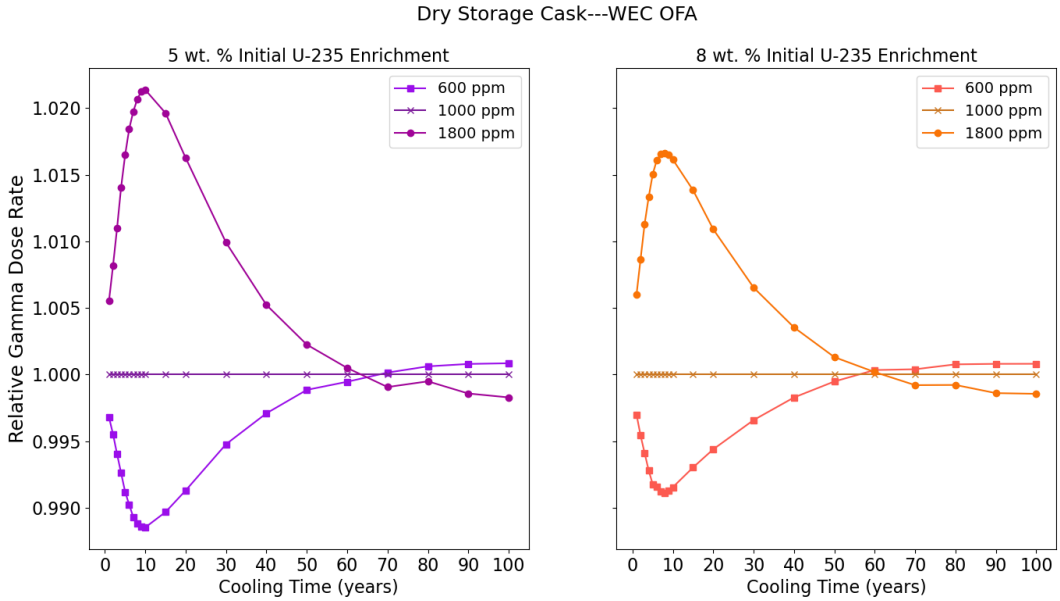

Figure 7-22 Comparative Effects of Varying Average Boron Concentration on Primary Gamma Dose Rate from PWR Fuel with Different Enrichments (Normalization to Dose Rate Values for a 1,000 ppm Boron Concentration)

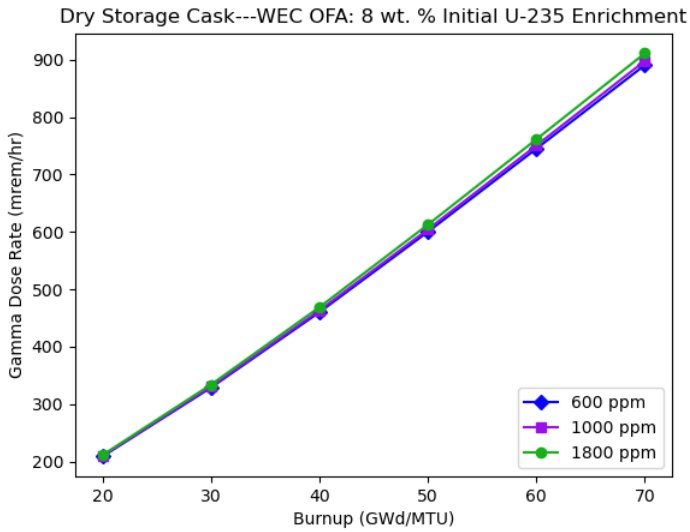

Figure 7-23 Primary Gamma Dose Rate Trends of Variation with PWR Average Boron Concentration and Burnup (GWd/MTU)

7.1.5.3 Cobalt-60 Dose Rate Trends

Figure 7-24 illustrates the effects on the ^{60}Co dose rate of varying average boron concentration (in ppm) in the coolant for PWR fuel with 8 wt % enrichment at fixed assembly average burnup (75 GWd/MTU) over a range of cooling times. The graphs in Figure 7-25 illustrate these effects at different initial enrichments and cooling time at fixed assembly average burnup (75 GWd/MTU). These graphs show that ^{60}Co dose rate increases with increasing average soluble boron concentration, and the effects are slightly greater for a higher initial fuel enrichment (e.g., 8 wt %) compared to a lower initial fuel enrichment (e.g., 5 wt %). Overall, the ^{60}Co dose rate is relatively insensitive to the average soluble boron concentration, as the dose rates only changed by approximately 1%. As expected, these effects do not vary with fuel cooling time. Similar to the primary gamma dose rate, for a given cooling time (5 yr) the effect of soluble boron concentration on ^{60}Co dose rate is insensitive to increasing burnup.

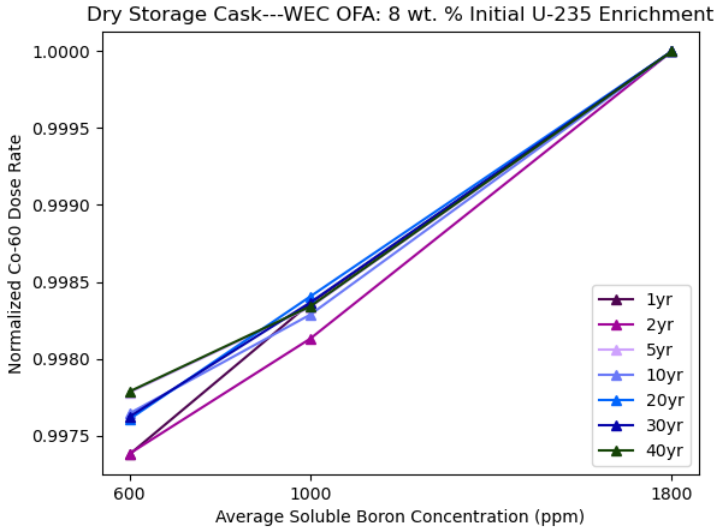

Figure 7-24 PWR ^{60}Co Dose Rate Trends of Variation with Soluble Boron Concentration (ppm) and Cooling Time (years) (Normalization to Highest Dose Rate Value at Each Cooling Time)

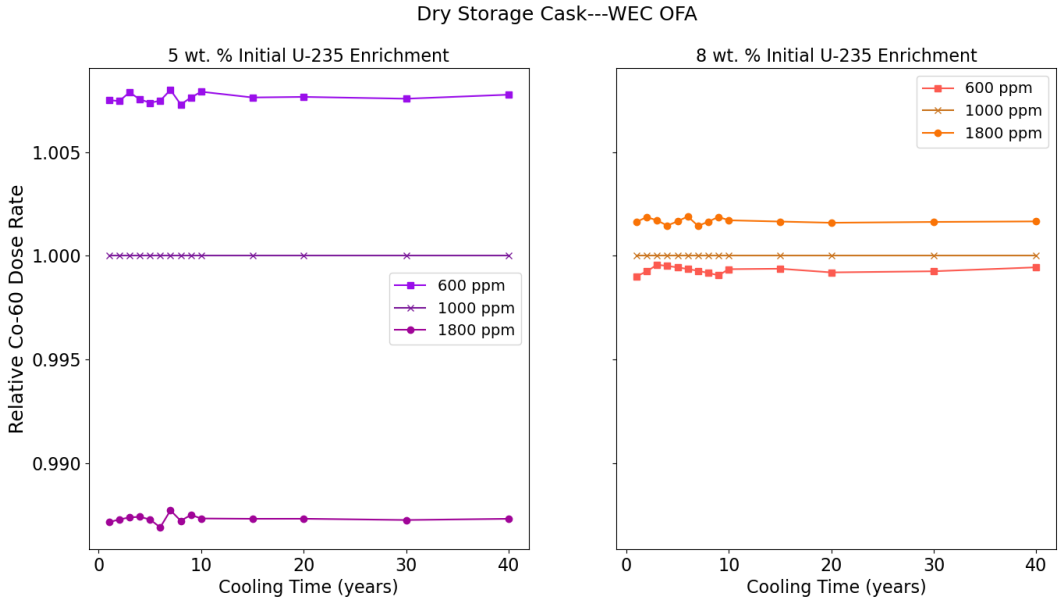

Figure 7-25 Comparative Effects of Varying Average Boron Concentration on ^{60}Co Dose Rate from PWR Fuel with Different Enrichments (Normalization to Dose Rate Values for a 1,000 ppm Boron Concentration)

7.1.5.4 Boron Letdown Curve vs. Average Boron Value

The effect of modeling assembly soluble boron concentration using a letdown curve compared to using the average boron concentration on dry storage cask dose rates was presented for 5 and 8 wt % ^{235}U PWR fuel. The fuel was burned up to 75 GWd/MTU using a boron letdown curve or the corresponding average soluble boron value. The letdown curve (adapted from the LEU+ letdown curves in [17]) and corresponding burnup-weighted average value are provided in Figure 7-26. The stepped-down specific power used in [17] was also used for this study.

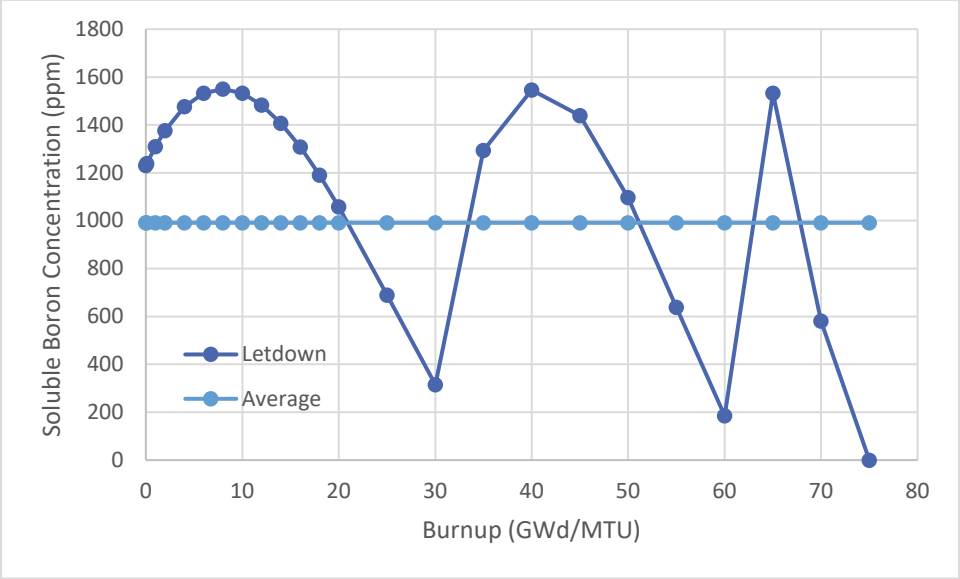

Figure 7-26 Boron Letdown Curve and Corresponding Average Boron Value

7.1.5.5 Neutron Dose Rate Trends

A comparison between the effects of the average soluble boron concentration and the effects of a boron letdown curve on neutron dose rate is shown in Figure 7-27. These graphs show that the neutron dose rate when using a boron letdown curve matched the dose rate when using the associated average boron concentration very closely. The difference in the dose rates between each method was consistent and negligible across all analyzed cooling times and enrichments.

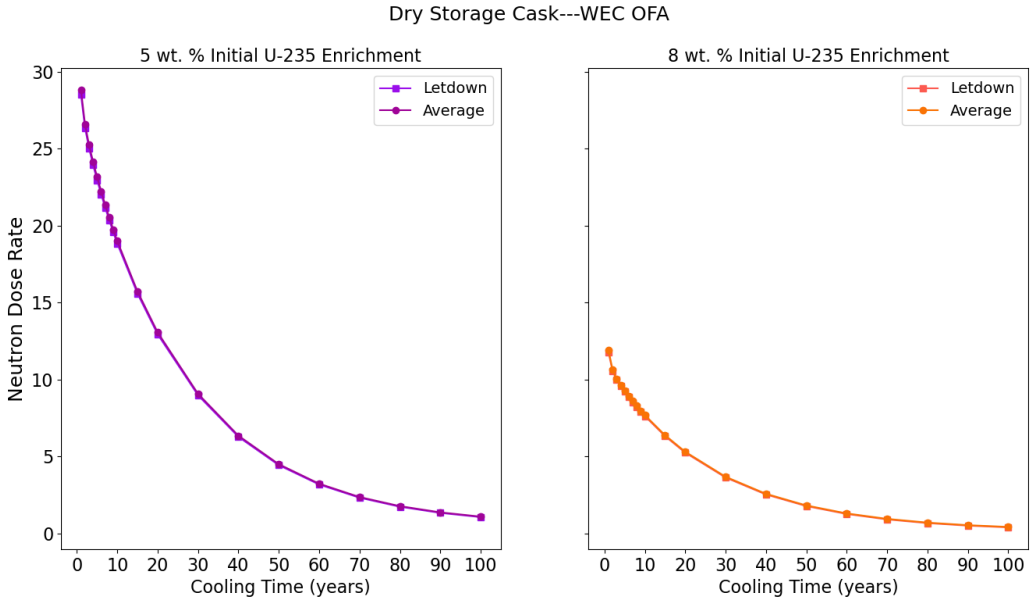

Figure 7-27 Comparative Effects of an Average Boron Concentration and a Boron Letdown Curve on Primary Neutron Dose Rate

7.1.5.6 Gamma Dose Rate Trends

A comparison between the effects of the average soluble boron concentration and the effects of a boron letdown curve on the primary gamma dose rate is shown in Figure 7-28. These graphs show that the primary gamma dose rate when using a boron letdown curve matched the dose rate when using the associated average boron concentration very closely. The difference in the dose rates between each method was consistent and negligible across all analyzed cooling times and enrichments.

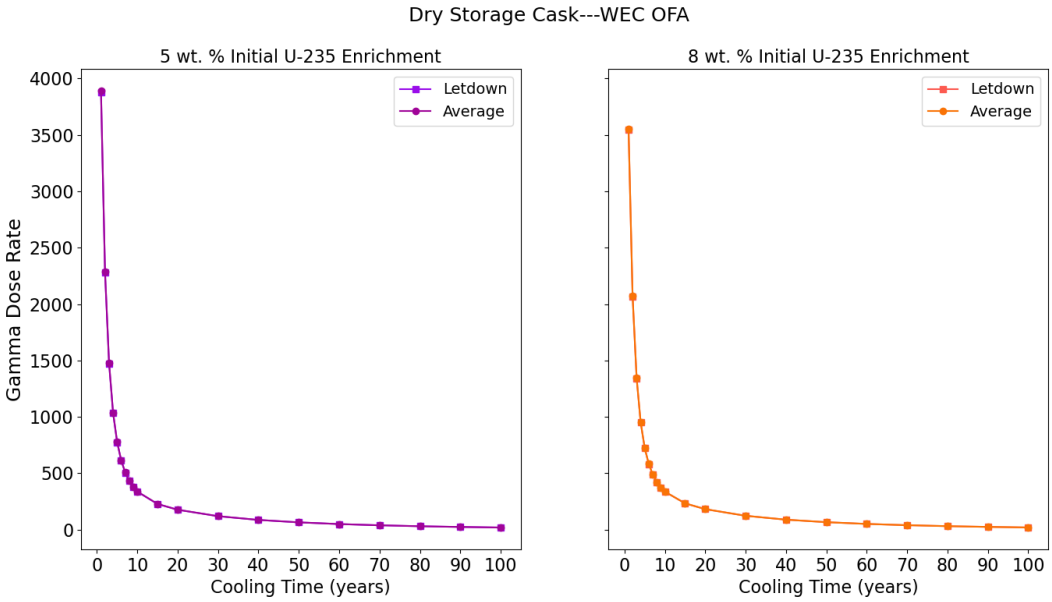

Figure 7-28 Comparative Effects of an Average Boron Concentration and a Boron Letdown Curve on Primary Gamma Dose Rate

7.1.5.7 Cobalt-60 Dose Rate Trends

The ^{60}Co dose rate was highly insensitive to the use of a boron letdown curve compared to the use of the associated average boron concentration. The difference in the dose rates between each method was consistent and negligible across all analyzed cooling times and enrichments.

7.1.6 Moderator Density/Temperature

The effect of assembly moderator density on cask dose rates was presented for 5 and 8 wt % ^{235}U PWR fuel. The moderator temperature was also appropriately varied along with the moderator density. The moderator density–temperature pairs are provided in Section 3.1.

7.1.6.1 Neutron Dose Rate Trends

Figure 7-29 illustrates the effects of moderator density (in g/cm^3), which also relates to the moderator temperature, on the neutron dose rate for PWR fuel with 8 wt % enrichment at fixed assembly average burnup (75 GWd/MTU) over a range of cooling times. The graphs in Figure 7-30 illustrate the moderator temperature effect for different initial fuel enrichments and cooling times at fixed assembly average burnup (75 GWd/MTU) relative to the baseline. The neutron dose rate decreases with increasing moderator density. The moderator density effect is slightly greater for 8 wt % enrichment compared to 5 wt % enrichment. The variation is approximately 5 percent for 5 wt % fuel and 10 percent for 8 wt % fuel in the moderator density range of approximately 0.6–0.7 g/cm^3. The trends observed in this analysis are consistent with the analysis in Section 3.4.2.5 in NUREG/CR-6716 [63], which was performed for BWR fuel with 4 wt % enrichment and 40 GWd/MTU burnup. As shown in Figure 7-31, for a given cooling time (5 yr), the effect of moderator density on neutron dose rate increases with increasing burnup, and the effect is slightly greater at 8 wt % enrichment than at 5 wt %.

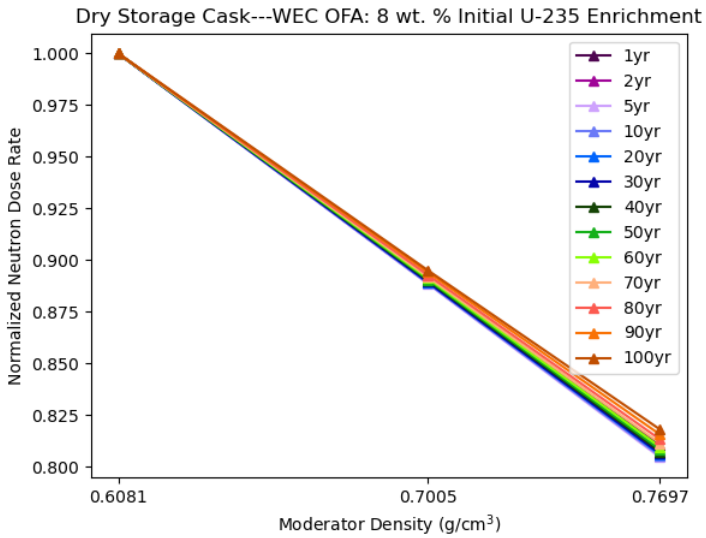

Figure 7-29 Neutron Dose Rate Trends of Variation with PWR Moderator Density (g/cm^3) and Cooling Time (years) (Normalization to Highest Dose Rate Value at Each Cooling Time)

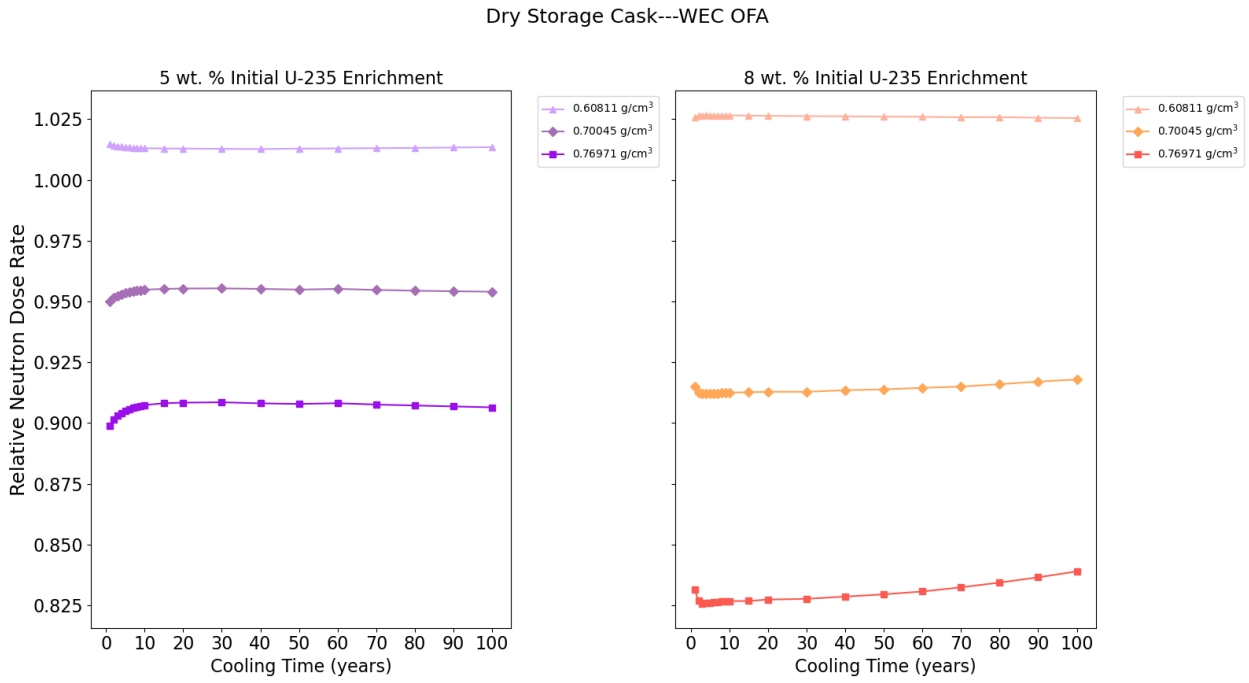

Figure 7-30 Comparative Effects of Varying Moderator Density on Neutron Dose Rate from PWR Fuel with Different Enrichments (Normalization to Dose Rate Values for a 0.63 g/cm³ Moderator Density)

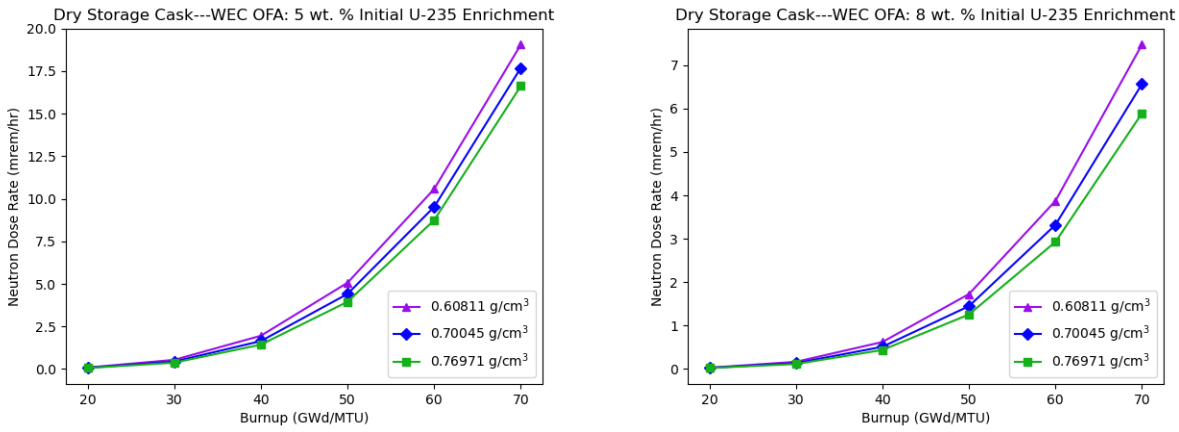

Figure 7-31 Neutron Dose Rate Trends of Variation with PWR Moderator Density (g/cm³) and Burnup (GWd/MTU)

7.1.6.2 Gamma Dose Rate Trends

Figure 7-32 illustrates the effect of moderator density, which also relates to the moderator temperature, on the primary gamma dose rate for PWR fuel with 8 wt % enrichment at fixed assembly average burnup (75 GWd/MTU) over a range of cooling times. The graphs in Figure 7-33 illustrate these effects at different initial enrichments and cooling time at fixed assembly average burnup (75 GWd/MTU). The gamma dose rate decreases with increasing moderator density until a cooling time of approximately 70 yr, beyond which the effect is mitigated. These effects are slightly greater at 8 wt % enrichment compared to 5 wt % enrichment. The trends up to approximately 70 yr of cooling time in this analysis are consistent with the trends described in Section 3.4.2.5 in NUREG/CR-6716 [63], which was performed for BWR fuel with 4 wt % enrichment and 40 GWd/MTU burnup. As shown in Figure 7-34, for a given cooling time (5 yr), the effect of moderator density on primary gamma dose rate increases with increasing burnup.

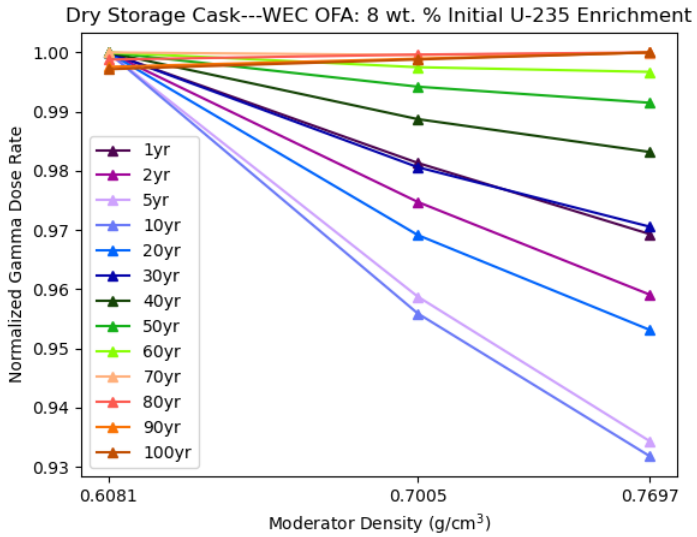

Figure 7-32 Primary Gamma Dose Rate Trends of Variation with PWR Moderator Density (g/cm^3) and Cooling Time (years) (Normalization to Highest Dose Rate Value at Each Cooling Time)

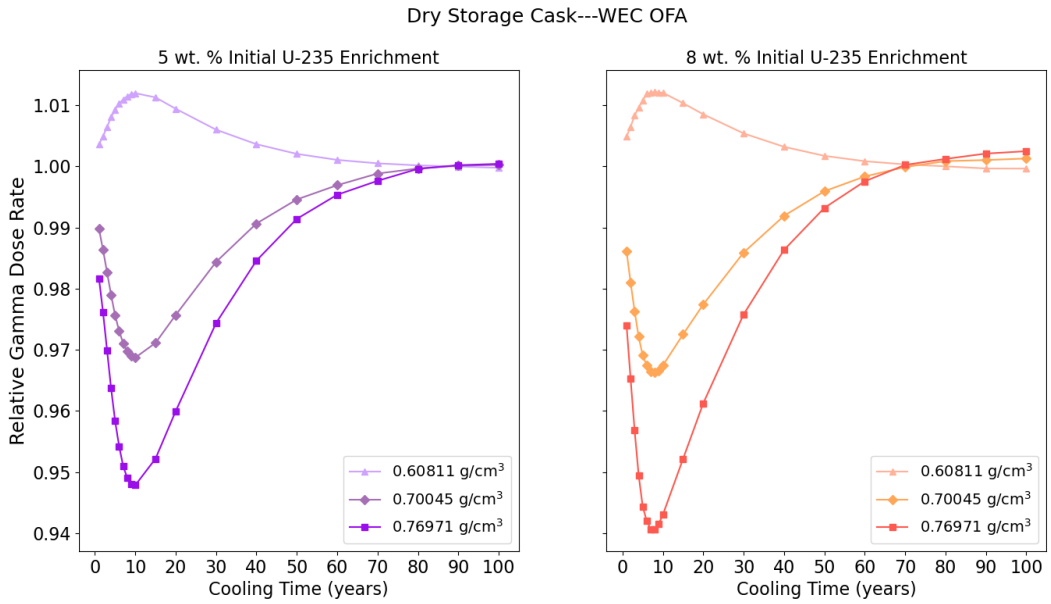

Figure 7-33 Comparative Effects of Varying Moderator Density on Primary Gamma Dose Rate from PWR Fuel with Different Enrichments (Normalization to Dose Rate Values for a 0.63 g/cm³ Moderator Density)

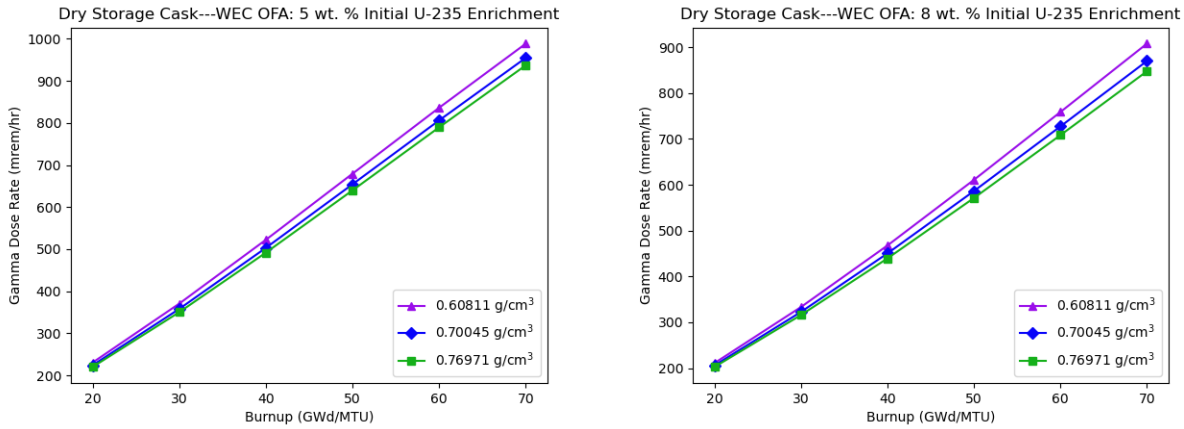

Figure 7-34 Primary Gamma Dose Rate Trends of Variation with PWR Moderator Density (g/cm³) and Burnup (GWd/MTU)

7.1.6.3 Cobalt-60 Dose Rate Trends

Figure 7-35 illustrates the effect of moderator density, which also relates to the moderator temperature effects, on the ^{60}Co dose rate for PWR fuel with 8 wt % enrichment at fixed

assembly average burnup (75 GWd/MTU) over a range of cooling times. The graphs in Figure 7-36 illustrate these effects at different initial enrichments and cooling time at fixed assembly average burnup (75 GWd/MTU). These graphs show that for all cooling times analyzed, the ^{60}Co dose rate decreases with increasing moderator density (and corresponding decreasing temperature) for 8 wt % fuel, and the opposite trend is displayed for 5 wt % fuel. ^{60}Co decreasing with increasing moderator density is also observed for 12 wt % fuel with 80 GWd/MTU burnup in [41] and is explained by the increased moderator density softening the relatively hard neutron spectrum and resulting in less neutron capture in ^{59}Co. For 5 wt % fuel, the relatively soft neutron spectrum results in ^{59}Co neutron capture increasing with increased moderator density and a corresponding higher ^{60}Co production. The (n,g) cross sections for ^{59}Co are provided in [64] and show the increasing cross section with decreasing neutron energy in the thermal range. As shown in Figure 7-37, for a given cooling time (5 yr), the ^{60}Co dose rate for 5 wt % fuel begins to increase with increasing moderator density at a burnup of 50 GWd/MTU, indicating that the trends are burnup- and enrichment-dependent. At 75 GWd/MTU, the effect of moderator density on the ^{60}Co dose rate was more significant at 5 wt % enrichment than at 8 wt % enrichment over all cooling times analyzed.

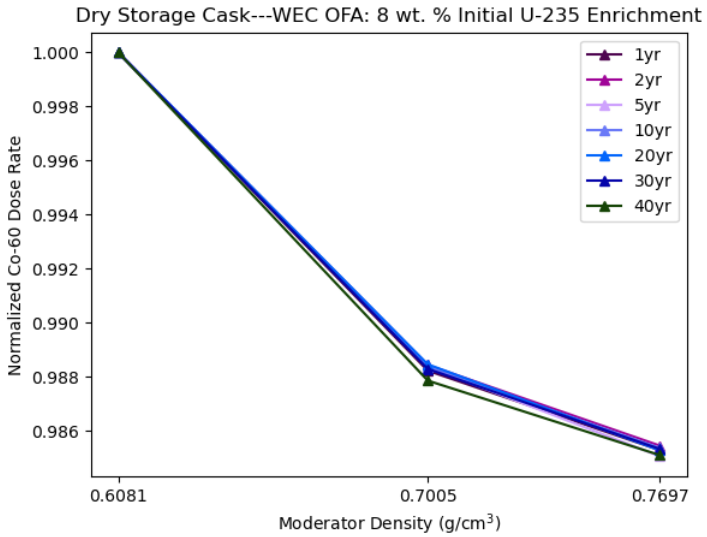

Figure 7-35 Cobalt-60 Dose Rate Trends of Variation with PWR Moderator Density (g/cm^3) and Cooling Time (years) (Normalization to Highest Dose Rate Value at Each Cooling Time)

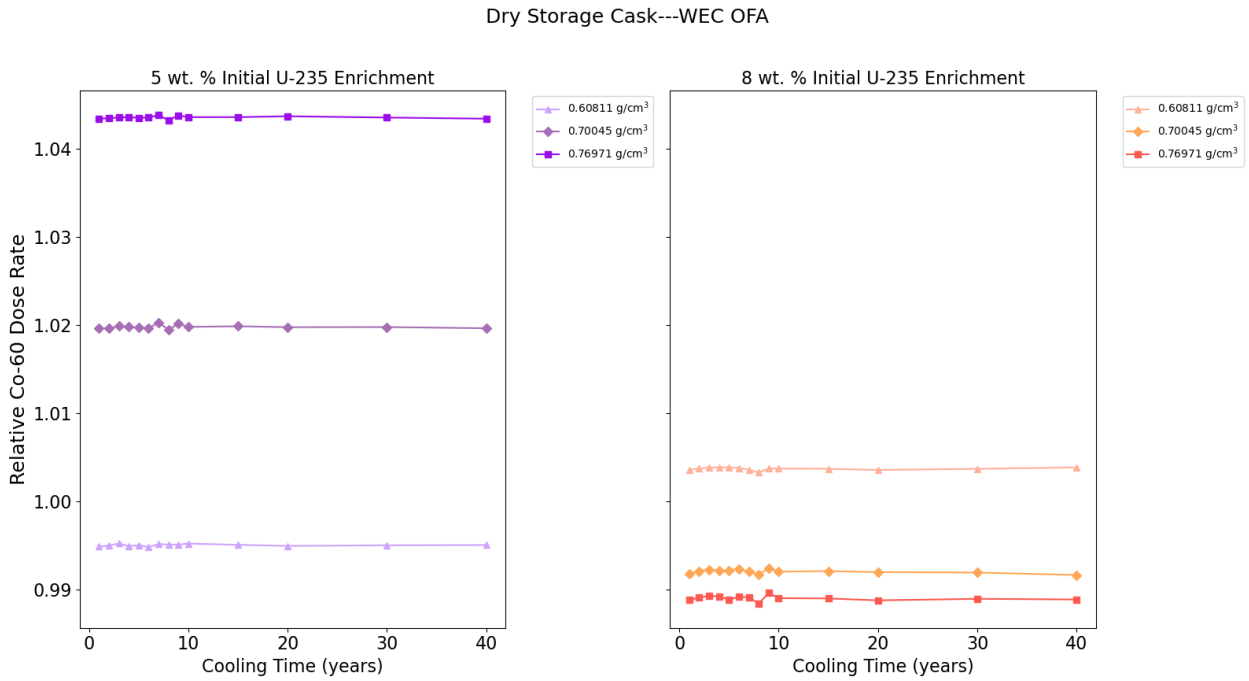

Figure 7-36 Comparative Effects of Varying Moderator Density on ^{60}Co Gamma Dose Rate from PWR Fuel with Different Enrichments (Normalization to Dose Rate Values for a 0.63 g/cm^3 Moderator Density)

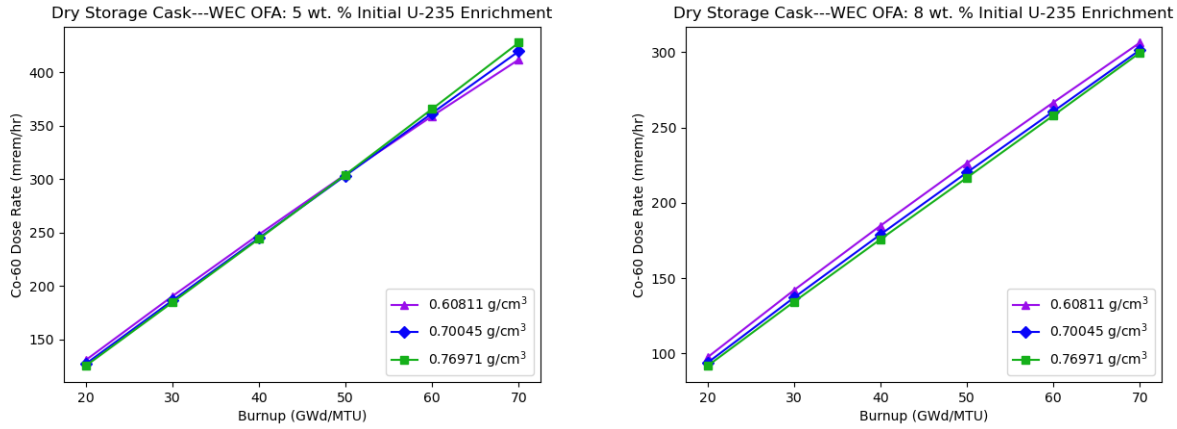

Figure 7-37 Cobalt-60 Dose Rate Trends of Variation with PWR Moderator Density (g/cm^3) and Burnup (GWd/MTU)

7.1.7 Fuel Temperature

The effect of fuel temperature on cask dose rates was presented for 5 and 8 wt % ^{235}U PWR fuel. The fuel temperatures analyzed are provided in Section 3.1.

7.1.7.1 Neutron Dose Rate Trends

Figure 7-38 illustrates the effects on the neutron dose rate of varying fuel temperature for PWR fuel with 8 wt % enrichment at fixed assembly average burnup (75 GWd/MTU) over a range of cooling times. The graphs in Figure 7-39 illustrate these effects at different initial enrichments and cooling times at fixed assembly average burnup (75 GWd/MTU). The effects were different at each enrichment analyzed. For 5 wt % enrichment, the neutron dose rate did not display a clear trend between cooling times of approximately 5 and 60 yr and generally increased with decreasing fuel temperature outside of this range. For 8 wt % enrichment, the neutron dose rate increased with increasing fuel temperature over the entire range of cooling times analyzed, and the effect was slightly reduced at long cooling times. As shown in Figure 7-40, for a given cooling time (5 yr), the effect of fuel temperature on neutron dose rate slightly increases with increasing burnup, and the effect is more pronounced at 8 wt % than at 5 wt % enrichment.

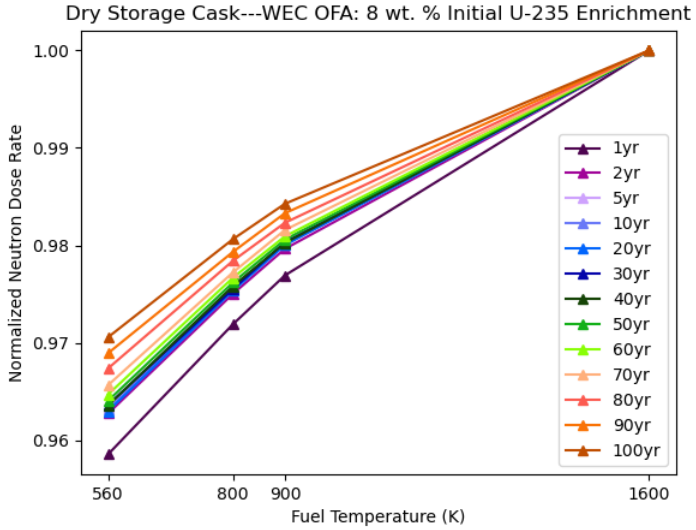

Figure 7-38 Neutron Dose Rate Trends of Variation with PWR Fuel Temperature (K) and Cooling Time (years) (Normalization to Highest Dose Rate Value at Each Cooling Time)

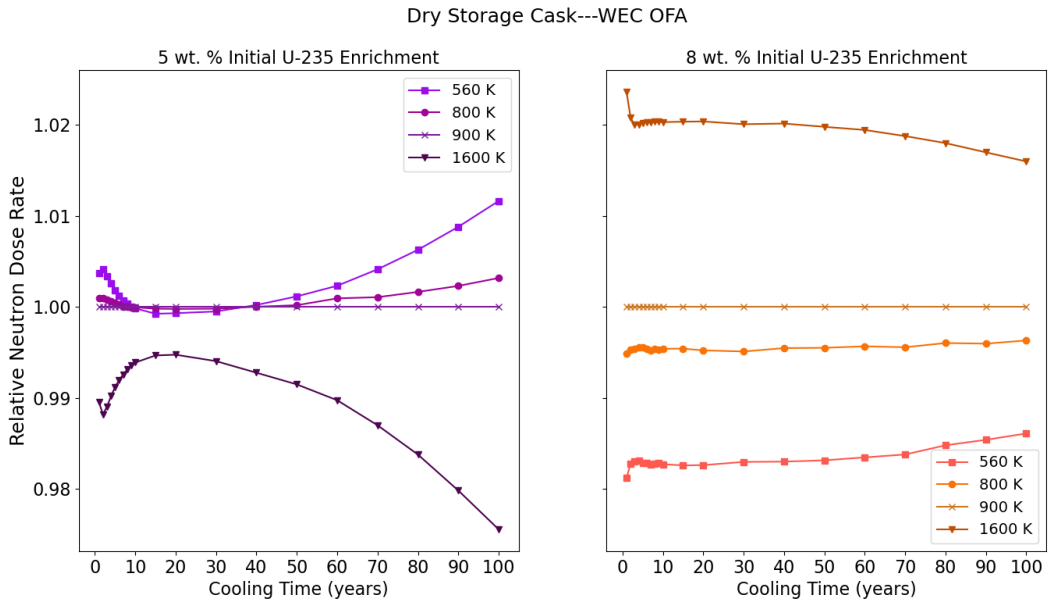

Figure 7-39 Comparative Effects of Varying Fuel Temperature on Neutron Dose Rate from PWR Fuel with Different Enrichments (Normalization to Dose Rate Values for a 900 K Fuel Temperature)

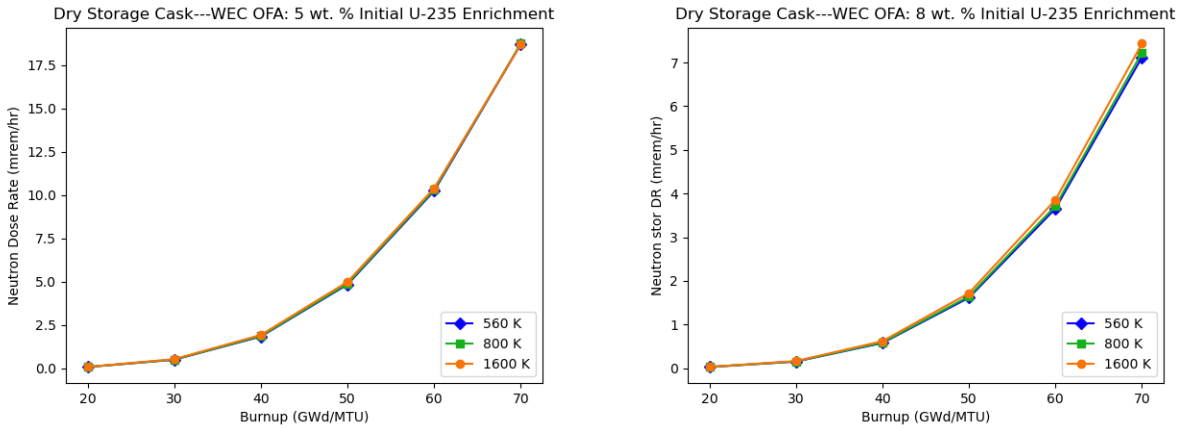

Figure 7-40 Neutron Dose Rate Trends of Variation with PWR Fuel Temperature and Burnup (GWd/MTU)

7.1.7.2 Gamma Dose Rate Trends

Figure 7-41 illustrates the effects on the primary gamma dose rate of varying fuel temperature for PWR fuel with 8 wt % enrichment at fixed assembly average burnup (75 GWd/MTU) over a

range of cooling times. The graphs in Figure 7-42 illustrate these effects at different initial enrichments and cooling times at fixed assembly average burnup (75 GWd/MTU). Temperature effects are greater for the 5 wt % enrichment compared with the 8 wt % enrichment. Maximum effects were observed at a cooling time of 15 yr. These graphs show that the primary gamma dose rate is relatively insensitive to fuel temperature, as the dose rate changed only by 1–2 percent. As shown in Figure 7-43, for a given cooling time (5 yr), the effect of fuel temperature on the primary gamma dose rate was insensitive to burnup.

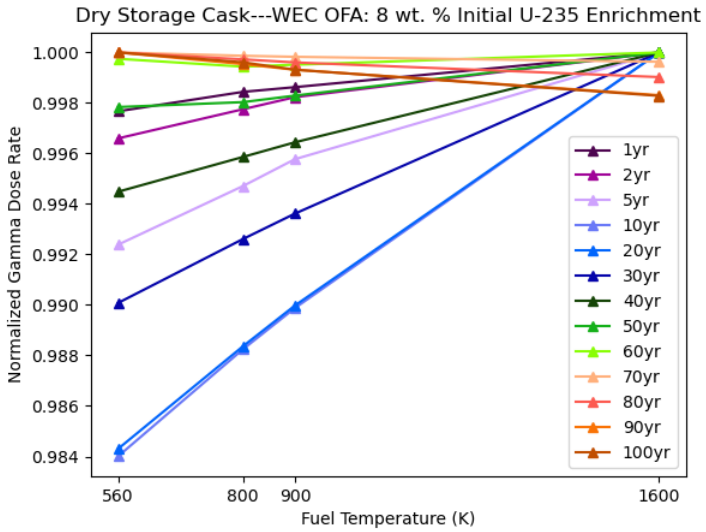

Figure 7-41 Primary Gamma Dose Rate Trends of Variation with PWR Fuel Temperature (K) and Cooling Time (years) (Normalization to Highest Dose Rate Value at Each Cooling Time)

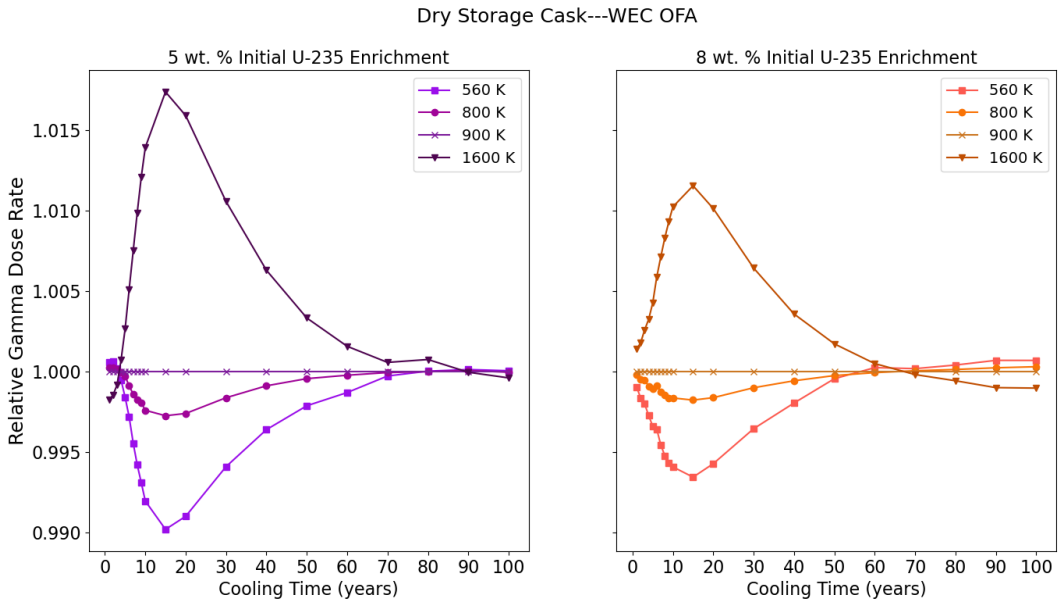

Figure 7-42 Comparative Effects of Varying Fuel Temperature on Primary Gamma Dose Rate from PWR Fuel with Different Enrichments (Normalization to Dose Rate Values for a 900 K Fuel Temperature)

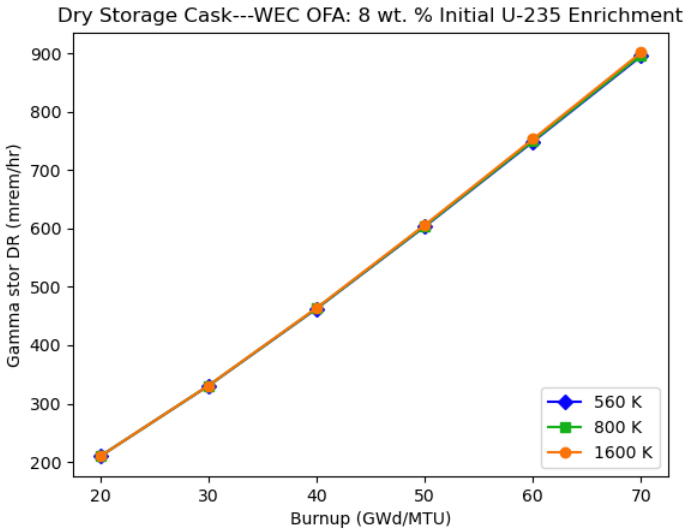

Figure 7-43 Primary Gamma Dose Rate Trends of Variation with PWR Fuel Temperature and Burnup (GWd/MTU)

7.1.7.3 Cobalt-60 Dose Rate Trends

Figure 7-44 illustrates the effects on the ^{60}Co dose rate of varying fuel temperature for PWR fuel with 8 wt % enrichment at fixed assembly average burnup (75 GWd/MTU) over a range of cooling times. The graphs in Figure 7-45 illustrate these effects at different initial enrichments and cooling times at fixed assembly average burnup (75 GWd/MTU). These graphs show that the ^{60}Co dose rate decreased with increasing fuel temperature. Fuel temperature effects are greater for the 5 wt % enrichment compared to the 8 wt % enrichment. Maximum effects are observed at a cooling time of 15 yr. As shown in Figure 7-46, for a given cooling time (5 yr), the effect of fuel temperature on the ^{60}Co dose rate increased very slightly with increasing burnup, and the effect was slightly greater at 5 wt % enrichment than at 8 wt % enrichment.

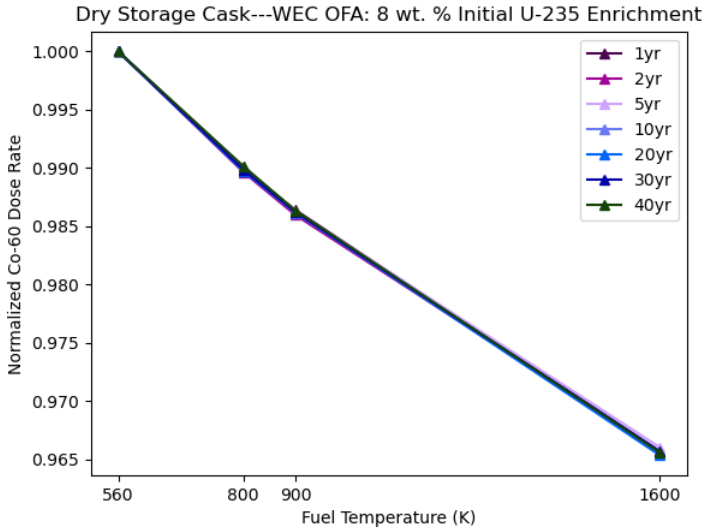

Figure 7-44 Cobalt-60 Dose Rate Trends of Variation with PWR Fuel Temperature (K) and Cooling Time (years) (Normalization to Highest Dose Rate Value at Each Cooling Time)

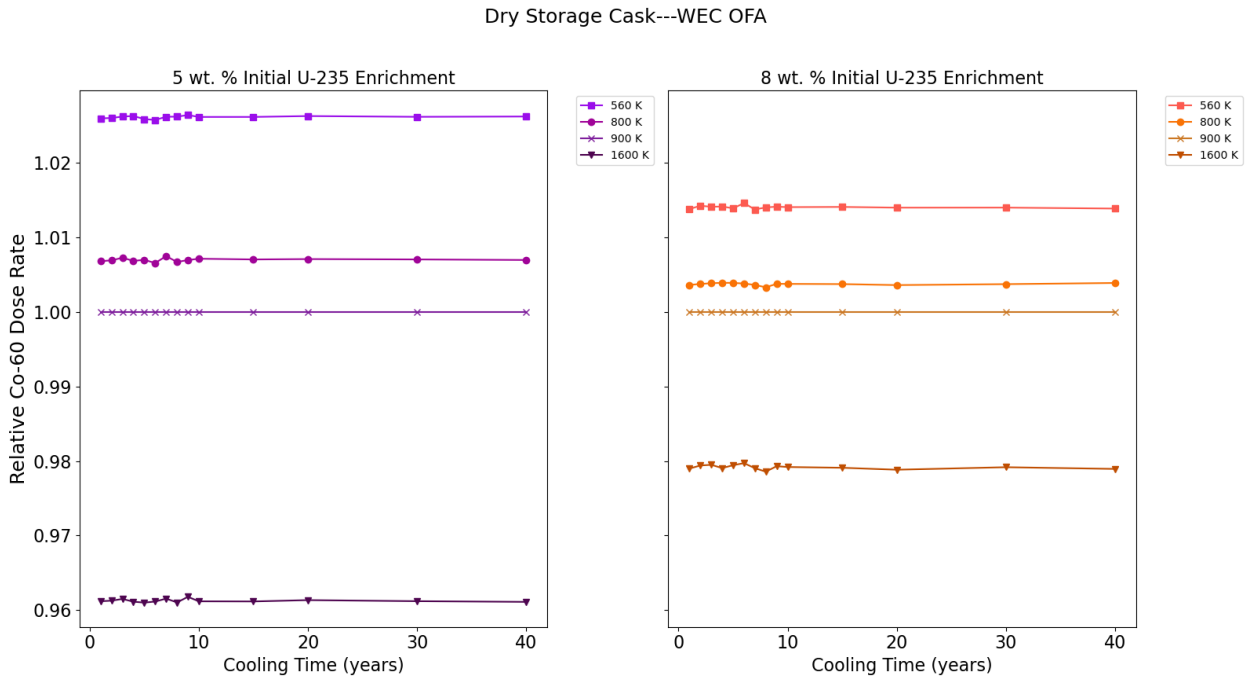

Figure 7-45 Comparative Effects of Varying Fuel Temperature on ^{60}Co Gamma Dose Rate from Fuel with Different Enrichments (Normalization to Dose Rate Values for a 900 K Fuel Temperature)

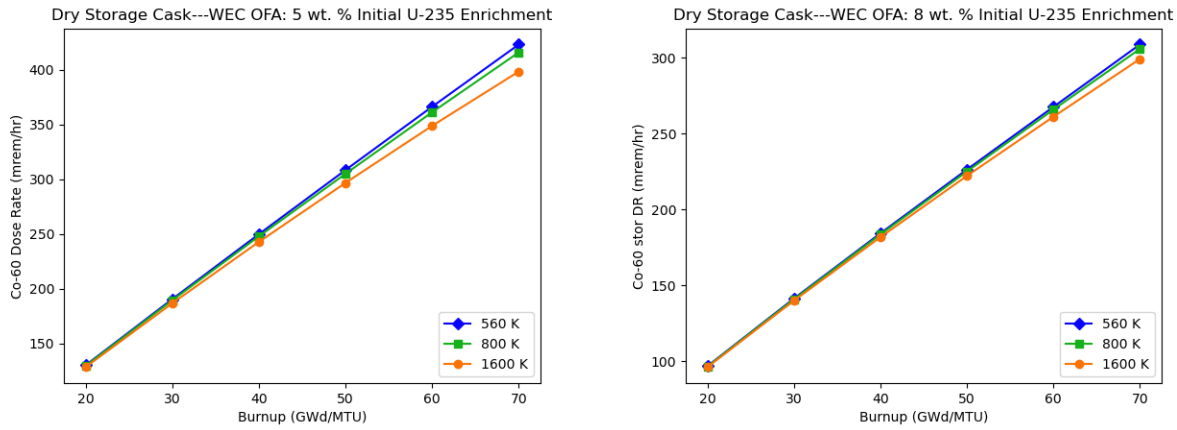

Figure 7-46 Cobalt-60 Dose Rate Trends of Variation with PWR Fuel Temperature and Burnup (GWd/MTU)

7.1.8 Fuel Density

The effect of fuel density on cask dose rates was presented for 5 and 8 wt % ^{235}U PWR fuel. The fuel densities analyzed are provided in Section 3.1. In this parametric study, the fuel density was perturbed without dimensional changes, and the same specific power and set of burnup values were used in all perturbed cases.

7.1.8.1 Neutron Dose Rate Trends

The graphs in Figure 7-47 illustrate the effects on the neutron dose rate of varying fuel density for PWR fuel with 8 wt % enrichment at fixed assembly average burnup (75 GWd/MTU) over a range of cooling times. The graphs in Figure 7-48 illustrate these effects at different initial enrichments and cooling times at fixed assembly average burnup (75 GWd/MTU). The neutron dose rate was observed to increase with increasing fuel density. These effects are slightly greater at 8 wt % enrichment compared to 5 wt % enrichment. The effect of fuel density on neutron dose rate was not significant because the dose rate only changed by approximately 2%. Increasing the fuel density (without changing fuel dimensions to conserve MTU) has the effect of increasing MTU and increasing the degree of self-shielding. These trends agree with the uranium mass analysis in Section 3.4.2.3 in NUREG/CR-6716 [63], which was performed using fuel with lower burnup and enrichment than used in this analysis. As shown in Figure 7-49, for a given cooling time (5 yr), the effect of fuel density on the neutron dose rate increased very slightly with increasing burnup.

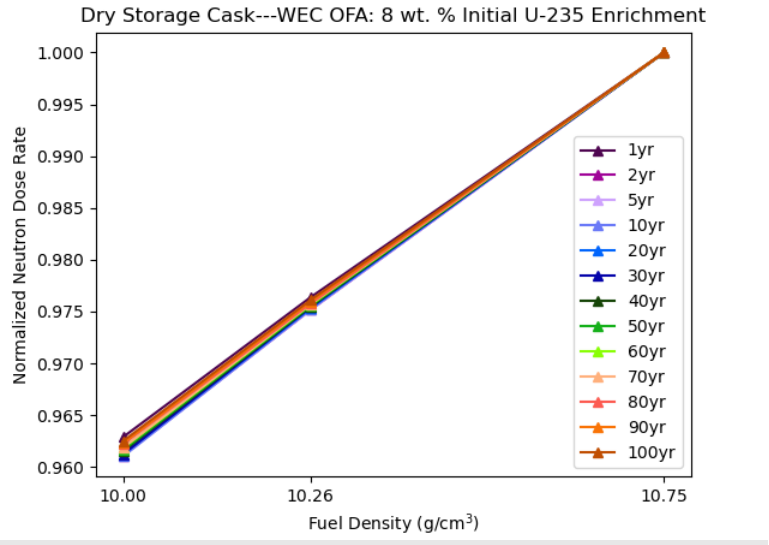

Figure 7-47 Neutron Dose Rate Trends of Variation with PWR Fuel Density (g/cm^3) as a Function of Cooling Time (years) (Normalization to Highest Dose Rate Value at Each Cooling Time)

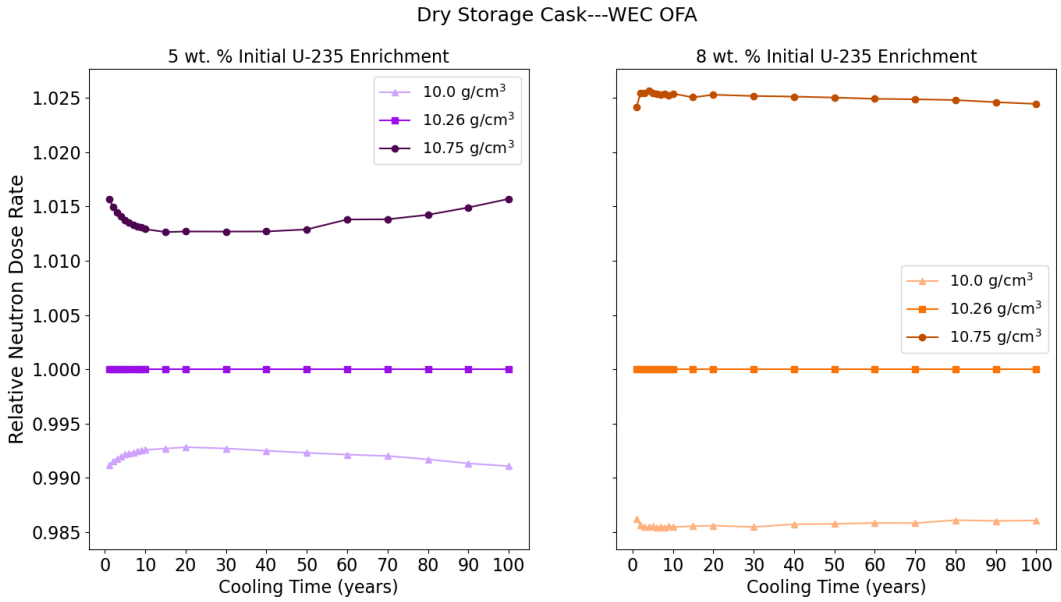

Figure 7-48 Comparative Effects of Varying Fuel Density on Neutron Dose Rate from PWR Fuel with Different Enrichments (Normalization to Dose Rate Values for a 10.26 g/cm^3 Fuel Density)

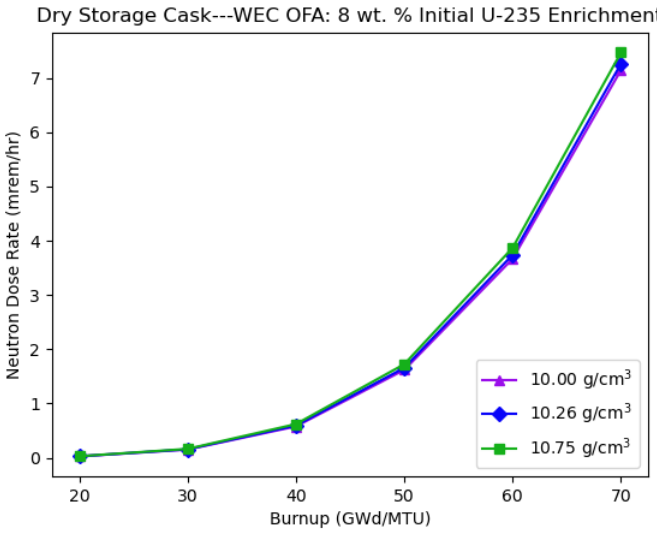

Figure 7-49 Neutron Dose Rate Trends of Variation with PWR Fuel Density (g/cm^3) and Burnup (GWd/MTU)

7.1.8.2 Gamma Dose Rate Trends

The graphs in Figure 7-50 illustrate the effects on the primary gamma dose rate of varying fuel density for PWR fuel with 8 wt % enrichment at fixed assembly average burnup (75 GWd/MTU) over a range of cooling times. The graphs in Figure 7-51 illustrate these effects at different initial enrichments and cooling times at fixed assembly average burnup (75 GWd/MTU). Changes in fuel density at fixed initial enrichment and average assembly burnup were observed to have negligible effects on the primary gamma dose rate. The primary gamma dose rate only changed by approximately 1% over the range of fuel densities analyzed. The smaller effect of fuel density on gamma dose rate than neutron dose rate is supported by the uranium mass analysis in Section 3.4.2.3 of NUREG/CR-6716 [63], which was performed using fuel with lower burnup and enrichment than used in this analysis. The maximum effects were achieved for the 10-year cooling time. These effects were approximately equal for both fuel enrichments analyzed. As shown in Figure 7-52, for a given cooling time (5 yr), the effect of fuel density on primary gamma dose rate increased very slightly with increasing burnup.

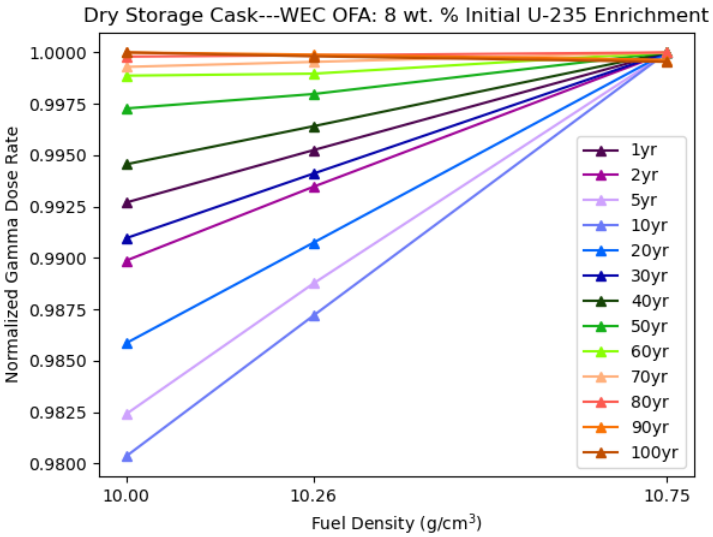

Figure 7-50 Primary Gamma Dose Rate Trends of Variation with PWR Fuel Density (g/cm^3) and Cooling Time (years) (Normalization to Highest Dose Rate Value at Each Cooling Time)

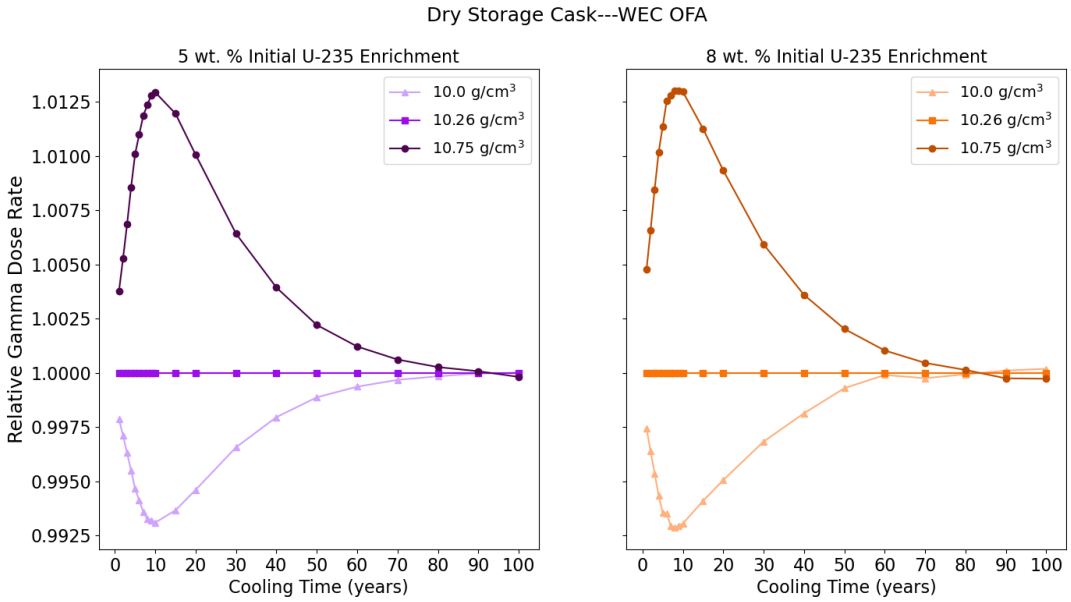

Figure 7-51 Comparative Effects of Varying Fuel Density on Primary Gamma Dose Rate from PWR Fuel with Different Enrichments (Normalization to Dose Rate Values for a 10.26 g/cm^3 Fuel Density)

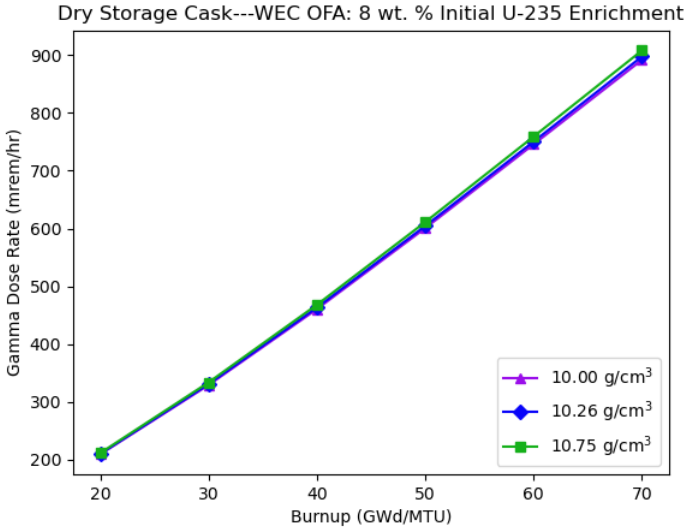

Figure 7-52 Primary Gamma Dose Rate Trends of Variation with PWR Fuel Density (g/cm^3) and Burnup (GWd/MTU)

7.1.8.3 Cobalt-60 Dose Rate Trends

The graph in Figure 7-53 illustrates the effects on the ^{60}Co dose rate of varying fuel density for PWR fuel with 8 wt % enrichment at fixed assembly average burnup (75 GWd/MTU) over a range of cooling times. The graphs in Figure 7-54 illustrate these effects at different initial enrichments and cooling times at fixed assembly average burnup (75 GWd/MTU). These effects are slightly greater for the 5 wt % enrichment compared to the 8 wt % enrichment. The change in ^{60}Co dose rate displayed a trend opposite to that of the primary gamma dose rate; the slight increase in ^{60}Co dose rate with decreasing fuel density indicated that the reduced self-shielding outweighed the increase in source term intensity for ^{60}Co. For a given cooling time (5 yr), the effect of fuel density on ^{60}Co dose rate increased with increasing burnup.

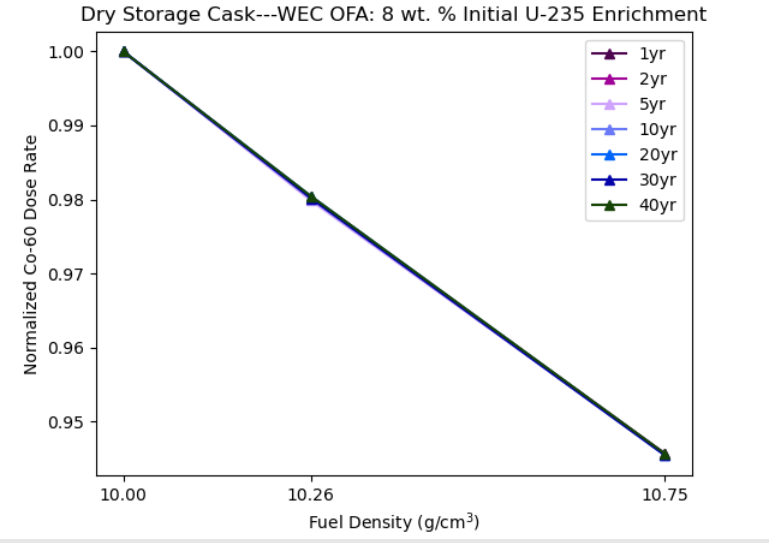

Figure 7-53 Cobalt-60 Gamma Dose Rate Trends of Variation with PWR Fuel Density (g/cm^3) and Cooling Time (years) (Normalization to Highest Dose Rate Value at Each Cooling Time)

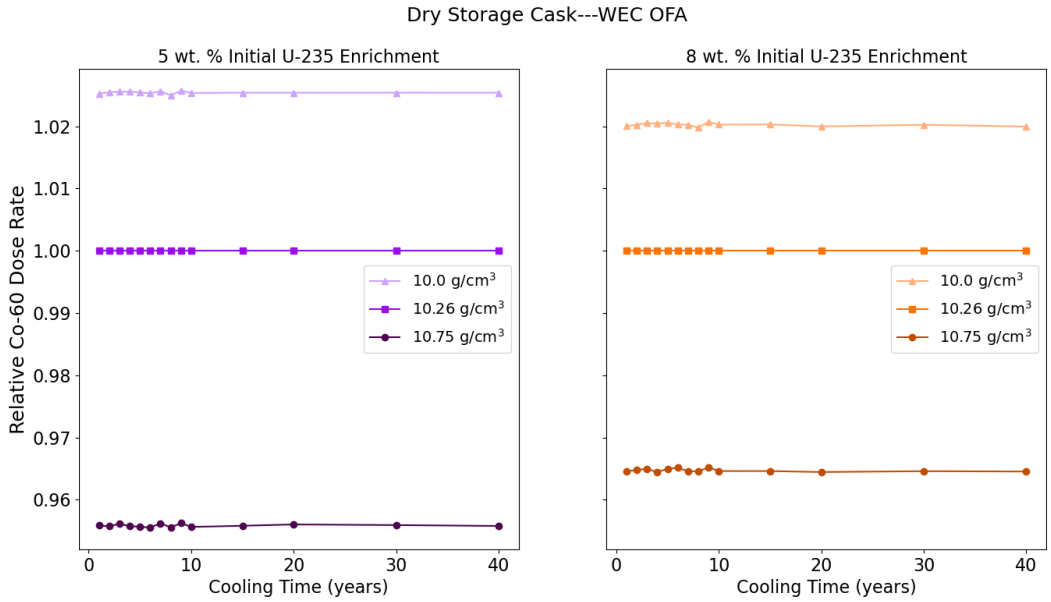

Figure 7-54 Comparative Effects of Varying Fuel Density on ^{60}Co Gamma Dose Rate from PWR Fuel with Different Enrichments (Normalization to Dose Rate Values for a 10.26 g/cm^3 Fuel Density)

7.1.9 Burnable Absorbers

The effects of IFBAs, WABAs, and fuel rods containing gadolinia on cask dose rates were presented for 5 and 8 wt % ^{235}U PWR fuel. The absorber configurations provided in Section 3.1 are described further in this section.

7.1.9.1 Integral Fuel Burnable Absorbers

PWR assembly lattices containing various numbers of IFBA rods were considered. The numbers of IFBA rods considered in this study are provided in Table 7-1.

Table 7-1 Number of IFBA Rods Used in PWR Study

Number of IFBAs
0
80
104
128
156
200

7.1.9.2 Integral Fuel Burnable Absorbers/Wet Annular Burnable Absorbers

PWR assembly lattices containing various numbers of IFBA and WABA rods were considered. The combinations of IFBA and WABA rods considered in this study are provided in Table 7-2.

Table 7-2 Combinations of IFBA and WABAs Used in PWR Study

Number of IFBAs	Number of WABAs
80	24
200	8
200	20
200	24

7.1.9.3 Integral Fuel Burnable Absorbers/Gadolinia

One PWR assembly lattice containing gadolinia was considered. The lattice, adapted from [15], contained 148 UO_2 rods, 104 IFBA rods, and 12 UO_2 rods containing Gd_2O_3.

A second lattice containing 160 UO_2 rods, 104 IFBA rods, and 0 Gd_2O_3 rods was also analyzed to serve as a point of comparison. The fuel pin layout of this lattice was identical to the first case but with the 12 Gd_2O_3 rods replaced with normal UO_2 rods. In each case, the UO_2 and IFBA rods contained 7 wt % ^{235}U. The rods containing Gd_2O_3 consisted of UO_2 with 5 wt % ^{235}U and contained 8 wt % Gd_2O_3.

7.1.9.4 Neutron Dose Rate Trends

The graphs in Figure 7-55 illustrate the effects on the neutron dose rate of varying number of IFBAs and WABAs for PWR fuel at fixed assembly average burnup (75 GWd/MTU) over a range of cooling times. The dose rates in this figure were normalized to the dose rates for the baseline case, which contained 80 IFBAs and 0 WABAs. The neutron dose rates generally increased with higher numbers of IFBAs and WABAs across the range of cooling times analyzed. The effect was largest at long cooling times, when the neutron dose rate is dominating compared to the gamma dose rate. The lattice with the highest number of IFBAs and WABAs (200 IFBAs, 24 WABAs) produced the highest dose rates, and the lattice with the lowest number (0 IFBAs, 0 WABAs) produced the lowest dose rates. Burnable absorbers were modeled in Polaris in generating the sources and were not included in the homogenized mixture inside the transportation package and dry storage cask in the simplified model as described in Appendix A. The addition of burnable absorbers hardens the neutron spectrum and results in more neutron capture and more transuranic production. The effect of IFBAs and WABAs was more significant at 8 wt % initial enrichment than at 5 wt %.

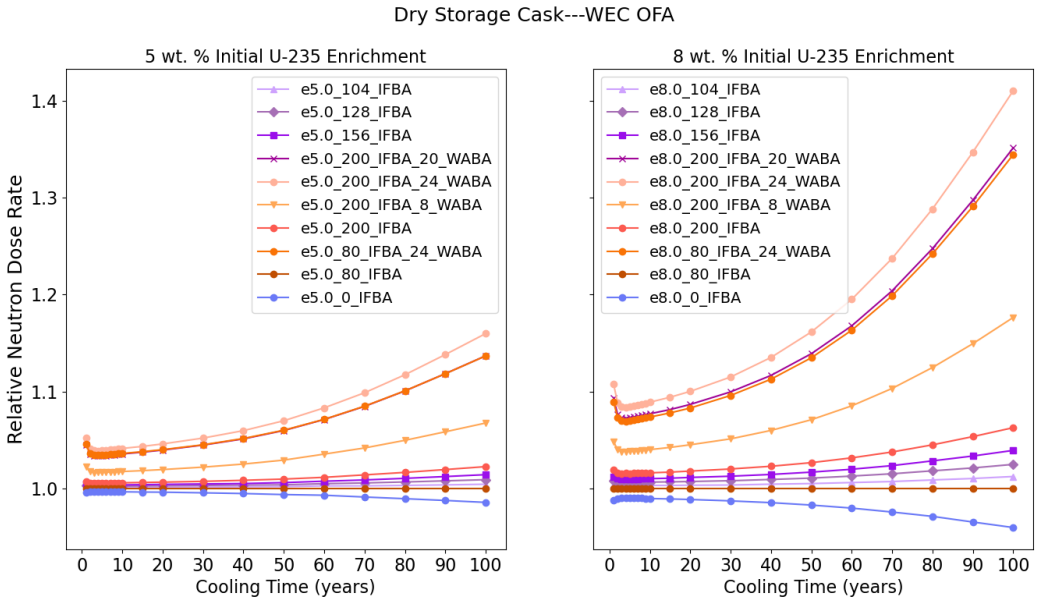

Figure 7-55 Comparative Effects of Varying Number of IFBAs and WABAs on Neutron Dose Rate from PWR Fuel (Normalization to Dose Rate Values for an Assembly with 80 IFBAs)

Figure 7-56 illustrates the effects on the neutron dose rate due to the presence of gadolinia-containing fuel rods for PWR fuel at fixed enrichment (7 wt %) and fixed assembly average burnup (75 GWd/MTU) over a range of cooling times. The dose rates in this figure were normalized to the dose rates for the 7 wt % baseline case with 80 IFBA rods. The neutron dose rate increased by approximately 4% over the range of cooling times analyzed with the presence of gadolinia. As discussed in Section 3.4.2.2 of NUREG/CR-6716 [63] for 4 wt % fuel burned up to 60 GWd/MTU, the effect of burnable absorbers such as Gd_2O_3 is relatively small at higher burnups. The increase in neutron dose rate is due to the hardening of the neutron spectrum during irradiation from neutron absorption by gadolinia.

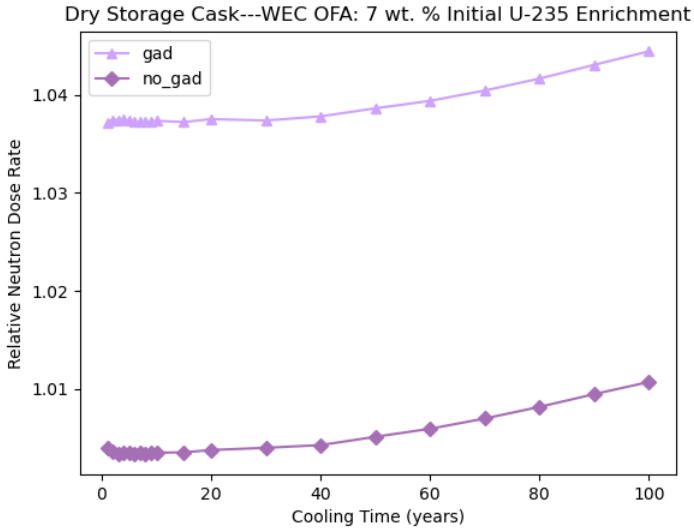

Figure 7-56 Comparative Effects of Varying Number of Gadolinia Rods on Neutron Dose Rate from PWR Fuel (Normalization to Dose Rate Values for Baseline 7 wt % Assembly with 0 Gadolinia Rods)

7.1.9.5 Gamma Dose Rate Trends

The graphs in Figure 7-57 illustrate the effects on the primary gamma dose rate of varying the number of IFBAs and WABAs for PWR fuel at fixed assembly average burnup (75 GWd/MTU) over a range of cooling times. The dose rates in this figure were normalized to the dose rates for the baseline case, which contained 80 IFBAs and 0 WABAs. The primary gamma dose rates generally increased with higher numbers of IFBAs and WABAs for cooling times up to 50 yr, beyond which the trend was reversed. The effect was largest at short cooling times, when the gamma dose rate is dominating compared to the neutron dose rate. Across all cooling times analyzed, the effect of IFBAs and WABAs on the primary gamma dose rate was relatively insignificant, and the dose rates changed by less than 2%. The effect of IFBAs and WABAs was generally similar at 5 and 8 wt % initial enrichments.

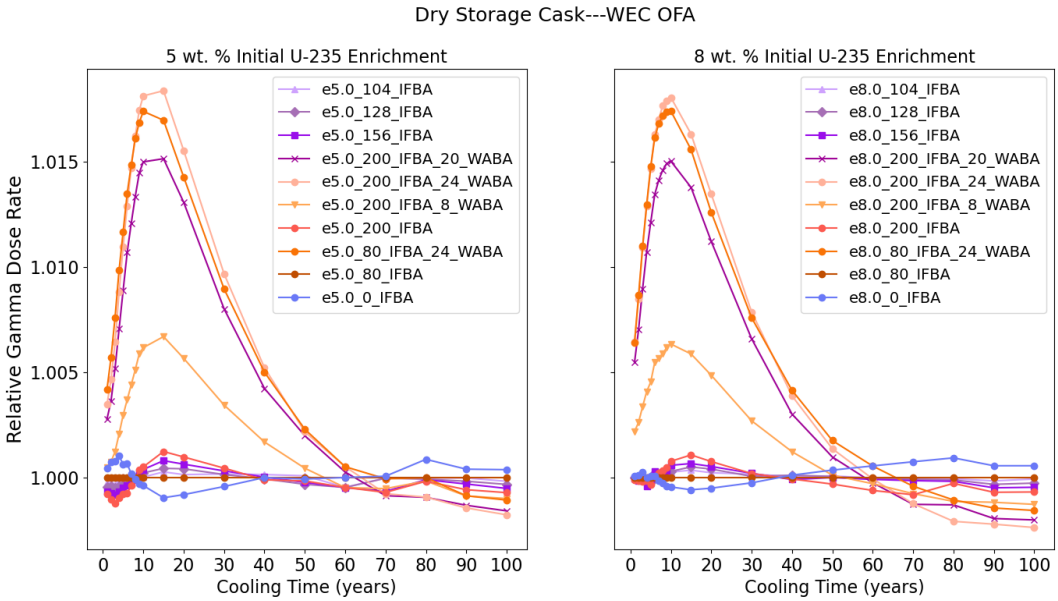

Figure 7-57 Comparative Effects of Varying Number of IFBAs and WABAs on Primary Gamma Dose Rate from PWR Fuel (Normalization to Dose Rate Values for an Assembly with 80 IFBAs)

The effects on the primary gamma dose rate due to the presence of gadolinia-containing fuel rods for PWR fuel at fixed enrichment (7 wt %) and fixed assembly average burnup (75 GWd/MTU) were analyzed over a range of cooling times. The effect of gadolinia-containing rods on the primary gamma dose rate was relatively insignificant compared to the effect on the neutron dose rate, and the primary gamma dose rates varied by less than 1% over the range of cooling times analyzed.

7.1.9.6 Cobalt-60 Dose Rate Trends

The graphs in Figure 7-58 illustrate the effects on the ^{60}Co dose rate of varying number of IFBAs and WABAs for PWR fuel at fixed assembly average burnup (75 GWd/MTU) over a range of cooling times. The dose rates in this figure were normalized to the dose rates for the baseline case, which contained 80 IFBAs and 0 WABAs. The ^{60}Co dose rates displayed opposite trends with increasing numbers of IFBAs and WABAs. Generally, the ^{60}Co dose rate increased with increasing number of WABAs and decreasing number of IFBAs. Across all cooling times analyzed, the effect of IFBAs and WABAs on the ^{60}Co dose rate was significant, and the dose rates changed by approximately 20 percent. The effect of IFBAs and WABAs was generally similar at 5 and 8 wt % initial enrichments.

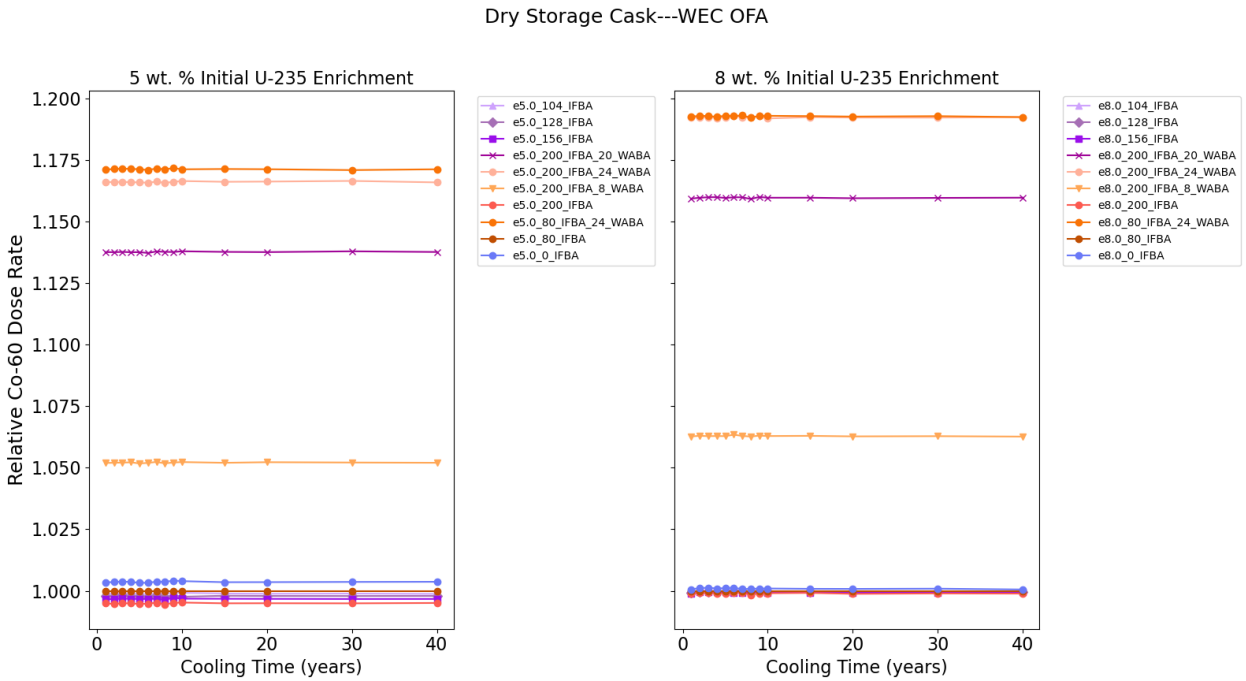

Figure 7-58 Comparative Effects of Varying Number of IFBAs and WABAs on ^{60}Co Dose Rate from PWR Fuel (Normalization to Dose Rate Values for an Assembly with 80 IFBAs)

The effects on the ^{60}Co dose rate due to the presence of gadolinia-containing fuel rods for PWR fuel at fixed enrichment (7 wt %) and fixed assembly average burnup (75 GWd/MTU) were analyzed over a range of cooling times. The effect of gadolinia-containing rods on the ^{60}Co dose rate, as with the primary gamma dose rate, was relatively insignificant compared with the effect on the neutron dose rate. The ^{60}Co dose rates changed by less than 1% over the range of cooling times analyzed.

7.1.10 Rod Cluster Control Assembly

Two removable burnable poison rod designs (as described in Section 3.1) were considered: AIC control rods and B_4C control rods. Cask dose rates were calculated for the WEC 17 × 17 OFA

fuel design using either 16 AIC control rods or 16 B_4C control rods. This analysis assumed that all assemblies in the cask contained fuel with the same control rod exposure during irradiation. These studies were performed at 8 wt % ^{235}U enrichment.

For the AIC control rods, studies were performed with all the control rods fully inserted at the beginning of fuel depletion, with all rods later removed once a variable burnup had been reached. An additional study was performed assuming the rods were inserted only from 70 to 75 GWd/MTU assembly burnup. For the B_4C control rods, only a single study was performed due to the possibility of the boron completely depleting at the high burnups analyzed in these studies. A summary of all control rod studies performed is provided in Table 7-3.

Table 7-3 PWR Control Rod Studies

Control Rod Type	Assembly Burnup at Rod Insertion (GWd/MTU)	Assembly Burnup at Rod Removal (GWd/MTU)
AIC	0	45
	0	55
	0	65
	0	75
	70	75
B_4C	0	75

7.1.10.1 Neutron Dose Rate Trends

Figure 7-59 illustrates the effects on the neutron dose rate due to control rod insertion and type for PWR fuel at fixed enrichment (8 wt %) and fixed assembly average burnup (75 GWd/MTU) over a range of cooling times. The dose rate results are normalized to the 8 wt % baseline case, which did not contain any control rods. For the AIC control rod initially inserted at the beginning of irradiation, the neutron dose rate generally increased over all cooling times with increased control rod insertion duration. For control rods inserted from 0 to 75 GWd/MTU, the B_4C control rods produced larger neutron dose rates than the AIC control rods. For the AIC control rod, inserting the control rod from 70 to 75 GWd/MTU had a relatively insignificant effect on the neutron dose rate, which only changed by approximately 2% and generally decreased with increasing cooling time.

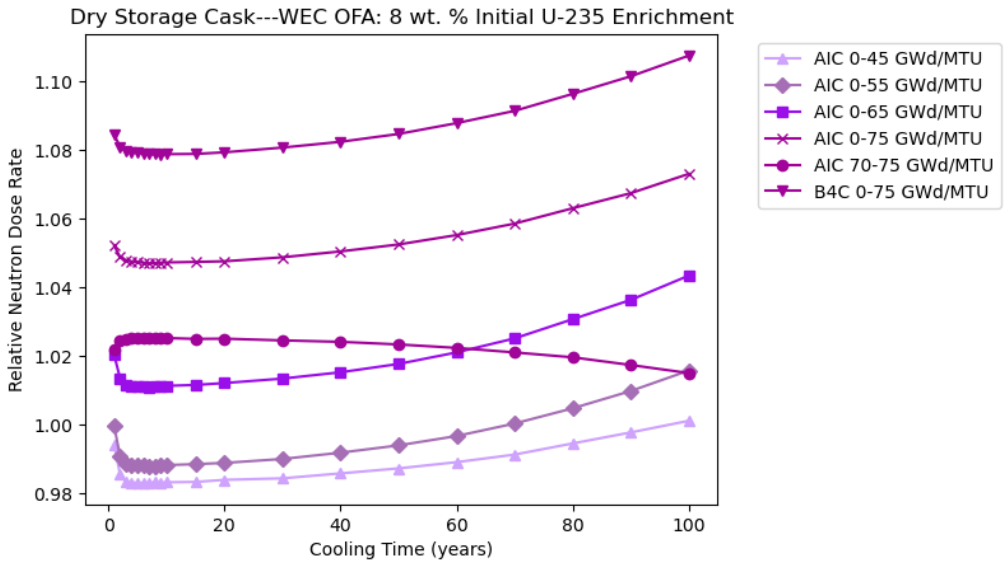

Figure 7-59 PWR Neutron Dose Rate Trends of Variation with Control Rod Insertion and Type as a Function of Cooling Time (years)

7.1.10.2 Gamma Dose Rate Trends

Figure 7-60 illustrates the effects on the primary gamma dose rate due to control rod insertion and type for PWR fuel at fixed enrichment (8 wt %) and fixed assembly average burnup (75 GWd/MTU) over a range of cooling times. The dose rate results are normalized to the 8 wt % baseline case, which did not contain any control rods. For the AIC control rod initially inserted at the beginning of irradiation, the primary gamma dose rate increased with increased control rod insertion duration. These gamma dose rates were larger than the baseline dose rates until approximately 50 yr of cooling time. For control rods inserted from 0 to 75 GWd/MTU, the B_4C control rods produced larger primary gamma dose rates than the AIC control rods. For the AIC control rod, inserting the control rod from 70 to 75 GWd/MTU had a larger effect on the primary gamma dose rate than all the cases with control rods initially and continuously inserted up to 65 GWd/MTU for cooling times greater than 40 yr. For all control rod cases analyzed, the effect on the primary gamma dose rate was highest at approximately 10 yr of cooling time.

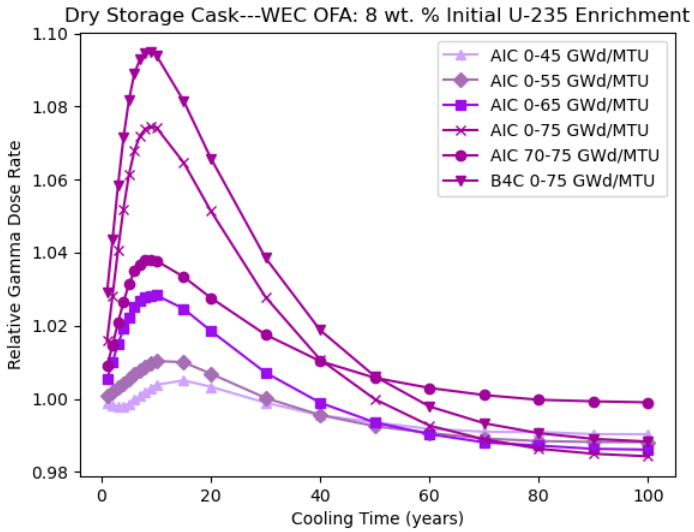

Figure 7-60 PWR Primary Gamma Dose Rate Trends of Variation with Control Rod Insertion and Type as a Function of Cooling Time (years)

7.1.10.3 Cobalt-60 Dose Rate Trends

Figure 7-61 illustrates the effects on the ^{60}Co dose rate due to control rod insertion and type for PWR fuel at fixed enrichment (8 wt %) and fixed assembly average burnup (75 GWd/MTU) over a range of cooling times. The dose rate results are normalized to the 8 wt % baseline case, which did not contain any control rods. For the AIC control rod initially inserted at the beginning of irradiation, the ^{60}Co dose rate increased with increased control rod insertion duration. For control rods inserted from 0 to 75 GWd/MTU, the B_4C control rods produced larger ^{60}Co dose rates than the AIC control rods. For the AIC control rod, inserting the control rod from 70 to 75 GWd/MTU had a larger effect on the ^{60}Co dose rate than all the cases with control rods initially and continuously inserted up to 65 GWd/MTU. The effects were generally similar to the effects on the primary gamma dose rate. For all control rod cases analyzed, the effect on the ^{60}Co dose rate was consistent over the range of cooling times analyzed.

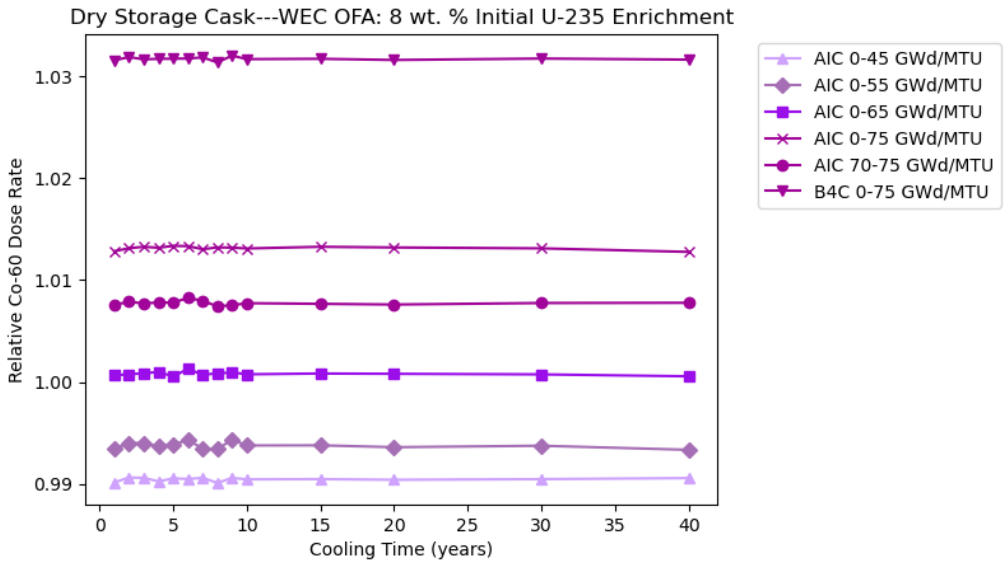

Figure 7-61 PWR ^{60}Co Dose Rate Trends of Variation with Control Rod Insertion and Type as a Function of Cooling Time (years)

7.1.11 Fuel Assembly Type

All parametric studies performed for the WEC 17 × 17 OFA PWR fuel assembly were repeated for the WEC 17 × 17 RFA PWR fuel assembly. The only difference between the OFA and RFA fuel assemblies is the slightly larger fuel pin diameter (and consequently slightly greater MTU) used in the RFA assembly. For all parameters analyzed, identical trends were observed for both fuel types, with the only difference being the magnitude of the dose rates. For the dry storage cask over the range of cooling times analyzed, the maximum difference in dose rates between the fuel types at 75 GWd/MTU was approximately 15% for neutrons, 5% for primary gammas, and 8% for ^{60}Co. The difference in gamma dose rates decreased beyond cooling times of approximately 20 yr. Similar studies were performed in Section 3.4.1.2 of NUREG/CR-6716 [63] at enrichments up to 5 wt % and burnups up to 60 GWd/MTU, which suggested that differences in total dose rate due to fuel assembly type are likely to be less than 10%. This result was also observed at higher burnups and enrichments analyzed in this study, as the total dose rates changed by less than 3 percent at 75 GWd/MTU over the range of cooling times analyzed.

7.1.12 Axial Burnup Profile

The effect of varying axial burnup profiles on dry storage cask and transportation package dose rates was qualitatively analyzed for PWR fuel. A reference profile was chosen from Table 43 of ORNL/SPR-2021/2093 [12]. The axial burnup profiles in Table 43 of ORNL/SPR-2021/2093 [12] were obtained by comparing data from more than 3,000 PWR fuel assemblies with average assembly burnups ranging up to approximately 55.3 GWd/MTU. Table 43 of ORNL/SPR-2021/2093 [12] gives bounding axial burnup profiles for fuel assembly average burnups less than 18 GWd/MTU, 18–30 GWd/MTU, 30–45 GWd/MTU, and 45 to less than 60 GWd/MTU. For the current study, the bounding profile for the range 45 GWd/MTU to less than 60 GWd/MTU was chosen. This axial burnup profile characterizes blanketed PWR fuel assemblies.

Two additional axial burnup profiles were chosen from ORNL/TM-2022/1831 [17] as example profiles from low-enriched uranium plus (LEU+) PWR fuel assemblies with high burnup. These profiles, referred to as P1 and P2, were obtained by condensing 24-node axial burnup profiles calculated in ORNL/TM-2022/1831 [17] to 18 nodes. P1 is from a fuel assembly with 6.2 wt % ^{235}U enrichment with 200 IFBA rods and 8 WABA rods and an assembly average burnup of 61.5 GWd/MTU. P2 is from a fuel assembly with 6.2 wt % ^{235}U enrichment with 200 IFBA rods and an average burnup of 72.0 GWd/MTU. The IFBA blankets were not modeled for these fuel assemblies.

The three selected profiles are provided in Table 7-4. The maximum axial peaking factor for each profile is bolded in the table. For all three profiles analyzed, the peaking factor occurred in the same axial node, and was largest in the reference profile. Peaking factors in the central nodes of the reference axial burnup profile were greater than those in LEU+ profiles. However, at the top and bottom nodes, the peaking factor in the reference profile was lower than those in LEU+ profiles. These comparisons suggest that the reference axial burnup profile will be bounding in calculating maximum dose rates compared to the LEU+ axial burnup profiles.

Table 7-4 PWR Axial Burnup Profiles Used for Qualitative Shielding Analysis

Axial Node	Relative Axial Burnup Profile		
	Reference ORNL/SPR-2021/2093 [12]	P1 ORNL/TM-2022/1831 [17]	P2 ORNL/TM-2022/1831 [17]
1 (bottom)	0.328	0.665	0.659
2	0.932	0.946	0.943
3	1.102	1.060	1.059
4	1.159	1.093	1.094
5	**1.169**	**1.096**	**1.099**
6	1.164	1.094	1.097
7	1.157	1.090	1.092
8	1.149	1.086	1.089
9	1.142	1.083	1.085
10	1.135	1.080	1.082
11	1.133	1.078	1.080
12	1.112	1.075	1.077
13	1.108	1.071	1.073
14	1.095	1.063	1.064
15	1.064	1.044	1.044
16	0.983	0.985	0.982
17	0.800	0.843	0.838
18 (top)	0.269	0.548	0.542

7.2 Dry Storage Cask and Transportation Package Shielding Evaluation for Boiling-Water Reactors

The parameters considered in this study included burnup, enrichment, cooling time, specific power, coolant void fraction, fuel temperature, fuel density, control rod blade exposure, gadolinia concentration, and axial burnup profile. The following parametric studies were performed for the GEH 10 × 10 GE14 BWR fuel assembly. All parametric studies were performed with a storage cask and a transportation package, which each contained 68 identical BWR fuel assemblies. The dose location for all analysis was the mid-height external surface of the cask/package.

7.2.1 Burnup

The effect of assembly burnup on cask dose rates was analyzed for BWR fuel with maximum fuel pin enrichments of 5, 5.5, 6.0, 6.5, 7.0, 7.5, and 8 wt % ^{235}U. The fuel was burned up to a maximum of 75 GWd/MTU.

7.2.1.1 Neutron Dose Rate Trends

Figure 7-62 illustrates the effects on the neutron dose rate of varying burnup for BWR fuel with several different initial enrichments at 5 yr of cooling time. Neutron dose rates for a dry storage cask and a transportation package are provided. As discussed in Section 3.4.1.1 of NUREG/CR-6716 [63], the neutron dose rate has previously been observed to increase with the burnup approximately to the power of four. These same effects are observed in this analysis, with the highest burnup producing the highest neutron dose rates. This effect was most pronounced at lower enrichments. The absolute neutron dose rate was higher for the transportation package than for the storage cask.

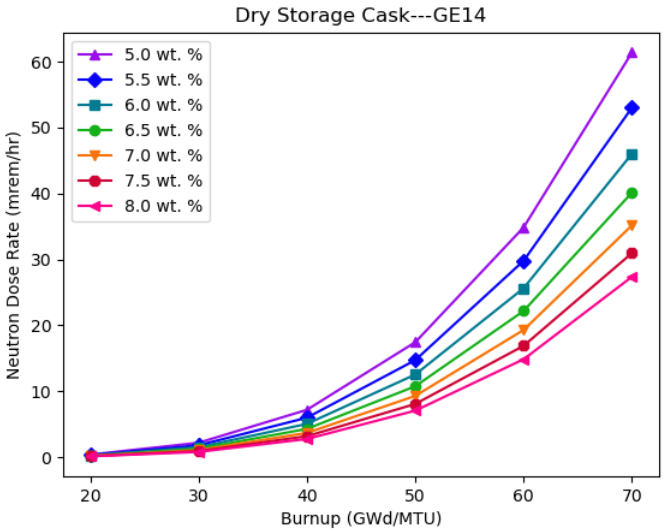

Figure 7-62 Neutron Dose Rate Trends of Variation with BWR Fuel Burnup (GWd/MTU) and Initial Enrichment (^{235}U wt %)

7.2.1.2 Gamma Dose Rate Trends

Figure 7-63 illustrates the effects on the primary gamma dose rate of varying burnup for BWR fuel with several different initial enrichments at 5 yr of cooling time. Primary gamma dose rates for a dry storage cask and a transportation package are provided. As discussed in Section 3.4.1.1 of NUREG/CR-6716 [63], the gamma dose rate has previously been observed to increase linearly with burnup. This linear relationship was also observed in this analysis, with the highest burnup producing the highest neutron dose rates. The effect of increasing burnup on primary gamma dose rates was most pronounced at lower enrichments.

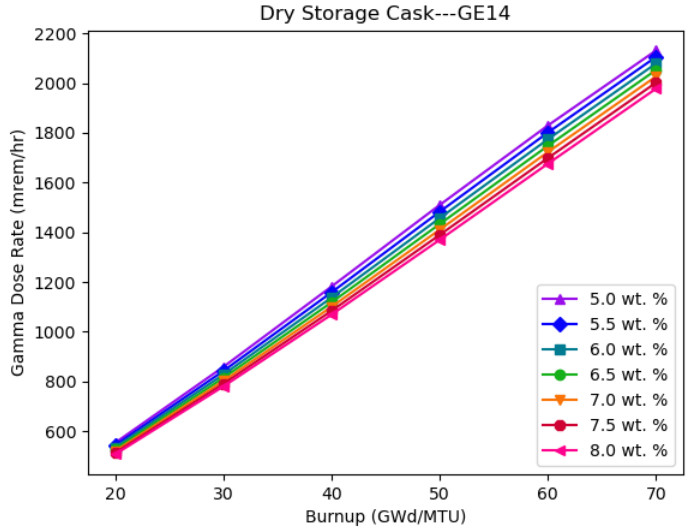

Figure 7-63 Primary Gamma Dose Rate Trends of Variation with BWR Fuel Burnup (GWd/MTU) and Initial Enrichment (^{235}U wt %)

7.2.1.3 Cobalt-60 Dose Rate Trends

Figure 7-64 illustrates the effects on the ^{60}Co dose rate of varying burnup for BWR fuel with several different initial enrichments at 5 yr of cooling time. Cobalt-60 dose rates for a dry storage cask and a transportation package are provided. As discussed in Section 3.4.1.1 of NUREG/CR-6716 [63], the primary gamma dose rate has previously been observed to increase linearly with burnup. This linear relationship was also observed with the ^{60}Co dose rates, with the highest burnup producing the highest neutron dose rates. The effect of increasing burnup on ^{60}Co dose rates was most pronounced at lower enrichments.

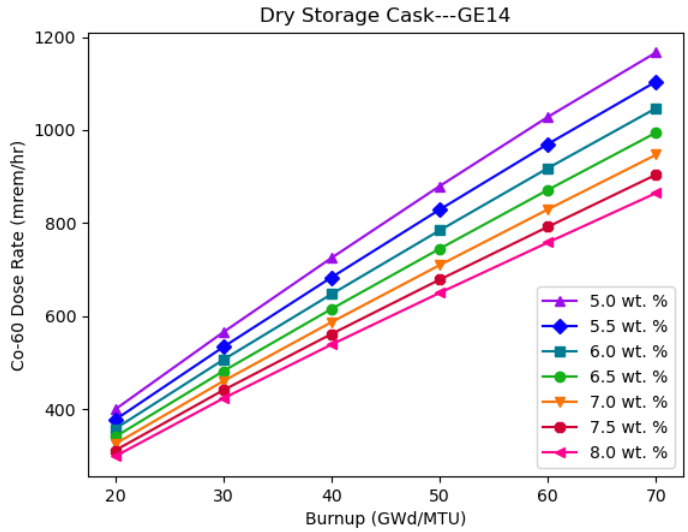

Figure 7-64 Cobalt-60 Dose Rate Trends of Variation with BWR Fuel Burnup (GWd/MTU) and Initial Enrichment (^{235}U wt %)

7.2.2 Initial Fuel Enrichment

The effect of initial ^{235}U enrichment on cask dose rates was analyzed for BWR fuel with maximum fuel pin enrichments of 5, 5.5, 6.0, 6.5, 7.0, 7.5, and 8 wt % ^{235}U. The fuel was burned up to 75 GWd/MTU.

7.2.2.1 Neutron Dose Rate Trends

Figure 7-65 illustrates the effects on the neutron dose rate of varying enrichment for BWR fuel at constant burnup (75 GWd/MTU) at several different cooling times. Neutron dose rates for a dry storage cask and a transportation package are provided. These graphs show that the neutron dose rate increases with decreasing enrichment. At a constant burnup of 75 GWd/MTU, the neutron dose rate decreased by a factor of two with an increase from 5 to 8 wt % enrichment. Similar effects were observed at lower enrichments and burnups in Section 3.4.1.2 of NUREG/CR-6716 [63], where neutron dose rate decreased by a factor of two with an increase from 2.5 to 5 wt. %.

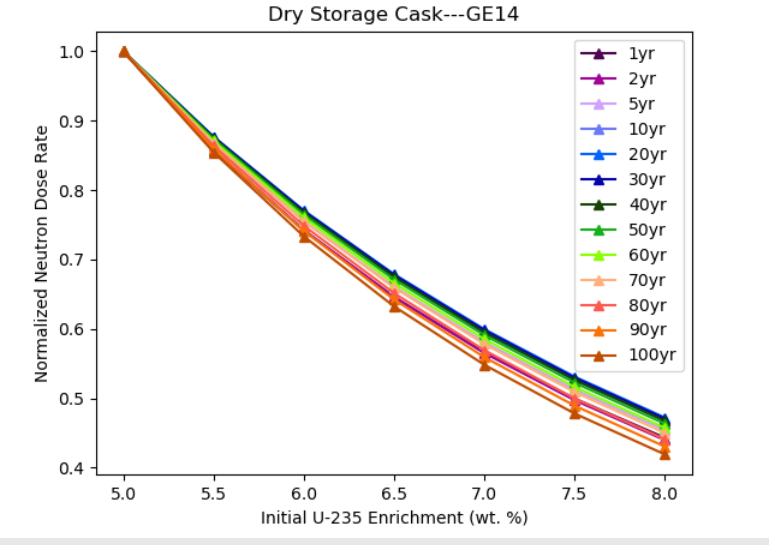

Figure 7-65 Neutron Dose Rate Trends of Variation with BWR Initial Fuel Enrichment (^{235}U wt %) and Cooling Time (years)

7.2.2.2 Gamma Dose Rate Trends

Figure 7-66 illustrates the effects on the primary gamma dose rate of varying enrichment for BWR fuel at constant burnup (75 GWd/MTU) at several different cooling times. Primary gamma dose rates for a dry storage cask and a transportation package are provided. These graphs show that for cooling times less than or equal to 5 yr, the primary gamma dose rate decreases with increasing fuel enrichment at a constant burnup of 75 GWd/MTU. These same effects were observed at lower enrichments (up to 5 wt. % ^{235}U) and burnups (up to 60 GWd/MTU) in Section 3.4.1.2 of NUREG/CR-6716 [63]. Figure 7-66 shows that the primary gamma dose rate changes its trend of variation with initial fuel enrichment at the 10-year cooling time. The primary gamma dose rate increases with increasing initial fuel enrichment for longer (i.e., greater than 10 yr) cooling times. At 75 GWd/MTU, the primary gamma dose rate was observed to be significantly less sensitive to fuel enrichment than the neutron dose rate.

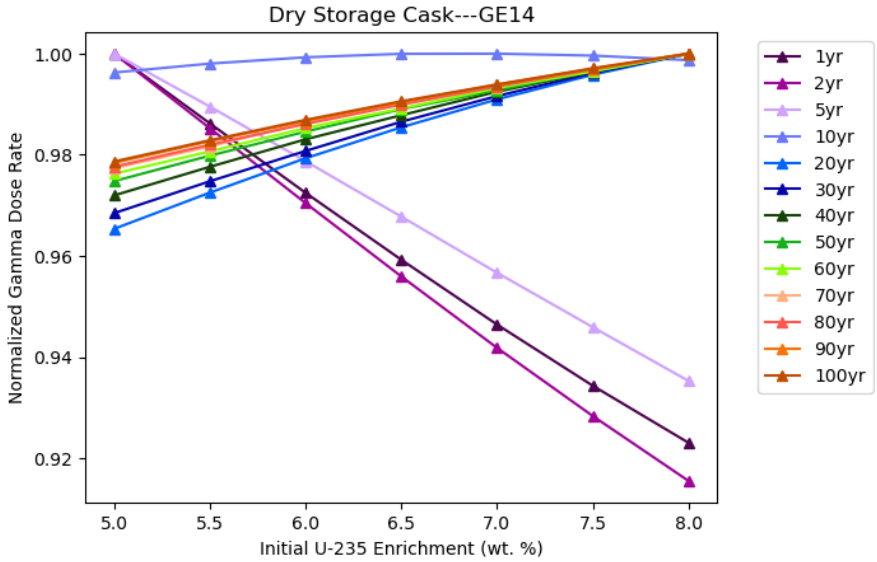

Figure 7-66 Primary Gamma Dose Rate Trends of Variation with BWR Initial Fuel Enrichment (^{235}U wt %) and Cooling Time (years)

7.2.2.3 Cobalt-60 Dose Rate Trends

Figure 7-67 illustrates the effects on the ^{60}Co dose rate of varying enrichment for BWR fuel at constant burnup (75 GWd/MTU) at several different cooling times. Cobalt-60 dose rates for a dry storage cask and a transportation package are provided. These graphs show that for all cooling times analyzed, the ^{60}Co dose rate decreased with increasing fuel enrichment. At a constant burnup of 75 GWd/MTU, the ^{60}Co dose rate was observed to be more sensitive to fuel enrichment than the primary gamma dose rate, but it was not as sensitive to fuel enrichment as the neutron dose rate.

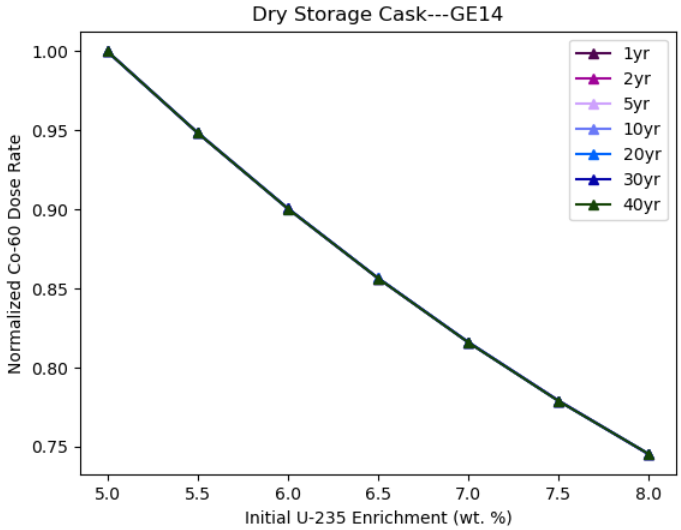

Figure 7-67 Cobalt-60 Dose Rate Trends of Variation with BWR Initial Fuel Enrichment (^{235}U wt %) and Cooling Time (years)

7.2.3 Cooling Time

The effect of postirradiation cooling time on cask dose rates was analyzed for BWR fuel with maximum fuel pin enrichments of 5, 5.5, 6.0, 6.5, 7.0, 7.5, and 8 wt % ^{235}U. The fuel was burned up to 75 GWd/MTU.

7.2.3.1 Neutron Dose Rate Trends

Figure 7-68 illustrates the effects on the neutron dose rate of varying cooling time for BWR fuel with several different initial enrichments. Neutron dose rates for a dry storage cask and a transportation package are provided. As discussed in Section 3.4.1.1 of NUREG/CR-6716 [63], the neutron dose rate decreased constantly and approximately exponentially with increasing cooling time over the range of cooling times analyzed.

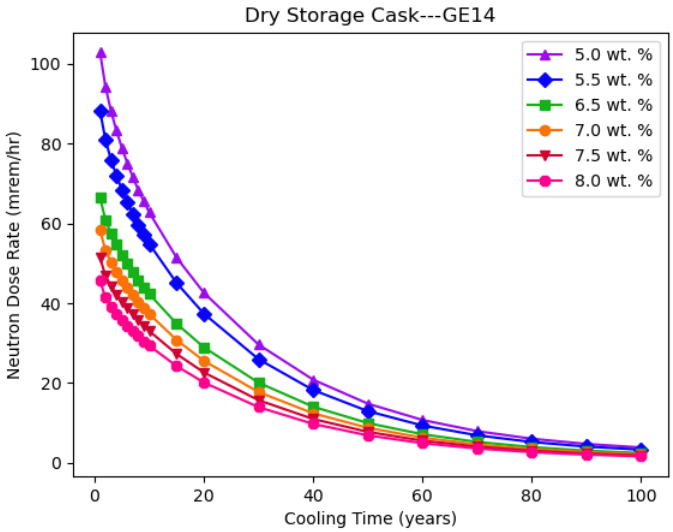

Figure 7-68 Neutron Dose Rate Trends of Variation with BWR Fuel Cooling Time (years)

7.2.3.2 Gamma Dose Rate Trends

Figure 7-69 illustrates the effects on the primary gamma dose rate of varying cooling time for BWR fuel with several different initial enrichments. Primary gamma dose rates for a dry storage cask and a transportation package are provided. As discussed in Section 3.4.1.1 of NUREG/CR-6716 [63], the primary gamma dose rate decreased very quickly between cooling times of approximately 5 and 20 yr. Beyond 20 yr, the primary gamma dose rate decreased approximately exponentially over the range of cooling times analyzed.

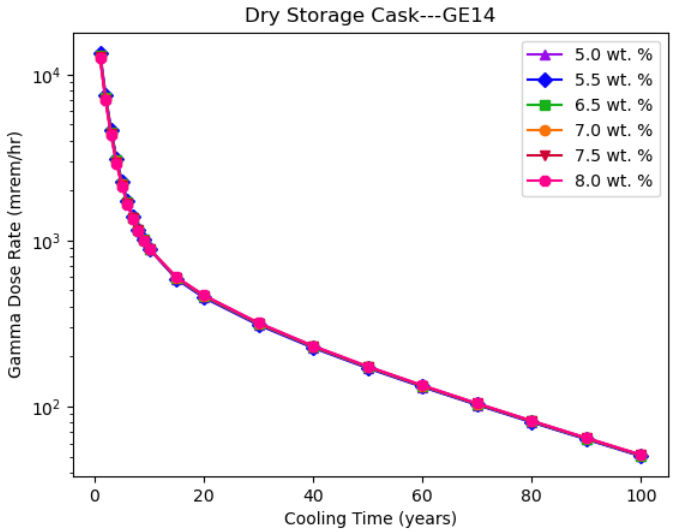

Figure 7-69 Primary Gamma Dose Rate Trends of Variation with BWR Fuel Cooling Time (years)

7.2.3.3 Cobalt-60 Dose Rate Trends

Figure 7-70 illustrates the effects on the ^{60}Co gamma dose rate of varying cooling time for BWR fuel with several different initial enrichments. Cobalt-60 dose rates for a dry storage cask and a transportation package are provided. The ^{60}Co dose rate decreased constantly and approximately exponentially with increasing cooling time over the range of cooling times analyzed.

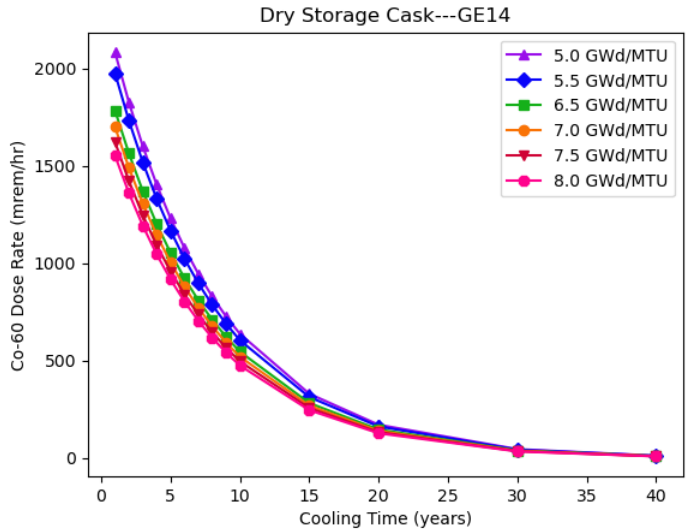

Figure 7-70 Cobalt-60 Dose Rate Trends of Variation with BWR Fuel Cooling Time (years)

7.2.4 Specific Power

The effect of assembly specific power on cask dose rates was analyzed for BWR fuel with maximum fuel pin enrichments of 5 and 8 wt % ^{235}U. The fuel was burned up to 75 GWd/MTU using specific powers of 15, 20, 30, 40, and 50 MW/MTU.

7.2.4.1 Neutron Dose Rate Trends

The graphs in Figure 7-71 illustrate the effects on the neutron dose rate of varying specific power for BWR fuel with 8 wt % enrichment at fixed assembly average burnup (75 GWd/MTU) over a range of cooling times. The graphs in Figure 7-72 illustrate these effects at different initial enrichments and cooling times at fixed assembly average burnup (75 GWd/MTU). These graphs show that neutron dose rate increases with increasing specific power, and the effects were approximately equal for both initial fuel enrichments analyzed. These effects decrease with increasing specific power at longer cooling times. The relatively small effect of specific power on the neutron dose rate was also observed for 3.5 wt % PWR fuel burned to 40 GWd/MTU over a range of specific powers in Section 3.4.2.4 of NUREG/CR-6716 [63]. As shown in Figure 7-73, for a given cooling time (5 yr), the effect of specific power on neutron dose rate slightly increases with increasing burnup.

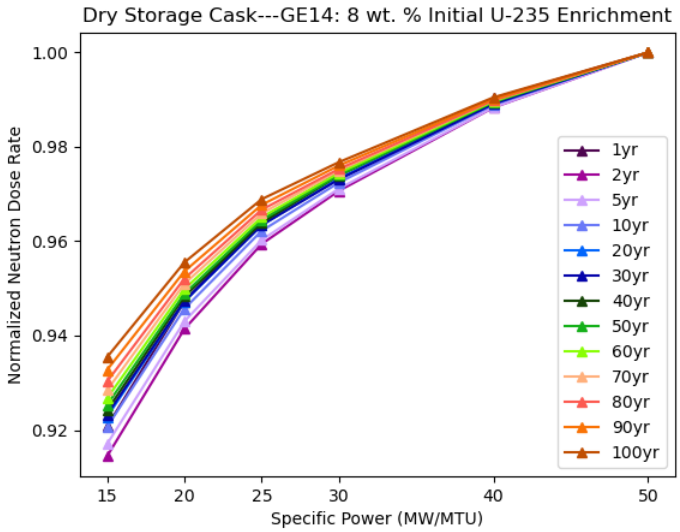

Figure 7-71 Neutron Dose Rate Trends of Variation with BWR Specific Power (MW/MTU) and Cooling Time (years) (Normalization to Highest Dose Rate Value at Each Cooling Time)

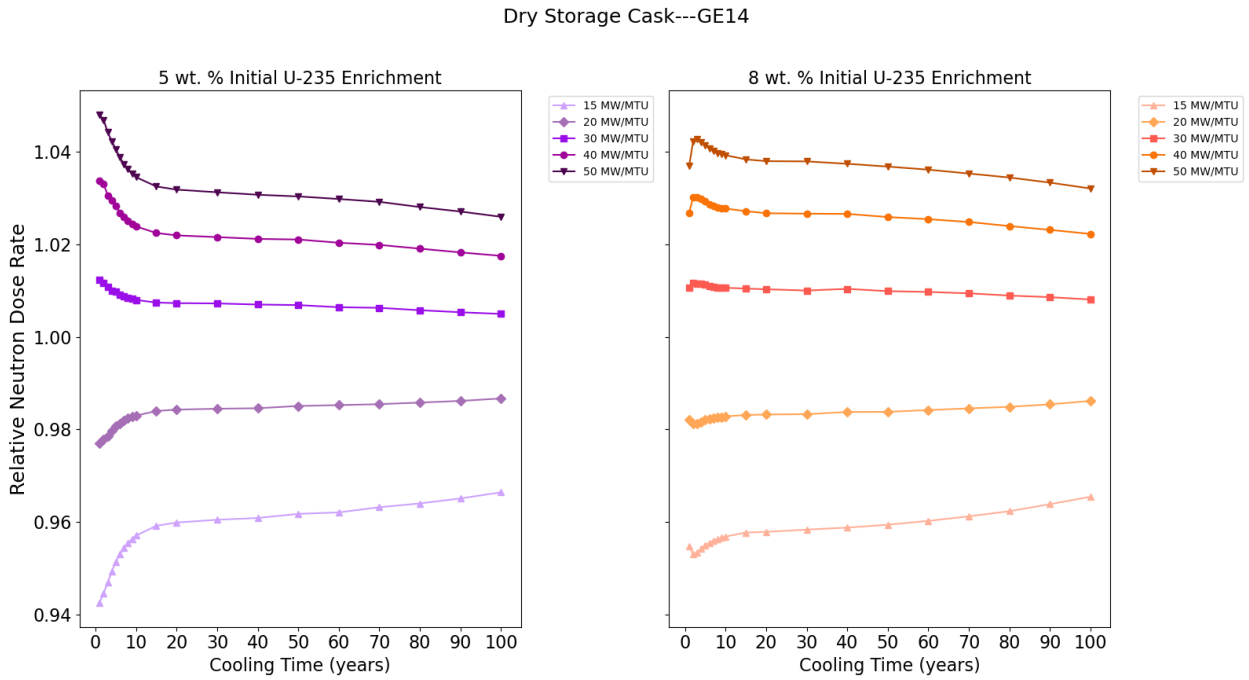

Figure 7-72 Comparative Effects of Varying Specific Power on Neutron Dose Rate from BWR Fuel with Different Enrichments (Normalization to Dose Rate Values for a 25 MW/MTU Specific Power)

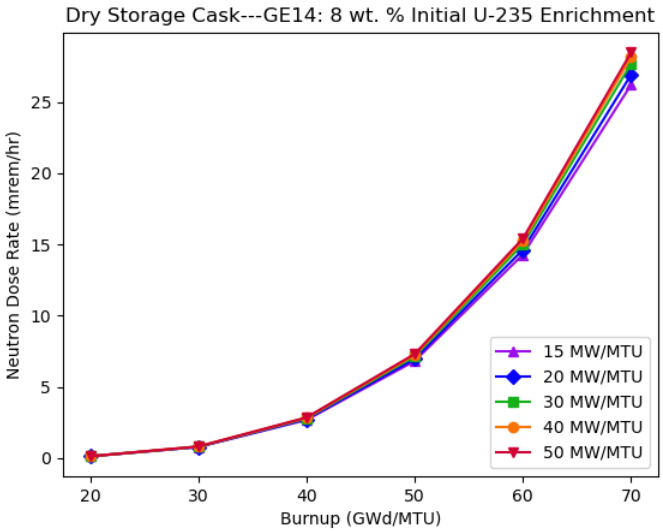

Figure 7-73 Neutron Dose Rate Trends of Variation with BWR Specific Power (MW/MTU) and Burnup (GWd/MTU)

7.2.4.2 Gamma Dose Rate Trends

Figure 7-74 illustrates the effects on the primary gamma dose rate of varying specific power for BWR fuel with 8 wt % enrichment at fixed assembly average burnup (75 GWd/MTU) over a range of cooling times. The graphs in Figure 7-75 illustrate these effects at different initial enrichments and cooling times at fixed assembly average burnup (75 GWd/MTU). These graphs show that the primary gamma dose rate increases with increasing specific power over the range of cooling times analyzed. As with the PWR assembly, the effects were greatest at approximately 1 yr of cooling time, indicating that shorter-lived fission products are more sensitive to the specific power than longer-lived fission products. Beyond approximately 10 yr of cooling time, the gamma dose rate decreased exponentially, independent of specific power. The effects were generally the same for 5 and 8 wt % initial enrichments. These same effects were observed for 3.5 wt % PWR fuel burned to 40 GWd/MTU over a range of specific powers in Section 3.4.2.4 of NUREG/CR-6716 [63]. As shown in Figure 7-76, for a given cooling time (5 yr), the effect of specific power on primary gamma dose rate increases with increasing burnup.

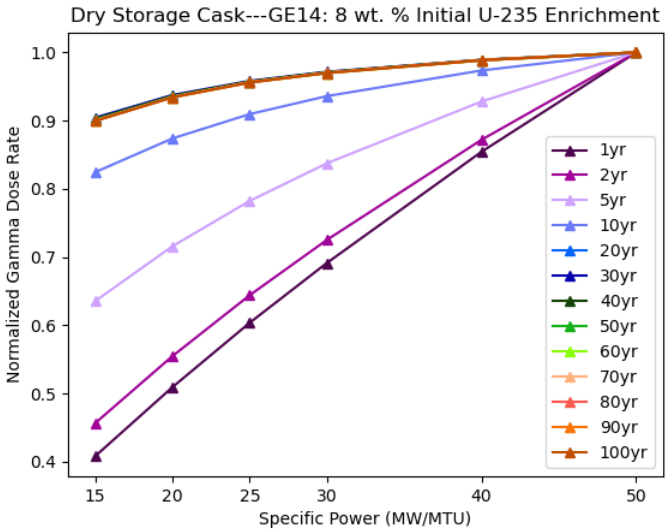

Figure 7-74 Primary Gamma Dose Rate Trends of Variation with BWR Specific Power (MW/MTU) and Cooling Time (years) (Normalization to Highest Dose Rate Value at Each Cooling Time)

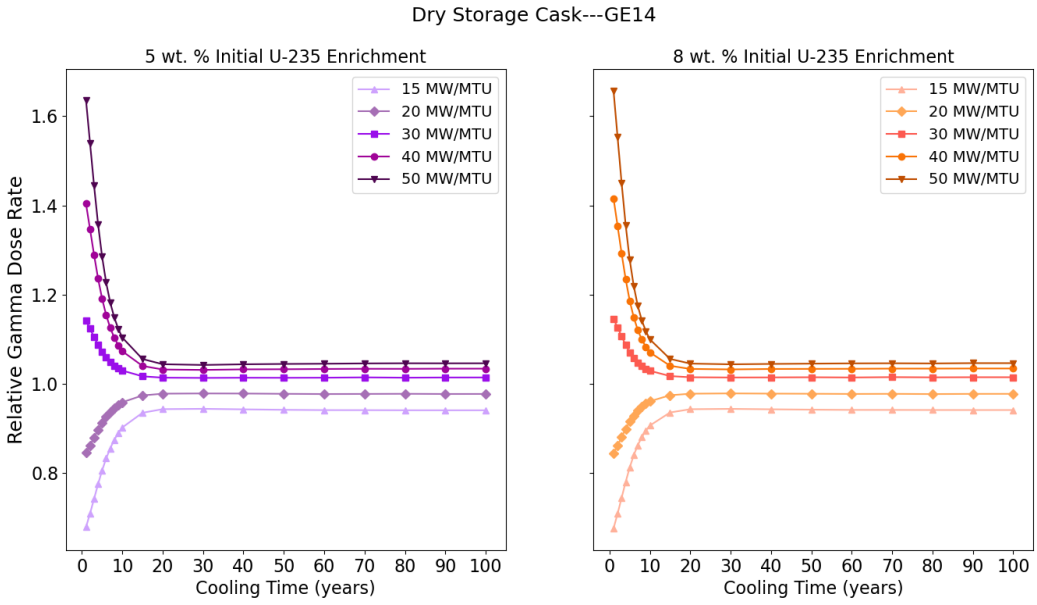

Figure 7-75 Comparative Effects of Varying Specific Power on Primary Gamma Dose Rate from BWR Fuel with Different Enrichments (Normalization to Dose Rate Values for a 25 MW/MTU Specific Power)

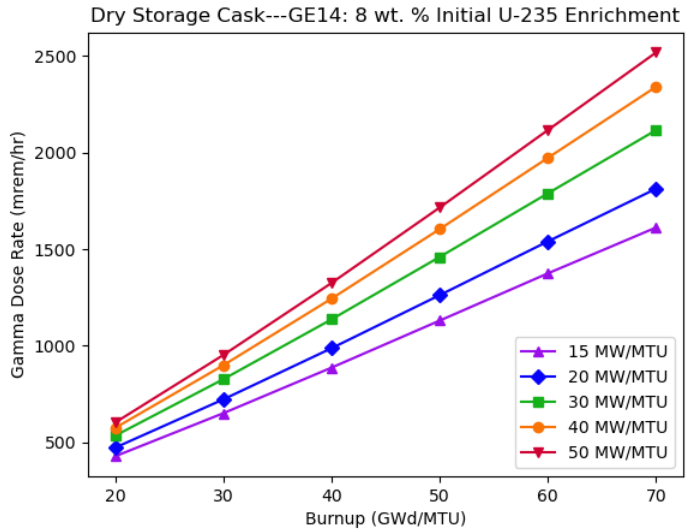

Figure 7-76 Primary Gamma Dose Rate Trends of Variation with BWR Specific Power (MW/MTU) and Burnup (GWd/MTU)

7.2.4.3 Cobalt-60 Dose Rate Trends

Figure 7-77 illustrates the effects on the ^{60}Co dose rate of varying specific power for BWR fuel with 8 wt % enrichment at fixed assembly average burnup (75 GWd/MTU) over a range of cooling times. The graphs in Figure 7-78 illustrate these effects at different initial enrichments and cooling time at fixed assembly average burnup (75 GWd/MTU). These graphs show that ^{60}Co dose rate increases with increasing specific power over the range of cooling times analyzed, and the effects are independent of initial fuel enrichment. Similar to the primary gamma dose rate, for a given cooling time (5 yr) the effect of specific power on ^{60}Co dose rate increases with increasing burnup.

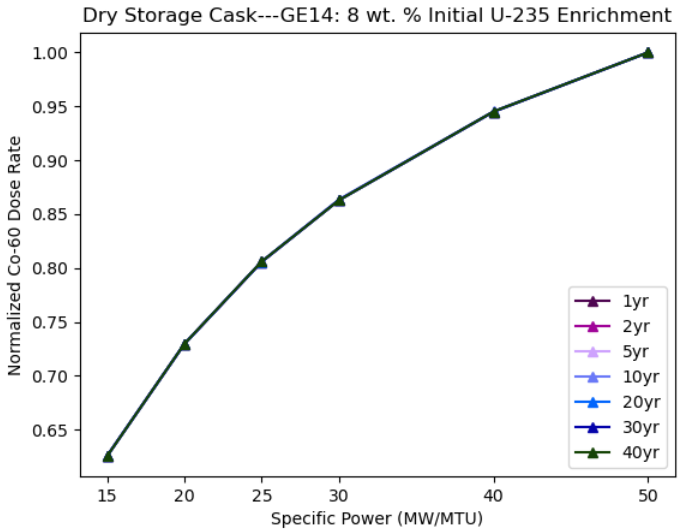

Figure 7-77 Cobalt-60 Dose Rate Trends of Variation with BWR Specific Power (MW/MTU) and Cooling Time (years) (Normalization to Highest Dose Rate Value at Each Cooling Time)

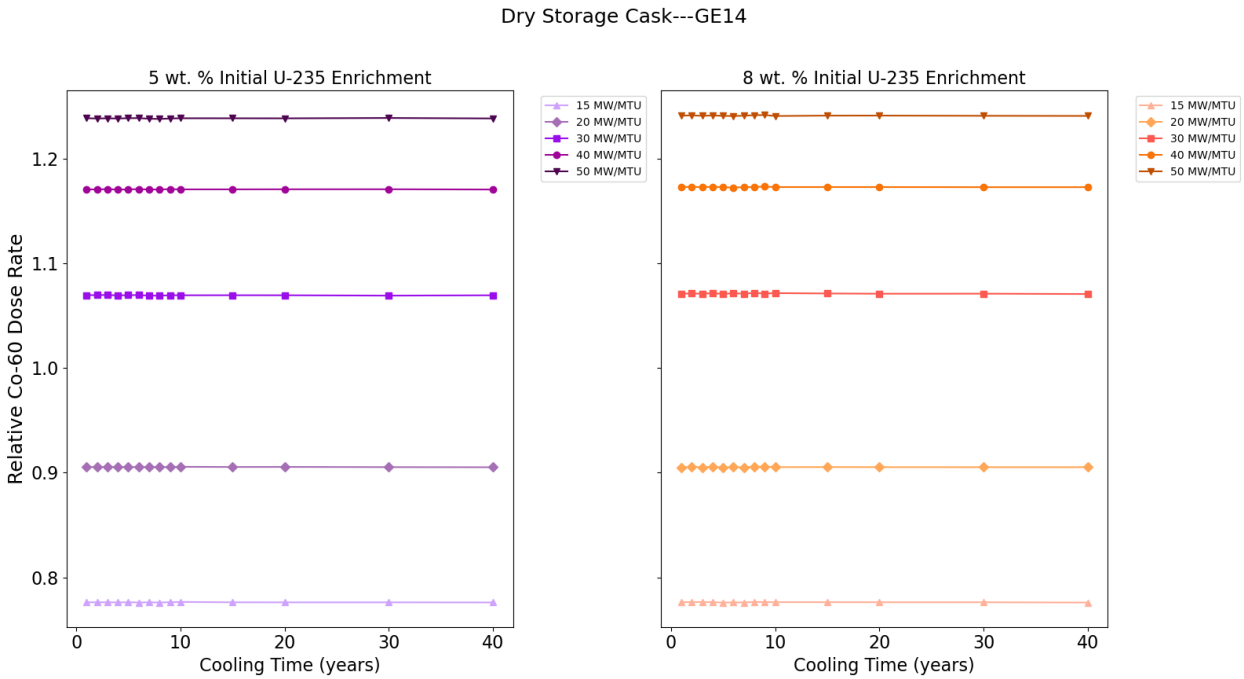

Figure 7-78 Comparative Effects of Varying Specific Power on ^{60}Co Dose Rate from BWR Fuel with Different Enrichments (Normalization to Dose Rate Values for a 25 MW/MTU Specific Power)

7.2.5 Coolant Void Fraction

The effect of coolant void fraction on cask dose rates was presented for 5 and 8 wt % ^{235}U BWR fuel. The fuel was burned up to 75 GWd/MTU using coolant void fractions of 20, 40, 60, and 80 percent.

7.2.5.1 Neutron Dose Rate Trends

Figure 7-79 illustrates the effects on the neutron dose rate of varying coolant void fraction for BWR fuel with 8 wt % enrichment at fixed assembly average burnup (75 GWd/MTU) over a range of cooling times. The graphs in Figure 7-80 illustrate these effects at different initial enrichments and cooling time at fixed assembly average burnup (75 GWd/MTU). The neutron dose rate was observed to increase with increasing coolant void fraction. These effects are slightly greater for 8 wt % enrichment compared to 5 wt % enrichment. The effect of coolant void fraction on neutron dose rates was significant, especially at large coolant void fractions. The trends observed in this analysis were consistent with the moderator density analysis in Section 3.4.2.5 in NUREG/CR-6716 [63], which was performed for fuel with 4 wt % enrichment and 40 GWd/MTU burnup. As shown in Figure 7-81, for a given cooling time (5 yr), the effect of coolant void fraction on neutron dose rate increases with increasing burnup.

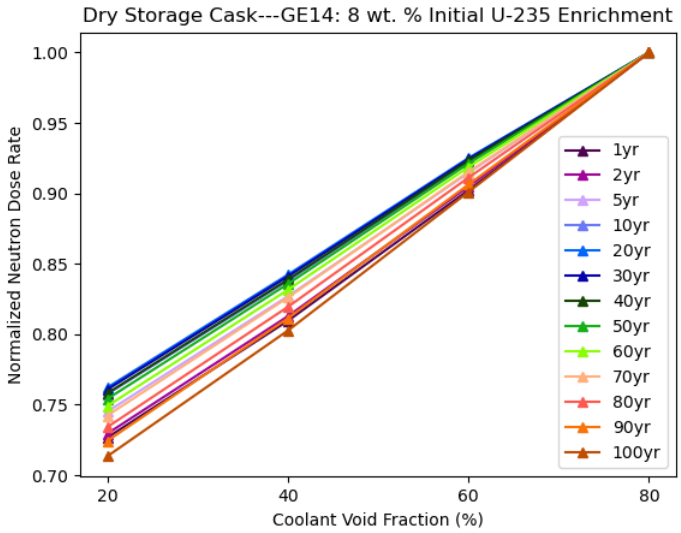

Figure 7-79 Neutron Dose Rate Trends of Variation with BWR Coolant Void Fraction and Cooling Time (years) (Normalization to Highest Dose Rate Value at Each Cooling Time)

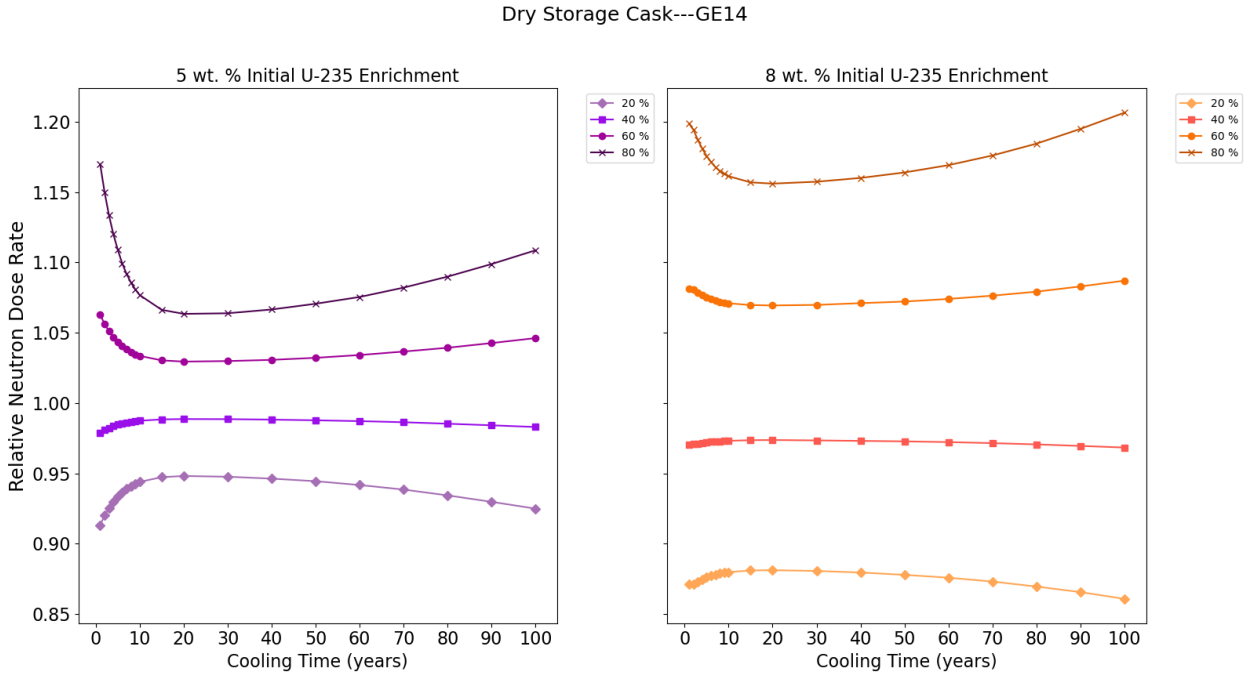

Figure 7-80 Comparative Effects of Varying Coolant Void Fraction on Neutron Dose Rate from BWR Fuel with Different Enrichments (Normalization to Dose Rate Values for Baseline Assembly with 45.5% Void)

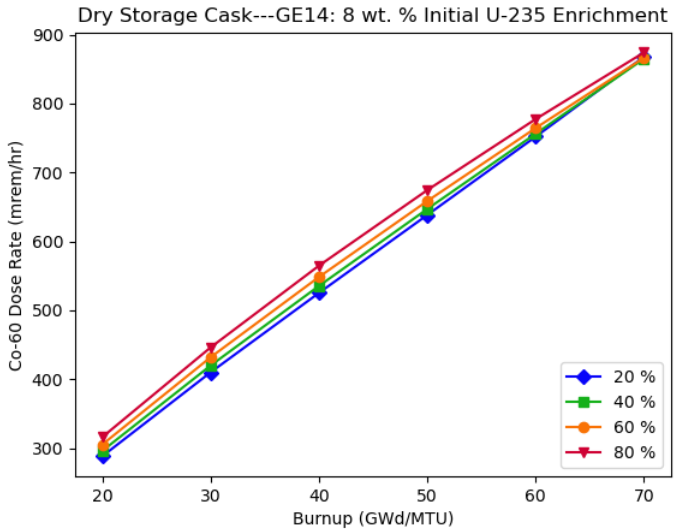

Figure 7-81 Neutron Dose Rate Trends of Variation with BWR Coolant Void Fraction and Burnup (GWd/MTU)

7.2.5.2 Gamma Dose Rate Trends

Figure 7-82 illustrates the effects on the primary gamma dose rate of varying coolant void fraction for BWR fuel with 8 wt % enrichment at fixed assembly average burnup (75 GWd/MTU) over a range of cooling times. The graphs in Figure 7-83 illustrate these effects at different initial enrichments and cooling times at fixed assembly average burnup (75 GWd/MTU). The gamma dose rate was observed to increase with increasing coolant void fraction until a cooling time of approximately 80 yr, beyond which the effect was mitigated. The trends observed in this analysis were consistent with the moderator density analysis in Section 3.4.2.5 in NUREG/CR-6716 [63], which was performed for fuel with 4 wt % enrichment and 40 GWd/MTU burnup. As shown in Figure 7-84, for a given cooling time (5 yr), the effect of coolant void fraction on the primary gamma dose rate increases with increasing burnup.

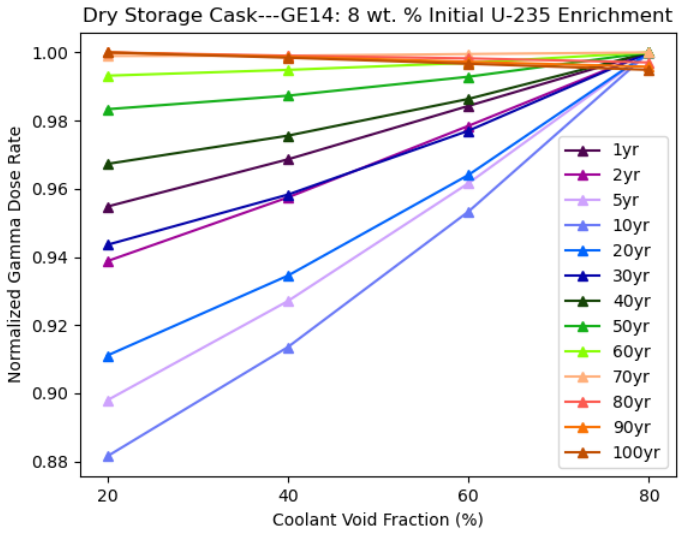

Figure 7-82 Primary Gamma Dose Rate Trends of Variation with BWR Coolant Void Fraction and Cooling Time (years) (Normalization to Highest Dose Rate Value at Each Cooling Time)

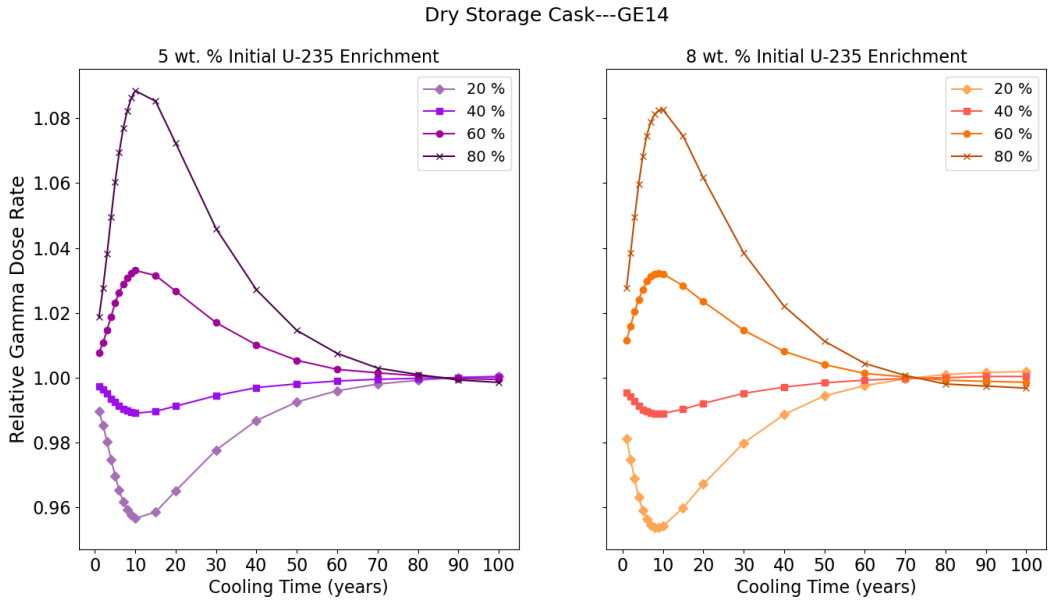

Figure 7-83 Comparative Effects of Varying Coolant Void Fraction on Primary Gamma Dose Rate from BWR Fuel with Different Enrichments (Normalization to Dose Rate Values for Baseline Assembly with 45.5% Void)

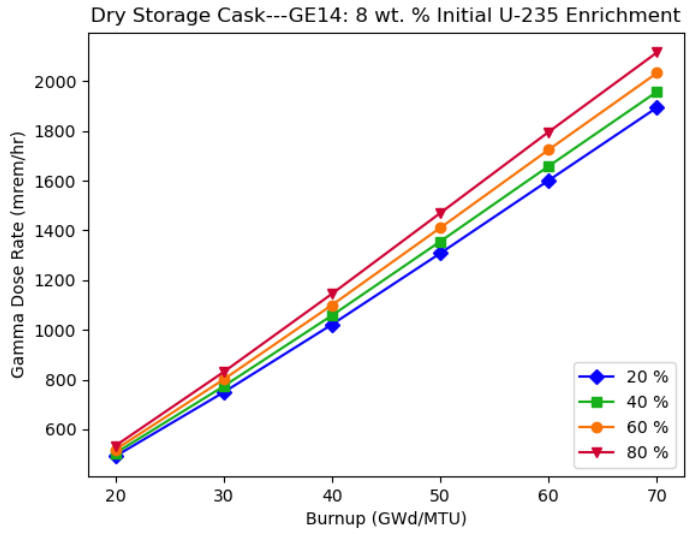

Figure 7-84 Primary Gamma Dose Rate Trends of Variation with BWR Coolant Void Fraction and Burnup (GWd/MTU)

7.2.5.3 Cobalt-60 Dose Rate Trends

Figure 7-85 illustrates the effects on the ^{60}Co dose rate of varying coolant void fraction for BWR fuel with 8 wt % enrichment at fixed assembly average burnup (75 GWd/MTU) over a range of cooling times. The graphs in Figure 7-86 illustrate these effects at different initial enrichments and cooling times at fixed assembly average burnup (75 GWd/MTU). These graphs show that, for 8 wt % fuel over all cooling times analyzed, the ^{60}Co dose rate decreases with increasing coolant void fraction until the coolant void fraction reaches a certain value, beyond which the trend is reversed. For 5 wt % fuel, the ^{60}Co dose rate decreases with increasing coolant void fraction. The value of the coolant void fraction at which the trend reverses is dependent on the initial enrichment and burnup achieved. As with the PWR fuel, the relatively soft neutron spectrum of the 5 wt % fuel results in ^{59}Co neutron capture increasing with decreasing coolant void fraction due to larger cross sections in the thermal range. The 8 wt % fuel generally displays this same trend but is offset at higher coolant void fractions due to the relatively hard spectrum of higher-enriched fuel and the large ^{59}Co neutron capture resonance peak at approximately 100 eV [64]. As shown in Figure 7-87, for a given cooling time (5 yr), the ^{60}Co dose rate for 5 wt % fuel begins to increase with decreasing coolant density at a burnup of 50 GWd/MTU, and for 8 wt % fuel, this trend occurs beyond 70 GWd/MTU (also demonstrated in Figure 7-85).

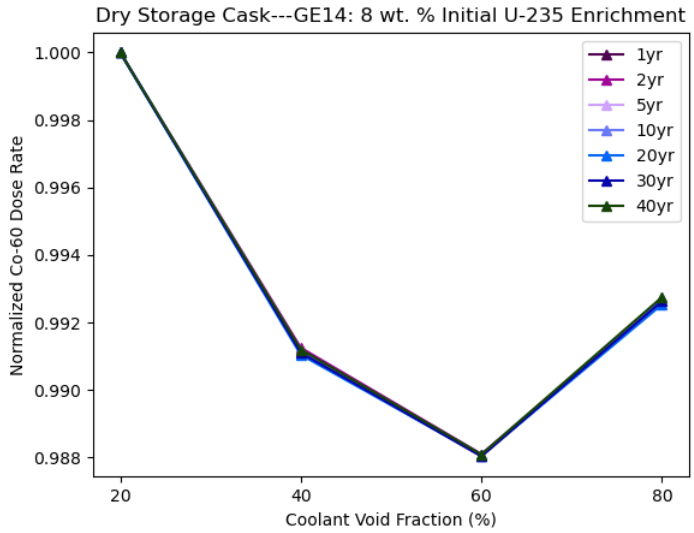

Figure 7-85 Cobalt-60 Dose Rate Trends of Variation with BWR Coolant Void Fraction and Cooling Time (years) (Normalization to Highest Dose Rate Value at Each Cooling Time)

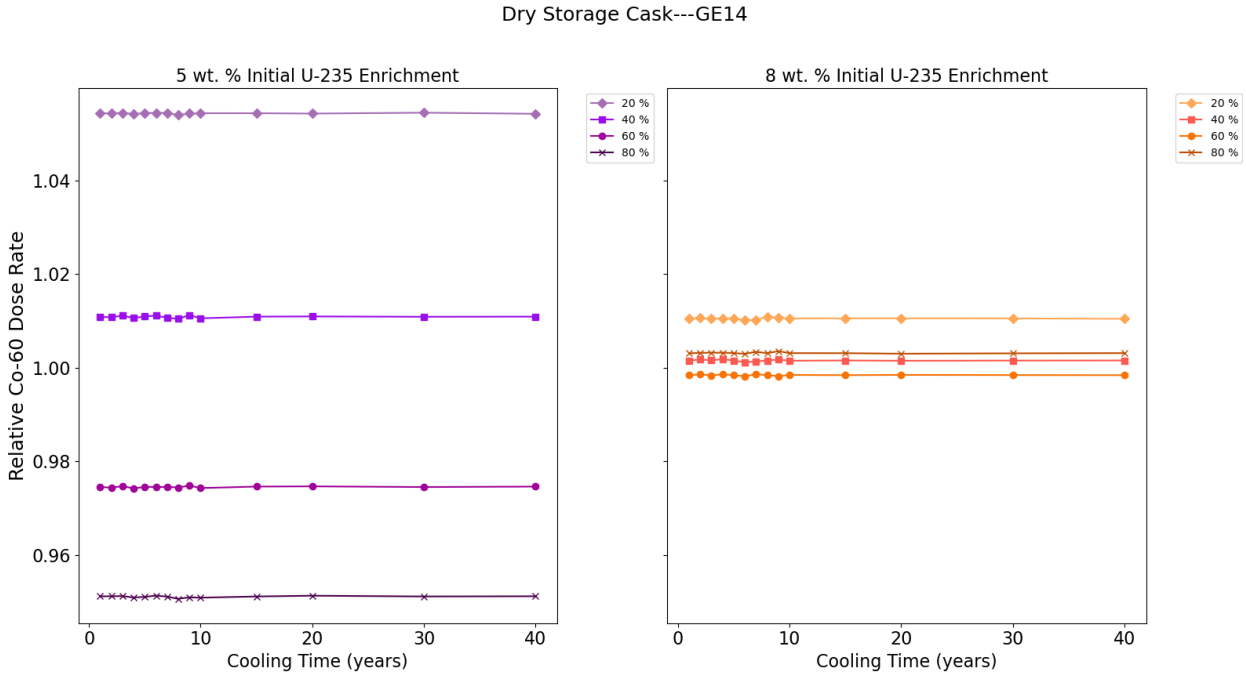

Figure 7-86 Comparative Effects of Varying Coolant Void Fraction on ^{60}Co Dose Rate from BWR Fuel with Different Enrichments (Normalization to Dose Rate Values for Baseline Assembly with 45.5% Void)

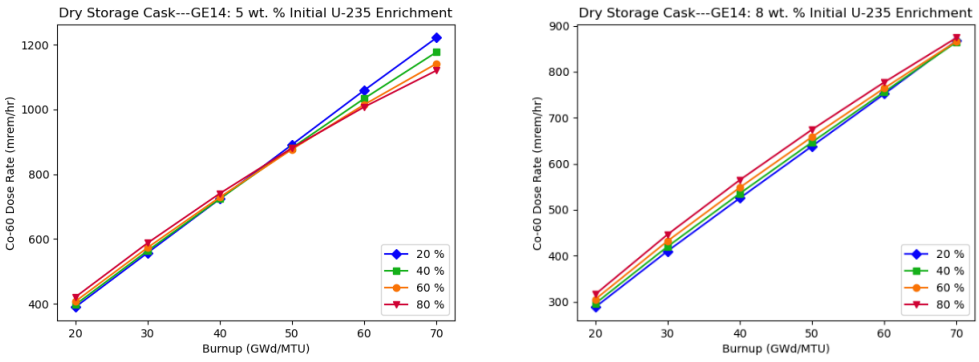

Figure 7-87 Cobalt-60 Dose Rate Trends of Variation with BWR Coolant Void Fraction and Burnup (GWd/MTU)

7.2.6 Fuel Temperature

The effect of fuel temperature on cask dose rates was presented for 5 and 8 wt % ^{235}U BWR fuel. The fuel temperatures analyzed are provided in Section 3.2.

7.2.6.1 Neutron Dose Rate Trends

Figure 7-88 illustrates the effects on the neutron dose rate of varying fuel temperature for BWR fuel with 8 wt % enrichment at fixed assembly average burnup (75 GWd/MTU) over a range of cooling times. The graphs in Figure 7-89 illustrate these effects at different initial enrichments and cooling times at fixed assembly average burnup (75 GWd/MTU). These graphs show that neutron dose rate is relatively insensitive to fuel temperature, as the dose rate only changed by 1%–2%. The effects were different at each enrichment analyzed. For 5 wt % enrichment, the neutron dose rate increased with increasing fuel temperature between cooling times of approximately 5 and 70 yr, but the trend was reversed outside of this range. For 8 wt % enrichment, the neutron dose rate increased with increasing fuel temperature over the entire range of cooling times analyzed, and the effect was slightly reduced at long cooling times. As shown in Figure 7-90, for a given cooling time (5 yr), the effect of fuel temperature on neutron dose rate slightly increases with increasing burnup.

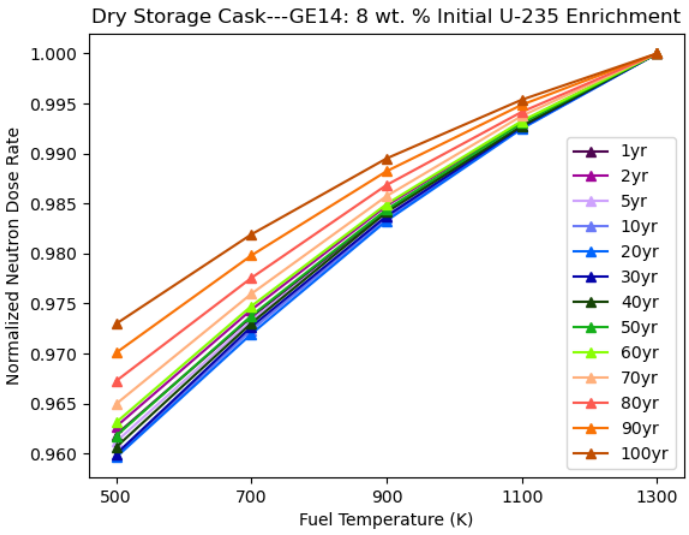

Figure 7-88 Neutron Dose Rate Trends of Variation with BWR Fuel Temperature (K) and Cooling Time (years) (Normalization to Highest Dose Rate Value at Each Cooling Time)

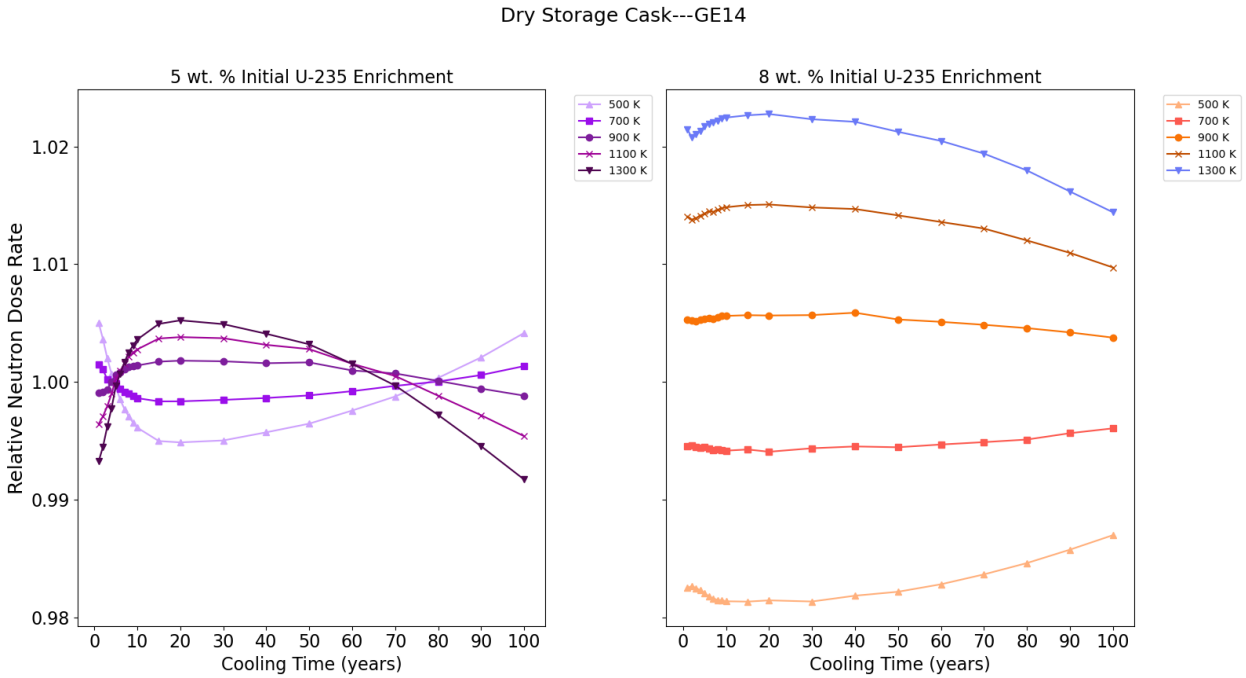

Figure 7-89 Comparative Effects of Varying Fuel Temperature on Neutron Dose Rate from BWR Fuel with Different Enrichments (Normalization to Dose Rate Values for a 800 K Fuel Temperature)

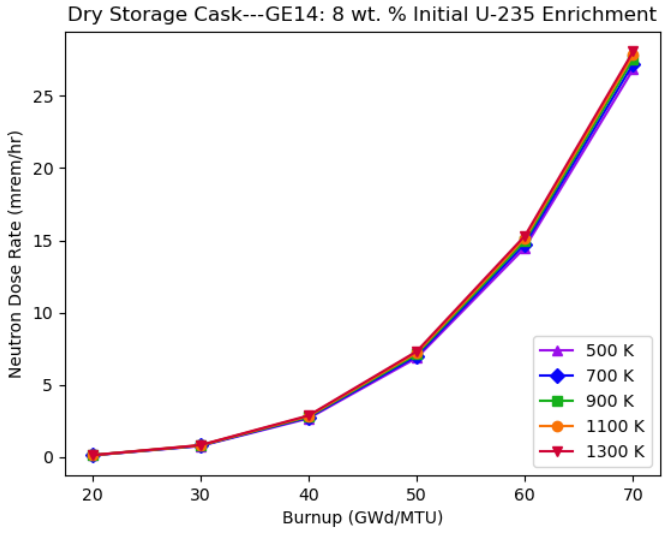

Figure 7-90 Neutron Dose Rate Trends of Variation with BWR Fuel Temperature and Burnup (GWd/MTU)

7.2.6.2 Gamma Dose Rate Trends

Figure 7-91 illustrates the effects on the primary gamma dose rate of varying fuel temperature for BWR fuel with 8 wt % enrichment at fixed assembly average burnup (75 GWd/MTU) over a range of cooling times. The graphs in Figure 7-92 illustrate these effects at different initial enrichments and cooling times at fixed assembly average burnup (75 GWd/MTU). These graphs show that the primary gamma dose rate is relatively insensitive to fuel temperature, as the dose rate changed by less than 1%. Maximum effects were observed at a cooling time of approximately 15 yr. These effects were slightly higher at 5 wt % enrichment than at 8 wt % enrichment. As shown in Figure 7-93, for a given cooling time (5 yr), the effect of fuel temperature on primary gamma dose rate is insensitive to fuel burnup.

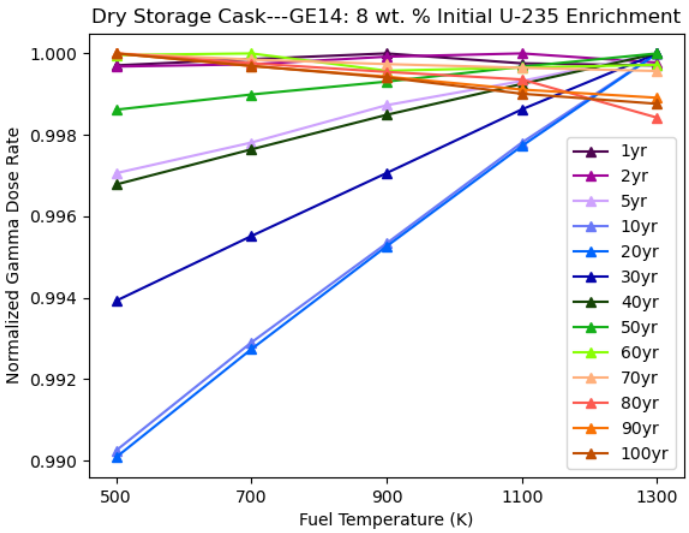

Figure 7-91 Primary Gamma Dose Rate Trends of Variation with BWR Fuel Temperature (K) and Cooling Time (years) (Normalization to Highest Dose Rate Value at Each Cooling Time)

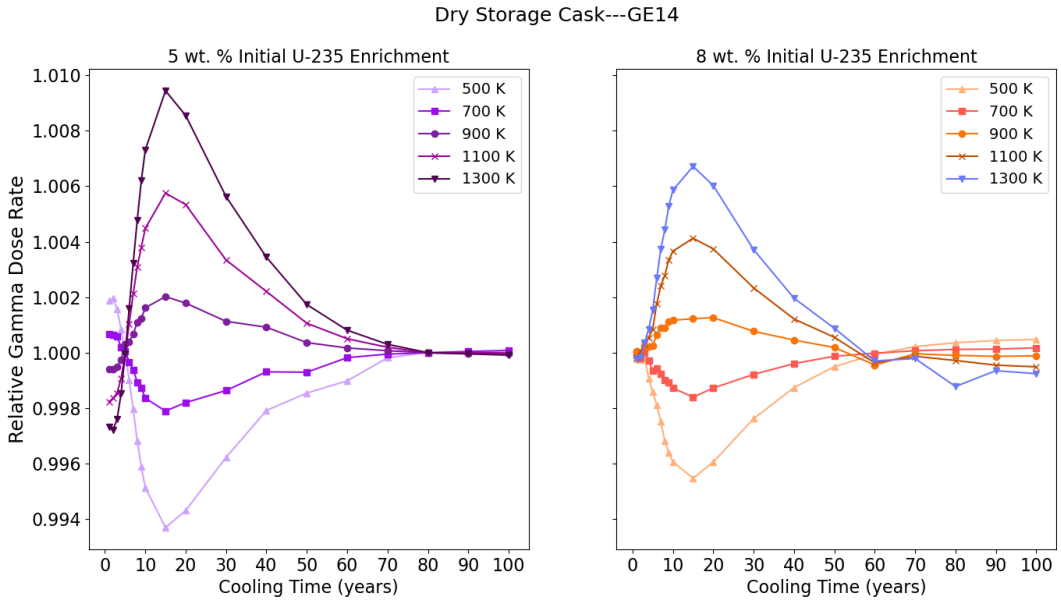

Figure 7-92 Comparative Effects of Varying Fuel Temperature on Primary Gamma Dose Rate from BWR Fuel with Different Enrichments (Normalization to Dose Rate Values for a 800 K Fuel Temperature)

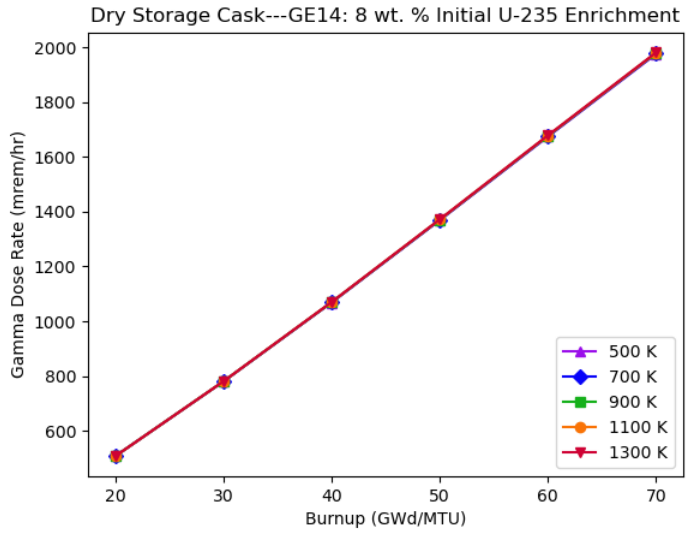

Figure 7-93 Primary Gamma Dose Rate Trends of Variation with BWR Fuel Temperature and Burnup (GWd/MTU)

7.2.6.3 Cobalt-60 Dose Rate Trends

Figure 7-94 illustrates the effects on the ^{60}Co dose rate of varying fuel temperature for BWR fuel with 8 wt % enrichment at fixed assembly average burnup (75 GWd/MTU) over a range of cooling times. The graphs in Figure 7-95 illustrate these effects at different initial enrichments and cooling times at fixed assembly average burnup (75 GWd/MTU). These graphs show that across all the cooling times analyzed, the ^{60}Co dose rate increased with decreasing fuel temperature. As shown in Figure 7-96, for a given cooling time (5 yr), the effect of fuel temperature on the ^{60}Co dose rate increases slightly with increasing fuel burnup.

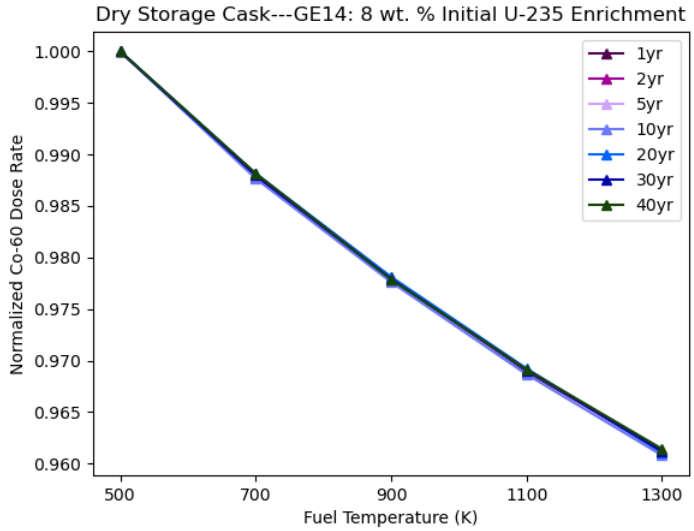

Figure 7-94 Cobalt-60 Dose Rate Trends of Variation with BWR Fuel Temperature (K) and Cooling Time (years) (Normalization to Highest Dose Rate Value at Each Cooling Time)

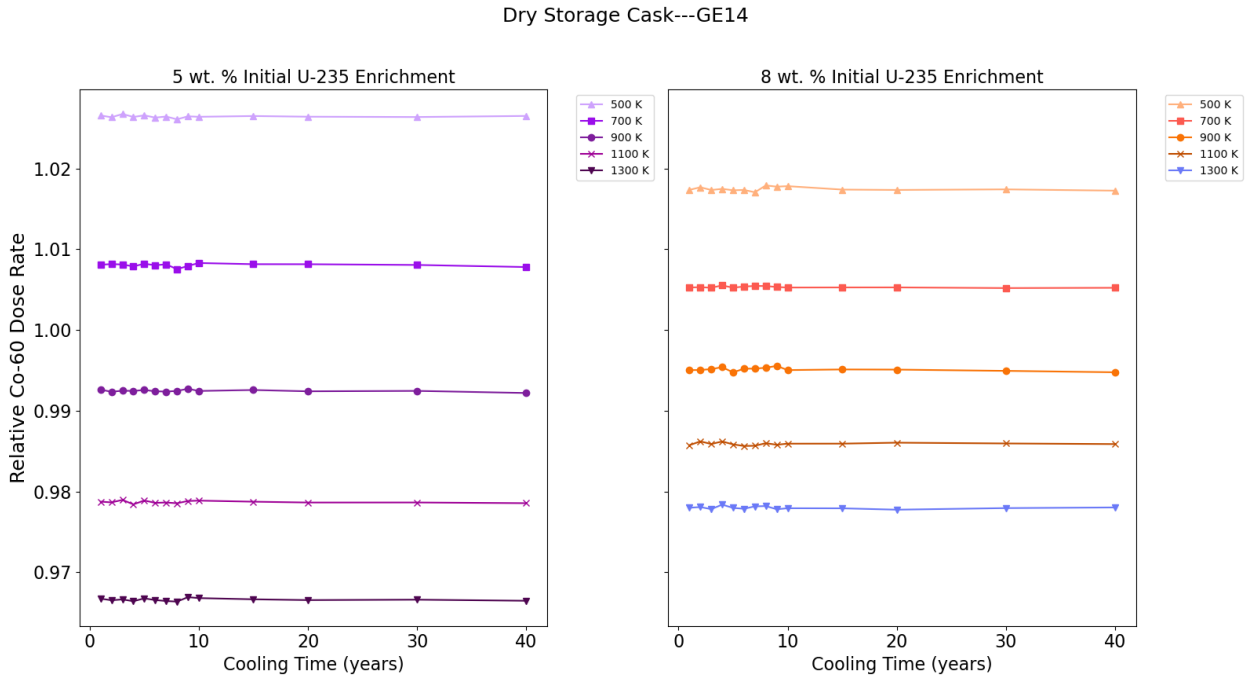

Figure 7-95 Comparative Effects of Varying Fuel Temperature on ^{60}Co Dose Rate from BWR Fuel with Different Enrichments (Normalization to Dose Rate Values for a 800 K Fuel Temperature)

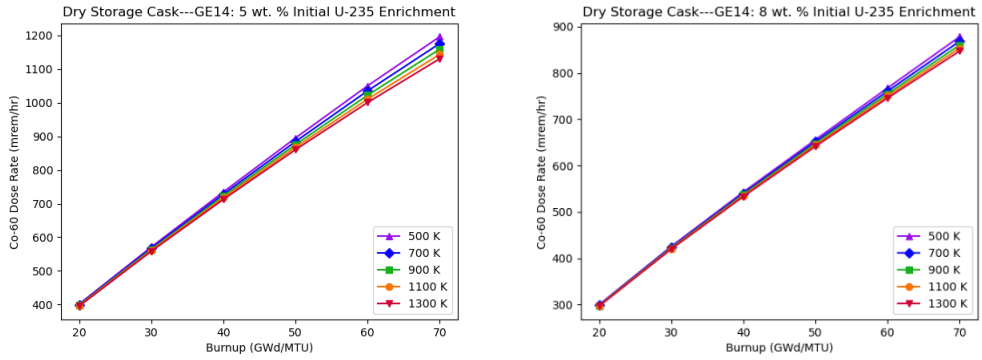

Figure 7-96 Cobalt-60 Dose Rate Trends of Variation with BWR Fuel Temperature and Burnup (GWd/MTU)

7.2.7 Fuel Density

The effect of fuel density on cask dose rates was presented for 5 and 8 wt % ^{235}U BWR fuel. The fuel densities analyzed are provided in Section 3.2. In this parametric study, the fuel density was perturbed without dimensional changes, and the same specific power and set of burnup values were used in all perturbed cases.

7.2.7.1 Neutron Dose Rate Trends

Figure 7-97 illustrates the effects on the neutron dose rate of varying fuel density for BWR fuel with 8 wt % enrichment at fixed assembly average burnup (75 GWd/MTU) over a range of cooling times. The graphs in Figure 7-98 illustrate these effects at different initial enrichments and cooling times at fixed assembly average burnup (75 GWd/MTU). The neutron dose rate was observed to increase with increasing fuel density. These effects are slightly greater at 8 wt % enrichment compared to 5 wt % enrichment. The effect of fuel density on neutron dose rate was not significant, as the dose rate only changed by approximately 2%. Increasing the fuel density (without changing fuel dimensions to conserve MTU) has the effect of increasing MTU while also increasing the degree of self-shielding. These trends agree with the analysis in Section 3.4.2.3 in NUREG/CR-6716 [63], which was performed using fuel with lower burnup and enrichment than what was used in this analysis. As shown in Figure 7-99, for a given cooling time (5 yr), the effect of fuel density on neutron dose rate increases very slightly with increasing fuel burnup.

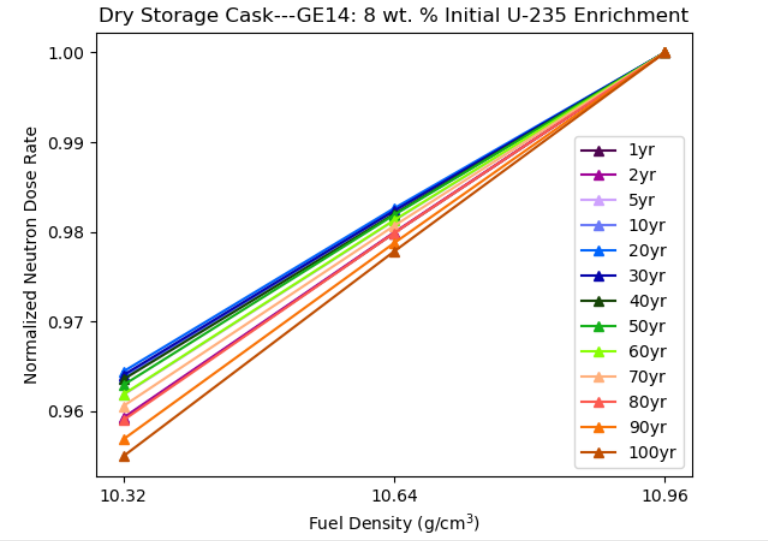

Figure 7-97 Neutron Dose Rate Trends of Variation with BWR Fuel Density (g/cm^3) as a Function of Cooling Time (years) (Normalization to Highest Dose Rate Value at Each Cooling Time)

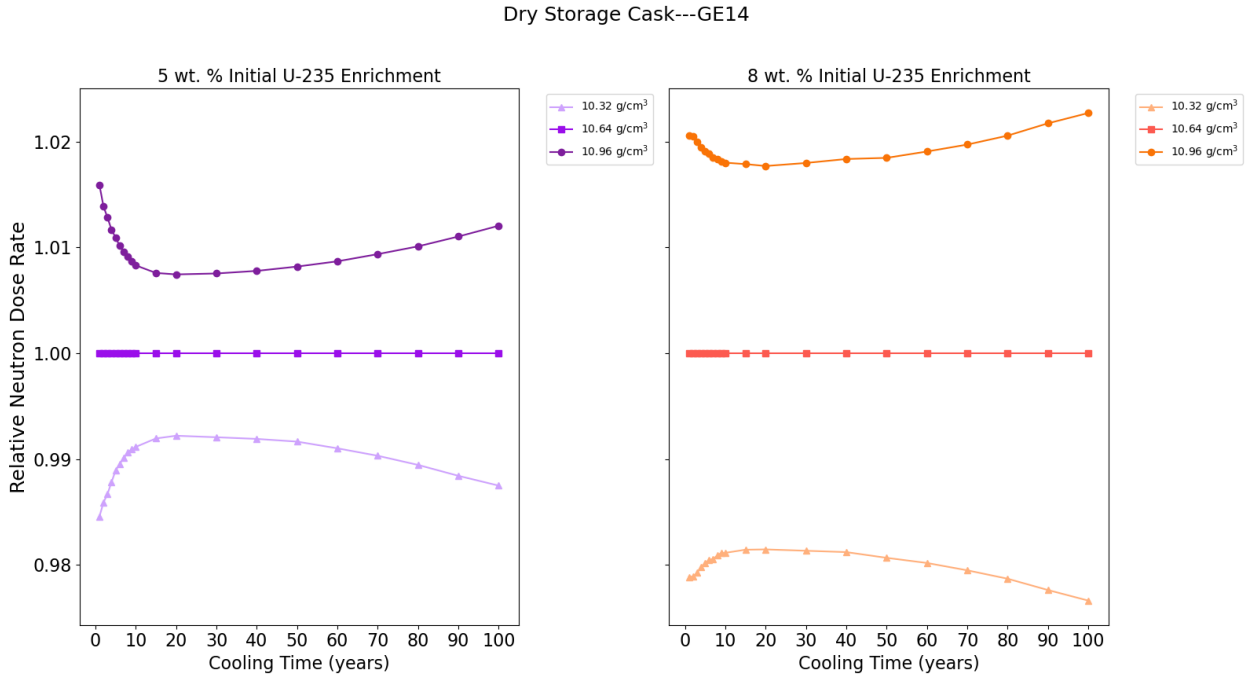

Figure 7-98 Comparative Effects of Varying Fuel Density on Neutron Dose Rate from BWR Fuel with Different Enrichments (Normalization to Dose Rate Values for a 10.64 g/cm³ Maximum Fuel Density)

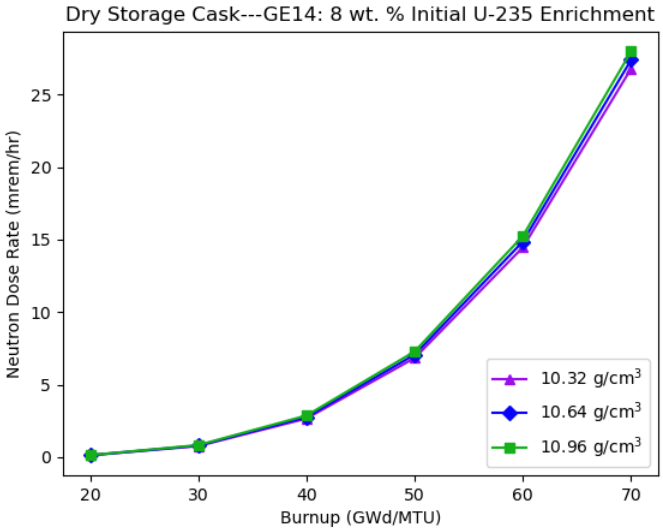

Figure 7-99 Neutron Dose Rate Trends of Variation with BWR Fuel Density and Burnup (GWd/MTU)

7.2.7.2 Gamma Dose Rate Trends

Figure 7-100 illustrates the effects on the primary gamma dose rate of varying fuel density for BWR fuel with 8 wt % enrichment at fixed assembly average burnup (75 GWd/MTU) over a range of cooling times. Changes in fuel density at fixed initial enrichment and average assembly burnup had negligible effects on the primary gamma dose rate, as the dose rates changed by less than 1% relative to the baseline. The smaller effect of fuel density on the gamma dose rate than neutron dose rate is supported by the analysis in Section 3.4.2.3 of NUREG/CR-6716 [63], which was performed using fuel with lower burnup and enrichment than what was used in this analysis. The maximum effects were achieved for the 10-year cooling time. These effects were approximately equal for both fuel enrichments analyzed. As shown in Figure 7-101, for a given cooling time (5 yr), the effect of fuel density on primary gamma dose rate is insensitive to fuel burnup.

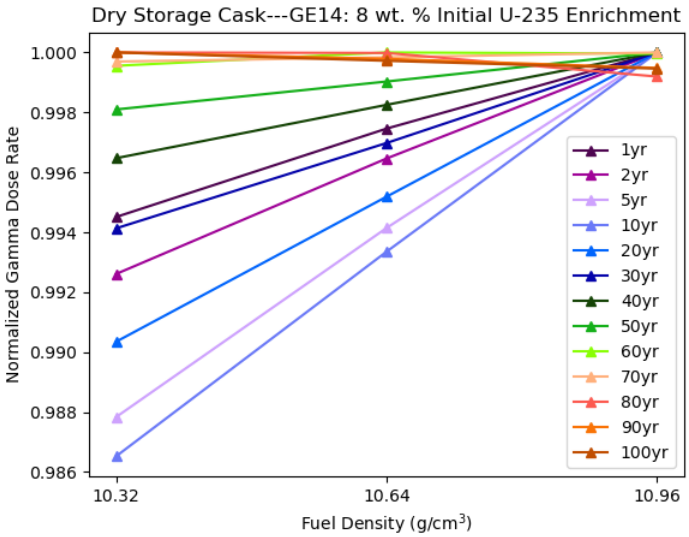

Figure 7-100 Primary Gamma Dose Rate Trends of Variation with BWR Fuel Density (g/cm^3) and Cooling Time (years) (Normalization to Highest Dose Rate Value at Each Cooling Time)

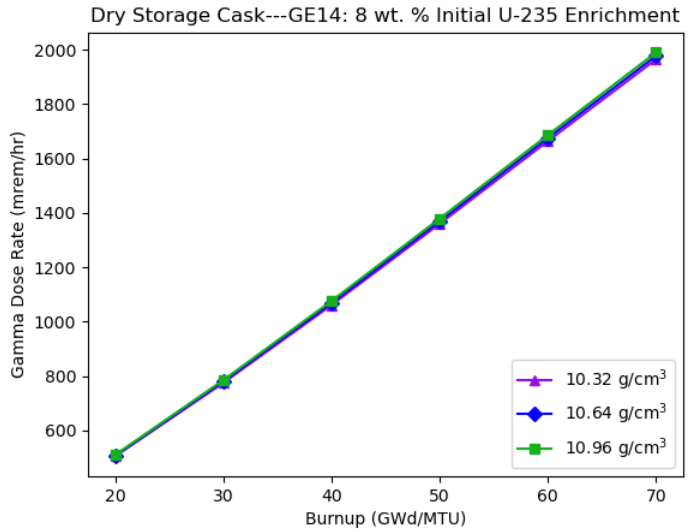

Figure 7-101 Primary Gamma Dose Rate Trends of Variation with BWR Fuel Density and Burnup (GWd/MTU)

7.2.7.3 Cobalt-60 Dose Rate Trends

Figure 7-102 illustrates the effects on the ^{60}Co dose rate of varying fuel density for BWR fuel with 8 wt % enrichment at fixed assembly average burnup (75 GWd/MTU) over a range of cooling times. The graphs in Figure 7-103 illustrate these effects at different initial enrichments and cooling times at fixed assembly average burnup (75 GWd/MTU). These graphs show that for all cooling times analyzed, the ^{60}Co dose rate decreased with increasing fuel density. These effects are slightly greater at 5 wt % enrichment compared to 8 wt % enrichment. As shown in Figure 7-104, for a given cooling time (5 yr), the effect of fuel density on ^{60}Co dose rate increases with increasing fuel burnup.

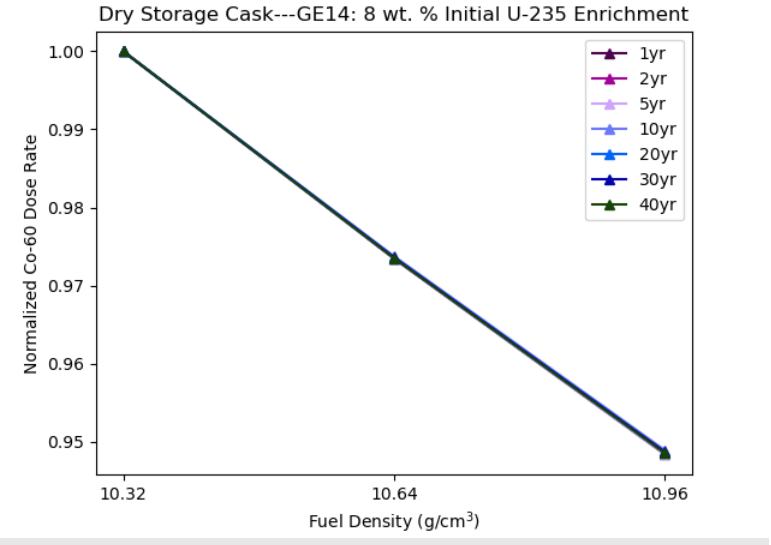

Figure 7-102 Cobalt-60 Dose Rate Trends of Variation with BWR Fuel Density (g/cm^3) and Cooling Time (years) (Normalization to Highest Dose Rate Value at Each Cooling Time)

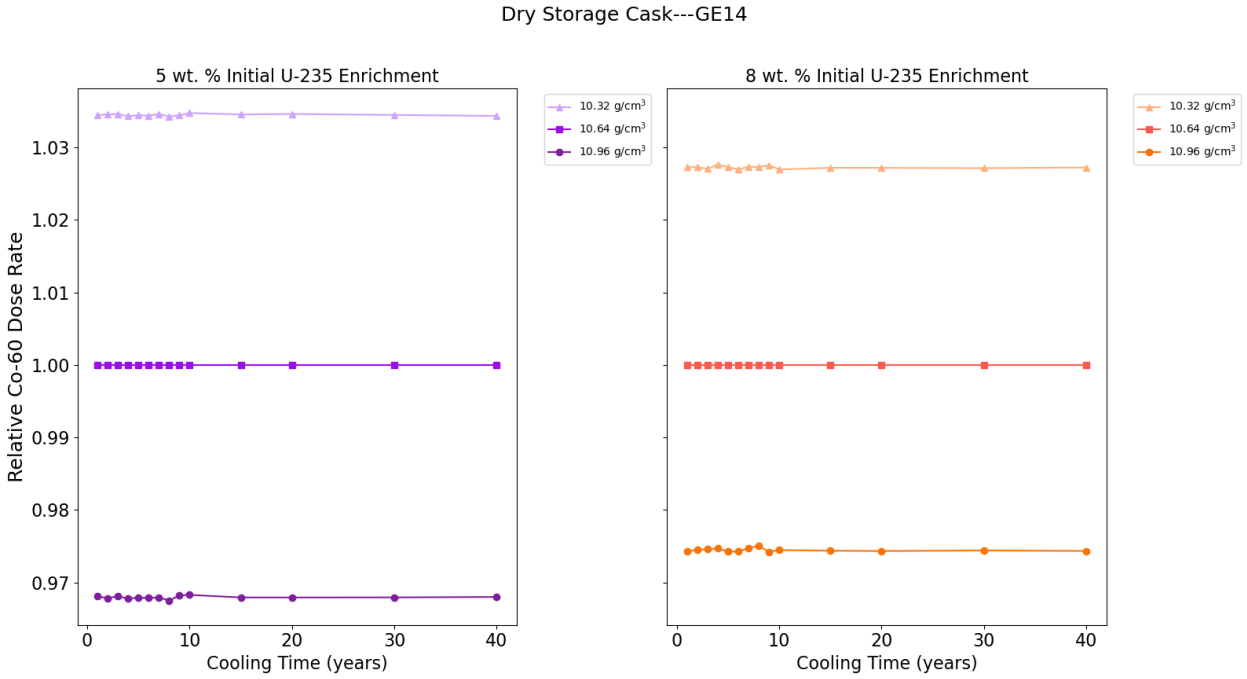

Figure 7-103 Comparative Effects of Varying Fuel Density on ^{60}Co Dose Rate from BWR Fuel with Different Enrichments (Normalization to Dose Rate Values for a 10.64 g/cm^3 Maximum Fuel Density)

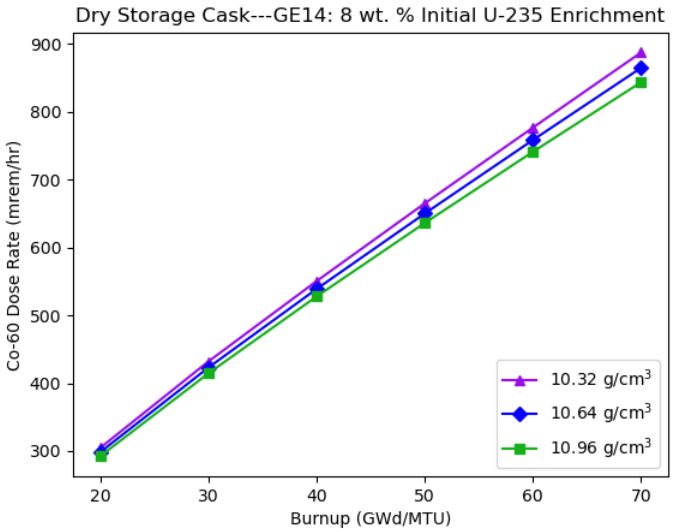

Figure 7-104 Cobalt-60 Dose Rate Trends of Variation with BWR Fuel Density and Burnup (GWd/MTU)

7.2.8 Control Rod Blade

For this study, the BWR control rod blade (described in Section 3.2) was considered. This analysis assumed that all assemblies in the cask contained fuel with the same exposure to the control blades. These studies were performed at 8 wt % ^{235}U enrichment. Studies were performed with the control blade fully inserted at the beginning of fuel depletion, with the blade later removed once a variable burnup had been reached. An additional study was performed assuming the blade was inserted only from 70 to 75 GWd/MTU assembly burnup. A summary of all control blade studies performed is provided in Table 7-5.

Table 7-5 BWR Control Rod Blade Studies

Assembly burnup at rod insertion (GWd/MTU)	Assembly burnup at rod removal (GWd/MTU)	Figure 7-105, Figure 7-106, and Figure 7-107 legend
0	45	0-45
0	55	0-55
0	65	0-65
0	75	0-75
70	75	70-75

7.2.8.1 Neutron Dose Rate Trends

The neutron dose rate trends of variation with control blade insertion at constant burnup (75 GWd/MTU) for BWR fuel are illustrated in Figure 7-105. The dose rate results are normalized to the 8 wt % baseline case, which did not contain any control blades. For the cases

with control blades initially inserted at the beginning of irradiation, the neutron dose rate generally increased with increased control rod insertion duration over all cooling times analyzed. For cooling times up to 40 yr, inserting the control blades only from 70 to 75 GWd/MTU had approximately the same effect on the neutron dose rate as inserting the control blades from 0 to 65 GWd/MTU.

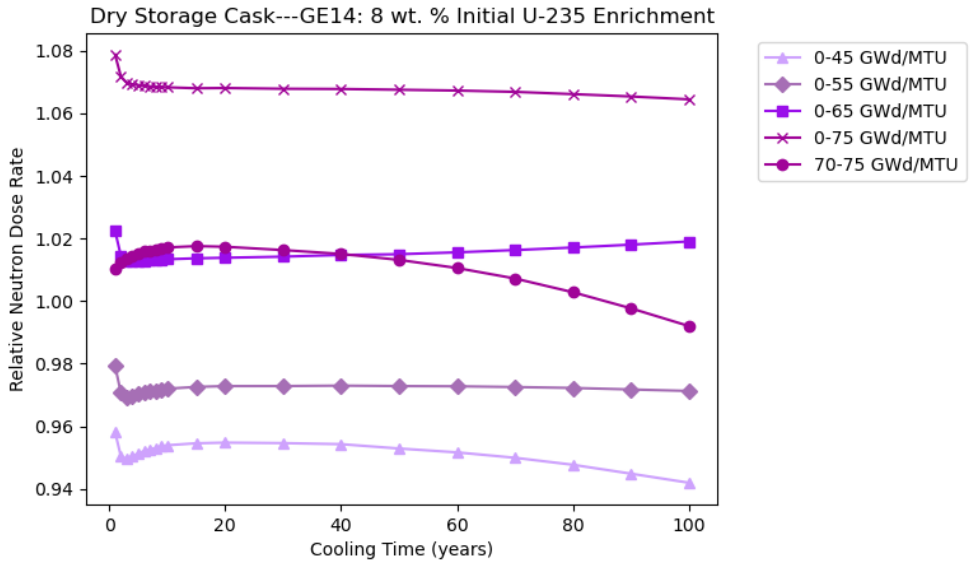

Figure 7-105 BWR Neutron Dose Rate Trends of Variation with Control Blade Insertion and Type as a Function of Cooling Time (years)

7.2.8.2 Gamma Dose Rate Trends

The primary gamma dose rate trends of variation with control blade insertion at constant burnup (75 GWd/MTU) for BWR fuel are illustrated in Figure 7-106. The dose rate results are normalized to the 8 wt % baseline case, which did not contain any control blades. For the cases with control blades initially inserted at the beginning of irradiation, the primary gamma dose rate generally increased with increased control rod insertion duration until approximately 60 yr of cooling time. Beyond 60 yr of cooling time, inserting the rods until 45, 55, and 65 GWd/MTU had approximately the same effect on the primary gamma dose rate. Beyond cooling times of 40 yr, inserting the control blades only from 70 to 75 GWd/MTU produced higher dose rates than the other cases analyzed.

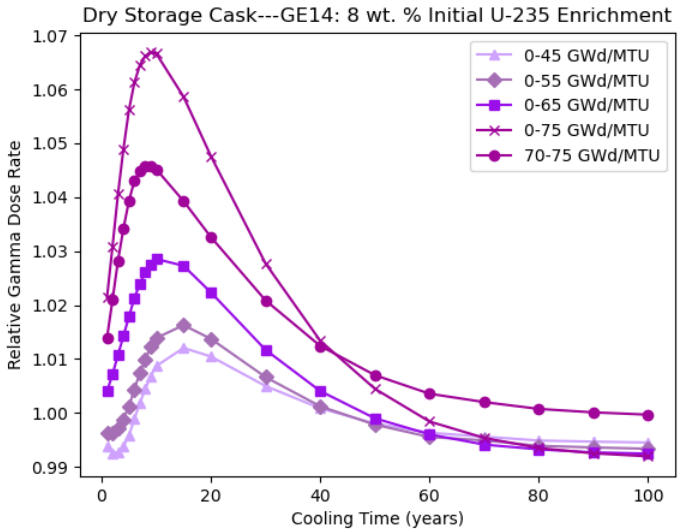

Figure 7-106 BWR Primary Gamma Dose Rate Trends of Variation with Control Rod Blade Insertion and Type as a Function of Cooling Time (years)

7.2.8.3 Cobalt-60 Dose Rate Trends

The ^{60}Co dose rate trend of variation with control blade insertion at constant burnup (75 GWd/MTU) for BWR fuel is illustrated in Figure 7-107. The dose rate results are normalized to the 8 wt % baseline case, which did not contain any control blades. Inserting the control rod from 70 to 75 GWd/MTU had a negligible effect on the ^{60}Co dose rates compared to the baseline case. For all control blade cases analyzed, the effect on the ^{60}Co dose rate was consistent over the range of cooling times analyzed. For the cases with the control blade initially inserted at the beginning of irradiation, the ^{60}Co dose rate generally decreased compared to the baseline case but did not uniformly change with increasing control blade insertion duration. These results indicate that for control blades inserted at the beginning of irradiation, there exists a specific burnup value at which the control blade withdrawal will produce a minimum ^{60}Co dose rate.

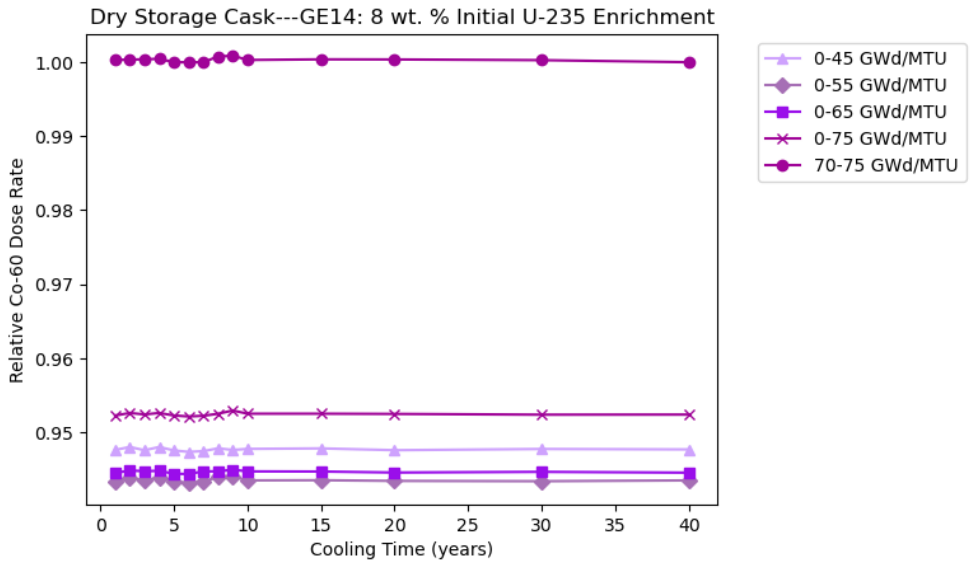

Figure 7-107 BWR ^{60}Co Dose Rate Trends of Variation with Control Blade Insertion and Type as a Function of Cooling Time (years)

7.2.9 Integral Burnable Absorbers

The effects of integral burnable absorbers (i.e., Gd_2O_3 fuel rods) on cask dose rates were presented for 5 and 8 wt % ^{235}U BWR fuel. The absorber configuration provided in Section 3.2 is further analyzed in this section. In this study, various Gd_2O_3 loadings were uniformly applied to every Gd_2O_3 rod in the assembly. The Gd_2O_3 loadings used in this study are provided in Table 7-6.

Table 7-6 Uniform Gd_2O_3 Loadings Used for BWR Absorber Study

Gd_2O_3 Loading (wt %)
1.5
4
6
8

7.2.9.1 Neutron Dose Rate Trends

Figure 7-108 illustrates the effects on the neutron dose rate of varying integral burnable absorber loading (in wt % Gd_2O_3) for BWR fuel with 8 wt % enrichment at fixed assembly average burnup (75 GWd/MTU) over a range of cooling times. The graphs in Figure 7-109 illustrate these effects at different initial enrichments and cooling times at fixed assembly average burnup (75 GWd/MTU). The neutron dose rate increased with increasing burnable absorber loading. These effects are greater at 8 wt % enrichment than at 5 wt % enrichment. For both enrichments, the effect was generally smallest at intermediate cooling times of

approximately 20-40 years. As shown in Figure 7-110, for a given cooling time (5 yr), the effect of burnable absorber loading on neutron dose rate increases very slightly with increasing fuel burnup, and the effect is more pronounced at 8 wt % enrichment than at 5 wt % enrichment.

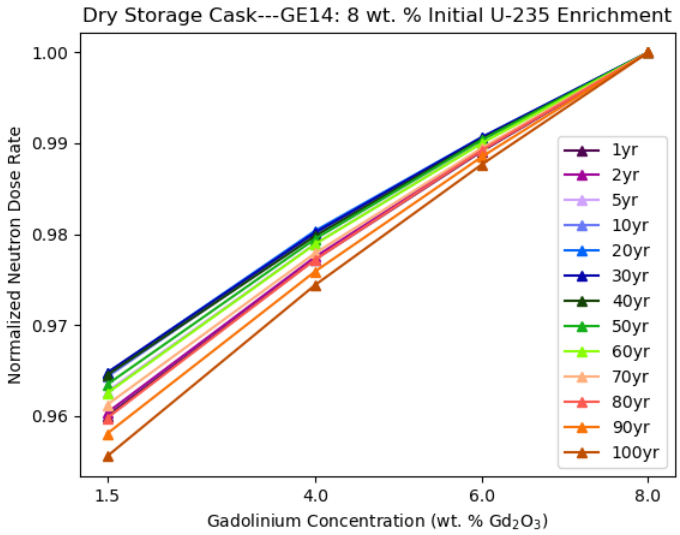

Figure 7-108 Neutron Dose Rate Trends of Variation with BWR Burnable Absorber Loading (wt % Gd_2O_3) as a Function of Cooling Time (years) (Normalization to Highest Dose Rate Value at Each Cooling Time)

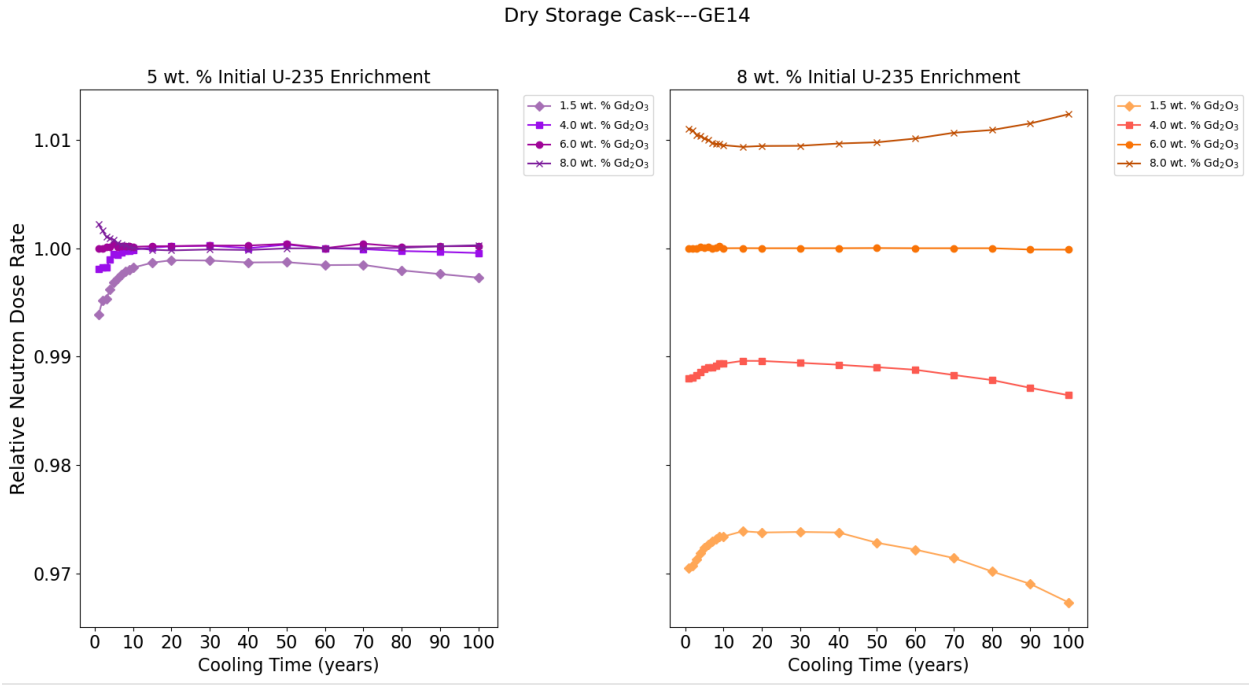

Figure 7-109 Comparative Effects of Varying Burnable Absorber Loading on Neutron Dose Rate from BWR Fuel with Different Enrichments (Normalization to Dose Rate Values for Baseline BWR Fuel Assembly)

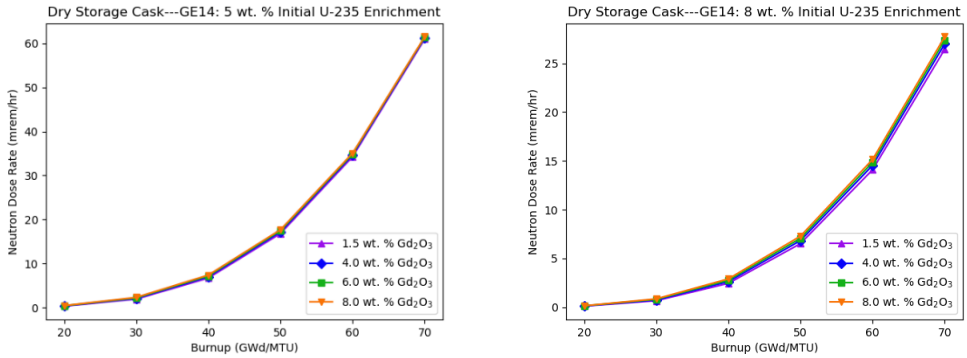

Figure 7-110 Neutron Dose Rate Trends of Variation with BWR Burnable Absorber Loading (wt % Gd_2O_3) and Burnup (GWd/MTU)

7.2.9.2 Gamma Dose Rate Trends

Figure 7-111 illustrates the effects on the primary gamma dose rate of varying integral burnable absorber loading (in wt % Gd_2O_3) for BWR fuel with 8 wt % enrichment at fixed assembly average burnup (75 GWd/MTU) over a range of cooling times. The primary gamma dose rate was highly insensitive to the burnable absorber loading, and the dose rates changed by less than 1% relative to the baseline over all cooling times analyzed. The negligible effect of

varying integral burnable absorber on primary gamma dose rate was similar for 5 and 8 wt % enrichment. As shown in Figure 7-112, for a given cooling time (5 yr), the effect of burnable absorber loading on primary gamma dose rate is insensitive to fuel burnup.

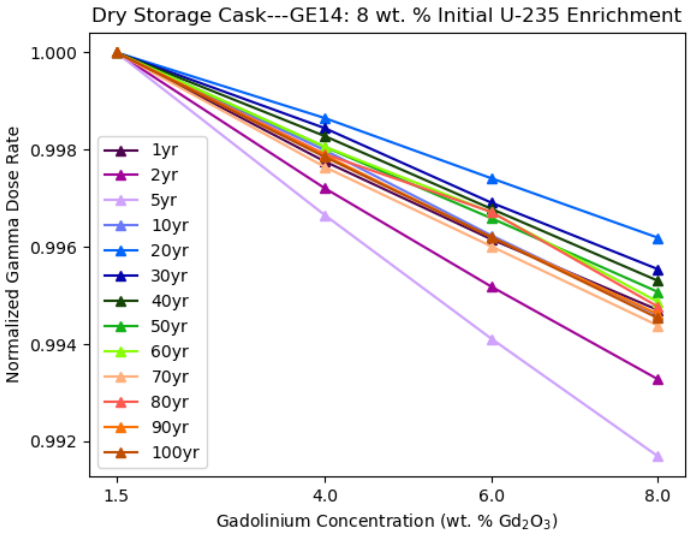

Figure 7-111 Primary Gamma Dose Rate Trends of Variation with BWR Burnable Absorber Loading (wt % Gd_2O_3) as a Function of Cooling Time (years) (Normalization to Highest Dose Rate Value at Each Cooling Time)

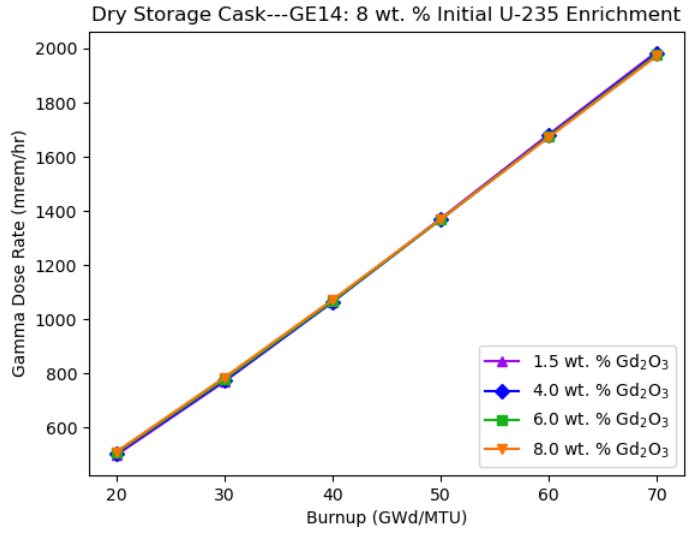

Figure 7-112 Primary Gamma Dose Rate Trends of Variation with BWR Burnable Absorber Loading (wt % Gd_2O_3) and Burnup (GWd/MTU)

7.2.9.3 Cobalt-60 Dose Rate Trends

Figure 7-113 illustrates the effects on the ^{60}Co dose rate of varying integral burnable absorber loading (in wt % Gd_2O_3) for BWR fuel with 8 wt % enrichment at fixed assembly average burnup (75 GWd/MTU) over a range of cooling times. The ^{60}Co dose rate was highly insensitive overall to the burnable absorber loading, and the dose rates changed by less than 1% relative to the baseline over all cooling times analyzed. Similar to the primary gamma dose rate, for a given cooling time (5 yr) the effect of burnable absorber loading on ^{60}Co dose rate is insensitive to fuel burnup.

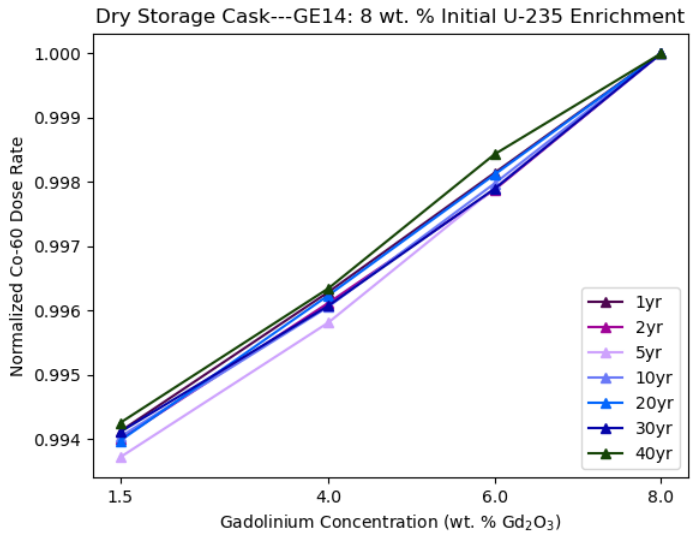

Figure 7-113 Cobalt-60 Dose Rate Trends of Variation with BWR Burnable Absorber Loading (wt % Gd_2O_3) as a Function of Cooling Time (years) (Normalization to Highest Dose Rate Value at Each Cooling Time)

7.2.10 Axial Burnup Profile

The effect of varying axial burnup profiles on dose rates was qualitatively analyzed for BWR fuel. A reference profile was chosen from Table 45 of ORNL/SPR-2021/2093 [12]. The axial burnup profiles in Table 45 of ORNL/SPR-2021/2093 [12] were obtained by comparing data from more than 2,000 BWR fuel assemblies with average assembly burnups up to greater than 46 GWd/MTU. Table 45 of ORNL/SPR-2021/2093 [12] gives bounding axial burnup profiles for fuel assembly average burnups in various burnup ranges. For the current study, the bounding profile for the range greater than 46 GWd/MTU chosen.

Two additional axial burnup profiles were chosen from LEU+ BWR fuel with high burnup. These profiles, referred to as P1 and P2, were calculated in concurrent ORNL analysis. P1 is from a fuel assembly with 9 wt % maximum enrichment and an average burnup of 60.6 GWd/MTU. P2 is from a fuel assembly with 9 wt % maximum enrichment and an average burnup of 72.0 GWd/MTU.

For all three profiles analyzed, the maximum peaking factor occurred in similar axial nodes and was largest in the P1 profile. Although the reference bounding profile was generally similar to the two LEU+ profiles across the axial height of the assembly, the LEU+ profiles had higher relative burnup than the reference profile in various nodes. The higher relative burnup in these nodes of LEU+ fuel may require newly bounding profiles to be generated for LEU+ and high burnup BWR fuel.

7.3 Summary of Dry Storage Cask Dose Rate Sensitivity to Select Irradiation and Decay Parameters

Summaries of the dose rate sensitivities to select irradiation parameters for the dry storage cask are provided in Table 7-7 through Table 7-10. The dose location for all results was the mid-height external surface of the cask/package. Irradiation parameters without clearly defined upper and lower bounds (such as burnable absorber exposure, assembly type, and control rod usage) are omitted from these tables. For each irradiation parameter and source component, dose rate sensitivities are calculated by comparing the dose rates at the baseline value to dose rates at the lower and upper bounds of the selected range. The sensitivities are provided as percentage differences from the baseline dose rate.

Table 7-7 5 wt % PWR Dose Rate Sensitivity Summary

Parameter	Lower bound	Baseline	Upper bound	Component	Cooling time (years)							
					Bound	1	3	5	10	20	30	40
Specific Power (MW/MTU)	15	40	50	Neutron	Lower	-6.3	-6.5	-6.3	-6.0	-5.8	-5.7	-5.6
					Upper	0.9	1.0	1.0	1.0	0.9	0.9	0.9
				Primary Gamma	Lower	-51.7	-42.4	-32.3	-16.1	-8.8	-8.6	-8.7
					Upper	16.5	12.0	7.8	2.9	1.2	1.1	1.1
				Co-60	Lower	-33.9	-33.8	-33.9	-33.9	-33.9	-33.9	-33.9
					Upper	5.8	5.8	5.8	5.8	5.8	5.8	5.8
Fuel Density (g/cm^3)	10	10.26	10.75	Neutron	Lower	-0.9	-0.8	-0.8	-0.7	-0.7	-0.7	-0.8
					Upper	1.6	1.4	1.4	1.3	1.3	1.3	1.3
				Primary Gamma	Lower	-0.2	-0.4	-0.5	-0.7	-0.5	-0.3	-0.2
					Upper	0.4	0.7	1.0	1.3	1.0	0.6	0.4
				Co-60	Lower	2.5	2.6	2.5	2.5	2.5	2.5	2.5
					Upper	-4.4	-4.4	-4.4	-4.4	-4.4	-4.4	-4.4
Fuel Temperature (K)	560	900	1600	Neutron	Lower	0.4	0.3	0.2	0.0	-0.1	-0.1	0.0
					Upper	-1.0	-1.1	-0.9	-0.6	-0.5	-0.6	-0.7
				Primary Gamma	Lower	0.1	0.0	-0.2	-0.8	-0.9	-0.6	-0.4
					Upper	-0.2	-0.1	0.3	1.4	1.6	1.1	0.6
				Co-60	Lower	2.6	2.6	2.6	2.6	2.6	2.6	2.6
					Upper	-3.9	-3.9	-3.9	-3.9	-3.9	-3.9	-3.9
Soluble Boron (ppm)	600	1000	1800	Neutron	Lower	-1.9	-1.7	-1.7	-1.7	-1.7	-1.7	-1.8
					Upper	3.3	3.0	3.0	3.0	3.0	3.1	3.3
				Primary Gamma	Lower	-0.3	-0.6	-0.9	-1.1	-0.9	-0.5	-0.3
					Upper	0.6	1.1	1.6	2.1	1.6	1.0	0.5
				Co-60	Lower	0.8	0.8	0.7	0.8	0.8	0.8	0.8
					Upper	-1.3	-1.3	-1.3	-1.3	-1.3	-1.3	-1.3
Moderator Density (g/cm3)	0.60811	0.63	0.76971	Neutron	Lower	1.5	1.4	1.3	1.3	1.3	1.3	1.3
					Upper	-10.1	-9.7	-9.5	-9.3	-9.2	-9.2	-9.2
				Primary Gamma	Lower	0.4	0.6	0.9	1.2	0.9	0.6	0.4
					Upper	-1.8	-3.0	-4.2	-5.2	-4.0	-2.6	-1.5
				Co-60	Lower	-0.5	-0.5	-0.5	-0.5	-0.5	-0.5	-0.5
					Upper	4.3	4.4	4.4	4.4	4.4	4.4	4.3

Table 7-8 8 wt % PWR Dose Rate Sensitivity Summary

Parameter	Lower bound	Baseline	Upper bound	Component	Cooling time (years)							
					Bound	1	3	5	10	20	30	40
Specific Power (MW/MTU)	15	40	50	Neutron	Lower	-5.2	-6.6	-6.6	-6.5	-6.4	-6.3	-6.0
					Upper	0.5	1.1	1.1	1.1	1.1	1.1	1.0
				Primary Gamma	Lower	-52.3	-42.3	-31.4	-15.5	-9.0	-8.8	-8.9
					Upper	17.1	12.2	7.7	2.8	1.2	1.1	1.1
				Co-60	Lower	-34.3	-34.2	-34.2	-34.3	-34.3	-34.2	-34.3
					Upper	5.9	5.9	5.9	5.9	5.9	5.9	5.9
Fuel Density (g/cm³)	10	10.26	10.75	Neutron	Lower	-1.4	-1.5	-1.4	-1.5	-1.4	-1.5	-1.4
					Upper	2.4	2.5	2.5	2.5	2.5	2.5	2.5
				Primary Gamma	Lower	-0.3	-0.5	-0.6	-0.7	-0.5	-0.3	-0.2
					Upper	0.5	0.8	1.1	1.3	0.9	0.6	0.4
				Co-60	Lower	2.0	2.1	2.1	2.0	2.0	2.0	2.0
					Upper	-3.5	-3.5	-3.5	-3.5	-3.6	-3.5	-3.5
Fuel Temperature (K)	560	900	1600	Neutron	Lower	-1.9	-1.7	-1.7	-1.7	-1.7	-1.7	-1.7
					Upper	2.4	2.0	2.0	2.0	2.0	2.0	2.0
				Primary Gamma	Lower	-0.1	-0.2	-0.3	-0.6	-0.6	-0.4	-0.2
					Upper	0.1	0.3	0.4	1.0	1.0	0.6	0.4
				Co-60	Lower	1.4	1.4	1.4	1.4	1.4	1.4	1.4
					Upper	-2.1	-2.1	-2.1	-2.1	-2.1	-2.1	-2.1
Soluble Boron (ppm)	600	1000	1800	Neutron	Lower	-2.5	-2.4	-2.4	-2.4	-2.5	-2.6	-2.8
					Upper	4.8	4.5	4.5	4.6	4.7	4.9	5.3
				Primary Gamma	Lower	-0.3	-0.6	-0.8	-0.8	-0.6	-0.3	-0.2
					Upper	0.6	1.1	1.5	1.6	1.1	0.7	0.4
				Co-60	Lower	-0.1	0.0	-0.1	-0.1	-0.1	-0.1	-0.1
					Upper	0.2	0.2	0.2	0.2	0.2	0.2	0.2
Moderator Density (g/cm³)	0.60811	0.63	0.76971	Neutron	Lower	2.6	2.7	2.7	2.7	2.6	2.6	2.6
					Upper	-16.8	-17.4	-17.4	-17.3	-17.3	-17.2	-17.1
				Primary Gamma	Lower	0.5	0.8	1.1	1.2	0.9	0.5	0.3
					Upper	-2.6	-4.3	-5.6	-5.7	-3.9	-2.4	-1.4
				Co-60	Lower	0.4	0.4	0.4	0.4	0.4	0.4	0.4
					Upper	-1.1	-1.1	-1.1	-1.1	-1.1	-1.1	-1.1
Enrichment (wt % U-235)	5	8	8	Neutron	Lower	142.6	152.2	150.4	147.4	146.2	146.3	146.8
				Primary Gamma	Lower	8.2	10.1	8.4	0.6	-3.3	-3.1	-2.8
				Co-60	Lower	35.4	35.4	35.4	35.4	35.4	35.4	35.4

Table 7-9 5 wt % BWR Dose Rate Sensitivity Summary

Parameter	Lower bound	Baseline	Upper bound	Component	Cooling time (years)							
					Bound	1	3	5	10	20	30	40
Specific Power (MW/MTU)	15	25	50	Neutron	Lower	-5.7	-5.3	-4.9	-4.3	-4.0	-4.0	-3.9
					Upper	4.8	4.4	4.1	3.5	3.2	3.1	3.1
				Primary Gamma	Lower	-32.2	-25.8	-19.4	-9.8	-5.7	-5.6	-5.7
					Upper	63.7	44.5	28.5	10.4	4.4	4.2	4.4
				Co-60	Lower	-22.4	-22.4	-22.4	-22.3	-22.4	-22.4	-22.4
					Upper	23.9	23.8	23.9	23.8	23.8	23.9	23.8
Fuel Density (g/cm^3)	10.26	10.64	10.96	Neutron	Lower	-1.5	-1.3	-1.1	-0.9	-0.8	-0.8	-0.8
					Upper	1.6	1.3	1.1	0.8	0.7	0.8	0.8
				Primary Gamma	Lower	-0.2	-0.3	-0.5	-0.7	-0.5	-0.3	-0.2
					Upper	0.2	0.3	0.5	0.7	0.5	0.3	0.2
				Co-60	Lower	3.4	3.5	3.4	3.5	3.5	3.4	3.4
					Upper	-3.2	-3.2	-3.2	-3.2	-3.2	-3.2	-3.2
Fuel Temperature (K)	500	800	1300	Neutron	Lower	0.5	0.2	0.0	-0.4	-0.5	-0.5	-0.4
					Upper	-0.7	-0.4	0.0	0.4	0.5	0.5	0.4
				Primary Gamma	Lower	0.2	0.2	0.0	-0.5	-0.6	-0.4	-0.2
					Upper	-0.3	-0.2	0.0	0.7	0.9	0.6	0.3
				Co-60	Lower	2.7	2.7	2.7	2.6	2.6	2.6	2.7
					Upper	-3.3	-3.3	-3.3	-3.3	-3.3	-3.3	-3.4
Moderator Void (%)	20	45.5	80	Neutron	Lower	-8.7	-7.5	-6.6	-5.6	-5.2	-5.2	-5.4
					Upper	17.0	13.4	10.9	7.7	6.3	6.4	6.7
				Primary Gamma	Lower	-1.0	-2.0	-3.0	-4.3	-3.5	-2.2	-1.3
					Upper	1.9	3.8	6.0	8.8	7.2	4.6	2.7
				Co-60	Lower	5.4	5.4	5.4	5.4	5.4	5.4	5.4
					Upper	-4.9	-4.9	-4.9	-4.9	-4.9	-4.9	-4.9

Table 7-10 8 wt % BWR Dose Rate Sensitivity Summary

Parameter	Lower bound	Baseline	Upper bound	Component	Cooling time (years)							
					Bound	1	3	5	10	20	30	40
Specific Power (MW/MTU)	15	25	50	Neutron	Lower	-4.5	-4.7	-4.5	-4.3	-4.2	-4.2	-4.1
					Upper	3.7	4.3	4.1	3.9	3.8	3.8	3.7
				Primary Gamma	Lower	-32.4	-25.6	-18.8	-9.4	-5.7	-5.6	-5.7
					Upper	65.7	45.0	27.8	9.9	4.5	4.4	4.4
				Co-60	Lower	-22.4	-22.3	-22.4	-22.4	-22.4	-22.4	-22.4
					Upper	24.1	24.1	24.1	24.1	24.1	24.1	24.1
Fuel Density (g/cm^3)	10.26	10.64	10.96	Neutron	Lower	-2.1	-2.1	-2.0	-1.9	-1.9	-1.9	-1.9
					Upper	2.1	2.0	1.9	1.8	1.8	1.8	1.8
				Primary Gamma	Lower	-0.3	-0.5	-0.6	-0.7	-0.5	-0.3	-0.2
					Upper	0.3	0.5	0.6	0.7	0.5	0.3	0.2
				Co-60	Lower	2.7	2.7	2.7	2.7	2.7	2.7	2.7
					Upper	-2.6	-2.5	-2.6	-2.6	-2.6	-2.6	-2.6
Fuel Temperature (K)	500	800	1300	Neutron	Lower	-1.7	-1.7	-1.8	-1.9	-1.9	-1.9	-1.8
					Upper	2.1	2.1	2.2	2.2	2.3	2.2	2.2
				Primary Gamma	Lower	0.0	0.0	-0.1	-0.4	-0.4	-0.2	-0.1
					Upper	0.0	0.0	0.2	0.6	0.6	0.4	0.2
				Co-60	Lower	1.7	1.7	1.7	1.8	1.7	1.7	1.7
					Upper	-2.2	-2.2	-2.2	-2.2	-2.2	-2.2	-2.2
Moderator Void (%)	20	45.5	80	Neutron	Lower	-12.9	-12.7	-12.4	-12.0	-11.9	-11.9	-12.1
					Upper	19.9	18.7	17.6	16.1	15.6	15.7	16.0
				Primary Gamma	Lower	-1.9	-3.1	-4.1	-4.6	-3.3	-2.0	-1.1
					Upper	2.8	4.9	6.8	8.3	6.2	3.9	2.2
				Co-60	Lower	1.1	1.0	1.0	1.1	1.1	1.1	1.0
					Upper	0.3	0.3	0.3	0.3	0.3	0.3	0.3
Enrichment (wt % U-235)	5	8	8	Neutron	Lower	125.7	125.2	120.3	114.0	111.8	112.5	113.9
				Primary Gamma	Lower	8.3	9.2	6.9	-0.2	-3.5	-3.2	-2.8
				Co-60	Lower	34.2	34.2	34.2	34.2	34.2	34.2	34.2

8 PARAMETRIC STUDY FOR CRITICALITY SAFETY

8.1 Dry Storage Cask and Transportation Package Criticality Safety Evaluation for Pressurized-Water Reactors

This section details the results of sensitivity studies related to criticality safety analysis of SNF transportation packages and dry storage casks. As a parametric study, the intent is not to demonstrate subcriticality of the contents within the modeled GBC-32 cask, but to identify trends and behaviors of k_{eff} with various parametrizations and whether such trends vary when compared to conventional operation and experience with current PWR enrichments and burnups. Parameters and their ranges are discussed in Section 3.1; the parametric analysis investigates these variables as they relate to reactor operation (fuel depletion). Thus, when investigating soluble boron as an example, the boron content of the GBC-32 cask design is not the investigated parameter—the boron content in the reactor during operation is of interest. The baseline fuel depletion conditions are noted in Section 3.1. When one parameter is adjusted, others are set to the baseline values to isolate the effect of the parameter of interest. The following formula is used in plotting the relative difference in k_{eff} (i.e., Δk_{eff}).

$$\Delta k_{eff} = k_{eff,i} - k_{eff,reference}$$

where $k_{eff,i}$ is the k_{eff} obtained by varying a parameter i and $k_{eff,reference}$ is the k_{eff} obtained using the parameter reference value. For example, in the fuel temperature study analyzing the effect of increasing the fuel temperature to 1600 K with respect to a reference value of 900 K, the relative difference in k_{eff} is calculated as:

$$\Delta k_{eff} = k_{eff,1600\,K} - k_{eff,900\,K}$$

where $k_{eff,1600\,K}$ and $k_{eff,900\,K}$ are the k_{eff} values calculated with a fuel temperature of 1600 K and reference fuel temperature of 900 K, respectively, while keeping the remaining parameters the same.

No adjustments are made to the CSAS5 model because parameters of interest effect only fuel depletion conditions, and all fuel compositions are directly imported from ORIGAMI. Residual poisons are not considered in any calculation. Sections 8.1.1 through 8.1.10 use the WEC 17 × 17 OFA design.

8.1.1 Burnup

Current burnup and enrichment limits allowing BUC in NUREG-2216 [8] and NUREG-2215 [7] are demonstrated with a previous analysis of existing radiochemical assay data in NUREG/CR-7108 [65]. A separate effort is ongoing to analyze radiochemical assay data not addressed by the publication of NUREG/CR-7108 [65] and other data generated after its publication with the goal of extending the validation basis of inventories at higher enrichments and burnups where possible. Variations of k_{eff} with burnup are detailed in each of the following parametric studies. Figure 8-1 and Figure 8-2 present the variation of k_{eff} with varying enrichment and burnup. The stochastic uncertainties in the calculations are less than 0.02 percent Δk (20 pcm) and are too small to be visualized in the figures. The rate at which different enrichments deplete relative to 15 GWd/MTU is depicted in Figure 8-2. The rate at which eigenvalues decrease with fuel

depletion is slightly lower at higher enrichments. This effect results in an approximately 600 pcm difference in the eigenvalue reduction between 15 and 75 GWd/MTU for each 0.5 wt % enrichment increment. This slope reduction is approximately 10 pcm per GWd/MTU for each 0.5 wt % enrichment increase. Figure 8-3 shows the behavior of the GBC-32 cask at various enrichments and burnups as a function of the energy of average lethargy of fission (EALF). The burnup, in 10 GWd/MTU increments, is expressed within each enrichment data series, progressing through each series from an initial burnup of 15 GWd/MTU to the final burnup of 75 GWd/MTU, shown as dashed lines bounding the data sets. Less burned fuel spans a greater range of EALF values, with 15 GWd/MTU fuel having an approximately 0.12 electron volt (eV) difference between 5 and 8 wt % fuel at 15 GWd/MTU and an approximately 0.06 eV difference at 75 GWd/MTU. Below 6 wt % fuel, increasing burnup hardens the spectrum of the spent fuel within GBC-32. Above 6 wt %, the opposite effect is observed, with increasing burnup leading to a softer spectrum of the fuel stored in the cask.

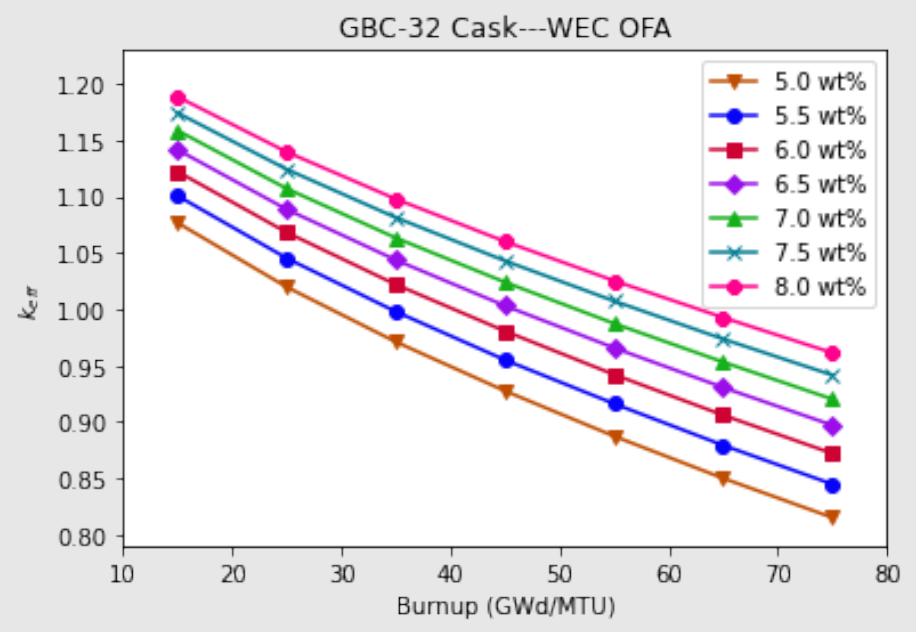

Figure 8-1 GBC-32 k_{eff} as a Function of Burnup for Multiple Initial ^{235}U Enrichments

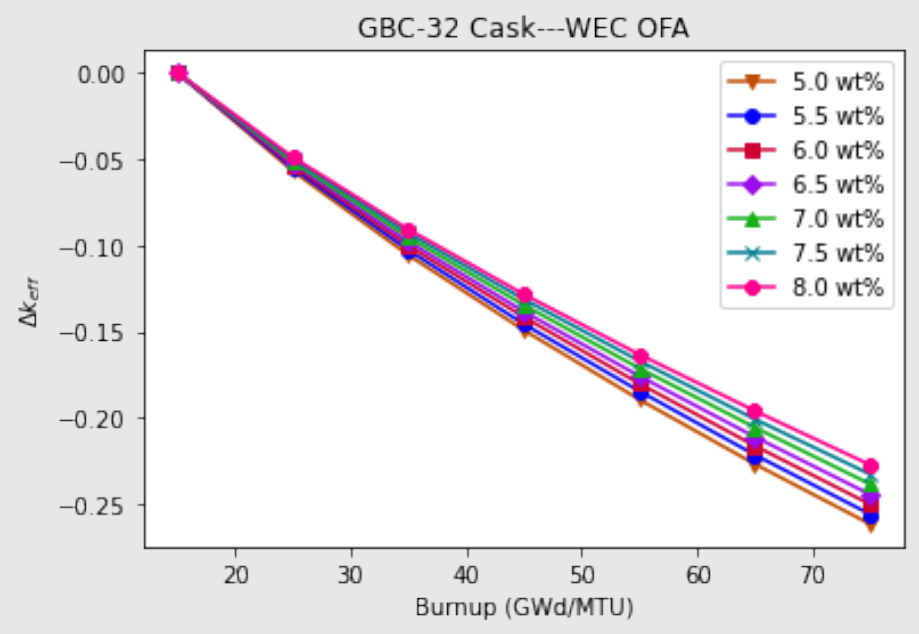

Figure 8-2 Relative Decrease in GBC-32 k_{eff} as a Function of Burnup for Multiple Initial ^{235}U Enrichments with Respect to a Reference of 15 GWd/MTU

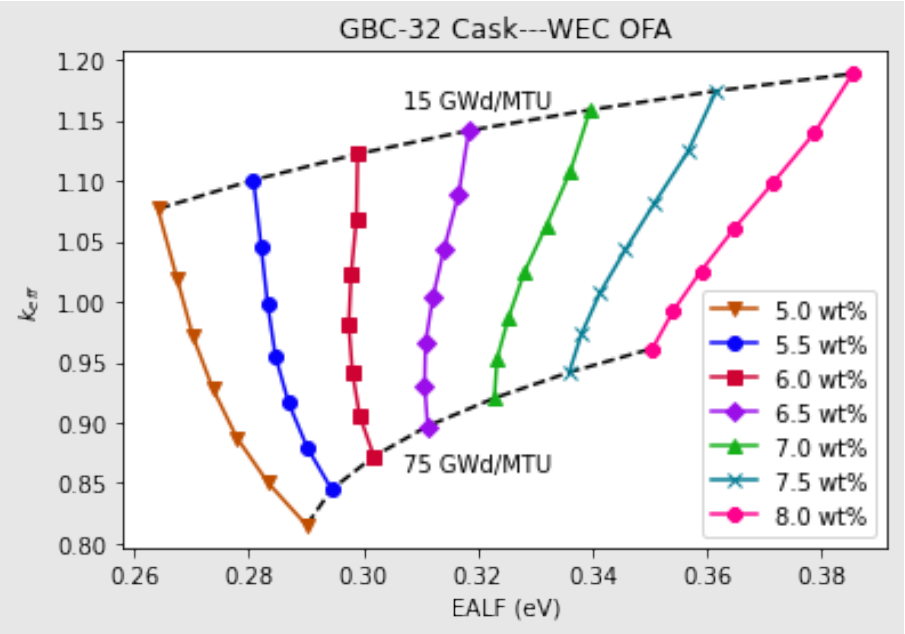

Figure 8-3 GBC-32 k_{eff} as a Function of EALF for Multiple Initial ^{235}U Enrichments and Burnups

8.1.2 Initial Fuel Enrichment

The effect of initial ^{235}U enrichment on cask reactivity was analyzed for 5.0, 5.5, 6.0, 6.5, 7.0, 7.5, and 8.0 wt % ^{235}U fuel. Depleted fuel inventories were generated in intervals of 10 GWd/MTU from 15 to 75 GWd/MTU.

Trends of k_{eff} variation with initial uranium enrichment (in ^{235}U wt %) at various burnup fuels are illustrated in Figure 8-1. Uncertainties are less than 0.02% Δk and too small to be visualized in the figure. The plot illustrates the expected positive correlation between eigenvalue and enrichment and inverse correlation between eigenvalue and burnup. Figure 8-3 demonstrates behavior with EALF. Higher enrichment levels lead to an increase in EALF, with increased ^{235}U and ^{239}Pu at the equivalent burnup point. At around 6.5 wt %, an increase in burnup causes the spectrum to soften. It is important to note that burnable absorber and soluble boron loading, which significantly affect the spectrum, are kept constant in this sensitivity study of enrichment on eigenvalue, although this would not be the case in actual operation.

8.1.3 Cooling Time

The effect of assembly cooldown post-irradiation on cask reactivity was analyzed for 5, 6.5, and 8 wt % ^{235}U fuel. The fuel was burned up to 75 GWd/MTU using cooling times of 1, 3, 5, 7, 10, 20, 30, 40, 50, 70, and 100 yr. Depleted fuel inventories were generated in intervals of 10 GWd/MTU from 15 to 75 GWd/MTU. Figure 8-4 plots relative decreases in reactivity with increased cooling time and burnup. This is not an absolute trend as the examined cooling times were limited to 100 yr, with reactivity expected to increase with cooling time with the decay of ^{241}Am and ^{240}Pu beyond 100 years and decrease again, though not demonstrated in this report [66].

With increasing enrichment, the behavior of k_{eff} is generally the same as a function of cooling time, but at a lower magnitude. The lower magnitude is a result of decreased ^{241}Pu and ^{155}Gd content with increasing enrichment. Less ^{241}Pu to decay into ^{241}Am reduces the reactivity effect of the ^{241}Pu decay at different cooling times. Less ^{155}Gd content with increased enrichment reduces the poison effect of a major fission product. All else equal, the same cooling period will result in a lessened reduction in reactivity within 100 yr of cooling for higher-enriched fuel. All else equal, the same cooling period will result in a greater reduction in reactivity within 100 yr of cooling for higher burned fuel. The behavior noted in NUREG-2216 [8] and NUREG/CR-6781 [66] as the basis for the recommendations provided in Attachment 6A of NUREG-2216 [8] is in line with the observations with increased enrichment and burnup analyzed.

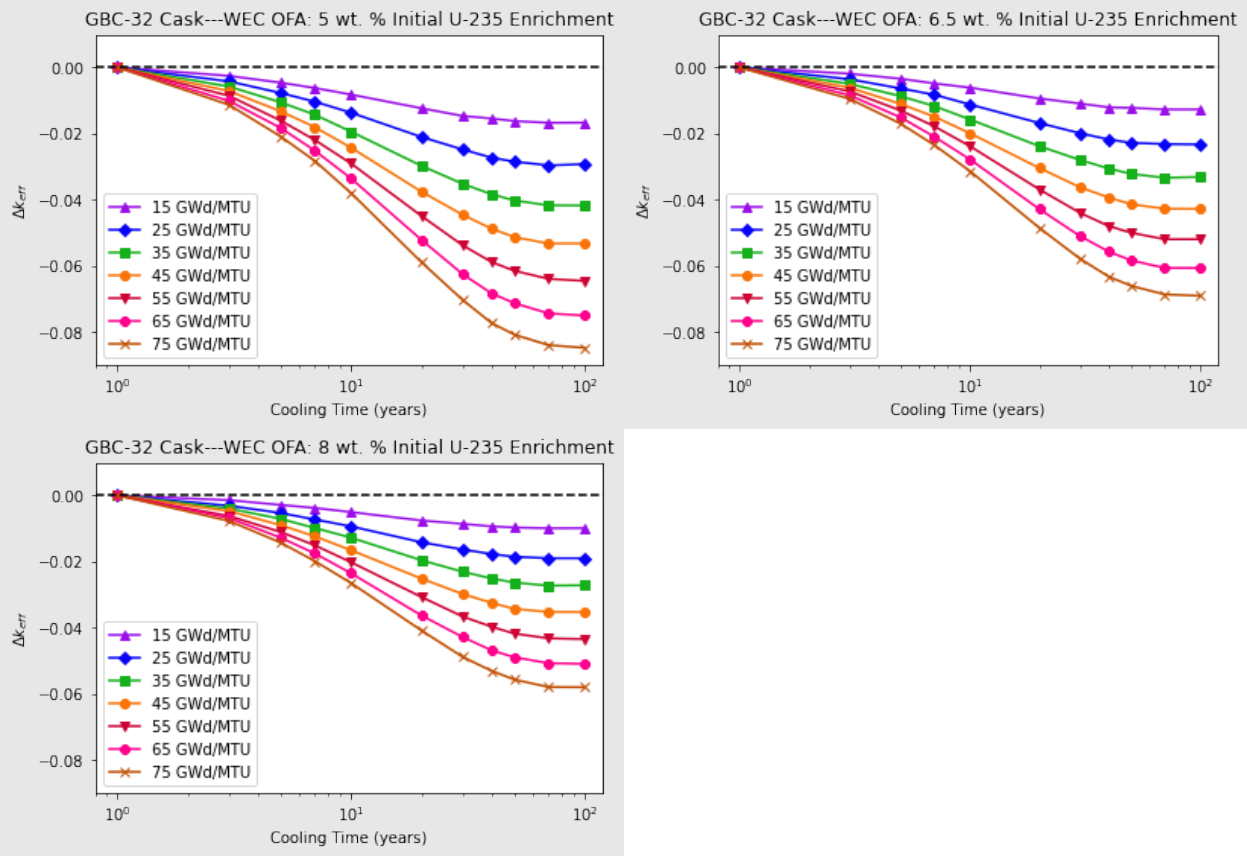

Figure 8-4 Relative Difference in k_{eff} at 5.0, 6.5, and 8.0 wt % ^{235}U Fuel as a Function of Cooling Time for Different Burnups with Respect to a Reference of 1-year Cooling Time

8.1.4 Specific Power

The effect of assembly specific power on cask reactivity was analyzed for 5, 6.5, and 8 wt % ^{235}U fuel. The fuel was burned up to 75 GWd/MTU using specific powers of 15, 20, 30, 40, and 50 MW/MTU. Depleted fuel inventories were generated in intervals of 10 GWd/MTU from 15 to 75 GWd/MTU.

Figure 8-5 plots the differences in discharged fuel reactivity relative to the 40 MW/MTU case. Negative values in the figure demonstrate that an increase in specific power results in a decrease in reactivity at that burnup, and the opposite for positive values. Uncertainties are displayed to 2σ for improved visibility. The specific power range of 15 to 50 MW/MTU bounds lifetime average values for standard LWR operation. ORNL/TM-12973 [67] indicates that more complicated trends are expected for specific power than for other parametric effects of fuel depletion, including by BUC nuclide set. This study used AFP nuclides exclusively and did not make determinations about specific power behavior with actinide-only BUC. Prior evidence notes the magnitude of the variation is more strongly related to fuel burnup than enrichment [67].

Behavior at all burnups is similar at different specific powers. At a burnup of 15 GWd/MTU, increasing specific power reduces discharged fuel reactivity, with approximately 100 pcm additional reduction per 10 MW/MTU within a range of specific powers from 20 to 50 MW/MTU. The reactivity of fuel depleted at higher specific powers increases relative to the lower specific powers with increasing burnup. The burnup at which the higher specific powers become bounding generally increases slightly with burnup. Increased enrichment slightly lowers the sensitivity to specific power. The maximum difference relative to 15 MW/MTU at 5 wt % is approximately 430 pcm opposed to approximately 240 pcm at 8 wt %. Fission product inventory is directly correlated to the specific power (a specific power of 40 MW/MTU will produce fission products at twice the rate of 20 MW/MTU). Thus, reactivity differences at higher specific powers are more sensitive to burnup as fission product production is increased while decay rate is constant.

The behavior noted here is consistent with that seen in NUREG-2216 [8] Figure 6A-6 drawn from NUREG/CR-6665 [54] and ORNL/TM-12973 [67]. Lower burnups are limited by the lower specific power, while higher burnups limited by the higher specific power. The point at which this transition between lower and higher burnups is likely system dependent but demonstrates a shift to a higher burnup with increased enrichment.

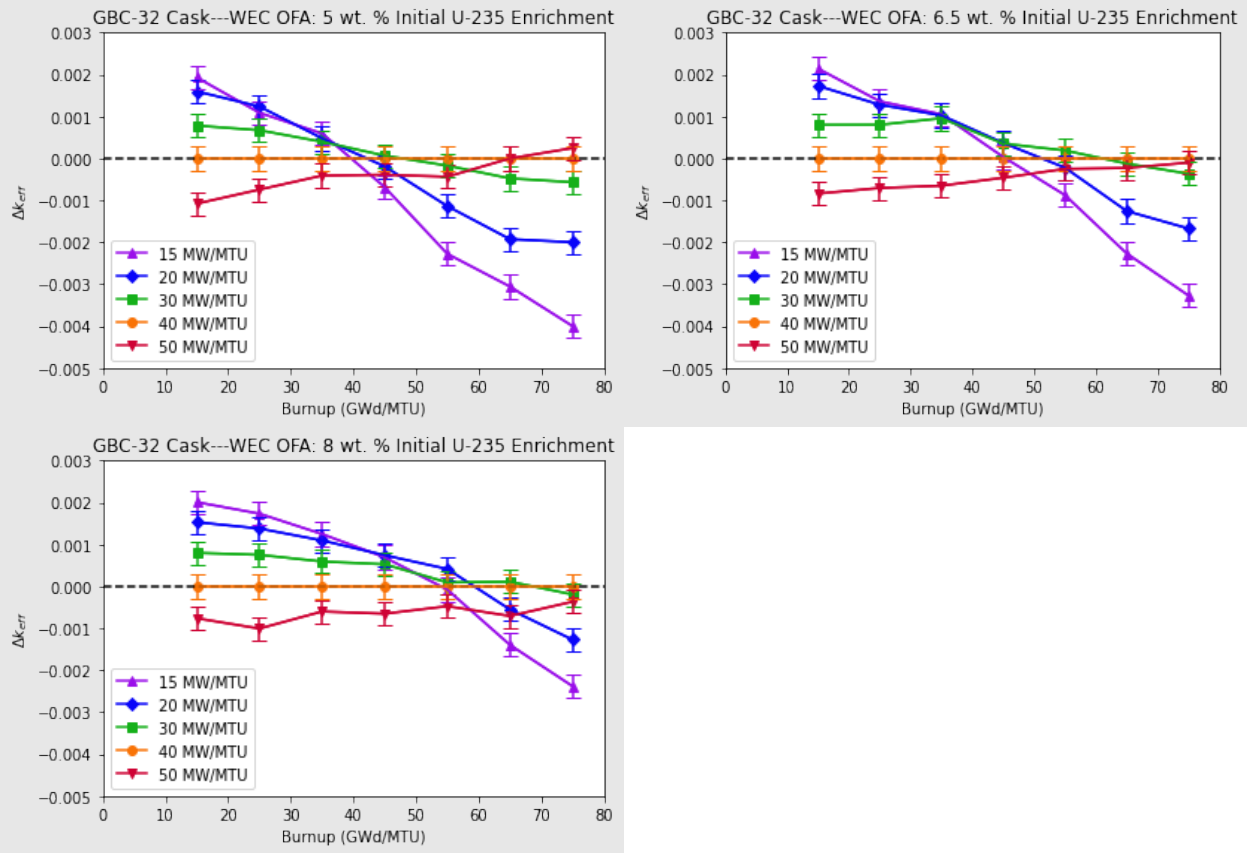

Figure 8-5 Relative Difference in k_{eff} (±2σ) at 5.0, 6.5, and 8.0 wt % ^{235}U Fuel at Varying Specific Power (MW/MTU) with Respect to a Reference of 40 MW/MTU

8.1.5 Soluble Boron

The effect of soluble boron concentration in the coolant on discharged fuel k_{eff} was analyzed for 5, 6.5, and 8 wt % ^{235}U fuel. The fuel was burned up to 75 GWd/MTU using soluble boron concentrations of 600, 1,000, and 1,800, ppm. In each case, the soluble boron level was held at a constant value during the entire irradiation period. Figure 8-6 plots the differences in reactivity relative to 1,000 ppm with differences in soluble boron content.

As expected, discharged fuel reactivity increases with soluble boron concentration due to increased ^{239}Pu production in the harder energy spectrum. This behavior is consistent with current guidance [8]. The effect of soluble boron on spent fuel reactivity is significantly reduced at higher enrichment. Higher enrichments have higher net ^{239}Pu buildup as per Figure 4-4. This is due to both spectral hardening and a decreasing $^{239}Pu/^{235}U$ ratio from a higher initial ^{235}U content, reducing the likelihood of ^{239}Pu fissions (reduced depletion rate). However, the increase in ^{239}Pu because of soluble boron induced spectrum hardening becomes less effective with increasing enrichment because of the lessened $^{239}Pu/^{235}U$ ratio. Figure 8-7 shows the decrease in the $^{239}Pu/^{235}U$ ratio with increase in enrichment, while increases in soluble boron increases the ratio. Figure 8-7 ^{239}Pu and ^{235}U concentrations are axially integrated and are purposefully exposed to extreme boron concentrations to emphasize the difference in concentration ratios. This behavior of the $^{239}Pu/^{235}U$ ratio decreasing with enrichment and increasing due to soluble boron is similarly observed with other parameters.

Increasing the depletion soluble boron concentration to 1800 ppm increases GBC-32 reactivity by almost 1% Δk above the baseline 1000 ppm depletion for 5 wt % initial ^{235}U at 75 GWd/MTU. This impact drops to only 270 pcm with 8 wt % initial ^{235}U. This relative reduction is seen at other soluble boron concentrations and burnups as well. Figure 8-8 shows the reactivity worth of soluble boron changes for each enrichment considered here. It clearly shows the trends of worth increasing with burnup and lower enrichment.

Figure 8-9 demonstrates the shift in neutron spectrum. Increasing burnup softens the spectrum for higher enrichments rather than hardening the spectrum for lower enrichments. Data along each line represent increasing burnup, thus the collection of points at approximately 0.26, 0.32, and 0.39 eV representing 15 GWd/MTU.

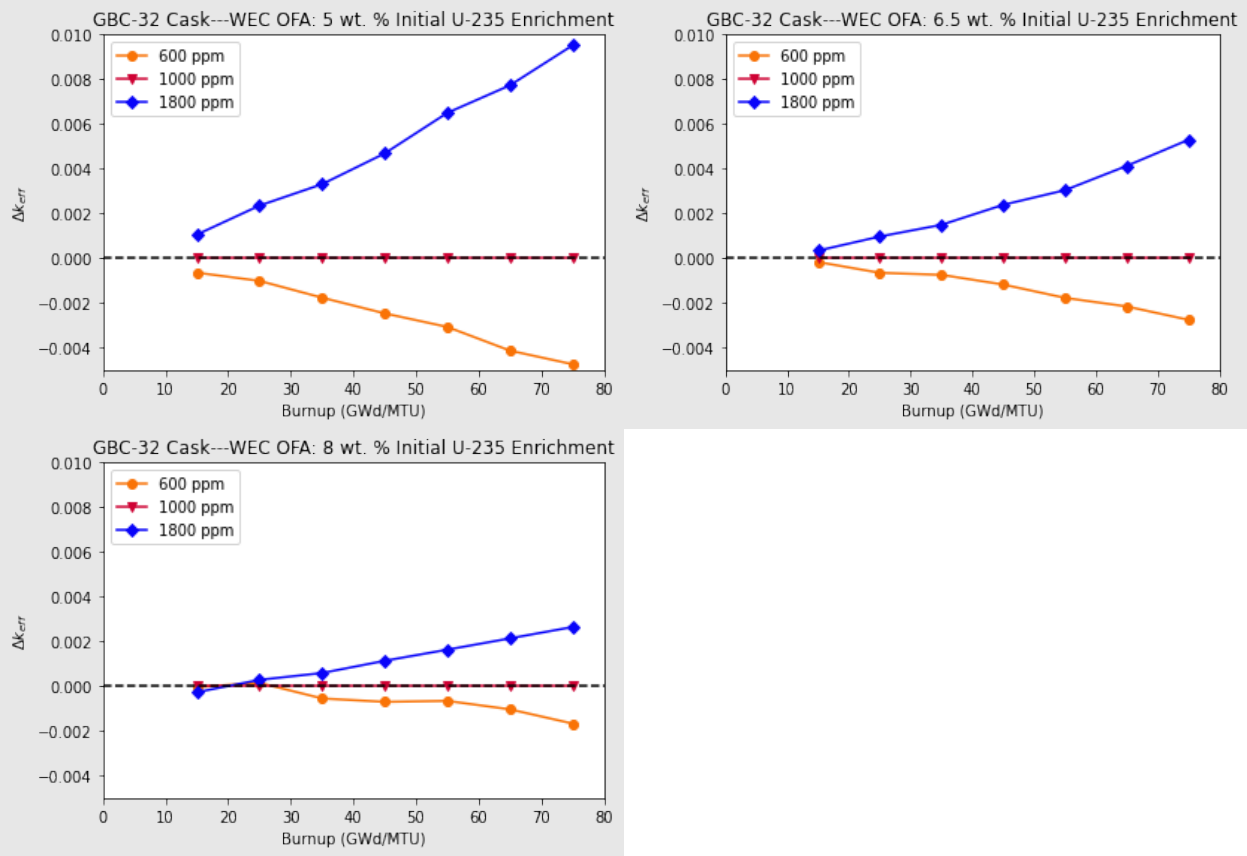

Figure 8-6 Relative difference in k_{eff} at 5.0, 6.5, and 8.0 wt % ^{235}U Fuel with Varying Soluble Boron (ppm) with Respect to a Reference of 1000 ppm

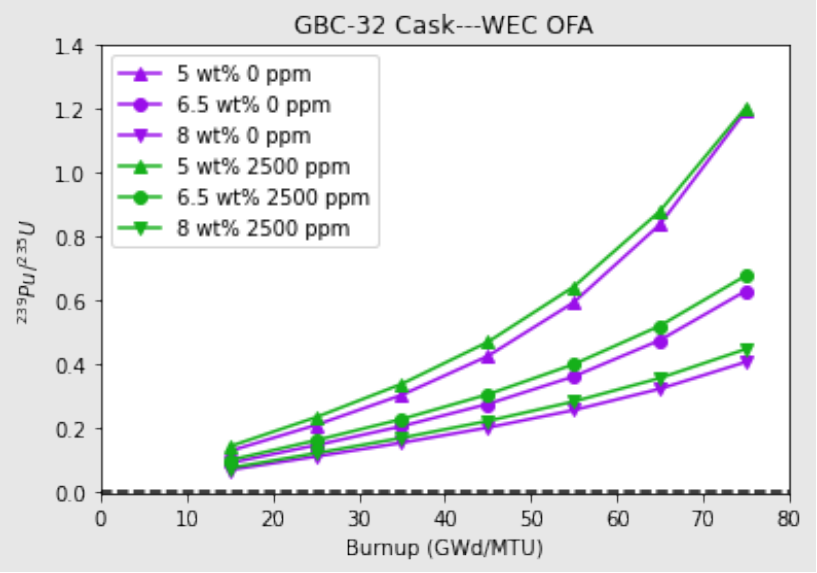

Figure 8-7 **Ratio of ^{239}Pu to ^{235}U Concentrations in Spent Fuel at 5.0, 6.5, and 8.0 wt % ^{235}U Fuel with Varying Soluble Boron (ppm)**

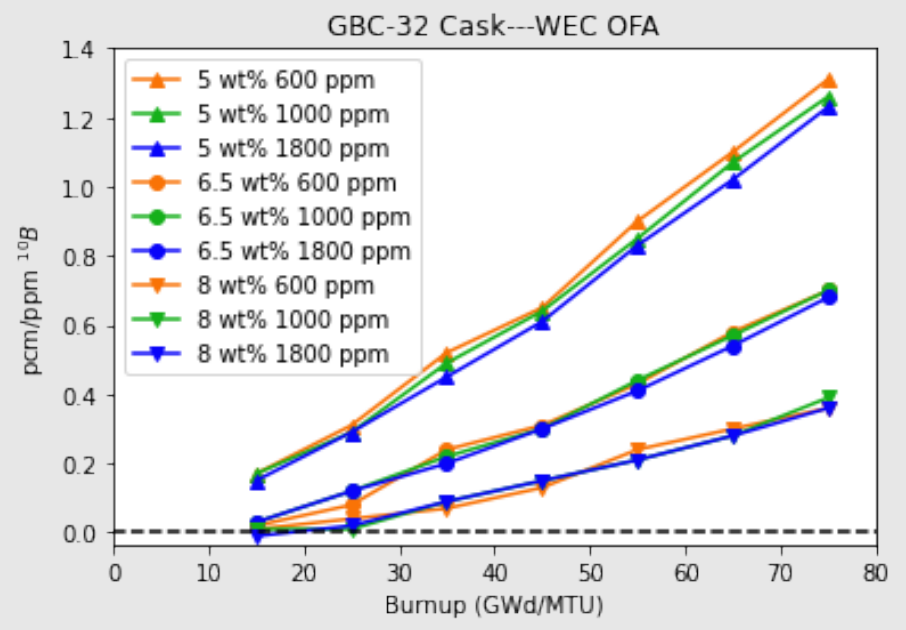

Figure 8-8 **^{10}B worth in Spent Fuel at 5.0, 6.5, and 8.0 wt % ^{235}U at Varying Soluble Boron (ppm) as a Function of Burnup (GWd/MTU)**

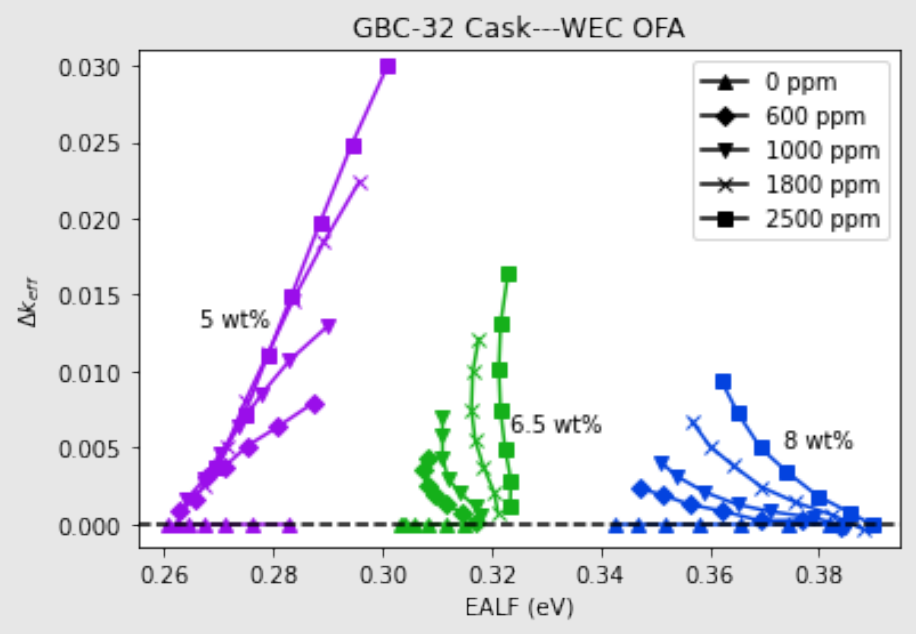

Figure 8-9 Relative Difference in k_{eff} at 5.0, 6.5, and 8.0 wt % ^{235}U at Varying Soluble Boron Concentrations (ppm) as a Function of Spectrum (EALF) with Respect to 0 ppm and Varying Burnup

All else equal, greater boron content will result in higher discharged fuel reactivity, with a smaller increase for higher enriched fuel. All else equal, increased boron content will result in a greater reactivity increase for fuel with a higher burnup. Behavior noted in NUREG-2216 [8] Figure 6A-4 drawn from NUREG/CR-6665 [54], as the basis for the recommendations provided in Attachment 6A of NUREG-2216 [8] is in line with the observations with increased enrichment and burnup analyzed.

8.1.5.1 Boron Letdown Curve

The effect of soluble boron concentration letdown in the coolant on discharged fuel k_{eff} was analyzed for 5, 6.5, and 8 wt % ^{235}U fuel, assuming a burnup-dependent soluble boron concentration. The fuel was burned up to 75 GWd/MTU using soluble boron letdown curves as described in Section 7.1.5.4. These curves were averaged to boron concentrations of 991 ppm. Figure 8-10 plots the relative changes in reactivity with changes in soluble boron content. Values presented are a comparison between the letdown and average curve. The use of the boron letdown curve is shown to be more limiting at most enrichments and burnups examined. Several points for 8 wt % fuel show the average is more limiting. In general, the deviation between the explicitly modeled letdown curve and the burnup averaged soluble boron is minimal, and further decreases as enrichment increases. At 75 GWd/MTU, the deviation between cycle average and boron letdown decreases.

With increasing enrichment, the reactivity difference between boron letdown and cycle averaged histories diminishes at all burnup points. The results for most scenarios indicate that discharged fuel reactivity is nearly equivalent between the letdown model and the constant average model at 75 GWd/MTU, when the burnup integrated average [68] soluble boron concentration are

equal. Differences from prior studies may be attributed to modeling a “sawtooth” expressed in operational days with cycle down powers, rather than an evenly divided burnup scheme at constant specific power. A more complete study of soluble boron letdown modeling including realistic combinations of enrichments, cycle lengths, and relative powers should be pursued in the future to fully investigate the phenomena involved.

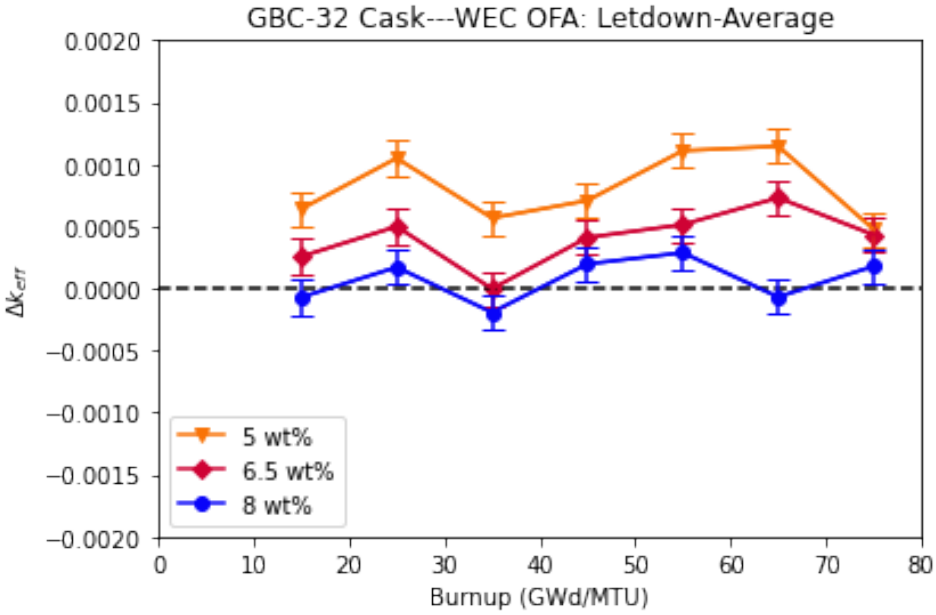

Figure 8-10 Relative Difference in k_{eff} of Boron Letdown Curve vs Cycle Average Soluble Boron (ppm) at 5.0, 6.5, and 8.0 wt % ^{235}U Fuel

8.1.6 Moderator Temperature

The effect of assembly moderator temperature on cask reactivity was analyzed for 5, 6.5, and 8 wt % ^{235}U fuel. The moderator density was appropriately varied along with the moderator temperature. The moderator density–temperature pairs are provided in Table 3-2. Moderator temperatures range between 550 and 615 K. Depleted fuel inventories were generated in intervals of 10 GWd/MTU from 15 to 75 GWd/MTU. Figure 8-11 plots the relative responses of k_{eff} to moderator temperature.

Temperature increases result in less moderation and a hardened spectrum. This generally results in more reactive spent fuel at higher operational temperatures. For 5 and 6.5 wt % fuel, this spectral hardening results in the expected increase in discharged fuel reactivity at all burnups. As with soluble boron, the variation in ^{239}Pu/^{235}U ratios mirrors the observed trending: the ratio decreases with enrichment as the increased moderator density hardens the spectrum. The impact of the increased ^{239}Pu content caused by the higher moderator temperature is reduced by the higher ^{235}U content, and the net effect at low burnups and higher enrichments is a reactivity reduction. All else equal, increasing enrichment lowers the moderator temperature

response, becoming slightly negative at lower burnups. All else equal, increasing burnup to 75 GWd/MTU continues the behavior established up to 60 GWd/MTU of increasing reactivity with increased moderator temperature.

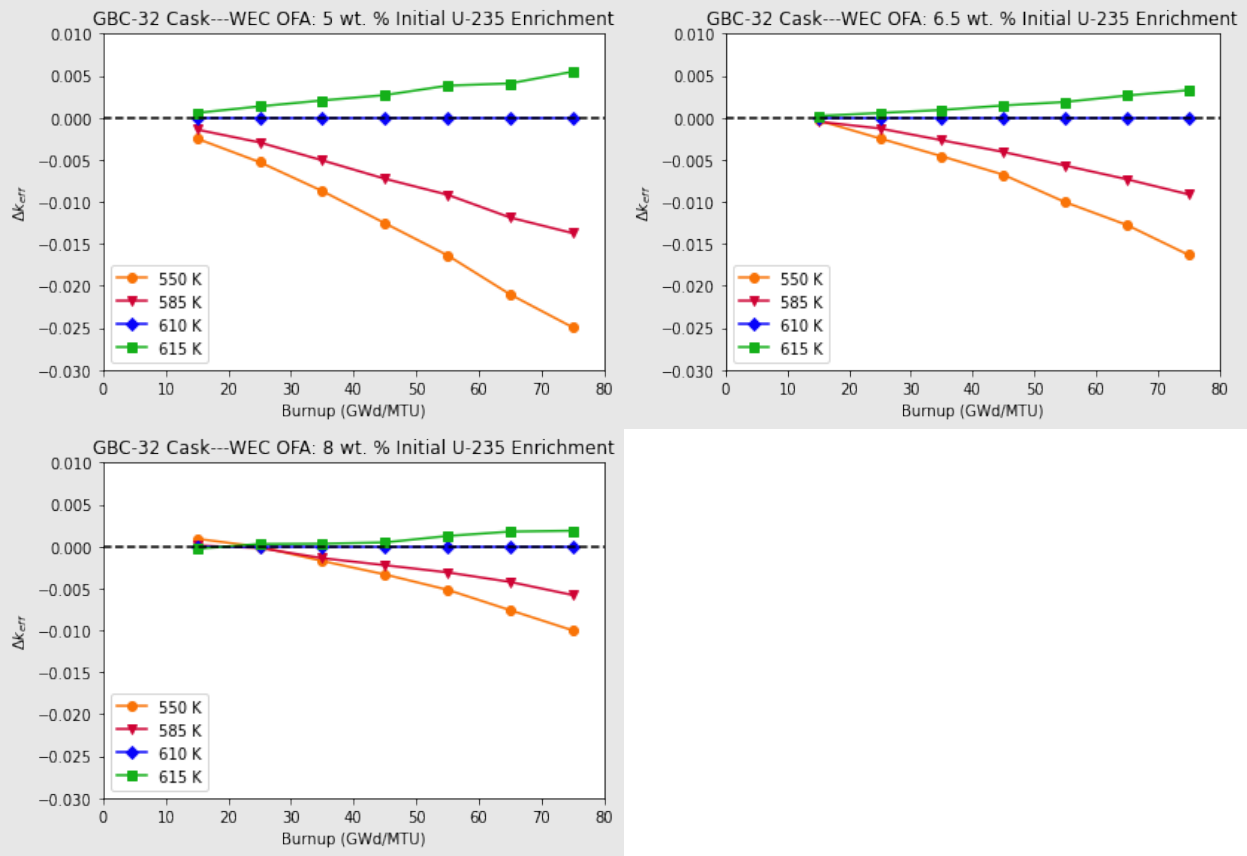

Figure 8-11 Relative Difference in k_{eff} at 5.0, 6.5, and 8.0 wt % ^{235}U Fuel with Varying Moderator Temperature (K) with Respect to a Reference of 610 K

8.1.7 Fuel Temperature

The effect of assembly fuel temperature on cask reactivity was analyzed for 5, 6.5, and 8 wt % ^{235}U fuel. Depleted fuel inventories were generated in intervals of 10 GWd/MTU from 15 to 75 GWd/MTU. Fuel temperatures of 560, 800, 900, and 1,600 K were investigated. In all instances, k_{eff} increases with increasing fuel temperature during fuel depletion as shown in Figure 8-12, similar to previous observed trends [67]. The effect decreases with increasing enrichment in a similar fashion to increased soluble boron content. The primary effect of increasing temperature is Doppler broadening of resonances, most importantly the ^{238}U capture resonances. As fuel temperature increases, ^{239}Pu production therefore also increases. However, the ^{239}Pu/^{235}U ratio is significantly reduced as a function of enrichment. Despite an increase in absolute ^{239}Pu production, the relative increase is lower and the reactivity impact is lessened. All else equal, increasing enrichment lowers the fuel temperature response. All else equal, increasing burnup to 75 GWd/MTU increases the integral effect of changes in the fuel temperature.

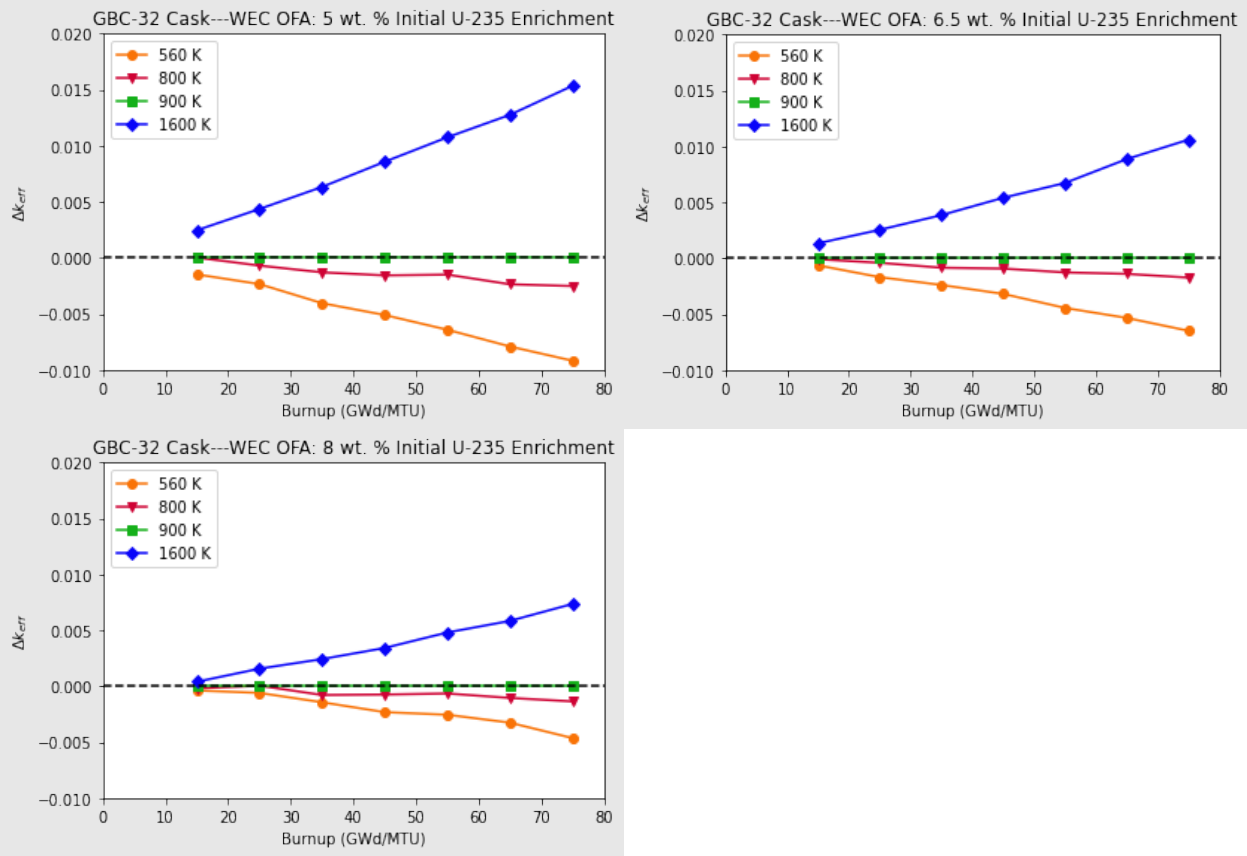

Figure 8-12 Relative Difference in k_{eff} at 5.0, 6.5, and 8.0 wt % ^{235}U Fuel with Varying Fuel Temperature (K) with Respect to a Reference of 900 K

8.1.8 Fuel Density

The effect of fuel density on cask reactivity was analyzed for 5, 6.5, and 8 wt % ^{235}U fuel. Depleted fuel inventories were generated in intervals of 10 GWd/MTU from 15 to 75 GWd/MTU. Fuel densities of 10.0, 10.26, and 10.75 g/cm^3 were investigated. Fuel density is not a parameter that is typically analyzed for BUC. Fuel density is not discussed in NUREG-2216 [8], with guidance only to "Ensure that the value of the fuel density used in calculations is justified to be realistic or conservative" in NUREG-2215 [7]. NUREG/CR-6716 [63] details fuel density parameterization of 1D and 3D k_{inf} calculations, though it ignores the use of BUC. A positive relation between fuel density and k_{inf} for 3D calculations was established in [63]. Fuel density is a known value for each batch of fuel, with higher density being more reactive. There is an observed variation of k_{eff} with burnup and enrichment, with higher burnups and densities having higher k_{eff} values. Increased density hardens the spectrum by introducing more fuel, marginally increasing ^{239}Pu production. NUREG/CR-6716 [63] reported a slight decrease in the trend slope of 3D eigenvalues with respect to fuel density with increasing enrichment. This is observed in Figure 8-13 with the slope of 8 wt % fuel approximately halved relative to 5 wt % fuel. All else equal, fuel density variation will have a lessened reactivity effect for higher enriched fuel. All else equal, fuel density increase will result in a greater reactivity effect for higher-burned fuel.

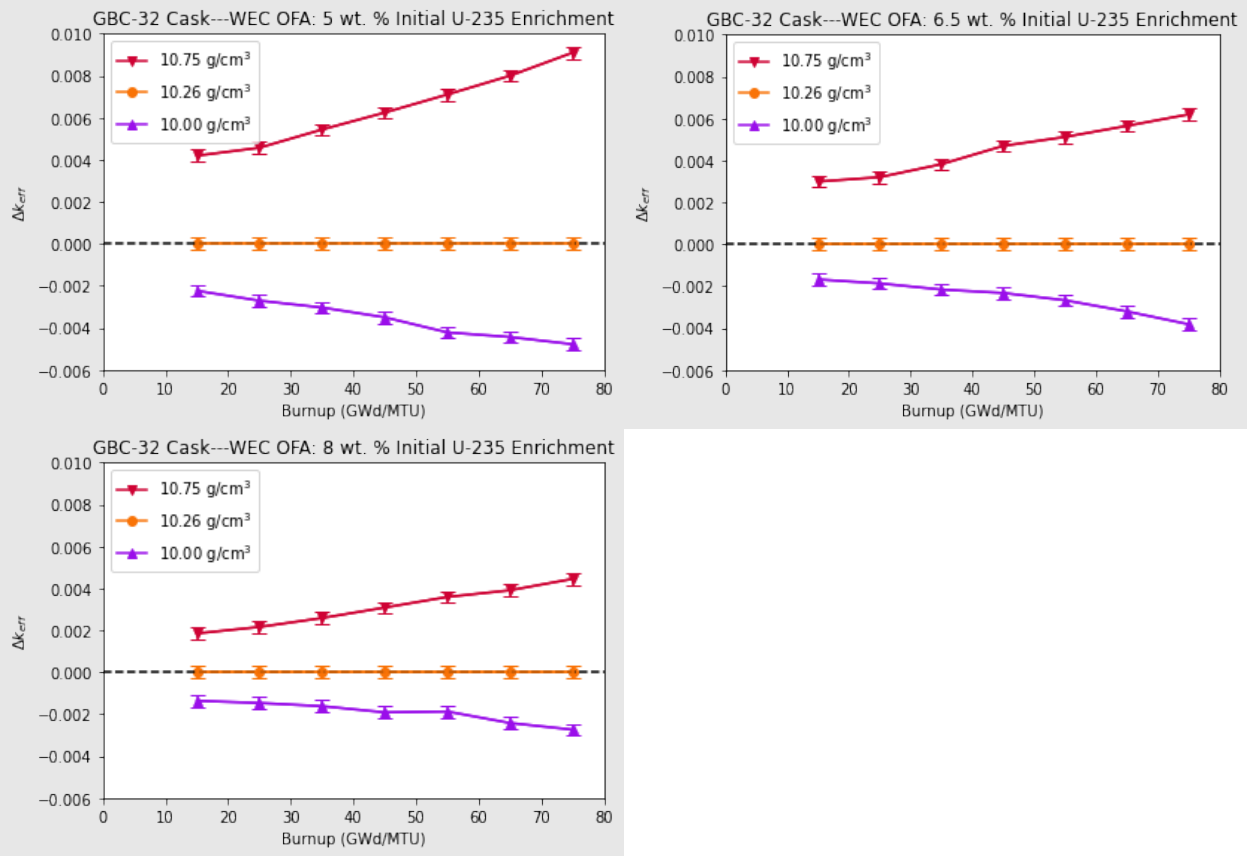

Figure 8-13 Relative Difference in k_{eff} (±2σ) at 5.0, 6.5, and 8.0 wt % ^{235}U Fuel with Varying Fuel Density (g/cm^3) with Respect to a Reference of 10.26 g/cm^3

8.1.9 Burnable Absorbers

8.1.9.1 Integral Fuel Burnable Absorbers

The effect of IFBA loading on cask reactivity was analyzed for 5, 6.5, and 8 wt % ^{235}U OFA fuel. Depleted fuel inventories were generated in intervals of 10 GWd/MTU from 15 to 75 GWd/MTU. IFBA loadings of 0, 80, 104, 128, 156, and 200 rods were investigated. Figure 8-14 shows variations in reactivity due to increased IFBA loading at different enrichments and burnups. In all cases analyzed, crediting IFBA in depletion increases the reactivity of spent fuel in storage, when neglecting residual boron in the cask model. The impact of IFBA variations on k_{eff} reduces with higher enrichments and increases with burnup. This results in very small differences for low burnups and high enrichment. As with soluble boron, integral burnable absorbers harden the spectrum. Accounting for the maximum credible absorber loading remains the more conservative approach, though the conservatism inherent in this approach is reduced with increased enrichment. With all else equal, an increase in IFBAs used in reactor operation increases discharged fuel reactivity, with higher burnups showing greater increases. Higher enrichments have a lower sensitivity to IFBA loading.

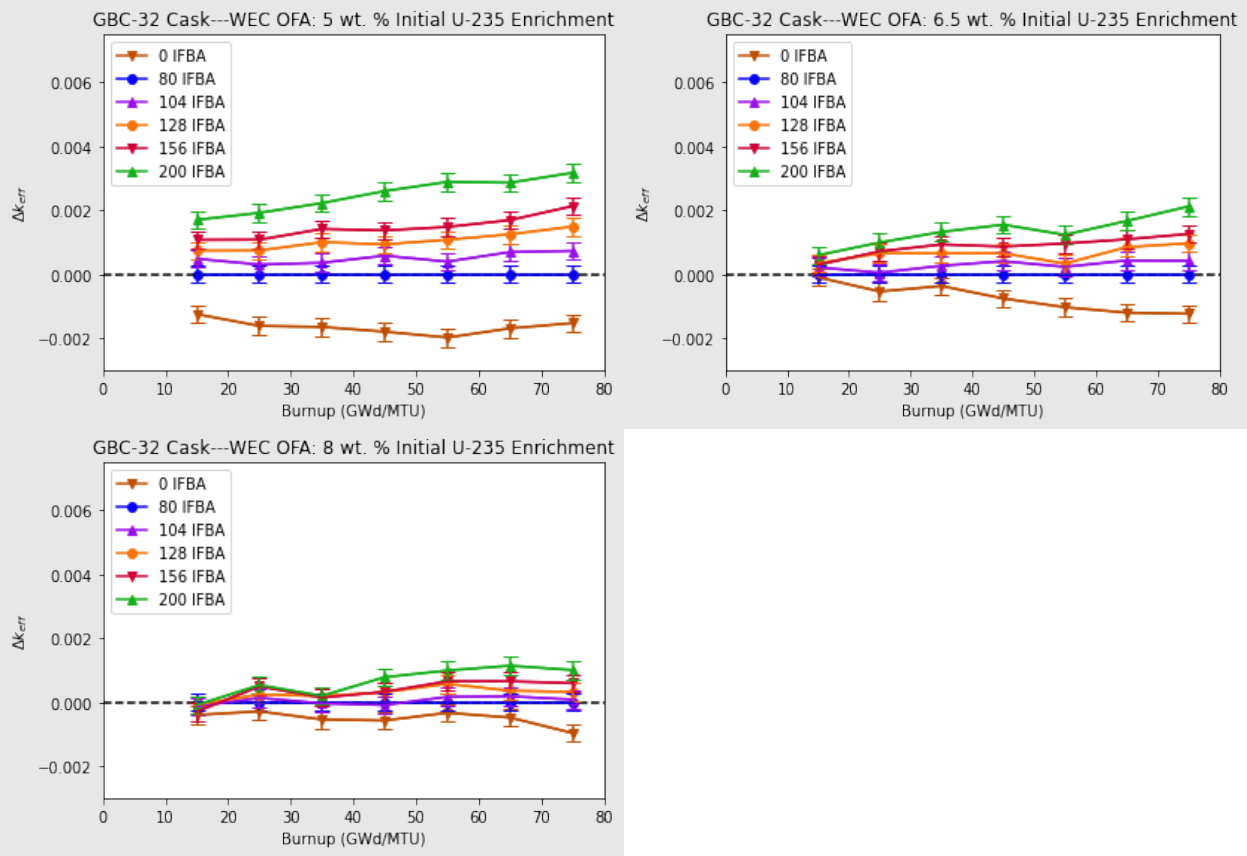

Figure 8-14 Relative Difference in k_{eff} (±2σ) at 5.0, 6.5, and 8.0 wt % ^{235}U Fuel with Varying IFBA Loading with Respect to a Reference of 80 IFBA Assembly

8.1.9.2 Integral Fuel Burnable Absorbers/Wet Annular Burnable Absorbers

The combined effect of IFBA and WABA loading on cask reactivity was analyzed for 5, 6.5, and 8 wt % ^{235}U OFA fuel. Depleted fuel inventories were generated in intervals of 10 GWd/MTU from 15 to 75 GWd/MTU. IFBA loadings of 200 rods were investigated in various combinations of 0, 8, 20, and 24 WABA. The use of 200 IFBA rods is the reference point for the study to isolate the impact of the WABA. Figure 8-15 shows variations in reactivity due to the loading of IFBA and WABA at different enrichments and burnups. In most cases analyzed, crediting WABA in depletion increases the reactivity of spent fuel in storage or transportation. At lower burnups and higher enrichments, there are reactivity fluctuations that approach statistical insignificance. For 200 IFBA and 24 WABA, a statistically insignificant decrease in reactivity results from the calculation. Again, a spectral hardening reactivity impact results from the presence of WABA and IFBA and decreases with enrichment. Accounting for the maximum credible absorber loading remains the conservative approach though the conservatism inherent in this approach decreases with increasing enrichment. With all else equal, an increase in the WABAs used in reactor operation would be the more reactive state with higher burnups showing greater increases. With equal burnup and WABA loading, higher enrichments have a lessened reactivity increase.

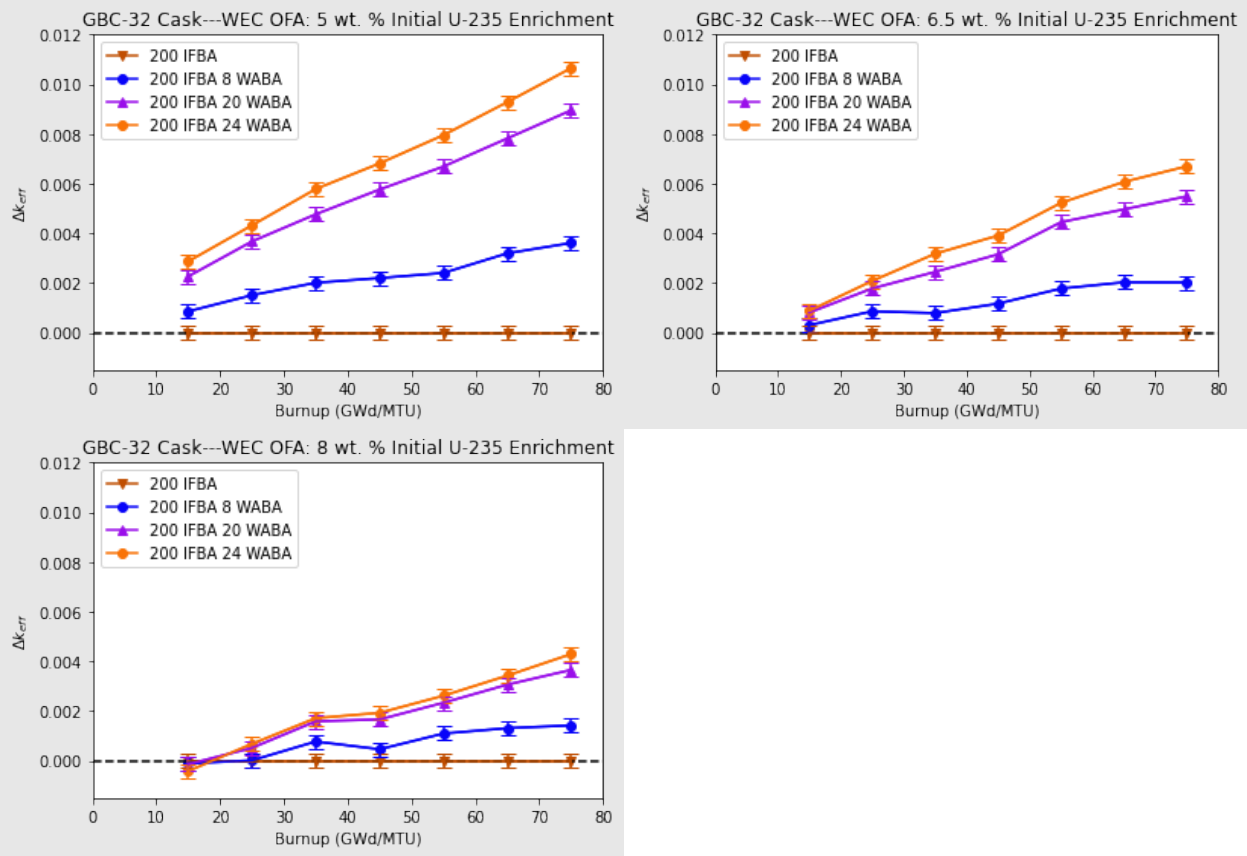

Figure 8-15 Relative Difference in k_{eff} (±2σ) at 5.0, 6.5, and 8.0 wt % ^{235}U fuel with Varying IFBA and WABA Loading with Respect to a Reference of 200 IFBA Assembly

8.1.9.3 Integral Fuel Burnable Absorbers/Gadolinia

The effect of IFBA and gadolinia on cask reactivity was analyzed for 7 wt % ^{235}U OFA fuel. Depleted fuel inventories were generated in intervals of 10 GWd/MTU from 15 to 75 GWd/MTU. Figure 8-16 shows variations in reactivity due to a single gadolinia loading of 12 rods with 8 wt % Gd_2O_3 and 104 IFBA for a range of different burnups. The presence of the gadolinia during depletion hardens the neutron energy spectrum, generating more plutonium and resulting in a slight increase to the reactivity of spent fuel in storage. At lower burnups, the reactivity fluctuations are statistically insignificant. The results of this limited study indicate that the presence of gadolinia during depletion increases discharged fuel reactivity when neglecting residual absorber. The impact appears to be small in combination with 104 IFBA but slowly increases with burnup. A more complete study is needed to characterize the impact of gadolinia as a function of content, number of rods, or fuel enrichment.

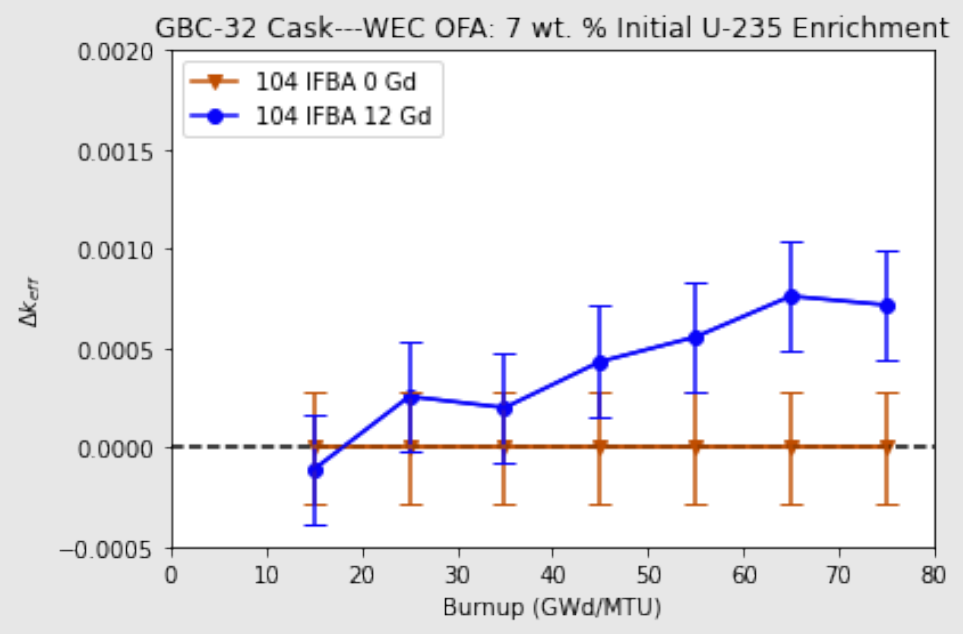

Figure 8-16 Relative Difference in k_{eff} (±2σ) at 7.0 wt % ^{235}U fuel with Varying IFBA and Gadolinia Loading with Respect to a Reference of 104 IFBA Assembly

8.1.10 Rod Cluster Control Assembly

The effect of RCCA history and material on cask reactivity was analyzed for 8 wt % ^{235}U OFA fuel. Depleted fuel inventories were generated in intervals of 10 GWd/MTU from 15 to 75 GWd/MTU. Multiple RCCA histories were investigated: AIC from startup (0 GWd/MTU) to 45, 55, 65, 75 GWd/MTU of burnup; AIC from 70 to 75 GWd/MTU of burnup; and boron carbide (B_4C) from startup to 75 GWd/MTU. RCCAs were modeled as fully inserted. A full insertion at power is precluded by the rod insertion limit. While a full insertion represents a nonphysical condition, analysis was performed to deliberately exaggerate the impact of RCCA insertion. This approach is also consistent with NUREG/CR-6759 [42], simplifying comparisons between these results and the available reference results. Figure 8-17 shows the variations in reactivity with the different RCCA histories and materials. In general, continuous RCCA insertion increases reactivity. Low burnup points in this analysis show a contradictory trend, but any conclusion is difficult given the nonphysical nature of the analysis. The results agree with the qualitative statement in NUREG-2216 Attachment 6A: "… the CR would have to be inserted for a significant fraction of the total irradiation time for these effects to be seen in terms of a positive Δk on the SNF package" [8]. While only 8 wt % fuel was examined, a spectral hardening effect would be expected to show an increase in the reactivity difference at lower enrichment as demonstrated thus far with other parameters. Additionally, such a decrease in the reactivity impact is established in NUREG/CR-6759 [42]. A more realistic analysis of rodded operation at power could be performed in the future to provide a more accurate estimate of the impact use during depletion.

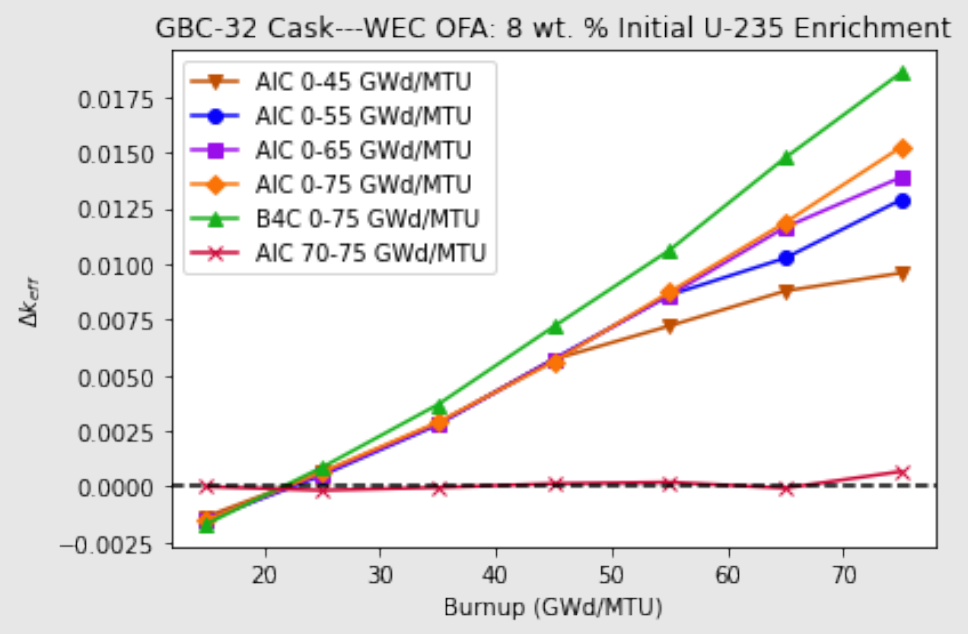

Figure 8-17 Relative Difference in k_{eff} at 8.0 wt % ^{235}U Fuel with Different RCCA Materials and Histories with Respect to a Reference of 0 RCCA Rod Insertion

8.1.11 Fuel Assembly Type

The baseline depletion calculations documented in Sections 8.1.1 through 8.1.10 were also performed with the WEC 17x17 RFA fuel assembly. The difference in the calculated k_{eff} in the GBC-32 cask for the two fuel assembly types is shown in Figure 8-18. The burnup at which RFA becomes more reactive than OFA increases with increasing enrichment, to the extent that for some of the highest enrichments considered in this report, the OFA design is more reactive than the RFA design at all burnups. This is the result of different response to burnup with increased enrichment between the two fuel assembly designs.

The parametric studies presented earlier in this section were repeated with the RFA fuel type. An example is demonstrated in Figure 8-19. The behavior of both fuel types is very similar as a function of burnup and enrichment. Figure 8-20 provides the difference in trend behavior—a difference of differences with the resulting increased uncertainties (20 pcm). Differences between OFA and RFA trends for specific power are thus largely, if not entirely, a result of Monte Carlo statistics and no trend between fuel types is observed as a function of enrichment burnup or specific power. This behavior is also observed with the other parameters studied.

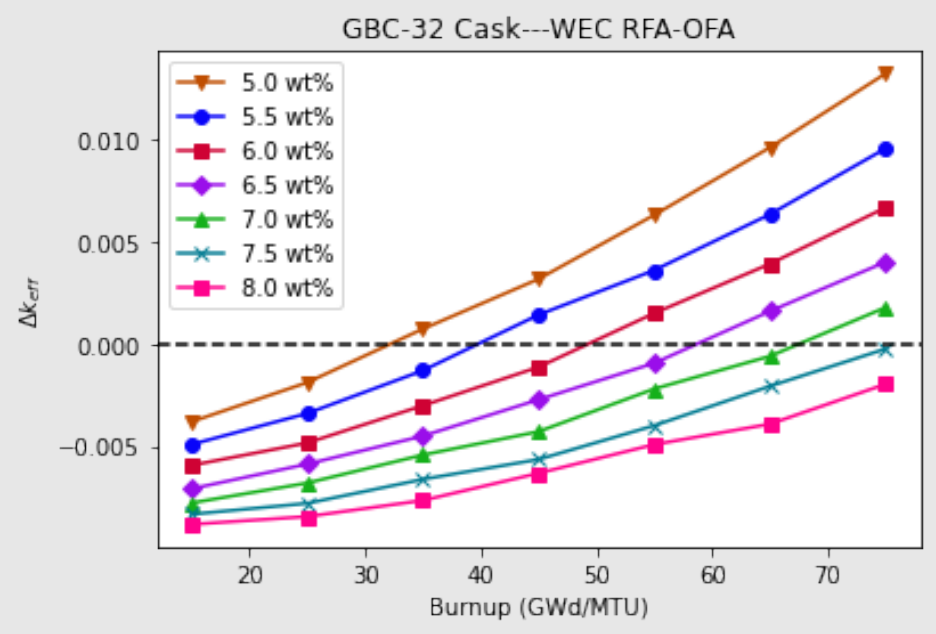

Figure 8-18 Relative Difference in GBC-32 Fuel Type k_{eff} as a Function of Burnup and Initial ^{235}U Enrichment

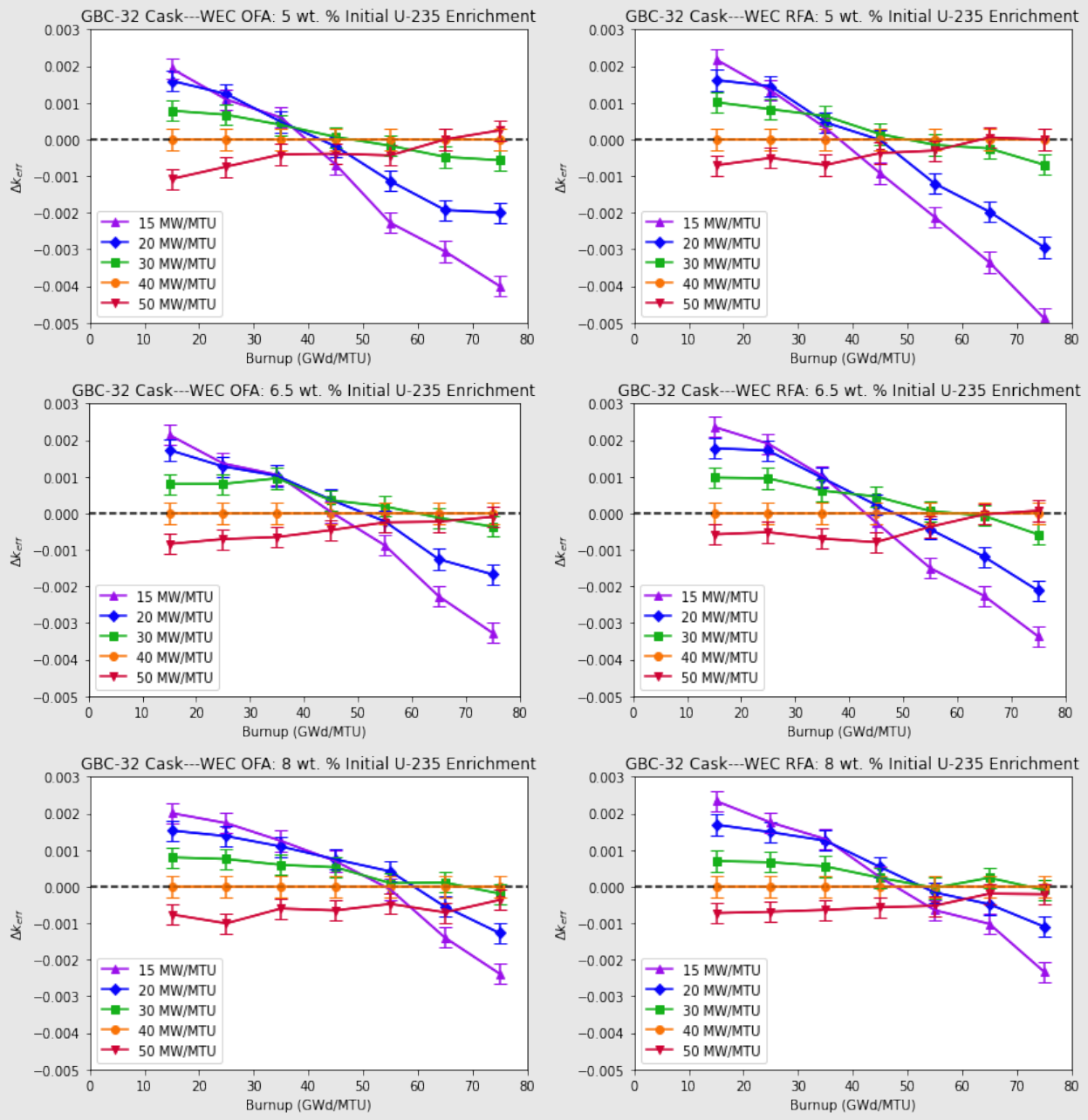

Figure 8-19 Relative Difference in k_{eff} (±2σ) at 5.0, 6.5, and 8.0 wt % ^{235}U Fuel with Varying Specific Power (MW/MTU) for OFA and RFA Fuel Rods with Respect to a Reference of 40 MW/MTU

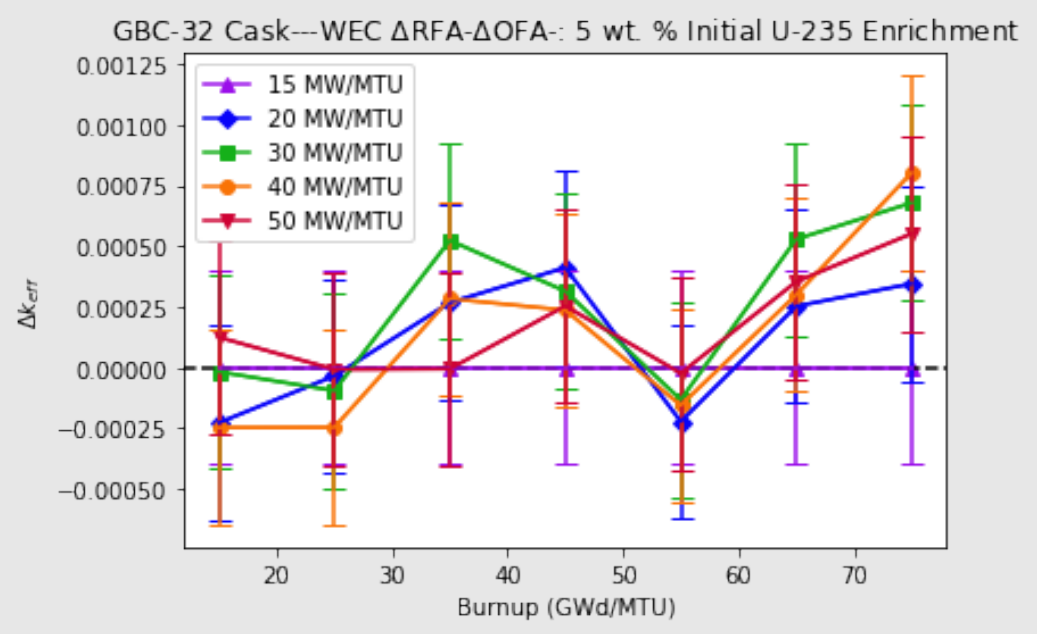

Figure 8-20 Differences (±2σ) in Trend Behavior for OFA and RFA Fuel Types for Varying Specific Powers (MW/MTU) with Respect to OFA

8.1.12 Axial Burnup Profile

The effect of different axial burnup profiles for criticality safety was analyzed using GBC-32 with WEC 17×17 OFA having 6 wt % initial ^{235}U enrichment. Four different axial burnup profiles, as given in Table 8-1, were used. The reference axial burnup profile was chosen from NUREG/CR-6801 [55] that corresponded to a burnup range of 30–34 GWd/MTU, as given in burnup group 5 of Table 5 in NUREG/CR-6801 [55]. This profile was chosen based on the results in [55] that bounding profiles from intermediate burnup ranges bound the available profiles at higher burnups. Profile 1 was also from NUREG/CR-6801 [55], corresponding to burnups greater than 46 GWd/MTU. This profile corresponded to burnup group 1 in Table 5 of NUREG/CR-6801 [55]. Profile 2 and Profile 3 were obtained from the LEU+ study in [17], corresponding to an initial ^{235}U enrichment of 6.2 wt % for WEC 17×17 RFA fuel rod design (noted as standard WEC 17×17 assembly design in [17]). Profile 2 was from an assembly with 200 IFBA fuel rods and 8 WABA rods and an average assembly burnup of 61.5 GWd/MTU. Profile 3 was from an assembly with 200 IFBA fuel rods and an average assembly burnup of 72.0 GWd/MTU. Profile 2 and Profile 3 were chosen for the purpose of comparing sample LEU+ and high assembly-average burnup axial burnup profiles with the baseline axial burnup profile.

Figure 8-21 shows k_{eff} for GBC-32 with WEC 17×17 OFA using the four axial profiles presented in Table 8-1. Results indicate that the reference axial burnup profile provides the highest k_{eff} in GBC-32, and is therefore the most conservative profile, in comparison to Profile 1 (i.e., LEU with burnups greater than 46 GWd/MTU), and sample LEU+ axial burnup profiles Profile 2 and Profile 3 (i.e., LEU+ with burnups at 61.5 GWd/MTU and 72.0 GWd/MTU).

At lower burnups, the uniform axial burnup profile provides less nonconservative k_{eff} values compared to the reference profile, as shown in Figure 8-22, since lower burnups have a more

uniform axial burnup profile compared to higher burnups. A reduced conservatism in k_{eff} is observed for the reference axial burnup profile with higher enrichment fuel compared to lower enrichment, as higher enrichment maintains a more uniform axial burnup profile.

Table 8-1 Relative Axial Burnup Profiles for Criticality Safety Burnup Credit Analysis

Axial Node No.	Relative Axial Burnup			
	Reference NUREG/CR-6801 [55]	Profile1 NUREG/CR-6801 [55]	Profile2 ORNL/TM-2022/1831 [17]	Profile3 ORNL/TM-2022/1831 [17]
1 (bottom)	0.652	0.582	0.659	0.665
2	0.967	0.920	0.943	0.946
3	1.074	1.065	1.059	1.060
4	1.103	1.105	1.094	1.093
5	1.108	1.113	1.099	1.096
6	1.106	1.110	1.097	1.094
7	1.102	1.105	1.092	1.090
8	1.097	1.100	1.089	1.086
9	1.094	1.095	1.085	1.083
10	1.094	1.091	1.082	1.080
11	1.095	1.088	1.080	1.078
12	1.096	1.084	1.077	1.075
13	1.095	1.080	1.073	1.071
14	1.086	1.072	1.064	1.063
15	1.059	1.050	1.044	1.044
16	0.971	0.992	0.982	0.985
17	0.738	0.833	0.838	0.843
18 (top)	0.462	0.515	0.542	0.548

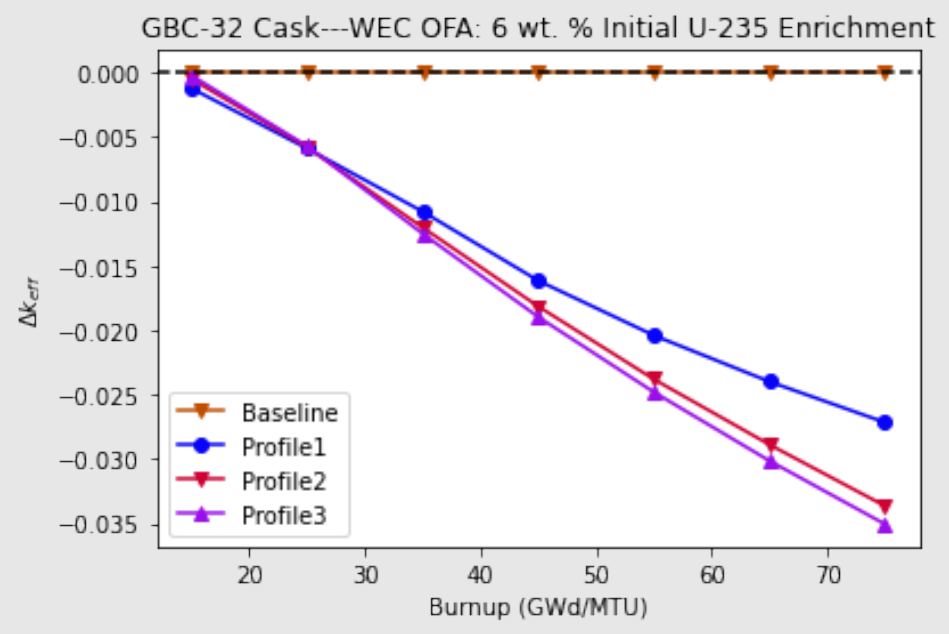

Figure 8-21 Relative k_{eff} for GBC-32 with WEC 17×17 OFA and 6 wt % Initial ^{235}U Enrichment for Different Axial Burnup Profiles with Respect to the Reference (Baseline) Profile

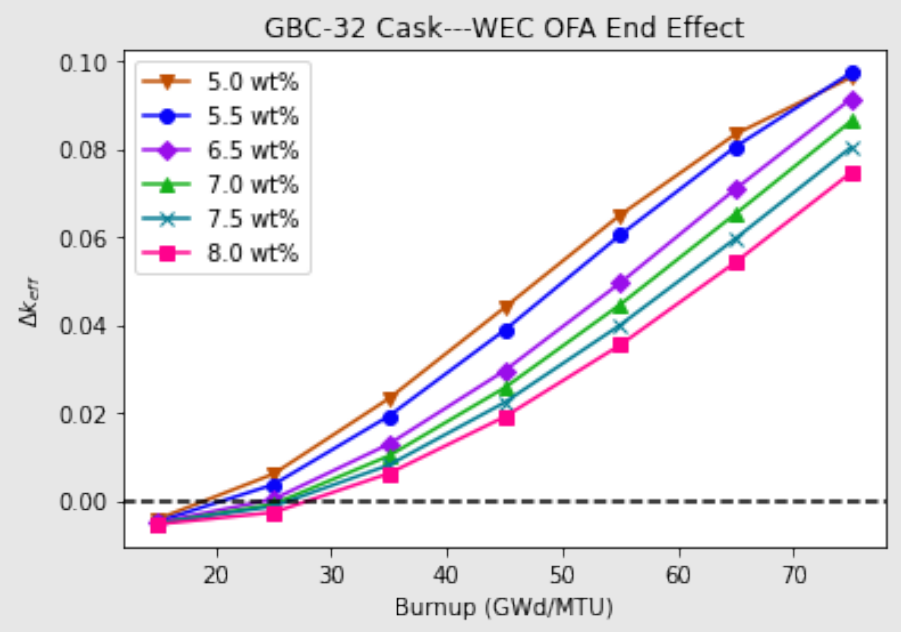

Figure 8-22 Relative k_{eff} for GBC-32 with WEC 17×17 OFA and Multiple Initial ^{235}U Enrichments for the Reference Axial Burnup Profile with Respect to a Uniform Distribution

8.1.13 Summary of Criticality Safety Parametric Sensitivities

Summaries of the k_{eff} sensitivities to select irradiation parameters for the GBC-32 cask are provided in Table 8-2 through Table 8-4. Irradiation parameters without clearly defined upper and lower bounds (such as burnable absorber exposure, assembly type, and control rod usage) are omitted from these tables. For each irradiation parameter and source component, the relative k_{eff} differences are calculated by comparing the eigenvalues at the baseline value to those at the lower and upper bounds of the selected range. The sensitivities are provided as differences in pcm from the baseline eigenvalue for the associated enrichment. Positive values are noted in italics.

Table 8-2 5 wt % PWR k_{eff} Sensitivity Summary

Parameter	Lower bound	Baseline	Upper bound	Burnup (GWd/MTU)							
				Bound	15	25	35	45	55	65	75
Specific Power (MW/MTU)	15	40	50	Lower	*161.5*	*143.4*	*30*	-77.9	-212.1	-320.7	-450
				Upper	-108	-74.5	-41.2	-51.5	-43.9	-0.3	*24.5*
Fuel Density (g/cm³)	10	10.26	10.75	Lower	-240	-261.7	-304.5	-364.2	-431.1	-451.2	-490
				Upper	*402.6*	*465.7*	*542.2*	*609.6*	*700.5*	*791.7*	*896.9*
Fuel Temperature (K)	560	900	1600	Lower	-165.9	-265.5	-393.2	-523.5	-678.9	-797.1	-939.3
				Upper	*238.2*	*435.6*	*641.2*	*811.1*	*1051.1*	*1301*	*1558.4*
Soluble Boron (ppm)	600	1000	1800	Lower	-70.3	-133.5	-160.1	-264.9	-342.2	-434.6	-506.1
				Upper	*95.3*	*207.4*	*344.7*	*470.9*	*610.8*	*773.4*	*943.9*
Moderator Temperature (K)	550	610	615	Lower	-265.3	-540.2	-872.5	-1264.5	-1668.3	-2067	-2493.2
				Upper	*62*	*145.9*	*212.6*	*249.2*	*318*	*430.6*	*515.5*
Cooling Time (years)	1	5	100	Lower	*444.9*	*753.7*	*1054.7*	*1299.9*	*1565.4*	*1829.2*	*2073.2*
				Upper	-1244.2	-2181.9	-3116.5	-4024.9	-4873.8	-5665.1	-6399.7

Table 8-3 6.5 wt % PWR k_{eff} Sensitivity Summary

Parameter	Lower bound	Baseline	Upper bound	Burnup (GWd/MTU)							
				Bound	15	25	35	45	55	65	75
Specific Power (MW/MTU)	15	40	50	Lower	*193.7*	*136*	*104.9*	*19.3*	-87.7	-226.8	-327
				Upper	-104.3	-70.7	-65.2	-30.3	-25.1	-23	-10.2
Fuel Density (g/cm³)	10	10.26	10.75	Lower	-201.6	-183.7	-209.7	-230.8	-279.2	-326.1	-373.2
				Upper	*265.1*	*322.8*	*388.1*	*470.5*	*499.4*	*558.2*	*627.2*
Fuel Temperature (K)	560	900	1600	Lower	-105.2	-155.8	-237.5	-344.7	-431	-542.2	-653
				Upper	*100.5*	*244*	*411.5*	*551.4*	*702.1*	*878.9*	*1055.6*
Soluble Boron (ppm)	600	1000	1800	Lower	-42.8	-39.4	-84.3	-111.5	-189.9	-221.2	-273.9
				Upper	*19.6*	*86.8*	*163.6*	*252.8*	*313.7*	*424.1*	*505.5*
Moderator Temperature (K)	550	610	615	Lower	-54	-200	-428.8	-698.8	-972.1	-1287.8	-1605.1
				Upper	*3.9*	*47.6*	*99.9*	*164.8*	*194.8*	*251.9*	*341.1*
Cooling Time (years)	1	5	100	Lower	*343.5*	*636.2*	*870.4*	*1106.1*	*1304.7*	*1513.7*	*1703.1*
				Upper	-926.2	-1693.3	-2440.2	-3172.4	-3889.6	-4549.3	-5201.3

Table 8-4 8 wt % PWR k_{eff} Sensitivity Summary

Parameter	Lower bound	Baseline	Upper bound	Burnup (GWd/MTU)							
				Bound	15	25	35	45	55	65	75
Specific Power (MW/MTU)	15	40	50	Lower	*200.7*	*173.3*	*124.7*	*69.2*	-7.9	-139.6	-238.1
				Upper	-76.2	-100.7	-60	-65.2	-47.4	-70.7	-36.6
Fuel Density (g/cm³)	10	10.26	10.75	Lower	-136.2	-146.6	-161.8	-191.3	-187.2	-242.1	-273.7
				Upper	*185*	*215.8*	*258.4*	*308.3*	*358.9*	*390.7*	*444.9*
Fuel Temperature (K)	560	900	1600	Lower	-35.5	-106.5	-153.8	-199.7	-256.6	-356.2	-447.1
				Upper	*42.9*	*140.1*	*250.4*	*349.7*	*476.7*	*591*	*704.9*
Soluble Boron (ppm)	600	1000	1800	Lower	-2.8	-16.8	-60.7	-43.2	-80.9	-122.6	-173.5
				Upper	-19.6	*17.3*	*58.6*	*113.3*	*169.6*	*196.9*	*271.1*
Moderator Temperature (K)	550	610	615	Lower	*91.4*	-33.6	-176.9	-322	-538.1	-775	-1017.7
				Upper	-11.1	*4.2*	*36.2*	*77.7*	*114.9*	*151.2*	*215.1*
Cooling Time (years)	1	5	100	Lower	*287*	*531.5*	*711.6*	*902.2*	*1107.5*	*1279.7*	*1430.1*
				Upper	-703.3	-1368.3	-2004.1	-2622.6	-3236.9	-3811.6	-4368.3

9 CONCLUSIONS

Parametric studies were performed to assess the effects of various fuel assembly, irradiation, and decay parameters on dose rates and discharge fuel reactivity of transportation packages and dry storage casks containing fuel with extended enrichment and high burnup. Extended enrichment refers to initial ^{235}U enrichment in the range of 5 to 8 wt %, and high burnup refers to assembly average burnups up to 75 GWd/MTU.

An analysis of nuclide importance to decay heat for 5 and 8 wt % ^{235}U at 75 GWd/MTU assembly average burnup demonstrated that changing enrichment does not cause a change in the top nuclide contributors, but the rankings of the top contributors show more variability at the 5-year cooling time compared to the 100-year cooling time. Nuclide importance to decay heat for 8 wt % ^{235}U at 40 and 75 GWd/MTU demonstrated that changing burnup can cause more variability in ranking at the 5-year cooling time compared to the 100-year cooling time. Nuclide importance to source terms and criticality safety demonstrated that the main nuclide contributors remain the same in comparing extended-enrichment and high-burnup fuel with LEU fuel.

A summary of the parameters studied and their effects on dose rates is provided in Table 9-1. Generally, burnup and cooling time had the largest effect on dose rates. The effect of the variation in the analyzed parameters were not consistently the same for 5 wt % and 8 wt % ^{235}U enrichments. Parameters that hardened the neutron spectrum, such as increased soluble boron concentration, increased burnable absorber presence, and RCCA insertion had the largest effect on neutron dose rates. The selected range of certain parameters (i.e., PWR moderator density and BWR coolant void fraction) and the corresponding dose rate trends are generally larger than the practical range in commercial reactors and are thus intended to be illustrative only. Although absolute dose rate values differed, generally similar trends were observed for burnup, initial enrichment, cooling time, specific power, moderator density/temperature, coolant void fraction, and fuel density compared to LEU publications.

Table 9-1 Summary of Shielding Parametric Study Results: Effects on Dose Rates

Parameter	Range	Neutron Dose Rate	Primary Gamma Dose Rate	Co-60 Dose Rate
Burnup (GWd/MTU)	20–75	Previously established LEU trends [63] were observed. Neutron dose rates increased with burnup to the power of four.	Previously established LEU trends [63] were observed. Primary gamma dose rates linearly increased with burnup.	^{60}Co dose rates linearly increased with burnup.
Initial ^{235}U enrichment (wt %)	5.0–8.0	Previously established LEU trends [63] were observed. Neutron dose rates decreased with	Primary gamma dose rates decreased with increasing enrichment up to 5 yr of cooling time. At cooling times of 20 yr and beyond, primary gamma dose	^{60}Co dose rates decreased with increasing enrichment.

Parameter	Range	Neutron Dose Rate	Primary Gamma Dose Rate	Co-60 Dose Rate
		increasing enrichment.	rate trends analyzed in this study were different compared to total gamma dose rate trends given in LEU publications, where total gamma dose rate decreases with cooling time. For LEU+, primary gamma dose rate increased with increasing enrichment at long cooling times, which is supported by LEU+ analysis in [41].	
Cooling Time (years)	1–100	Previously established LEU trends [63] were observed. Neutron dose rates decreased with increasing cooling time.	Previously established LEU trends [63] were observed. Primary gamma dose rates decreased with increasing cooling time, rapidly decreasing from 5 to 20 yr.	^{60}Co dose rates decreased with increasing cooling time.
Specific Power (MW/MTU)	15–50	Previously established LEU trends [63] were observed. Neutron dose rates increased with increasing specific power.	Previously established LEU trends [63] were observed. Primary gamma dose rates increased with increasing specific power.	^{60}Co dose rates increased with increasing specific power.
Soluble Boron (ppm)	600–1,800	Dose rates increased with increasing boron concentration. Effects were larger at higher enrichments. Differences in dose rates between a boron letdown curve and the associated average value were negligible.	Dose rates generally increased with increasing boron concentration. Dose rate effects were larger at lower enrichments; effects were mitigated at cooling times beyond 60 yr. Differences in dose rates between a boron letdown curve and the associated	Dose rates were relatively insensitive to boron concentration. Dose rate effects were larger at lower enrichments. Differences in dose rates between a boron letdown curve and the associated average value were negligible.

Parameter	Range	Neutron Dose Rate	Primary Gamma Dose Rate	Co-60 Dose Rate
			average value were negligible.	
Moderator Density (g/cm^3) /Temperature (K) (PWR) **Coolant Void (%) (BWR)**	0.60811/615 –1.0052/293 (PWR) 20–80 (BWR)	Previously established LEU trends [63] were observed. Dose rates decreased with increasing moderator density or decreasing coolant void; effects were greater at higher enrichments.	Previously established LEU trends [63] were observed. Dose rates decreased with increasing moderator density or decreasing coolant void.	^{60}Co dose rate trends displayed local minima, which depended on burnup and enrichment.
Fuel Temperature (K)	560–1,600 (PWR) 500–1,300 (BWR)	Dose rate effects were small. Neutron dose rates increased with increasing fuel temperature for 8 wt % ^{235}U enrichment.	Dose rate effects were small. Primary gamma dose rates generally decreased with increasing fuel temperature; effects were greater at lower enrichments.	Dose rate effects were small. ^{60}Co dose rates decreased with increasing fuel temperature; effects were greater at lower enrichments.
Fuel Density (g/cm^3)	10–10.75 (PWR) 10.26–10.96 (BWR)	Previously established LEU trends with uranium mass [63] were observed for neutron dose rates; dose rates generally increased with increasing fuel density.	Previously established LEU trends [63] with uranium mass were observed for primary gamma dose rates; dose rates generally increased with increasing fuel density.	^{60}Co dose rates decreased with increasing fuel density; effects were small.
Burnable Absorbers	0–200 IFBAs, 8–24 WABAs, 12 Gd_2O_3 rods at 8 wt % loading (PWR) 1.5–8 wt % Gd_2O_3 (BWR)	Neutron dose rates increased with increasing IFBAs/WABAs, and the change was greater at higher enrichment; gadolinia rods did not greatly affect neutron dose rates. BWR neutron dose rates increased with increasing gadolinia, and the	IFBA/WABA effects on primary gamma dose rates did not vary with enrichment; dose rates were also insensitive to gadolinia rods. BWR primary gamma dose rates were insensitive to gadolinium loading.	^{60}Co dose rates increased with increasing WABAs and decreasing IFBAs over all enrichments and were insensitive to gadolinia rods. BWR ^{60}Co dose rates were insensitive to gadolinium loading.

Parameter	Range	Neutron Dose Rate	Primary Gamma Dose Rate	Co-60 Dose Rate
		effect was greater at higher enrichments.		
RCCA /Control Rod Blades	—	Increased control rod insertion increased PWR neutron dose rates by up to 10% at short cooling times, with slightly increased effects at longer cooling times. BWR neutron dose rates increased with increased blade insertion by up to 8% over all cooling times analyzed.	Increased control rod/blade insertion increased primary gamma dose rates by up to 10% at short cooling times for PWRs; effects were mitigated beyond 50 yr of cooling time. Effects were slightly smaller for BWRs.	Increased control rod/blade insertion increased ^{60}Co dose rates by up to 3% over all analyzed cooling times for PWR. For BWRs, the ^{60}Co dose rate reached a local minimum at an intermediate control blade withdrawal.
Fuel Assembly Type	WEC OFA and RFA	Trends were identical between the fuel assembly types analyzed; total dose rate variation was less than 3% at 75 GWd/MTU.		
Axial Burnup Profile	—	PWR LEU+ profiles were bounded by reference LEU profile; BWR LEU+ profiles suggest that new bounding profiles may need to be generated for LEU+ designs.		

In most instances, criticality safety behavior for high-burnup and extended-enrichment assemblies followed expectations established by decades of BUC analysis. A summary of the parameters studied and their effects on reactivity is provided in Table 9-2. Results demonstrated an increased magnitude of the accrued effect at an increased burnup—the slope behavior was unchanged by the increase in burnup alone. Several parameters exhibited unexpected behavior at lower burnups, but this was determined to be a result of select parameter responses to increased enrichment rather than a burnup-specific behavior. The impact of enrichment appears to be more complicated. Competing effects in play for different parameters resulted in minor unexpected effects. Although the spectral hardening effect of several parameters and the resulting increase in spent fuel reactivity are well established, the magnitude of the enrichment effect is much lower for extended enrichments. A significant reduction in the ratio of ^{239}Pu/^{235}U concentrations is observed as enrichment is increased within the extended enrichment range. At higher enrichments, less ^{239}Pu production relative to the ^{235}U inventory results in a lesser effect on k_{eff}. Thus, the impact of the magnitude of several parameters on k_{eff} with an enrichment increase from 5 to 8 wt % presents a significant reduction of conservatism compared to LEU fuel. Despite increased burnup and increased enrichment each individually increase ^{239}Pu content, the ^{239}Pu buildup from the examined parametric effects is lessened and, thus, produces a lessened response.

Table 9-2 Summary of Burnup Credit Parametric Study Results

Parameter	Range	Observation
Burnup (GWd/MTU)	15–75	Previously established LEU trends were observed. Cask reactivity decreased with burnup. The rate of decrease was slightly reduced with increased enrichment. Unless otherwise noted, all other trends have an increase in the integrated parameter effect as a function of burnup.
Initial Fuel Enrichment (wt %)	5.0–8.0	Previously established LEU trends were observed. Cask reactivity increased with increasing enrichment, though as noted above the magnitude of the increase is reduced at higher enrichments.
Cooling Time (years)	1–100	Previously established LEU trends were observed. A minimum in reactivity is observed at 100 yr. The magnitude of the reactivity shift is reduced because of less ^{241}Pu and ^{155}Gd generation at higher enrichments. This agrees with NUREG/CR-6781 [66].
Specific Power (MW/MTU)	15–50	Previously established LEU trends were observed. Lower specific powers are more conservative at lower burnups, and higher specific powers are more bounding at higher burnups, consistent with NUREG/CR-6665 [54] and ORNL/TM-12973 [67]. The burnup point at which the reverse occurs slightly delays with increased enrichment.
Soluble Boron (ppm)	600–1,800	Previously established LEU trends were observed. An increase in soluble boron increases discharged fuel reactivity. The magnitude of this increase is reduced with enrichment in line with ORNL/TM-12973 [67]. The boron letdown modeled resulted in a higher reactivity than the average cycle boron until assembly end of life. The detailed letdown and constant average boron concentration yield approximately equal reactivity after the single letdown has completed.
Moderator Temperature (g/cm^3) /Moderator Temperature (K) (PWR)	0.61/615–0.77/550	Previously established LEU trends were observed for cask reactivity with varied moderator density in most conditions. The magnitude of this increase is reduced with enrichment. At a burnup of 15 GWd/MTU and an initial enrichment of 8 wt % ^{235}U, minor deviations were observed, with increasing temperature (reduced density) slightly reducing reactivity.

Parameter	Range	Observation
Fuel Temperature (K)	560–1,600	Previously established LEU trends were observed. An increase in fuel temperature increases discharged fuel reactivity. The magnitude of this increase is reduced with enrichment in line with ORNL/TM-12973 [67].
Fuel Density (g/cm^3)	10–10.75	Previously established LEU trends are not overly detailed regarding 3D BUC analysis of fuel density. An increase in fuel density increases discharged fuel reactivity. The magnitude of this increase is reduced with enrichment. Available previous information is in line with observations.
Burnable Absorbers	0–200 IFBAs, 8–24 WABAs, 12 Gd_2O_3 rods at 8 wt % loading	Previously established LEU trends were observed. Increased burnable absorber loading hardens the neutron spectrum resulting in increased discharge fuel reactivity. The magnitude of this increase is reduced with enrichment- for low burnups at 8 wt % this effect becomes statistically negligible.
Rod Cluster Control Assembly	—	Analysis of RCCA effects was performed assuming full insertion, which is not customary for PWR operation. Results are consistent with qualitative statements from NUREG-2216 [8], requiring significant RCCA exposure for a significant discharge fuel reactivity increase.
Fuel Assembly Type	WEC OFA and RFA	Trends were identical between fuel types; in cases such as specific power the trends were so similar as to be statistically equivalent. In all other instances, the trend behavior, if not exact k_{eff} differences, performed identically (e.g., increased burnable absorber increased discharge fuel reactivity, reducing magnitude with enrichment).
Axial Burnup Profile	—	Sample profiles from previous LEU+ reports were bounded by the reference bounding LEU axial burnup profile for increased enrichment and burnup.

10 REFERENCES

1. Chadwick, M.B., et al., "ENDF/B-VII.1 Nuclear Data for Science and Technology: Cross Sections, Covariances, Fission Product Yields and Decay Data," *Nuclear Data Sheets*, Vol. 112, No. 12, pp. 2887-2996, December 2011, https://doi.org/10.1016/j.nds.2011.11.002.

2. Wagner, J.C., "Computational Benchmark for Estimation of Reactivity Margin from Fission Products and Minor Actinides in PWR Burnup Credit " NUREG/CR-6747 U.S. Nuclear Regulatory Commission, Washington, DC, October 2001, Agencywide Documents Access and Management System (ADAMS) Accession No. ML013060035.

3. Hall, R., et al., "Extended-Enrichment Accident-Tolerant LWR Fuel Isotopic and Lattice Parameter Trends," ORNL/TM-2021/1961, Oak Ridge National Laboratory, Oak Ridge, TN, March 2021, ADAMS Accession No. ML21088A254.

4. Shaw, A.M. and Clarity, J.B., "Impacts of LEU+ and ATF on Fresh Fuel Storage Criticality Safety," ORNL/TM-2021/2330, Oak Ridge National Laboratory, Oak Ridge, TN, February 2022, https://doi.org/10.2172/1843694.

5. Westinghouse Electric Company LLC, "Peripheral Power Suppression Assembly," NF-FE-0050, Cranberry Township, PA, September 2015, https://www.westinghousenuclear.com/Portals/0/flysheets/NF-FE-0050%20PPSA.pdf.

6. Westinghouse Electric Company LLC, "Shielding Fuel Assembly (SFA) – Generation III," NFCM-0012, Cranberry Township, PA, December 2016, https://www.westinghousenuclear.com/Portals/0/flysheets/NFCM-0012_SFA.pdf.

7. U.S. Nuclear Regulatory Commission, "Standard Review Plan for Spent Fuel Dry Storage Systems and Facilities," NUREG-2215, Washington, DC, April 2020, ADAMS Accession No. ML20121A190.

8. Borowski, J., et al., "Standard Review Plan for Transportation Packages for Spent Fuel and Radioactive Material," NUREG-2216, U.S. Nuclear Regulatory Commission, Washington, DC, August 2020 ADAMS Accession No. ML20234A651.

9. U.S. Nuclear Regulatory Commission, "Standard Review Plan for Transportation Packages for Spent Fuel and Radioactive Material," NUREG-2216, Washington, DC, August 2020, ADAMS Accession No. ML20234A651.

10. Barsic, J.A., et al., "17x17 Next Generation Fuel (17x17 NGF) Reference Core Report," WCAP-16498-NP Westinghouse Electric Company LLC, Monroeville, PA, March 2008, ADAMS Accession No. ML081010603.

11. U.S. Department of Energy, "Characteristics of Spent Fuel, High-Level Waste, and Other Radioactive Wastes Which May Require Long-Term Isolation, Appendix 2A. Physical Descriptions of LWR Fuel Assemblies," DOE/RW—0184-Vol. 3," Washington, DC, December 1987, https://www.osti.gov/servlets/purl/5258301.

12. Radulescu, G., Grogan, B.R., and Banerjee, K., "Fuel Assembly Reference Information for SNF Radiation Source Term Calculations," ORNL/SPR-2021/2093, Oak Ridge National Laboratory, Oak Ridge, TN, September 2021, https://doi.org/10.2172/1819561.

13. Bradfute, J.L., et al., "Westinghouse Fuel Designs and Performance Overview," *2012 Water Reactor Fuel Performance Meeting*, Manchester, UK, September 2-6, 2012, https://www.studsvik.com/SharepointFiles/2012%20TopFuel%20Operation%20and%20Experience.pdf.

14. Lam, H., et al., "Westinghouse Advanced Fuel Management Strategies Leveraging High Enrichment and High Burnup Fuel to Optimize PWR Economics," *PHYSOR 2022*, Pittsburgh, PA, May 15-20, 2022.

15. Franceschini, F., et al., "Reactor Physics Benchmark of Westinghouse PWR Core Design Suite for High Burnup/High Enrichment Fuel - Part I: Pin and Lattice," *PHYSOR 2022*, Pittsburgh, PA, May 15-20, 2022.

16. Mangham, G., et al., "Reactor Physics Benchmark of Westinghouse PWR Core Design Suite for High Burnup/High Enrichment Fuel - Part II: 2D and 3D Core Simulations," *PHYSOR 2022*, Pittsburgh, PA, May 15-20, 2022.

17. Hu, J., Mertyurek, U., and Wieselquist, W.A., "Assessment of Core Physics Characteristics of Extended Enrichment and Higher Burnup LWR Fuels using the Polaris/PARCS Two-Step Approach, Vol. I: PWR Fuel," ORNL/TM-2022/1831, Oak Ridge National Laboratory, Oak Ridge, TN, June 2022, https://doi.org/10.2172/1905421.

18. Hall, R., et al., "Isotopic and Fuel Lattice Parameter Trends in Extended Enrichment and Higher Burnup LWR Fuel, Vol. I: PWR Fuel," ORNL/TM-2020/1833, Oak Ridge National Laboratory, Oak Ridge, TN, February 2021, https://doi.org/10.2172/1779134.

19. Capps, N., et al., "Full core LOCA safety analysis for a PWR containing high burnup fuel," *Nuclear Engineering and Design*, Vol. 379, August 2021, https://doi.org/10.1016/j.nucengdes.2021.111194.

20. Zhang, H., et al., "Fuel Rod Burst Potential Evaluation under LOCA Conditions for an Existing Plant with Extended Burnup Exceeding the Current Limit by 20%," INL/EXT-19-55888, Idaho National Laboratory, Idaho Falls, ID, September 2019, https://lwrs.inl.gov/RiskInformed%20Safety%20Margin%20Characterization/Fuel_Rod_Burst_Potential_Evaluation_under_LOCA_Conditions_for_an_Existing_Plant.pdf.

21. LaSalle, Units 1 and 2, Updated Final Safety Analysis Report (UFSAR), Revision 17, Chapter 4.0 - Reactor., April 2008, ADAMS Accession No. ML081330056.

22. Cumberland, R., et al., "Isotopic and Fuel Lattice Parameter Trends in Extended Enrichment and Higher Burnup LWR Fuel, Volume II: BWR Fuel," ORNL/TM-2020/1835, Oak Ridge National Laboratory, Oak Ridge, TN, March 2021, https://doi.org/10.2172/1782042.

23. Bae, J.W., Mertyurek, U., and Asgari, M., "Light Water Reactor LEU+ Lattice Optimization," ORNL/TM-2021/2366, Oak Ridge National Laboratory, Oak Ridge, TN, September 2022, https://doi.org/10.2172/1885360.

24. Wagner, J.C. and Sanders, C.E., "Investigation of the Effect of Fixed Absorbers on the Reactivity of PWR Spent Nuclear Fuel for Burnup Credit," *Nuclear Technology*, Vol. 139, pp. 91-126, April 2017, https://doi.org/10.13182/NT02-A3307.

25. Wagner, J.C. and Parks, C.V., "Parametric Study of the Effect of Burnable Poison Rods for PWR Burnup Credit," NUREG/CR–6761, U.S. Nuclear Regulatory Commission, Washington, DC, March 2002, https://www.nrc.gov/reading-rm/doc-collections/nuregs/contract/cr6761/cr6761.pdf.

26. Sanders, C.E. and Wagner, J.C., "Study of the Effect of Integral Burnable Absorbers for PWR Burnup Credit " NUREG/CR-6760, Nuclear Regulatory Commission, Washington, DC, March 2002, ADAMS Accession No. ML020770436.

27. Westinghouse Electric Company LLC, "Integral Fuel Burnable Absorber (IFBA) Fuel Cycles and IFBA/Gad Hybrid Fuel Cycles," NFCM-0015, Rev. 1, Cranberry Township, PA, April 2018, https://www.westinghousenuclear.com/Portals/0/operating%20plant%20services/fuel/fuel%20products/NFCM-0015%20IFBA.pdf.

28. Westinghouse Electric Company LLC, "Wet Annular Burnable Absorber (WABA) Assembly," NFCM-0016, Cranberry Township, PA, May 2017, https://www.westinghousenuclear.com/Portals/0/operating%20plant%20services/fuel/fuel%20products/NFCM-0016%20WABA.pdf.

29. Evans, J.A., et al., "Burnable Absorbers in Nuclear Reactors – A Review," *Nuclear Engineering and Design*, Vol. 391, May 2022, https://doi.org/10.1016/j.nucengdes.2022.111726.

30. ASTM International, ASTM B811-13 (Reapproved 2022), "Standard Specification For Wrought Zirconium Alloy Seamless Tubes For Nuclear Reactor Fuel Cladding," West Conshohocken, PA.

31. Watts Bar, Unit 2 - Final Safety Analysis Report (FSAR), Amendment 93, Section 4.0, Reactor, April 2009, ADAMS Accession No. ML091400651.

32. Westinghouse Electric Company LLC, "Optimized ZIRLO™ High-performance Fuel Cladding Material," NF-FE-0046, Cranberry Township, PA, September 2016, https://www.westinghousenuclear.com/Portals/0/operating%20plant%20services/fuel/fuel%20products/NF-FE-0046%20Optimized%20ZIRLO%20HP%20Fuel%20Clad%20Mtl.pdf.

33. Shah, H.H., "Optimized ZIRLO™," WCAP-14342-A & CENPD-404-NP-A, Addendum 1-A, Westinghouse Electric Company LLC, Pittsburgh, PA, July 2006, ADAMS Accession No. ML062080569.

34. Motta, A.T., Couet, A., and Comstock, R.J., "Corrosion of Zirconium Alloys Used for Nuclear Fuel Cladding," *Annual Review of Materials Research*, Vol. 45, pp. 311-343, April 2015, https://doi.org/10.1146/annurev-matsci-070214-020951.

35. Godfrey, A.T., "VERA Core Physics Benchmark Progression Problem Specifications," CASL-U-2012-0131-004, Revision 4, Oak Ridge National Laboratory, Oak Ridge, TN, August 2014, https://casl.gov/archive/.

36. Brown, J.A. and Lam, H.Q., "Hybrid IFBA Gad Assembly Designs for Long PWR Cycles," *2017 Water Reactor Fuel Performance Meeting*, Ramada Plaza Jeju, Jeju Island, Korea, September 10 -14, 2017.

37. Mays, C.W., "Summary Report of Commercial Reactor Criticality Data for McGuire Unit 1," B00000000-01717-5705-00063, Rev. 0, Civilian Radioactive Waste Management System, Las Vegas, NV, August 1997, ADAMS Accession No. ML033520310.

38. Lancaster, D., et al., "Nuclear Criticality Safety Engineering Training Module 16, Burnup Credit for Criticality Safety Analysis of Commercial Spent Nuclear Fuel," https://ncsp.llnl.gov/sites/ncsp/files/2021-05/Burnup_Credit_Module_Final_110309.pdf.

39. Scaglione, J.M., et al., "An Approach for Validating Actinide and Fission Product Burnup Credit Criticality Safety Analyses—Criticality (k_{eff}) Predictions," NUREG/CR-7109, U.S. Nuclear Regulatory Commission, Washington, DC, April 2012, ADAMS Accession No. ML12116A128.

40. The International Association for the Properties of Water and Steam, Revised Release on the IAPWS Industrial Formulation 1997 for the Thermodynamic Properties of Water and Steam, IAPWS R7-97(2012), Lucerne, Switzerland, August 2007.

41. Radulescu, G. and Stefanovic, P., "A Study on the Characteristics of the Radiation Source Terms of Spent Fuel and Various Non-Fuel Hardware for Shielding Applications," ORNL/SPR-2021/2373, Oak Ridge National Laboratory, Oak Ridge, TN May 2022, https://doi.org/10.2172/1867782.

42. Sanders, C.E. and Wagner, J.C., "Parametric Study of the Effect of Control Rods for PWR Burnup Credit," NUREG/CR-6759, U.S. Nuclear Regulatory Commission, Washington, DC, February 2002, ADAMS Accession No. ML020810111.

43. Code of Federal Regulations, *Title 10*, *Energy*, Part 71.4 "Packaging and Transportation of Radioactive Material".

44. Svensk Kärnbränslehantering AB, "Spent nuclear fuel for disposal in the KBS-3 repository," Technical Report TR-10-13, Stockholm, Sweden, December 2010, https://skb.se/upload/publications/pdf/TR-10-13.pdf.

45. Larsen, N.H., "Core Design and Operating Data for Cycles 1 and 2 of Peach Bottom 2 " EPRI NP-563, Electric Power Research Institute, Palo Alto, CA, June 1978.

46. Wieselquist, W.A. and Lefebvre, R.A., eds., "SCALE 6.3.1 User Manual," ORNL/TM-SCALE-6.3.1, Oak Ridge National Laboratory, Oak Ridge, TN, February 2023, https://info.ornl.gov/sites/publications/Files/Pub191420.pdf.

47. Gauld, I.C., et al., "Isotopic Depletion and Decay Methods and Analysis Capabilities in SCALE," *Nuclear Technology*, Vol. 174, No. 2, pp. 169-195, May 2011, https://doi.org/10.13182/NT11-3.

4 . Skutnik, S.E., Williams, M.L., and LeFebvre, R.A., "ORIGAMI: A New Interface for Fuel Assembly Characterization with ORIGEN," *2015 International High-Level Radioactive Waste Management Conference (IHLRWM 2015)*, Charleston, SC, April 12-16, 2015, https://www.researchgate.net/publication/279060360_ORIGAMI_A_New_Interface_for_Fuel_Assembly_Characterization_with_ORIGEN.

4 . Leal, L.C., et al., "ARP: Automatic Rapid Process for the Generation of Problem-Dependent SAS2H/ORIGEN-S Cross-Section Libraries," ORNL/TM-13584, Oak Ridge National Laboratory, Oak Ridge, TN April 1998, https://doi.org/10.2172/296737.

50. Peplow, D.E., "Monte Carlo Shielding Analysis Capabilities with MAVRIC," *Nuclear Technology*, Vol. 174, No. 2, pp. 289-313, May 2011, https://doi.org/10.13182/NT174-289.

51. Wagner, J.C., et al., "Review of Hybrid (Deterministic/Monte Carlo) Radiation Transport Methods, Codes, and Applications at Oak Ridge National Laboratory," *Progress in Nuclear Science and Technology*, Vol. 2, pp. 808-814, October 2011, http://dx.doi.org/10.15669/pnst.2.808.

52. Wagner, J.C., Peplow, D.E., and Mosher, S.W., "FW-CADIS Method for Global and Regional Variance Reduction of Monte Carlo Radiation Transport Calculations," *Nuclear Science and Engineering*, Vol. 176, No. 1, pp. 37–57, January 2014, http://dx.doi.org/10.13182/NSE12-33.

53. Evans, T.M., et al., "Denovo: A New Three-Dimensional Parallel Discrete Ordinates Code in SCALE," *Nuclear Technology*, Vol. 171, No. 2, pp. 171-200, August 2010, https://doi.org/10.13182/NT171-171.

54. Parks, C.V., DeHart, M.D., and Wagner, J.C., "Review and Prioritization of Technical Issues Related to Burnup Credit for LWR Fuel " NUREG/CR-6665, U.S. Nuclear Regulatory Commission, Washington, DC, February 2000, ADAMS Accession No. ML003688150.

55. Wagner, J.C., DeHart, M.D., and Parks, C.V., "Recommendations for Addressing Axial Burnup in PWR Burnup Credit Analyses," NUREG/CR-6801, U.S. Nuclear Regulatory Commission, Washington, DC, March 2003, ADAMS Accession No. ML031110292.

56. Greene, T.M. and Marshall, W.J., "SCALE 6.2.4 Validation: Nuclear Criticality Safety," ORNL/TM-2020/1500/v2, Oak Ridge National Laboratory, Oak Ridge, TN, November 2022, https://doi.org/10.2172/1902815.

57. Ilas, G., et al., "SCALE 6.2.4 Validation: Reactor Physics," ORNL/TM-2020/1500/v3, Oa Rid e National La oratory, Oa Rid e, TN, Nove er 2022, htt s://doi.or /10.2172/1 02 1 .

58. Celik, C., et al., “SCALE 6.2.4 Validation: Radiation Shielding,” ORNL/TM-2020/1500/v4, Oak Ridge National Laboratory, Oak Ridge, TN, November 2022, https://doi.org/10.2172/1902814.

59. Marshall, W.J. and Rearden, B.T., “The SCALE Verified, Archived Library of Inputs and Data–VALID,” *Proceedings of the ANS Nuclear Criticality Safety Division Topical Meeting (NCSD2013)*, Wilmington, NC, September 29 – October 4, 2013, 2013.

60. Gauld, I.C. and Ryman, J.C., “Nuclide Importance to Criticality Safety, Decay Heating, and Source Terms Related to Transport and Interim Storage of High-Burnup LWR Fuel,” NUREG/CR-6700, Oak Ridge National Laboratory, Oak Ridge, TN, January 2001, ADAMS Accession No. ML010330186.

61. Gauld, I.C. and Parks, C.V., “Review of Technical Issues Related to Predicting Isotopic Compositions and Source Terms for High-Burnup LWR Fuel,” NUREG/CR-6701 U.S. Nuclear Regulatory Commission, Washington, DC, January 2001, ADAMS Accession No. ML010230244.

62. Broadhead, B.L., “Recommendations for Shielding Evaluations for Transport and Storage Packages,” NUREG/CR-6802, U.S. Nuclear Regulatory Commission, Washington, DC, May 2003, ADAMS Accession No. ML031330514.

63. Bowman, S.M., Gauld, I.C., and Wagner, J.C., “Recommendations on Fuel Parameters for Standard Technical Specifications for Spent Fuel Storage Casks,” NUREG/CR-6716, U.S. Nuclear Regulatory Commission, Washington, DC, March 2001, ADAMS Accession No. ML010820352.

64. Kopecky, J., “Atlas of Neutron Capture Cross Sections,” INDC(NDS)-362, International Atomic Energy Agency, Vienna, April 1997.

65. Radulescu, G., et al., “An Approach for Validating Actinide and Fission Product Burnup Credit Criticality Safety Analyses—Isotopic Composition Predictions,” NUREG/CR-7108 U.S. Nuclear Regulatory Commission, Washington, DC, April 2012, ADAMS Accession No. ML12116A124.

66. Wagner, J.C. and Parks, C.V., “Recommendations on the Credit for Cooling Time in PWR Burnup Credit Analyses,” NUREG/CR-6781 U.S. Nuclear Regulatory Commission, Washington, DC, January 2003 ADAMS Accession No. ML030290585.

67. DeHart, M.D., “Sensitivity and Parametric Evaluations of Significant Aspects of Burnup Credit for PWR Spent Fuel Packages,” ORNL/TM-12973, Oak Ridge National Laboratory, Oak Ridge, TN, May 1996, https://doi.org/10.2172/814237.

68. Wagner, J.C., “Impact of Soluble Boron Modeling for PWR Burnup Credit Criticality Safety Analyses,” *American Nuclear Society: International ANS/ENS (European Nuclear Society) 2003 Winter Meeting with cooperation with Nuclear Energy Institute on “Nuclear*

69. *Technology: Achieving Global Economic Growth While Safeguarding the Environment”, New Orleans, Louisiana, November 16–20, 2003.*

APPENDIX A
SIMPLIFICATIONS TO DOSE RATE CALCULATIONS FOR SHIELDING EVALUATIONS

A parametric study was performed to determine the effects of fuel depletion parameter variations on the radiation source terms of PWR and BWR fuel assemblies with extended enrichment and high burnup, affecting dose rates on a transportation package and spent fuel cask. Two simplifications were used in the shielding evaluations:

1. Representative geometrical models
2. On-the-fly dose rate calculation approach

This appendix describes these two simplifications. Due to the large number of parametric studies outlined for the shielding analyses, a simplified geometrical modeling approach was used as an alternative to using high-fidelity 3D shielding models with fuel rod–level detail. This approach is consistent with the analysis approach used in the parametric studies published in NUREG/CR-6716 [A-1]. Those studies essentially used 1D models of representative dry storage casks and transportation packages, where spent fuel was surrounded by gamma and neutron shielding materials. Simplified geometrical models such as these are advantageous for parametric studies because consideration of axial effects (i.e., an axial burnup profile) is not necessary when evaluating fuel and irradiation parameter changes on dose rate trends at a specific location outside of the transportation package or dry storage cask. Additionally, if a uniform axial burnup is assumed for purposes of a parametric study, overpack features (e.g., air inlets, trunnions) could affect external dose rates at the fuel midplane outside of the transportation package or dry storage cask and lead to incorrect conclusions. Therefore, it was appropriate to use a uniform axial burnup and exclude overpack features in the simplified model for the current analysis.

Compared to currently authorized SNF transportation/storage cask systems, LWR fuel with extended enrichment and high burnup may require additional shielding and/or longer cooling times to meet shielding regulatory requirements. However, the shielding models used herein are based on existing SNF transportation/dry storage cask designs because this parametric study evaluates relative dose rate effects produced by variations in fuel assembly characteristics (i.e., initial enrichment, average burnup, and cooling time) and fuel depletion parameters (e.g., specific power and moderator density) to identify the trends of dose rate variation with these parameters. The shielding models are based on the Holtec International Storage Module (HI-STORM) 100 dry storage cask [A-2] and Holtec International Storage, Transport and Repository (HI-STAR) 100 transportation package designs [A-3]. The PWR shielding models describe 32 homogeneous fuel assemblies based on the multipurpose canister (MPC)-32 basket assembly design, and the BWR shielding models describe 68 homogeneous fuel assemblies based on the MPC-68 basket assembly design. The shielding models are simplified 3D models based on detailed 3D models developed for the Used Nuclear Fuel Storage, Transportation & Disposal Analysis Resource and Data System [A-4]. The simplified model describes a homogenized fuel region within the canister cavity that is surrounded by shielding material. The dose rate location is specified at the axial fuel midplane on the surface of the transportation package or dry storage cask.

To further simplify shielding analyses and enable large numbers of calculations, an on-the-fly dose rate calculation approach [A-5] was used. This approach requires initial shielding

calculations for determining dose rate contributions of a single gamma or neutron associated with an energy group. These dose rates are then multiplied by the source strength (e.g., calculated using Polaris) to get the actual dose rate.

A.1 Simplified Transportation Package and Dry Storage Cask Models

The transportation package shielding model is based on the HI-STAR 100 transportation package design. The PWR shielding models describe 32 identical fuel assemblies based on the MPC-32 basket assembly design, and the BWR shielding models describe 68 identical fuel assemblies based on the MPC-68 basket assembly design. The detailed geometrical model for HI-STAR 100 containing PWR fuel is illustrated in Figure A-1, and its simplified shielding model is illustrated in Figure A-2. The detailed geometrical model includes the detailed transportation package model and materials. The fuel assembly is axially subdivided into fuel and bottom and top assembly hardware regions. The fuel region is represented as a homogeneous mixture within the outer dimensions of the fuel assembly that contains fuel and the hardware regions, which are represented as homogeneous mixtures within their respective outer dimensions. This fuel assembly model is typically used in licensing applications. Only the fuel region of the fuel assembly is included in the simplified model. In the simplified model, the fuel and fuel basket materials are homogenized within the canister cavity and surrounded by the stainless steel canister, carbon steel gamma shield, Holtite^{TM} neutron shield (hydrogen-rich polymer impregnated with uniformly dispersed boron carbide particles), and carbon steel overpack outer shell, as shown in Figure A-2. An annular region surrounding the outer surface of the cask at the fuel midplane is used for dose rate calculations. The tally region is segmented into 24 angular regions in the detailed model. Section A.1.1 demonstrates that the detailed and simplified models predict similar trends for the external dose rate.

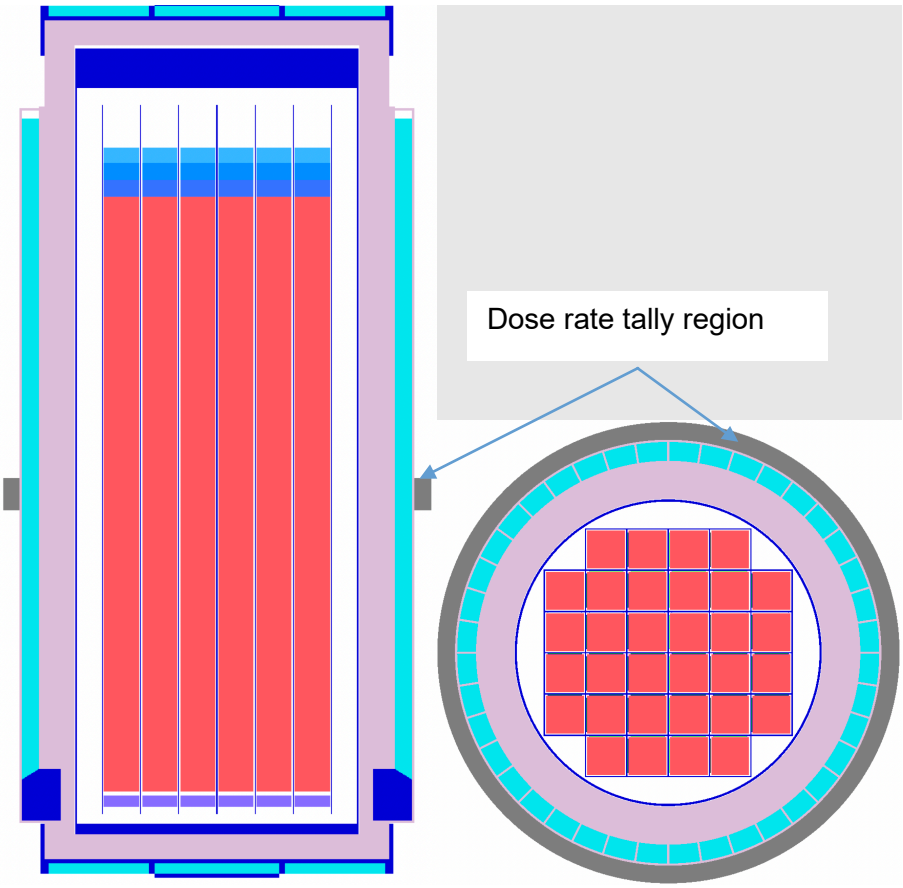

Figure A-1 Detailed Transportation Package Model with Simplified Fuel Assembly Model for HI-STAR 100 with MPC-32 for PWRs ([Left] Vertical Cross-Sectional View and [Right] Horizontal Cross-Sectional View)

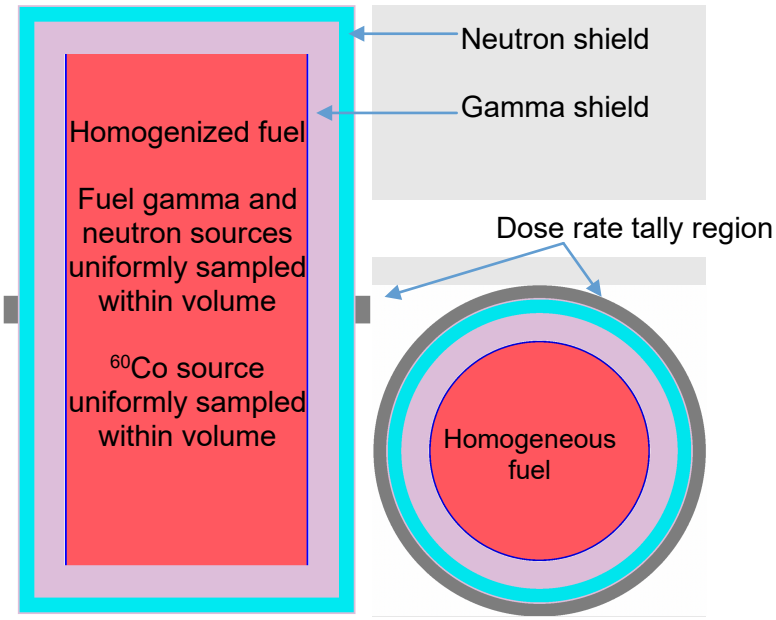

Figure A-2 Simplified Transportation Package Model for HI-STAR 100 with MPC-32 for PWRs ([Left] Vertical Cross-Sectional View and [Right] Horizontal Cross-Sectional View)

The dry storage cask shielding model is based on the HI-STORM 100 dry storage cask design. The detailed and simplified models are shown in Figure A-3 and Figure A-4, respectively. In the simplified model, the fuel and fuel basket materials are homogenized within the canister cavity and surrounded by the stainless-steel canister, concrete neutron and gamma shield, and carbon steel overpack outer shell, as shown in Figure A-4. As in the transportation cask models, an annular region surrounding the outer surface of the cask at the fuel midplane is used for dose rate calculations. The tally region is segmented into 24 angular regions in the detailed model. Similar to the transportation cask, Section A.1.1 demonstrates that the detailed and simplified models predict similar trends for the external dose rate.

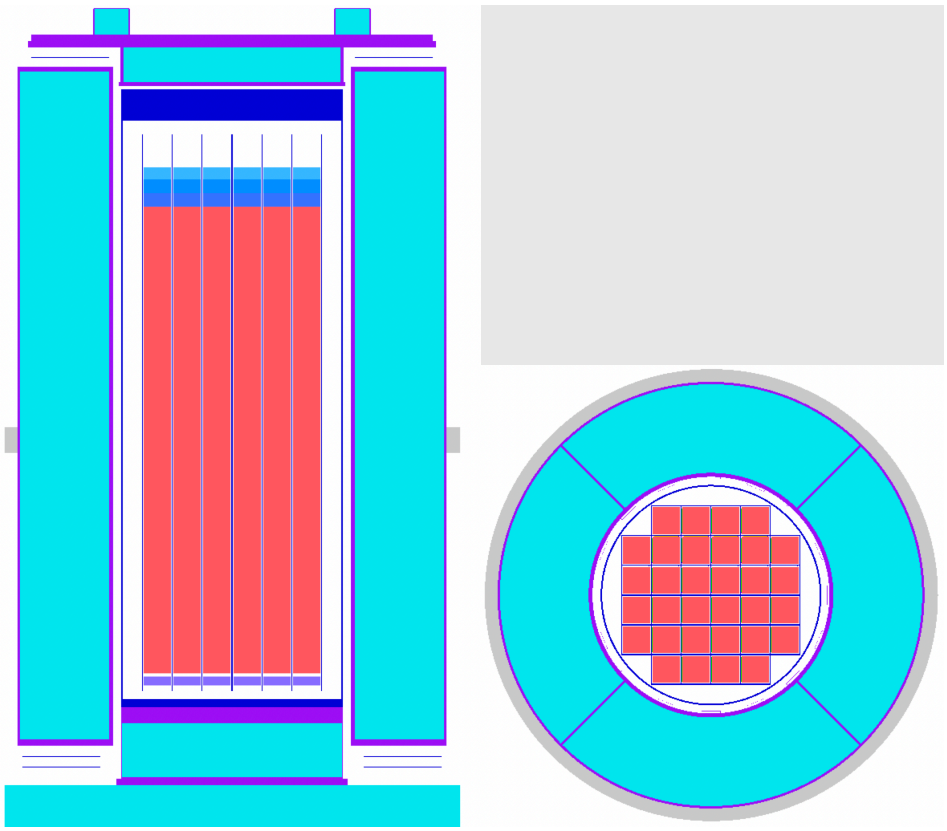

Figure A-3 Detailed Dry Storage Cask Model with Simplified Fuel Assembly Model for HI-STORM 100 with MPC-32 for PWRs ([Left] Vertical Cross-Sectional View and [Right] Horizontal Cross-Sectional View)

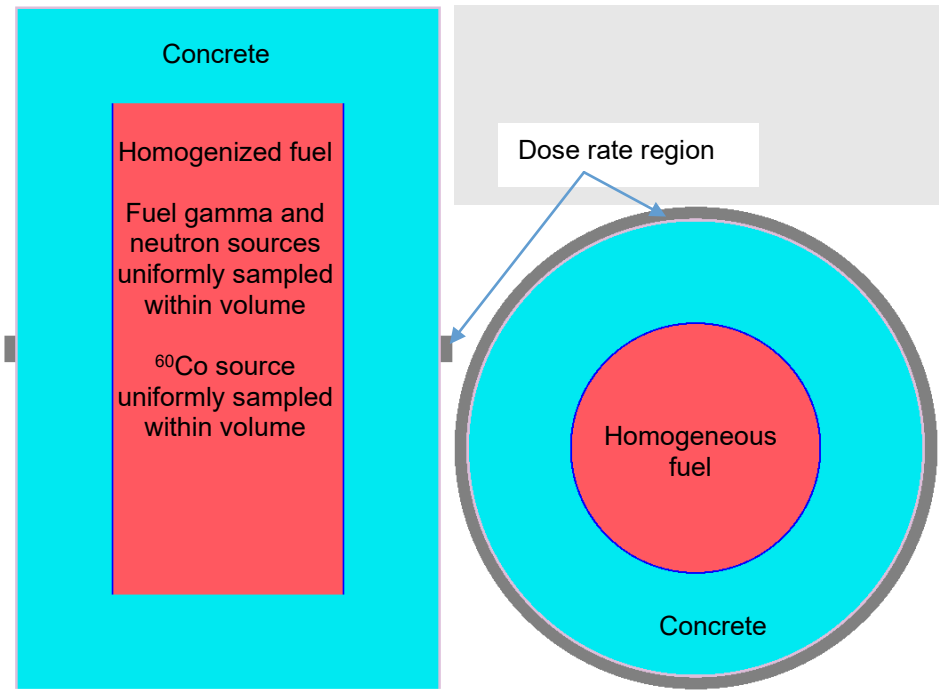

Figure A-4 Simplified Dry Storage Cask Model for HI-STORM 100 with MPC-32 for PWRs ([Left] Vertical Cross-Sectional View and [Right] Horizontal Cross-Sectional View)

A.1.1 Detailed and Simplified Model Dose Rate Comparisons

The detailed and simplified models presented in Section A.1 were analyzed in terms of their effect on dose rate trends. This section demonstrates that the detailed and simplified geometrical models predict the same trend for assembly burnup changes for the external dose rate. This conclusion can be generalized for fuel and other irradiation parameter changes. The dose rate was calculated within an annular region surrounding the outer surface of the cask at the fuel midplane, as shown in Figure A-1 through Figure A-4. However, because the radial dose rate varies as a function of azimuthal location for the detailed model, the annular region was subdivided into 24 angular segments, and the maximum dose rate value among these segments was reported. For the simplified model, the dose rate was averaged within the entire annular region because this model does not exhibit any dose rate azimuthal variation. The same axial burnup profile was used with the detailed and simplified models. To show that the two different models predict the same trend of dose rate with the variation of a fuel depletion parameter, external dose rates were calculated for fuel assemblies with assembly average burnup values of 60 and 75 GWd/MTU. The ratios of the dose rate values calculated with the detailed and simplified models for the gamma and neutron sources originating from the fuel region are presented in Table A-1 and in Table A-2. The American National Standards Institute/American Nuclear Society-6.1.1-1977 [A-6] neutron and gamma flux-to-dose-rate conversion factors were applied to the particle flux estimated by the Monte Carlo method to obtain the dose rates. Figure A-5 shows dose rates and relative errors for the detailed and simplified models of the transportation package for a burnup of 75 GWd/MTU.

Table A-1 Results of the Detailed and Simplified Model Dose Rate Comparison Study for the HI-STAR 100 Transportation Package with MPC-32 for PWRs

Particle type	Assembly average burnup (GWd/MTU)	Model	Dose rate (mrem/h)	Relative error	Dose rate ratio ±1σ, 75-to-60 GWd/MTU
Gamma	75	Detailed[a]	2.463×10^2	0.0018	1.215 ± 0.003
Gamma	60	Detailed[a]	2.027×10^2	0.0020	
Gamma	75	Simplified[b]	3.001×10^2	0.0005	1.223 ± 0.001
Gamma	60	Simplified[b]	2.452×10^2	0.0005	
Neutron	75	Detailed[a]	1.250×10^2	0.0552	2.153 ± 0.168
Neutron	60	Detailed[a]	5.806×10^1	0.0551	
Neutron	75	Simplified[b]	1.2373×10^2	0.0504	2.147 ± 0.155
Neutron	60	Simplified[b]	5.763×10^1	0.0516	

[a] See Figure A-1
[b] See Figure A-2

Table A-2 Results of the Detailed and Simplified Model Dose Rate Comparison Study for the HI-STORM 100 Dry Storage Cask with MPC-32 for PWRs

Particle type	Assembly average burnup (GWd/MTU)	Model	Dose rate (mrem/h)	Relative error	Dose rate ratio ±1σ, 75-to-60 GWd/MTU
Gamma	75	Detailed[a]	1.418×10^2	0.0044	1.218 ± 0.008
Gamma	60	Detailed[a]	1.164×10^2	0.0047	
Gamma	75	Simplified[b]	6.368×10^2	0.0005	1.230 ± 0.001
Gamma	60	Simplified[b]	5.177×10^2	0.0004	
Neutron	75	Detailed[a]	2.486×10^1	0.0868	2.245 ± 0.251
Neutron	60	Detailed[a]	1.1071×10^1	0.0702	
Neutron	75	Simplified[b]	3.965×10^1	0.0225	2.225 ± 0.061
Neutron	60	Simplified[b]	1.782×10^1	0.0154	

[a] See Figure A-3
[b] See Figure A-4

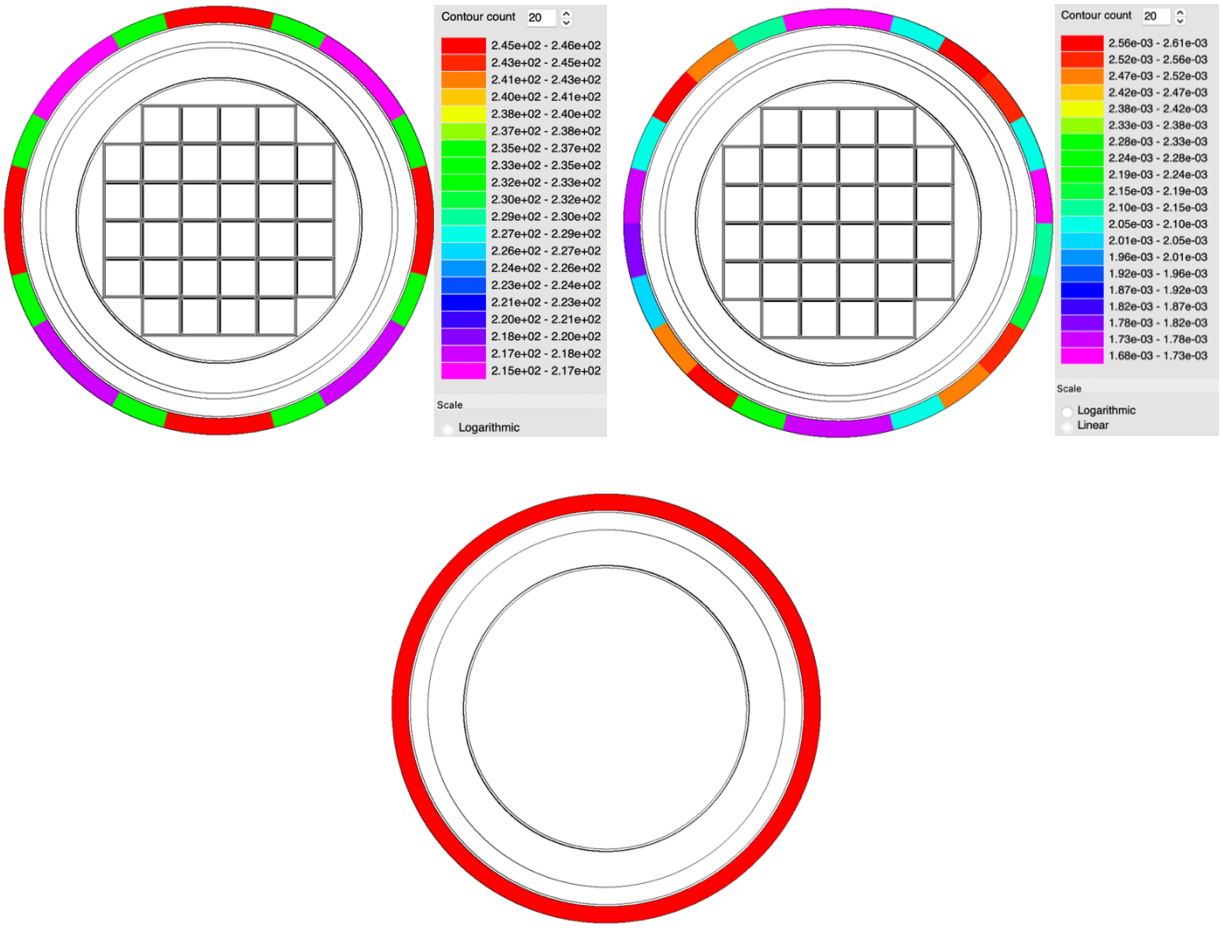

Figure A-5 Illustration of Gamma Dose Rates (mrem/h) and Statistical Uncertainties for the Transportation Package for an Assembly Average Burnup of 75 GWd/MTU

A.2 Response Functions for On-The-Fly Dose Rate Calculations

To calculate dose rates efficiently for the shielding evaluations, an on-the-fly approach was used. This approach involved calculating dose rates by the following steps:

1. Generating response functions in terms of dose rate on the transportation package or dry storage cask produced by a single-source photon or a single-source neutron within an energy group using MAVRIC. A uniform axial burnup profile and the SCALE 27n19g energy groups were used to generate the response functions.
2. Multiplying the response dose rate values for each energy group in Step 1 by the number of fuel assemblies in the cask (32 for PWR or 68 for BWR).
3. Multiplying the energy-group dependent values in Step 2 by the energy-group dependent assembly source intensities calculated using a fuel depletion computer code. The neutron source term includes neutrons from spontaneous fission and (α,n) reactions generated with the fuel depletion code; it does not include neutrons from subcritical multiplication (i.e., neutrons that are generated from fission events).
4. Summing the partial energy-dependent products in Step 3.

The gamma and neutron dose rate response functions for the simplified transportation package model containing PWR fuel are provided in Table A-3 and Table A-4, respectively. The dose rate from a ^{60}Co decay source, normalized to one gamma source, is 1.409×10^{-14} mrem/h with an associated relative error of 0.0003. The gamma and neutron dose rate response functions for the simplified dry storage cask model containing PWR fuel are provided in Table A-5 and Table A-6, respectively. The dose rate from a ^{60}Co decay source, normalized to one source photon, is 2.8214×10^{-14} mrem/h with an associated relative error of 0.0005. Slightly higher response function values were calculated for the BWR fuel, which are provided in Table A-7 and Table A-8 for the simplified transportation package model and Table A-9 and Table A-10 for the simplified storage cask model. Some of the neutron response functions in the lower energy range were negligible and were included as zero values in Table A-4 and Table A-8. The dose rate from a ^{60}Co decay source, normalized to one source photon, is 1.787×10^{-14} mrem/h (relative error of 0.0037) for the simplified BWR transportation model and 3.536×10^{-14} mrem/h (relative error of 0.0005) for the simplified BWR storage cask model.

Examples of total gamma and neutron dose rate calculations for the simplified transportation package with PWR fuel (MPC-32) are shown in Table A-11 and Table A-12, respectively. The fuel assembly is WEC 17 × 17, having an assembly average burnup of 75 GWd/MTU and a cooling time of 5 yr. The radiation source was generated with the SCALE 27n19g group structure.

Photons emitted with very low energies have no contributions to the total external dose rate because these photons are completely absorbed within fuel materials. The gamma energy range recommended in NUREG-2216 [A-7] for shielding evaluation of SNF transportation packages is 0.4–3 MeV. The gamma dose rate values in Table A-11 show that the photon energy range of 3–4 MeV has a small but significant contribution to the external dose rate. This contribution is slightly greater than that of the photons within the energy range of 0.4–0.6 MeV. Therefore, the 0.4–4 MeV gamma source energy range is recommended to be considered for the purpose of calculating external gamma dose rates produced by fuel with extended enrichment and high burnup. The gamma emission rates in the higher energy range, above 4 MeV at all cooling times and at energies above 3.5 MeV after 10 yr, come primarily from the actinides (e.g., ^{244}Cm). The low intensity of the high-energy photons from the heavy-metal isotopes may contribute a dose rate fraction comparable to that of activation and fission products for long cooling times and extremely thick shields [A-8].

Table A-3 PWR Fuel, Simplified Transportation Package Model—Primary Gamma Dose Rates Produced by a Single-Source Photon as a Function of Gamma Energy Bin

27n19g library gamma group number	Upper gamma energy bound (MeV)	Lower gamma energy bound (MeV)	Dose rate[a] (mrem/h)	Relative error
1	2.00×10^{1}	1.00×10^{1}	2.9471×10^{-12}	0.0004
2	1.00×10^{1}	8.00×10^{0}	3.3610×10^{-12}	0.0003
3	8.00×10^{0}	6.50×10^{0}	3.1312×10^{-12}	0.0003
4	6.50×10^{0}	5.00×10^{0}	2.5813×10^{-12}	0.0003
5	5.00×10^{0}	4.00×10^{0}	1.8209×10^{-12}	0.0003
6	4.00×10^{0}	3.00×10^{0}	1.0660×10^{-12}	0.0004
7	3.00×10^{0}	2.50×10^{0}	5.2958×10^{-13}	0.0004
8	2.50×10^{0}	2.00×10^{0}	2.5754×10^{-13}	0.0004
9	2.00×10^{0}	1.66×10^{0}	1.0550×10^{-13}	0.0004
10	1.66×10^{0}	1.33×10^{0}	3.8596×10^{-14}	0.0005
11	1.33×10^{0}	1.00×10^{0}	9.3364×10^{-15}	0.0008
12	1.00×10^{0}	8.00×10^{-1}	1.6096×10^{-15}	0.0006
13	8.00×10^{-1}	6.00×10^{-1}	2.6612×10^{-16}	0.0007
14	6.00×10^{-1}	4.00×10^{-1}	1.8417×10^{-17}	0.0011
15	4.00×10^{-1}	3.00×10^{-1}	3.3395×10^{-19}	0.0021
16	3.00×10^{-1}	2.00×10^{-1}	4.4212×10^{-21}	0.0053
17	2.00×10^{-1}	1.00×10^{-1}	4.5126×10^{-25}	0.0395
18	1.00×10^{-1}	4.50×10^{-2}	0.0	—
19	4.50×10^{-2}	1.00×10^{-2}	0.0	—

[a] Source normalization = one gamma per assembly.

Table A-4 PWR Fuel, Simplified Transportation Package Model—Neutron Dose Rate Produced by a Single-Source Neutron as a Function of Neutron Energy Bin

27n19g library neutron group number	Upper neutron energy bound (MeV)	Lower neutron energy bound (MeV)	Dose rate[a] (mrem/h)	Relative error
1	2.00×10^{1}	6.38×10^{0}	2.9048×10^{-9}	0.0003
2	6.38×10^{0}	3.01×10^{0}	1.1243×10^{-9}	0.0004
3	3.01×10^{0}	1.83×10^{0}	8.7847×10^{-10}	0.0004
4	1.83×10^{0}	1.42×10^{0}	6.2305×10^{-10}	0.0004
5	1.42×10^{0}	9.07×10^{-1}	5.7400×10^{-10}	0.0005
6	9.07×10^{-1}	4.08×10^{-1}	2.7085×10^{-10}	0.0008
7	4.08×10^{-1}	1.11×10^{-1}	3.5133×10^{-11}	0.0011
8	1.11×10^{-1}	1.50×10^{-2}	5.6784×10^{-12}	0.0019
9	1.50×10^{-2}	3.04×10^{-3}	2.3225×10^{-13}	0.0023
10	3.04×10^{-3}	5.83×10^{-4}	3.3461×10^{-14}	0.0083
11	5.83×10^{-4}	1.01×10^{-4}	3.2345×10^{-15}	0.0076
12	1.01×10^{-4}	2.90×10^{-5}	$3.2475E \times 10^{-16}$	0.0194
13	2.90×10^{-5}	1.07×10^{-5}	4.1270×10^{-17}	0.0620
14	1.07×10^{-5}	3.06×10^{-6}	0.0	—
15	3.06×10^{-6}	1.86×10^{-6}	0.0	—
16	1.86×10^{-6}	1.30×10^{-6}	0.0	—
17	1.30×10^{-6}	1.13×10^{-6}	0.0	—
18	1.13×10^{-6}	1.00×10^{-6}	0.0	—
19	1.00×10^{-6}	8.00×10^{-7}	0.0	—
20	8.00×10^{-7}	4.14×10^{-7}	0.0	—
21	4.14×10^{-7}	3.25×10^{-7}	0.0	—
22	3.25×10^{-7}	2.25×10^{-7}	0.0	—
23	2.25×10^{-7}	1.00×10^{-7}	0.0	—
24	1.00×10^{-7}	5.00×10^{-8}	0.0	—
25	5.00×10^{-8}	3.00×10^{-8}	0.0	—
26	3.00×10^{-8}	1.00×10^{-8}	0.0	—
27	1.00×10^{-8}	1.00×10^{-11}	0.0	—

[a]Source normalization = one neutron per assembly

Table A-5 PWR Fuel, Simplified Storage Cask Model—Primary Gamma Dose Rate Produced by a Single Source Photon as a Function of Photon Energy Bin

27n19g library gamma group number	Upper energy bound (MeV)	Lower energy bound (MeV)	Dose rate[a] (mrem/h)	Relative error
1	2.00×10^{1}	1.00×10^{1}	1.9768×10^{-11}	0.0004
2	1.00×10^{1}	8.00×10^{0}	1.4001×10^{-11}	0.0004
3	8.00×10^{0}	6.50×10^{0}	1.0780×10^{-11}	0.0004
4	6.50×10^{0}	5.00×10^{0}	7.4032×10^{-12}	0.0004
5	5.00×10^{0}	4.00×10^{0}	4.4163×10^{-12}	0.0004
6	4.00×10^{0}	3.00×10^{0}	2.2653×10^{-12}	0.0004
7	3.00×10^{0}	2.50×10^{0}	1.0207×10^{-12}	0.0004
8	2.50×10^{0}	2.00×10^{0}	4.7686×10^{-13}	0.0004
9	2.00×10^{0}	1.66×10^{0}	1.9337×10^{-13}	0.0004
10	1.66×10^{0}	1.33×10^{0}	7.2897×10^{-14}	0.0004
11	1.33×10^{0}	1.00×10^{0}	1.9157×10^{-14}	0.0001
12	1.00×10^{0}	8.00×10^{-1}	3.8242×10^{-15}	0.0005
13	8.00×10^{-1}	6.00×10^{-1}	7.4665×10^{-16}	0.0005
14	6.00×10^{-1}	4.00×10^{-1}	7.0092×10^{-17}	0.0008
15	4.00×10^{-1}	3.00×10^{-1}	2.6534×10^{-18}	0.0009
16	3.00×10^{-1}	2.00×10^{-1}	1.0466×10^{-19}	0.0011
17	2.00×10^{-1}	1.00×10^{-1}	3.5412×10^{-22}	0.0019
18	1.00×10^{-1}	4.50×10^{-2}	0.0	—
19	4.50×10^{-2}	1.00×10^{-2}	0.0	—

[a]Source normalization = one gamma per assembly.

Table A-6 PWR Fuel, Simplified Dry Storage Cask Model—Neutron Dose Rate Produced by a Single Source Neutron as a Function of Neutron Energy Bin

27n19g library neutron group number	Upper energy bound (MeV)	Lower energy bound (MeV)	Dose rate[a] (mrem/h)	Relative error
1	2.00×10^{1}	6.38×10^{0}	1.0898×10^{-9}	0.0006
2	6.38×10^{0}	3.01×10^{0}	6.0050×10^{-10}	0.0007
3	3.01×10^{0}	1.83×10^{0}	2.5438×10^{-10}	0.0009
4	1.83×10^{0}	1.42×10^{0}	3.0826×10^{-11}	0.0018
5	1.42×10^{0}	9.07×10^{-1}	1.5212×10^{-11}	0.0015
6	9.07×10^{-1}	4.08×10^{-1}	1.1028×10^{-11}	0.0014
7	4.08×10^{-1}	1.11×10^{-1}	6.9082×10^{-12}	0.0040
8	1.11×10^{-1}	1.50×10^{-2}	4.0429×10^{-12}	0.0016
9	1.50×10^{-2}	3.04×10^{-3}	1.9707×10^{-12}	0.0016
10	3.04×10^{-3}	5.83×10^{-4}	1.3427×10^{-12}	0.0016
11	5.83×10^{-4}	1.01×10^{-4}	7.2274×10^{-13}	0.0030
12	1.01×10^{-4}	2.90×10^{-5}	4.1771×10^{-13}	0.0019
13	2.90×10^{-5}	1.07×10^{-5}	2.8361×10^{-13}	0.0025
14	1.07×10^{-5}	3.06×10^{-6}	2.0704×10^{-13}	0.0018
15	3.06×10^{-6}	1.86×10^{-6}	2.2373×10^{-13}	0.0014
16	1.86×10^{-6}	1.30×10^{-6}	1.7244×10^{-13}	0.0040
17	1.30×10^{-6}	1.13×10^{-6}	1.2819×10^{-13}	0.0025
18	1.13×10^{-6}	1.00×10^{-6}	1.1899×10^{-13}	0.0015
19	1.00×10^{-6}	8.00×10^{-7}	1.1731×10^{-13}	0.0020
20	8.00×10^{-7}	4.14×10^{-7}	8.9623×10^{-14}	0.0020
21	4.14×10^{-7}	3.25×10^{-7}	5.6890×10^{-14}	0.0023
22	3.25×10^{-7}	2.25×10^{-7}	4.4019×10^{-14}	0.0017
23	2.25×10^{-7}	1.00×10^{-7}	3.1946×10^{-14}	0.0017
24	1.00×10^{-7}	5.00×10^{-8}	1.7180×10^{-14}	0.0015
25	5.00×10^{-8}	3.00×10^{-8}	9.8889×10^{-15}	0.0025
26	3.00×10^{-8}	1.00×10^{-8}	5.0284×10^{-15}	0.0019
27	1.00×10^{-8}	1.00×10^{-11}	1.2367×10^{-15}	0.0033

[a]Source normalization = one neutron per assembly

Table A-7 BWR Fuel, Simplified Transportation Package Model—Primary Gamma Dose Rate Produced by a Single-Source Photon as a Function of Gamma Energy Bin

27n19g library gamma group number	Upper energy bound (MeV)	Lower energy bound (MeV)	Dose rate[a] (mrem/h)	Relative error
1	2.00×10^{1}	1.00×10^{1}	3.717×10^{-12}	0.0004
2	1.00×10^{1}	8.00×10^{0}	4.2335×10^{-12}	0.0003
3	8.00×10^{0}	6.50×10^{0}	3.9444×10^{-12}	0.0003
4	6.50×10^{0}	5.00×10^{0}	3.2465×10^{-12}	0.0003
5	5.00×10^{0}	4.00×10^{0}	2.2882×10^{-12}	0.0003
6	4.00×10^{0}	3.00×10^{0}	1.3374×10^{-12}	0.0003
7	3.00×10^{0}	2.50×10^{0}	6.6376×10^{-13}	0.0004
8	2.50×10^{0}	2.00×10^{0}	3.2295×10^{-13}	0.0004
9	2.00×10^{0}	1.66×10^{0}	1.3219×10^{-13}	0.0004
10	1.66×10^{0}	1.33×10^{0}	4.8380×10^{-14}	0.0004
11	1.33×10^{0}	1.00×10^{0}	1.1725×10^{-14}	0.0005
12	1.00×10^{0}	8.00×10^{-1}	2.0236×10^{-15}	0.0006
13	8.00×10^{-1}	6.00×10^{-1}	3.3484×10^{-16}	0.0007
14	6.00×10^{-1}	4.00×10^{-1}	2.3284×10^{-17}	0.0011
15	4.00×10^{-1}	3.00×10^{-1}	4.2336×10^{-19}	0.0025
16	3.00×10^{-1}	2.00×10^{-1}	5.6064×10^{-21}	0.0050
17	2.00×10^{-1}	1.00×10^{-1}	5.7850×10^{-25}	0.0299
18	1.00×10^{-1}	4.50×10^{-2}	0.0	—
19	4.50×10^{-2}	1.00×10^{-2}	0.0	—

[a] Source normalization = one gamma per assembly.

Table A-8 BWR Fuel, Simplified Transportation Package Model—Neutron Dose Rate Produced by a Single-Source Neutron as a Function of Neutron Energy Bin

27n19g library neutron group number	Upper energy bound (MeV)	Lower energy bound (MeV)	Dose rate[a] (mrem/h)	Relative error
1	2.00×10^{1}	6.38×10^{0}	3.5517×10^{-9}	0.0003
2	6.38×10^{0}	3.01×10^{0}	1.3752×10^{-9}	0.0003
3	3.01×10^{0}	1.83×10^{0}	1.0746×10^{-9}	0.0003
4	1.83×10^{0}	1.42×10^{0}	7.6324×10^{-10}	0.0004
5	1.42×10^{0}	9.07×10^{-1}	7.0200×10^{-10}	0.0004
6	9.07×10^{-1}	4.08×10^{-1}	3.2879×10^{-10}	0.0004
7	4.08×10^{-1}	1.11×10^{-1}	4.2638×10^{-11}	0.0009
8	1.11×10^{-1}	1.50×10^{-2}	6.8487×10^{-12}	0.0018
9	1.50×10^{-2}	3.04×10^{-3}	2.8592×10^{-13}	0.0040
10	3.04×10^{-3}	5.83×10^{-4}	4.1166×10^{-14}	0.0043
11	5.83×10^{-4}	1.01×10^{-4}	3.9862×10^{-15}	0.0053
12	1.01×10^{-4}	2.90×10^{-5}	3.9682×10^{-16}	0.0032
13	2.90×10^{-5}	1.07×10^{-5}	4.5126×10^{-17}	0.0053
14	1.07×10^{-5}	3.06×10^{-6}	0.0	—
15	3.06×10^{-6}	1.86×10^{-6}	0.0	—
16	1.86×10^{-6}	1.30×10^{-6}	0.0	—
17	1.30×10^{-6}	1.13×10^{-6}	0.0	—
18	1.13×10^{-6}	1.00×10^{-6}	0.0	—
19	1.00×10^{-6}	8.00×10^{-7}	0.0	—
20	8.00×10^{-7}	4.14×10^{-7}	0.0	—
21	4.14×10^{-7}	3.25×10^{-7}	0.0	—
22	3.25×10^{-7}	2.25×10^{-7}	0.0	—
23	2.25×10^{-7}	1.00×10^{-7}	0.0	—
24	1.00×10^{-7}	5.00×10^{-8}	0.0	—
25	5.00×10^{-8}	3.00×10^{-8}	0.0	—
26	3.00×10^{-8}	1.00×10^{-8}	0.0	—
27	1.00×10^{-8}	1.00×10^{-11}	0.0	—

[a]Source normalization = one neutron per assembly

Table A-9 BWR Fuel, Simplified Storage Cask Model—Primary Gamma Dose Rate Produced by a Single-Source Photon as a Function of Gamma Energy Bin

27n19g library gamma group number	Upper energy bound (MeV)	Lower energy bound (MeV)	Dose rate[a] (mrem/h)	Relative error
1	2.00×10^{1}	1.00×10^{1}	2.4925×10^{-11}	0.0004
2	1.00×10^{1}	8.00×10^{0}	1.7648×10^{-11}	0.0004
3	8.00×10^{0}	6.50×10^{0}	1.3569×10^{-11}	0.0004
4	6.50×10^{0}	5.00×10^{0}	9.3095×10^{-12}	0.0004
5	5.00×10^{0}	4.00×10^{0}	5.5451×10^{-12}	0.0004
6	4.00×10^{0}	3.00×10^{0}	2.8420×10^{-12}	0.0004
7	3.00×10^{0}	2.50×10^{0}	1.2817×10^{-12}	0.0004
8	2.50×10^{0}	2.00×10^{0}	5.9815×10^{-13}	0.0004
9	2.00×10^{0}	1.66×10^{0}	2.4241×10^{-13}	0.0004
10	1.66×10^{0}	1.33×10^{0}	9.1426×10^{-14}	0.0006
11	1.33×10^{0}	1.00×10^{0}	2.4058×10^{-14}	0.0004
12	1.00×10^{0}	8.00×10^{-1}	4.8043×10^{-15}	0.0005
13	8.00×10^{-1}	6.00×10^{-1}	9.4128×10^{-16}	0.0010
14	6.00×10^{-1}	4.00×10^{-1}	8.8688×10^{-17}	0.0006
15	4.00×10^{-1}	3.00×10^{-1}	3.36768×10^{-18}	0.0012
16	3.00×10^{-1}	2.00×10^{-1}	1.3308×10^{-19}	0.0011
17	2.00×10^{-1}	1.00×10^{-1}	4.5374×10^{-22}	0.0017
18	1.00×10^{-1}	4.50×10^{-2}	0.0	—
19	4.50×10^{-2}	1.00×10^{-2}	0.0	—

[a]Source normalization = one gamma per assembly.

Table A-10 BWR Fuel, Simplified Storage Cask Model—Neutron Dose Rate Produced by a Single-Source Neutron as a Function of Neutron Energy Bin

27n19g library neutron group number	Upper energy bound (MeV)	Lower energy bound (MeV)	Dose rate[a] (mrem/h)	Relative error
1	2.00×10^{1}	6.38×10^{0}	1.3297×10^{-9}	0.0005
2	6.38×10^{0}	3.01×10^{0}	7.3630×10^{-10}	0.0023
3	3.01×10^{0}	1.83×10^{0}	3.0952×10^{-10}	0.0012
4	1.83×10^{0}	1.42×10^{0}	3.9460×10^{-11}	0.0585
5	1.42×10^{0}	9.07×10^{-1}	1.9875×10^{-11}	0.0850
6	9.07×10^{-1}	4.08×10^{-1}	1.2780×10^{-11}	0.0178
7	4.08×10^{-1}	1.11×10^{-1}	7.4319×10^{-12}	0.0150
8	1.11×10^{-1}	1.50×10^{-2}	4.6668×10^{-12}	0.0307
9	1.50×10^{-2}	3.04×10^{-3}	2.2938×10^{-12}	0.0489
10	3.04×10^{-3}	5.83×10^{-4}	1.7461×10^{-12}	0.0808
11	5.83×10^{-4}	1.01×10^{-4}	8.2009×10^{-13}	0.0493
12	1.01×10^{-4}	2.90×10^{-5}	4.4728×10^{-13}	0.0595
13	2.90×10^{-5}	1.07×10^{-5}	2.8538×10^{-13}	0.0532
14	1.07×10^{-5}	3.06×10^{-6}	1.8761×10^{-13}	0.1257
15	3.06×10^{-6}	1.86×10^{-6}	1.6782×10^{-13}	0.0627
16	1.86×10^{-6}	1.30×10^{-6}	1.8596×10^{-13}	0.3950
17	1.30×10^{-6}	1.13×10^{-6}	1.8352×10^{-13}	0.3565
18	1.13×10^{-6}	1.00×10^{-6}	9.8470×10^{-14}	0.0817
19	1.00×10^{-6}	8.00×10^{-7}	8.71296×10^{-14}	0.0904
20	8.00×10^{-7}	4.14×10^{-7}	7.2560×10^{-14}	0.0953
21	4.14×10^{-7}	3.25×10^{-7}	4.4565×10^{-14}	0.0429
22	3.25×10^{-7}	2.25×10^{-7}	5.5750×10^{-14}	0.2660
23	2.25×10^{-7}	1.00×10^{-7}	2.7777×10^{-14}	0.1085
24	1.00×10^{-7}	5.00×10^{-8}	1.3465×10^{-14}	0.0659
25	5.00×10^{-8}	3.00×10^{-8}	1.0154×10^{-14}	0.1710
26	3.00×10^{-8}	1.00×10^{-8}	0	—
27	1.00×10^{-8}	1.00×10^{-11}	0	—

[a] Source normalization = one neutron per assembly

Table A-11 Example of Total Gamma Dose Rate Calculation: Simplified Transportation Package Model Containing WEC 17 × 17 PWR Assembly (MPC-32); 75 GWd/MTU, 5-year Cooling Time

27n19g neutron group number	Upper energy bound[a] (MeV)	Lower energy bound[a] (MeV)	Primary gamma intensity[b] (s^{-1})	Gamma dose rate from Table A-3	Final gamma dose rate[c] (mrem/h)	Relative error	Group percentage contribution (%)
1	2.00×10^{1}	1.00×10^{1}	1.46×10^{5}	2.9465×10^{-12}	1.38×10^{-5}	0.0004	0.00
2	1.00×10^{1}	8.00×10^{0}	2.00E+06	3.3618×10^{-12}	2.15×10^{-4}	0.0003	0.00
3	8.00×10^{0}	6.50×10^{0}	9.30E+06	3.1313×10^{-12}	9.32×10^{-4}	0.0003	0.00
4	6.50×10^{0}	5.00×10^{0}	4.77E+07	2.5813×10^{-12}	3.94×10^{-3}	0.0004	0.00
5	5.00×10^{0}	4.00×10^{0}	1.17E+08	1.8223×10^{-12}	6.82×10^{-3}	0.0003	0.00
6	4.00×10^{0}	3.00×10^{0}	3.25E+10	1.0654×10^{-12}	1.11×10^{0}	0.0003	0.44
7	3.00×10^{0}	2.50×10^{0}	2.53E+11	5.2900×10^{-13}	4.28×10^{0}	0.0004	1.68
8	2.50×10^{0}	2.00×10^{0}	2.33E+12	2.5772×10^{-13}	1.92×10^{1}	0.0004	7.55
9	2.00×10^{0}	1.66×10^{0}	1.64E+12	1.0549×10^{-13}	5.54×10^{0}	0.0004	2.17
10	1.66×10^{0}	1.33×10^{0}	7.66E+13	3.8586×10^{-14}	9.46×10^{1}	0.0004	37.15
11	1.33×10^{0}	1.00×10^{0}	2.16E+14	9.3356×10^{-15}	6.45×10^{1}	0.0005	25.35
12	1.00×10^{0}	8.00×10^{-1}	2.28E+14	1.6099×10^{-15}	1.17×10^{1}	0.0006	4.61
13	8.00×10^{-1}	6.00×10^{-1}	6.25E+15	2.6598×10^{-16}	5.32×10^{1}	0.0007	20.89
14	6.00×10^{-1}	4.00×10^{-1}	6.60E+14	1.8410×10^{-17}	3.89×10^{-1}	0.0011	0.15
15	4.00×10^{-1}	3.00×10^{-1}	9.31E+13	3.3440×10^{-19}	9.96×10^{-4}	0.0029	0.00
16	3.00×10^{-1}	2.00×10^{-1}	1.52E+14	4.4639×10^{-21}	2.17×10^{-5}	0.0057	0.00
17	2.00×10^{-1}	1.00×10^{-1}	5.36E+14	4.5198×10^{-25}	7.75×10^{-9}	0.0327	0.00
18	1.00×10^{-1}	4.50×10^{-2}	7.45E+14	0.0	0.0	—	0.00
19	4.50×10^{-2}	1.00×10^{-2}	2.47E+15	0.0	0.0	—	0.00
Total primary gamma dose rate	—	—	—	—	2.55×10^{2}	0.0003	100
^{60}Co[d]	—	—	—	—	3.37×10^{0}	0.0012	—

[a] Groups 7 through 14 cover the gamma energy range recommended in NUREG-2216 [A-7]
[b] Calculated by ORIGEN Assembly Isotopics (ORIGAMI)
[c] (Primary gamma intensity) × (Gamma dose rate from Table A-3) × 32
[d] Assuming 100 Ci/assembly

Table A-12 Example of Total Neutron Dose Rate Calculation: Simplified Transportation Package Model Containing WEC 17 × 17 PWR Fuel (MPC-32); 75 GWd/MTU, 5-year Cooling Time

27n19g neutron group number	Upper energy bound (MeV)	Lower energy bound (MeV)	Neutron intensity[a] (s^{-1})	Neutron dose rate from Table A-4	Final neutron dose rate[b] (mrem/h)	Relative error
1	2.00×10^{1}	6.38×10^{0}	5.36×10^{7}	2.9056×10^{-9}	4.98×10^{0}	0.0004
2	6.38×10^{0}	3.01×10^{0}	5.24×10^{8}	1.1246×10^{-9}	1.89×10^{1}	0.0007
3	3.01×10^{0}	1.83×10^{0}	5.98×10^{8}	8.7861×10^{-10}	1.68×10^{1}	0.0004
4	1.83×10^{0}	1.42×10^{0}	2.79×10^{8}	6.2328×10^{-10}	5.56×10^{0}	0.0004
5	1.42×10^{0}	9.07×10^{-1}	4.00×10^{8}	5.7398×10^{-10}	7.35×10^{0}	0.0004
6	9.07×10^{-1}	4.08×10^{-1}	3.90×10^{8}	2.7068×10^{-10}	3.38×10^{0}	0.0006
7	4.08×10^{-1}	1.11×10^{-1}	1.79×10^{8}	3.5136×10^{-11}	2.01×10^{-1}	0.0009
8	1.11×10^{-1}	1.50×10^{-2}	3.14×10^{7}	5.6635×10^{-12}	5.69×10^{-3}	0.0018
9	1.50×10^{-2}	3.04×10^{-3}	1.54×10^{6}	2.3316×10^{-13}	1.15×10^{-5}	0.0025
10	3.04×10^{-3}	5.83×10^{-4}	1.41×10^{5}	3.3554×10^{-14}	1.51×10^{-7}	0.0039
11	5.83×10^{-4}	1.01×10^{-4}	1.21×10^{4}	3.2812×10^{-15}	1.27×10^{-9}	0.0171
12	1.01×10^{-4}	2.90×10^{-5}	7.98×10^{2}	3.3510×10^{-16}	8.56×10^{-12}	0.0665
13	2.90×10^{-5}	1.07×10^{-5}	1.12×10^{2}	4.1998×10^{-17}	1.51×10^{-13}	0.0461
14	1.07×10^{-5}	3.06×10^{-6}	2.72×10^{1}	0.00	0.00	—
15	3.06×10^{-6}	1.86×10^{-6}	2.60×10^{0}	0.00	0.00	—
16	1.86×10^{-6}	1.30×10^{-6}	9.61×10^{-1}	0.00	0.00	—
17	1.30×10^{-6}	1.13×10^{-6}	2.65×10^{-1}	0.00	0.00	—
18	1.13×10^{-6}	1.00×10^{-6}	1.78×10^{-1}	0.00	0.00	—
19	1.00×10^{-6}	8.00×10^{-7}	2.62×10^{-1}	0.00	0.00	—
20	8.00×10^{-7}	4.14×10^{-7}	4.13×10^{-1}	0.00	0.00	—
21	4.14×10^{-7}	3.25×10^{-7}	7.46×10^{-2}	0.00	0.00	—
22	3.25×10^{-7}	2.25×10^{-7}	7.23×10^{-2}	0.00	0.00	—
23	2.25×10^{-7}	1.00×10^{-7}	6.91×10^{-2}	0.00	0.00	—
24	1.00×10^{-7}	5.00×10^{-8}	1.88×10^{-2}	0.00	0.00	—
25	5.00×10^{-8}	3.00×10^{-8}	5.50×10^{-3}	0.00	0.00	—
26	3.00×10^{-8}	1.00×10^{-8}	3.86×10^{-3}	0.00	0.00	—
27	1.00×10^{-8}	1.00×10^{-11}	9.20×10^{-4}	0.00	0.00	—
Total					5.72×10^{1}	0.0003

[a] Calculated by ORIGAMI

[b] (Neutron intensity) × (Neutron dose rate from Table A-4) × 32

A.3 References

A-1. Bowman, S.M., Gauld, I.C., and Wagner, J.C., "Recommendations on Fuel Parameters for Standard Technical Specifications for Spent Fuel Storage Casks," NUREG/CR-6716, U.S. Nuclear Regulatory Commission, Washington, DC, March 2001, ADAMS Accession No. ML010820352.

A-2. Holtec International, "Final Safety Analysis Report for the HI-STORM 100 Cask System," Revision 13, Marlton, NJ, March 2016.

A-3. Holtec International, "Safety Analysis Report on the HI-STAR 100 Cask System," Revision 20, Camden, NJ, June 2019.

A-4. Lefebvre, R.A., et al., "Development of Streamlined Nuclear Safety Analysis Tool for Spent Nuclear Fuel Applications," *Nuclear Technology*, 199, 227-244, September 2017, https://doi.org/10.1080/00295450.2017.1314747227.

A-5. Radulescu, G., Banerjee, K., and Miller, L.P., "Demonstration of the On-the-Fly Shielding Analysis Method," ORNL/SPR-2021/1913, Oak Ridge National Laboratory, Oak Ridge, TN, March 2021, https://doi.org/10.2172/1813202.

A-6. American National Standards Institute / American Nuclear Society, "Neutron and Gamma-Ray Flux-to-Dose-Rate Factors," ANSI/ANS-6.1.1-1977 (N666), American Nuclear Society, La Grange Park, IL, 1977, https://www.osti.gov/biblio/5538262.

A-7. Borowski, J., et al., "Standard Review Plan for Transportation Packages for Spent Fuel and Radioactive Material," NUREG-2216, U.S. Nuclear Regulatory Commission, Washington, DC, August 2020 ADAMS Accession No. ML20234A651.

A-8. Shappert, L.B., ed., "The Radioactive Materials Packaging Handbook, Design, Operations, and Maintenance," ORNL/M-5003, Oak Ridge National Laboratory, Oak Ridge, TN, 1998, https://doi.org/10.2172/303938.

APPENDIX B
CONTINUOUS-ENERGY AND MULTIGROUP CALCULATION COMPARISONS FOR CRITICALITY SAFETY EVALUATIONS

Criticality safety calculations throughout this report are performed with the ENDF/B-VII.1 252-group multigroup (MG) library. Although this is an extensively validated library and generally accepted for LWR applications [B-1], it is still desired to demonstrate the suitability of the lower fidelity nuclear data for the calculations performed in this report. Several spot checks were performed at various state points to sample the different neutronic environments involved with variable enrichment, burnup, and spectrum to ensure the multigroup library remained applicable relative to the higher fidelity, CE counterpart. The baseline configuration, a case of 70-year cooling time with an initial enrichment of 8 wt %, and a case of 2,500 ppm depletion soluble boron with 5 wt % initial enrichment were selected. Each test involved the typical range of burnups—15 through 75 GWd/MTU with 10 GWd/MTU increments. The limited number of calculations covering some of the extremes of the analyses presented in this report is deemed to be acceptable given the broad range of systems for which comparisons of the 252-group and CE libraries have been performed [B-1]. The enrichments included cover 5, 6, and 8 wt % fuel, with burnups of 15–75 GWd/MTU, and conditions such as 70 yr of cooling time and 2,500 ppm of soluble boron. Figure B-1 demonstrates the excellent agreement between MG and CE calculations of the systems. The bias between the two libraries is below 50 pcm in all instances, with an uncertainty in the bias of 14 pcm. The MG calculation is consistently lower than the CE result. These results are in line with the results documented in Greene and Marshall [B-1], which show that the 252-group MG library generally calculated k_{eff} values that are approximately 50–70 pcm lower than the CE results for LEU or mixed uranium/plutonium pin array benchmarks. Results are statistically indistinguishable between burnups and libraries.

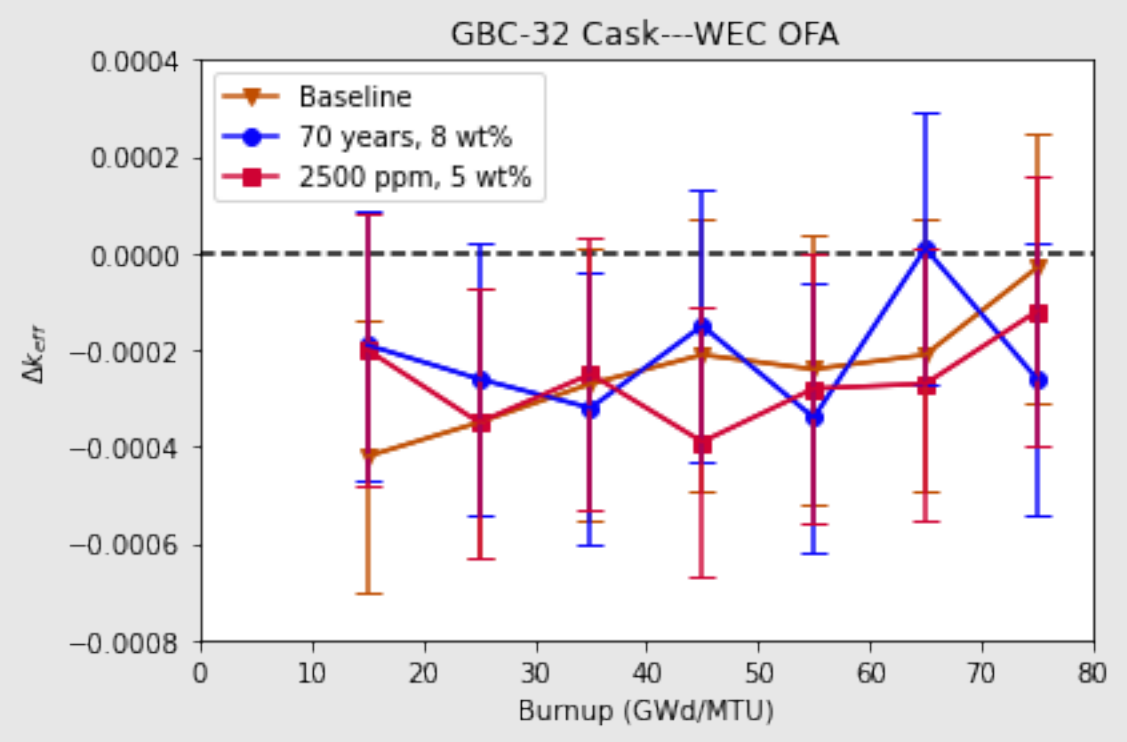

Figure B-1 Multigroup Bias (±2σ) as a Function of Burnup at Selected State Points

B.1 References

B-1. Greene, T.M. and Marshall, W.J., "SCALE 6.2.4 Validation: Nuclear Criticality Safety," ORNL/TM-2020/1500/v2, Oak Ridge National Laboratory, Oak Ridge, TN, November 2022, https://doi.org/10.2172/1902815.

NRC FORM 335
(12-2010)
NRCMD 3.7

U.S. NUCLEAR REGULATORY COMMISSION

BIBLIOGRAPHIC DATA SHEET

(See instructions on the reverse)

1. REPORT NUMBER
(Assigned by NRC, Add Vol., Supp., Rev., and Addendum Numbers, if any.)

NUREG/CR-7306
ORNL/TM-2023/2938

2. TITLE AND SUBTITLE

Fuel Assembly and Irradiation Parametric Study for Extended-Enrichment and High-Burnup Light-Water Reactor Spent Nuclear Fuel in Dry Storage Casks and Transportation Packages

3. DATE REPORT PUBLISHED

MONTH	YEAR
April	2024

4. FIN OR GRANT NUMBER

5. AUTHOR(S)

A. Alpan, N. Kucinski, A. Shaw, B. Hiscox, G. Radulescu

6. TYPE OF REPORT

Technical

7. PERIOD COVERED (Inclusive Dates)

8. PERFORMING ORGANIZATION - NAME AND ADDRESS (If NRC, provide Division, Office or Region, U. S. Nuclear Regulatory Commission, and mailing address; if contractor, provide name and mailing address.)

Oak Ridge National Laboratory
1 Bethel Valley Road
Oak Ridge, TN 37831

9. SPONSORING ORGANIZATION - NAME AND ADDRESS (If NRC, type "Same as above", if contractor, provide NRC Division, Office or Region, U. S. Nuclear Regulatory Commission, and mailing address.)

Division of Systems Analysis
Office of Nuclear Regulatory Research
U.S. Nuclear Regulatory Commission
Washington, D.C. 20555-0001

10. SUPPLEMENTARY NOTES

L. Kyriazidis, NRC Project Manager

11. ABSTRACT (200 words or less)

There is an increased interest in operating commercial light-water reactors (LWRs) in the United States with improved economics that would result from longer fuel cycle lengths, fewer and shorter refueling outages, and fewer fuel assemblies requiring storage at the back end of the fuel cycle. To support this, fuel discharge burnups, as well as initial ^{235}U enrichments, must be higher than those used in current commercial LWRs. The typical upper limit considered for assembly average burnup in this report is 75 gigawatt-days (GWd) per metric ton of uranium (MTU), as opposed to the current typical upper bound of approximately 62 GWd/MTU. The upper limit considered for initial ^{235}U enrichment is 8 weight percent (8 wt %), as opposed to the current regulatory limit of 5 wt %. The enrichment range from 5 to 8 wt % is referred to in this report as *extended enrichment*. To investigate the effect of high burnup and extended enrichment conditions on dose rates and burnup credit for dry storage casks and transportation packages, a fuel assembly and irradiation parametric study was performed. The conclusions from this study will assist U.S. Nuclear Regulatory Commission staff in reviewing applications for dry storage casks and transportation packages that contain high-burnup and extended enrichment fuel.

12. KEY WORDS/DESCRIPTORS (List words or phrases that will assist researchers in locating the report.)

light-water reactor
extended enrichment
high burnup
dry storage cask
transportation package
radiation shielding
criticality safety

13. AVAILABILITY STATEMENT

unlimited

14. SECURITY CLASSIFICATION

(This Page)
unclassified

(This Report)
unclassified

15. NUMBER OF PAGES

16. PRICE

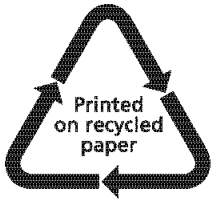

Federal Recycling Program

UNITED STATES
NUCLEAR REGULATORY COMMISSION
WASHINGTON, DC 20555-0001

OFFICIAL BUSINESS

NUREG/CR-7306 **Fuel Assembly and Irradiation Parametric Study for Extended-Enrichment and High-Burnup Light-Water Reactor Spent Nuclear Fuel in Dry Storage Casks and Transportation Packages** April 2024